

**Development of molten salt electrochemical process for  
electrolytic reduction of uranium oxide**

*By*

**NAGARAJ ALANGI**

**Enrolment No: ENGG01200704009**

**Bhabha Atomic Research Center, Mumbai**

*A thesis submitted to the*

*Board of Studies in Engineering Sciences*

*In partial fulfillment of requirements*

*For the Degree of*

**DOCTOR OF PHILOSOPHY**

*of*

**HOMI BHABHA NATIONAL INSTITUTE**



**March 2016**

**Homi Bhabha National Institute**

## Recommendation of the Viva Voce Board

As members of the Viva Voce Board, we certify that we have read the dissertation prepared by Nagaraj Alangi entitled "Development of molten salt electrochemical process for electrolytic reduction of uranium oxide" and recommend that it may be accepted as fulfilling the dissertation requirement for the Degree of Doctor of Philosophy.

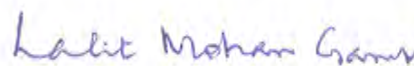
**Date:**

Chairman: Prof Smt Roy S B

  
1.4.2016

**Date:**

Guide / Convener: Prof L M Gantayet

  
31.3.16

**Date:**

Member 1: Prof Dinesh Srivastava

  
31.3.16

**Date:**

Member 2: Prof Smt Mukhopadhyaya S

  
31/3/2016

**Date:**

Member 3: Prof Rajeev Kapoor

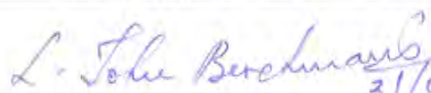
  
31/3/2016

**Date:**

Member 4:

**Date:**

External Examiner: Dr. L John Berchmans

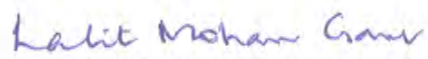
  
31/03/2016

Final approval and acceptance of this dissertation is contingent upon the candidate's submission of the final copies of the dissertation to HBNI.

I hereby certify that I have read this dissertation prepared under my direction and recommend that it may be accepted as fulfilling the dissertation requirement.

**Date: March 31, 2016**

**Place: HBNI, Anushakthi Nagar, Mumbai-94**

  
31.3.16  
**Guide: Prof L M Gantayet**

## **STATEMENT BY AUTHOR**

This dissertation has been submitted in partial fulfillment of requirement for an advance degree at Homi Bhabha National Institute (HBNI) and is deposited in the library to be made available to borrowers under rules of the HBNI.

Brief quotations from the dissertation are allowable without special permission, provided that accurate acknowledgement of source is made. Requests for permission for extended quotation from or reproduction of this manuscript in whole or in part may be granted by the Competent Authority of HBNI when in his or her judgment the proposed use of the material is in the interests of scholarship. In all other instances, however, permission must be obtained from the author.



Nagaraj Alangi

## **DECLARATION**

I hereby declare that the investigation presented in the thesis has been carried out by me. The work is original and has not been submitted earlier as a whole or in part for a degree / diploma at this or any other Institution / University.



Nagaraj Alangi

*Dedicated to  
my wife, Gouri  
son, Tarit  
parents and in-laws  
for their constant support and unconditional love*

## ACKNOWLEDGEMENTS

It has been a long road, and finally I am at the end, but there are so many people to whom I extend thanks. First and foremost I want to thank my advisor Dr. L. M. Gantayet for his support, encouragement and advice throughout this project. I am very pleased to acknowledge with gratitude the generous help, invaluable guidance and constant inspiration at every stage provided to me by him throughout the course of this work. I am truly thankful for his unwavering veracity, and altruistic dedication to both my personal and academic development. The enthusiasm he has for the research and innovation was contagious and motivational for me, during all times in the Ph.D. pursuit. His forensic scrutiny of new ideas always helped to recommend consistently excellent improvements.

I would like to express my deepest thanks to my co-advisor Dr A K Suri for his guidance in solubility studies, valuable suggestions in electrolysis experiments which brought forth the culmination of this study. His patience and enormous knowledge were key motivations throughout my PhD. I deeply appreciate the contribution of his specific scientific advice and positive outlook under all circumstances.

I would like to extend thanks to current Head of Division, L&PTD, BARC Dr K Dasgupta and former Head of Division Dr A K Das for enabling me work in this project of paramount importance by providing facilities and constant encouragement. I am extremely thankful to Dr Jaya Mukherjee, Head, ICPEs, L&PTD for always being with me at the moment of need. Her untiring efforts with a professional outlook guided me conduct a large number of experiments, involving hazardous chemicals in a safe and efficient manner.

I will forever be thankful to my colleague Smt Anupama. She has been supportive since the days I began working on this project, not only limited to motivate to work in the lab, but also academically and emotionally through the road to finish this thesis.

I would like to express my sincere thanks to Dr P V A Padmanabhan for generously sharing his time and knowledge in the development of plasma spray coatings. Thanks are also due to Chakravarthy and Sreekumar for help in preparation of coatings.

I want to thank present and past members of my PhD committee guiding me through all these years, with their advice and suggestions in general.

I would specially thank Dr. R. Mishra from Chemistry Division, BARC for his help in TG-DTA experiments and useful discussions while XRD data analysis. My special thanks are to Shri Hareendran, UED, BARC for allowing helping me with the chemical analysis of samples. I am also thankful to Dr Nagarajan V, Dr Prabhakara Reddy and Shri S Ghosh from IGCAR for their help in electrochemical experiments, useful discussions and data analysis. Thanks are due to Dr Arun Kumar and Dr K B Khan, RMD, BARC for providing me the glove box cutting facility to collect samples from graphite crucibles of experiments.

My sincere thanks also go to our team members Shri S. Sethi, Shri S.P. Dey, Shri Devranjan das, Ms Anchal Gupta, Shri Aditya, Shri Devendra and Shri Paramjit for their useful design discussions and support during the experiments. Special thanks to Shri V S Rawat for guidance in completion of thesis during the last phase of my work.

I would like to convey my sincere thanks to Shri Sunil Dehade and Shri Mukesh Verma for extending all possible and sincere help throughout the course of experiments. Also thanks to Shri Prashant Malonkdar for his help in up keeping the lab.

Again, support of my friends Murthy, Manoj, Mani can never be forgotten.

Last but not the least, I would like to thank my family for all their love and encouragement. This PhD thesis is a testimony to your faith in me and I hope I have made you proud. Finally, I would like to thank my better half, Gouri. I cannot find words that can express my gratitude for everything you have done. Thank you for accompanying me on this arduous adventure, and I will look forward to our next one!

My note of thanks would be incomplete without mentioning my six year old son Tarit. He was to me, an epitome of perseverance, an incessant source of energy to spring back on my feet.



Nagaraj Alangi

## Table of Contents

	<b>Content</b>	<b>Page no.</b>
	Abbreviations	xiv
	Nomenclature	xv
	List of Figures	xvi
	List of Tables	xxiii
 <b>CHAPTER I</b>		
	INTRODUCTION	1
1.1	Considerations for uranium feed metal production	2
1.2	Electrolytic reduction process	3
1.3	Objectives and scope	12
1.4	Organization of the thesis	13
	References	15
 <b>CHAPTER II</b>		
	LITERATURE REVIEW AND THERMO-CHEMISTRY OF ELECTROLYTIC REDUCTION PROCESS	17
2.1	Electrolytic Reduction of Uranium oxides to Uranium	17
2.1.1	Electrolytic Reduction of Uranium oxides in Chloride Electrolytes	17
2.1.2	Electrolytic Reduction of Uranium oxides in Fluoride electrolytes	21
2.2	Summary of the literature reviewed	30
2.3	UO <sub>2</sub> Solubility studies	35
2.4	Thermo-chemistry of the electrolytic reduction process	41
2.5	Associated Problems in electrolytic reduction of uranium oxides	48

	<b>Content</b>	<b>Page no.</b>
	References	50
<b>CHAPTER III</b>		
	THERMO-PHYSICAL CHARACTERIZATION AND MATERIALS FOR ELECTROLYTE HANDLING	55
3.1	Introduction	55
3.1.1	Importance of purity of the molten salt	56
3.1.2	Selection of materials for the components of the electrolytic cell	57
3.2	Melting point determination	60
3.2.1	Experimental setup for salt mixture preparation	60
3.2.2	Testing and performance evaluation of experimental setup	66
3.2.3	Salt mixture preparation	68
3.2.4	TG-DTA experiments	70
3.3	Conditioning procedure for electrolyte	74
3.3.1	Chemicals and Electrodes	76
3.3.2	Apparatus and methods	77
3.3.3	Results of experiments and selection of conditioning procedure	79
3.4	Selection of materials for electrolytic cells	83
3.4.1	Reactions of molten fluoride with metallic materials	84
3.4.2	Effect of moisture	85
3.4.3	Reaction of molten fluoride salts with ceramic materials	85

	<b>Content</b>	<b>Page no.</b>
3.5	Experimental study for selection of materials for electrolytic cells	94
3.5.1	Experimental setup for testing compatibility of materials for electrolytic cells	94
3.5.2	Tests conducted	100
3.6	Conclusions	103
	References	104
 <b>CHAPTER IV</b>		
	SOLUBILITY OF UO <sub>2</sub> IN FLUORIDE MELTS	105
4.1	Introduction	105
4.1.1	Methods of determination of saturation solubility	108
4.2	Salt mixture preparation and their purification	111
4.3	Experimental setup for solubility studies	111
4.4	Experimental procedure	115
4.5	Sample dissolution and uranium analysis methods	118
4.6	Results and discussions	118
4.6.1	Uncertainties and errors	118
4.6.2	Effect of LaF <sub>3</sub> concentration	120
4.6.3	Effect of temperature	121
4.6.4	Effect of addition of UF <sub>4</sub> to LaF <sub>3</sub> (mixed electrolyte)	121
4.7	Conclusions	124
	References	125
 <b>CHAPTER V</b>		
	ELECTROCHEMICAL STUDIES OF URANIUM IN FLUORIDE MELTS	127

	<b>Content</b>	<b>Page no.</b>
5.1	Introduction	127
5.2	Experimental setup for electrochemical studies	128
5.3	Experimental materials and methods	133
5.4	Results and discussions	134
5.4.1	Analysis of cathodic peak IIc and anodic peak IIa	135
5.4.2	Analysis of cathodic peak IIIc and anodic peak IIIa	141
5.4.3	Chronopotentiometry in LiF-BaF <sub>2</sub> (1:1)25 wt% UF <sub>4</sub>	144
5.4.4	Effect of UO <sub>2</sub> addition in LiF-BaF <sub>2</sub> (1:1)25 wt% UF <sub>4</sub>	146
5.4.5	Investigations in LiF-BaF <sub>2</sub> (1:1)25 wt% LaF <sub>3</sub> melts with and without UO <sub>2</sub>	149
5.5	Conclusions	152
	References	153
 <b>CHAPTER VI</b>		
	ELECTROLYTIC REDUCTION OF URANIUM OXIDE TO URANIUM METAL	155
6.1	Introduction	155
6.2	Selection of electrolyte	156
6.3	Materials used in the electrolysis and salt preparation	159
6.3.1	Preparation of UO <sub>2</sub> +C pellets	160
6.4	Experimental setup for electrolysis studies	161
6.5	Experimental variables for electrolysis of UO <sub>2</sub> to U metal	165
6.6	Electrolysis experiments	171
6.6.1	Phase 1 electrolysis experiments (ES1-ES7a)	172
6.6.2	Phase 2 electrolysis experiments (ES8-ES9)	175

	<b>Content</b>	<b>Page no.</b>
6.6.3	Phase 3 electrolysis experiments (ES10-ES19)	178
6.6.4	Electrolysis experiments in Phase 4 (ES17-ES21)	187
6.7	Conclusions	193
	References	194
 <b>CHAPTER VII</b>		
PREPARATION AND TESTING OF YTTRIA COATINGS		197
7.1	Introduction	197
7.1.1	Yttria coating	199
 PART A		
7.2	Yttria coating preparation and thermal stability testing	202
7.2.1	Preparation of plasma spray grade Y <sub>2</sub> O <sub>3</sub> Powder	202
7.2.2	Preparation of coated samples	202
7.2.3	Thermal cycling test of coatings	205
7.2.4	Equipment for thermal cycling	206
7.2.5	Thermal cycling test procedure	209
7.3.	Results and Discussion for thermal cycling tests	210
 PART -B		
7.4	Liquid uranium corrosion studies of yttria coatings	214
7.4.1	Experimental setup for liquid uranium compatibility studies	215
7.5	Plasma spray coating on coupons and crucible	219
7.6.	Experimental procedure for liquid uranium corrosion studies	220
7.7	Results and Discussions for liquid uranium compatibility studies	221

	<b>Content</b>	<b>Page no.</b>
7.7.1	Analysis of penetration of uranium into pores of coating	231
7.7.2	EDS analysis of the cross section of immersed coupons	232
7.8	Conclusions	236
	References	237
 <b>CHAPTER VIII</b>		
	<b>SUMMARY AND CONCLUSIONS</b>	<b>239</b>
8.1	Thermo-physical characterization and preparation of electrolytes	240
8.2	Selection of materials to for the electrolysis setup	240
8.3	Solubility studies of UO <sub>2</sub> in the electrolyte baths	241
8.4	Electrochemical studies of uranium in the molten fluoride bath at 1473K	241
8.5	Electrolysis of UO <sub>2</sub> to U metal	243
8.6	Preparation of Y <sub>2</sub> O <sub>3</sub> coatings as chemical barrier	244
8.7	Qualification of coatings by thermal cycling	245
8.8	Compatibility of yttria coating with liquid uranium	246
8.9	Important Conclusions	247
8.10	Major contributions	249
8.11	Future work	250
	List of publications	251

## Abbreviations

AR	- Analytic reagent
AVLIS	- Atomic Vapor Laser Isotope Separation
BDL	- Below Detectable Limits
BN	- Boron Nitride
CAS	- Chemical Abstracts Service
CCD	- Cathode Current Density
CV	- Cyclic Voltammetry
EDS	- Energy Dispersive Spectroscopy
EXAFS	- Extended X-Ray Absorption Fine Structure
HAZOP	- Hazard and Operability study
He-MSLD	- Helium Mass Spectrometer Leak Detector
HEPA	- High Efficiency Particulate Arrestance
ICPMS	- Inductively coupled plasma mass spectrometry
ID	- Inner Diameter
KAPL	- Knolls Atomic Power Laboratory
LSV	- Linear Sweep Voltammetry
MCW	- Mallinckrodt Chemical Works
OD	- Outer Diameter
ORNL	- Oak Ridge National Laboratory
QRE	- Quasi-reference electrode
SEM	- Scanning Electron Microscope
TG-DTA	- Thermo Gravimetric and Differential Thermal Analysis
UNS	- Unified Numbering System
USBM	- United States Bureau of Mines
XRD	- X-Ray Diffraction

## Nomenclature

A	Electrode area	cm <sup>2</sup>
C <sub>o</sub>	Bulk concentration	mol/cm <sup>3</sup>
D	pore diameter	cm
D <sub>o</sub>	Diffusion coefficient	cm <sup>2</sup> /s
E <sub>p</sub>	Peak potential	Volts
E <sub>p1/2</sub>	Half peak potential	Volts
E <sub>pa</sub>	Anodic peak voltage	Volts
E <sub>pc</sub>	Cathodic peak voltage	Volts
ΔE <sub>p</sub>	Potential difference between the anodic and cathodic peaks	Volts
F	Faraday constant	C/mol
g	acceleration due to gravity	m <sup>2</sup> /s
h	Distance of penetration from a given datum line	cm
i <sub>p</sub>	Peak current	Amperes
n	Number of electrons involved	eq/mol
ΔP'	capillary pressure	Pascal
R	Universal gas constant	J / mol. K
r	radius of the oxide particle	cm
r <sub>o</sub>	Capillary radius	cm
t	Time	seconds
T	Temperature	Kelvin
μ	Viscosity of the liquid	centipoise
ν	Sweep rate	Volts/s
η	Viscosity of the electrolyte	centipoise
θ	contact angle between the liquid uranium and yttrium oxide	degree
ρ	Liquid density	g/cc
ρ	Density of uranium oxide	g/cc
ρ'	Density of the electrolyte	g/cc
σ	surface tension of liquid uranium	Dyne/cm
τ	Transition time	seconds

## List of figures

<b>Figure</b>	<b>Description</b>	<b>Page no</b>
1.1	Block diagram of different routes for preparing uranium metal from oxides	8
2.1	Different electrolytic cell designs by KAPL	23
2.2	Conceptual compartmental cell design for reduction of uranium oxides	25
2.3	Cell with basket anode used by Piper	27
2.4	UO <sub>2</sub> Solubility at 1423K in LiF-BaF <sub>2</sub> by Varwig	37
2.5	Solubility of UO <sub>2</sub> in LiF/UF <sub>4</sub> melts by Greenfield and Hyde	38
2.6	Solubility of UO <sub>2</sub> in BaF <sub>2</sub> /UF <sub>4</sub> melts by Greenfield and Hyde	39
2.7	Schematic of Electrolytic reduction cell	41
2.8	Pictorial representation of anode effect in electrolytic cells	49
3.1 (a)	Photograph of the argon purifier to generate argon with < 0.1ppm oxygen	59
3.1(b)	Copper mesh roll absorber used in purifier	59
3.2	Schematic of experimental assembly used for salt mixture preparation	64
3.3	Fabrication drawing of inconel 600 muffle of salt mixture preparation assembly	65
3.4	Photograph of the experimental setup for salt mixture with heating system	67
3.5	Temperature time characteristics of tubular furnace for ramp of 600K/hr	67
3.6	Temperature profile at the centre of the furnace at 1273K set point	68

<b>Figure</b>	<b>Description</b>	<b>Page no</b>
3.7	XRD pattern of LiF: BaF <sub>2</sub> (1:1 mole ratio) and 20 Wt % LaF <sub>3</sub> frozen salt mixture	73
3.8	XRD pattern of LiF: BaF <sub>2</sub> (1:1 mole ratio) and 20 Wt % UF <sub>4</sub> frozen salt mixture	74
3.9	Schematic of experimental assembly for preconditioning of molten salt	78
3.10	Heating cycle adopted for pre-conditioning the salt mixture	79
3.11	Voltammogram of LiF:BaF <sub>2</sub> (1:1) mixture, with short conditioning cycle, both graphite electrodes, at 1173K.	79
3.12	Voltammogram of LiF:BaF <sub>2</sub> (1:1) mixture, with 24hr conditioning cycle, both graphite electrodes, at 1173K.	80
3.13	Voltammogram comparing 2 electrode configuration and 3 electrode configuration in LiF:BaF <sub>2</sub> (1:1) electrolyte at 1173K.	81
3.14	Schematic of experimental assembly for material compatibility studies	98
3.15	Process and Instrumentation diagram of the typical fumehood experimental setup	99
4.1	Schematic of the experimental setup for solubility study	113
4.2	Photograph of the solubility study experimental setup inside fumehood	113
4.3	Variation of solubility of UO <sub>2</sub> with LaF <sub>3</sub> concentration in electrolytes	122
4.4	Variation of solubility of uranium oxide with temperature	123
4.5	Solubility of uranium oxide in mixed electrolytes	123

<b>Figure</b>	<b>Description</b>	<b>Page no</b>
4.6	Photographs of pellet holder, pellet and colors developed after experiment.	124
5.1	Schematic of setup for electrochemical studies	131
5.2a	Photograph of the setup inside fumehood for electrochemical studies	132
5.2b	Photograph of the components used for electrochemical studies	132
5.3	Voltammogram of LiF-BaF <sub>2</sub> equimolar electrolyte at 1473K	135
5.4	Cyclic voltammogram of LiF-BaF <sub>2</sub> (1:1)25 wt% UF <sub>4</sub> electrolyte	138
5.5	Linear variation of peak potential $E_p^{IIc}$ with sweep rate for peak IIc	140
5.6	Linear variation of peak current $I_p^{IIc}$ with square root of sweep rate for peak IIc	140
5.7	Linear variation of peak potential $E_p^{IIIc}$ with log of sweep rate for Peak IIIc	143
5.8	Linear variation of peak current $I_p^{IIIc}$ with square root of sweep rate for Peak IIIc	143
5.9	Chronopotentiogram of LiF-BaF <sub>2</sub> (1:1)25 wt% UF <sub>4</sub>	145
5.10	Product of $it^{1/2}$ for Chronopotentiogram of LiF-BaF <sub>2</sub> (1:1)25 wt% UF <sub>4</sub>	146
5.11	Cyclic voltammogram of LiF-BaF <sub>2</sub> (1:1)25 wt% UF <sub>4</sub> electrolyte with and without UO <sub>2</sub>	148
5.12	Chronopotentiogram of LiF-BaF <sub>2</sub> (1:1)25 wt% UF <sub>4</sub> electrolyte	148
5.13	Voltammogram of LiF-BaF <sub>2</sub> (1:1)25 wt% LaF <sub>3</sub> electrolyte with and without uranium oxide	151

<b>Figure</b>	<b>Description</b>	<b>Page no</b>
5.14	Comparison of chronopotentiograms of different electrolytes at 1473K	151
6.1	Photograph of experimental setup for electrolysis inside the fumehood	164
6.2	Schematic of the electrolysis assembly with setup A	165
6.3	Schematic of setup A, B, C D and E the for electrolysis experiments	166
6.4	Schematic of Setup F, G and H for the electrolysis experiments	167
6.5	Different anode designs used in the electrolysis studies	169
6.6	Photograph of different anodes of graphite used in the electrolysis experiment	169
6.7	Photographs of the components in assembled condition of Setup F	170
6.8	Photograph of S80 cell after the electrolysis with anode power holder embedded	173
6.9	Photograph of the BN tube used in experiment of electrowinning of uranium	178
6.10	Photographs of components depicting their typical state after the electrolysis experiments in phase 3 with tin cathode	185
6.11	Typical XRD analysis of cathode deposit sample confirming the formation of $USn_3$	186
6.12	Typical XRD analysis of cathode deposit sample confirming the formation of $Cu_5U$	186
7.1	General assembly of the thermal cycling setup for thermal cycling test of plasma coated coupons	209

<b>Figure</b>	<b>Description</b>	<b>Page no</b>
7.2	Heating and cooling cycle for thermal cycling experiments for test of yttria coating	210
7.3	Yttria coating on tantalum rectangular token, as coated surface micrograph at 100X	211
7.4	Yttria coating on tantalum rectangular token, as coated surface micrograph at 100X	211
7.5	Optical micrograph of Yttria coating on Ta coupon	212
7.6	SEM Picture of Ta-Yttria interface of yttria coating	212
7.7	SEM picture of yttria coating	212
7.8	Schematic of the experimental assembly for liquid uranium corrosion study	218
7.9	Photograph of the experimental assembly for liquid uranium corrosion study	218
7.10	Engineering safety arrangement of copper block to quench accidentally spilled liquid uranium inside the fumehood	219
7.11	Typical optical micrograph of surface of yttria coating on tantalum substrate (as coated)	224
7.12	Typical SEM micrograph of surface of yttria coating on tantalum substrate (as coated)	224
7.13	Typical optical micrograph of cross-sectional view of tantalum /yttria coating interface (as coated)	225
7.14	Typical SEM micrograph of cross-sectional view of tantalum /yttria coating interface (as coated)	225
7.15	Photographs of the Y <sub>2</sub> O <sub>3</sub> coated tantalum coupons	227

<b>Figure</b>	<b>Description</b>	<b>Page no</b>
7.16	Cross-sectional view of tantalum /yttria coating interface after 10hrs of immersion ( Sample UCOR-4)	227
7.17	Cross-sectional view of tantalum /yttria coating interface after 20hrs of immersion ( Sample UCOR-6)	228
7.18	Cross-sectional view of tantalum /yttria coating interface after 40hrs of immersion ( Sample UCOR-8)	228
7.19	Cross-sectional view of tantalum /yttria coating interface after 80hrs of immersion ( Sample UCOR-12)	229
7.20	Cross-sectional view of tantalum /yttria coating interface after 120hrs of immersion (Sample UCOR-14)	229
7.21	Cross-sectional view of tantalum /yttria coating interface after 200hrs of immersion (Sample UCOR-16)	230
7.22	Cross-sectional view of tantalum /yttria coating interface after 400hrs of immersion ( Sample UCOR-18)	230
7.23	EDS line scan of the cross-section of tantalum /yttria coating interface after 10hrs of immersion (Sample UCOR-4)	233
7.24	EDS line scan of the cross-section of tantalum /yttria coating interface after 20hrs of immersion (Sample UCOR-6)	233
7.25	EDS line scan of the cross-section of tantalum /yttria coating interface after 40hrs of immersion (Sample UCOR-8)	234
7.26	EDS line scan of the cross-section of tantalum /yttria coating interface after 80hrs of immersion (Sample UCOR-12)	234
7.27	EDS line scan of the cross-section of tantalum /yttria coating interface after 120hrs of immersion (Sample UCOR-14)	235

<b>Figure</b>	<b>Description</b>	<b>Page no</b>
7.28	EDS line scan of the cross-section of tantalum /yttria coating interface after 200hrs of immersion (Sample UCOR-16)	235
7.29	EDS line scan of the cross-section of tantalum /yttria coating interface after 400hrs of immersion (Sample UCOR-18)	236

## List of tables

<b>Table</b>	<b>Description</b>	<b>Page no</b>
1.1	Comparison of different uranium metal production techniques	4
2.1	Brief details of the reported fluoride electrolytes used, operating temperature and efficiencies reported for uranium metal production	31
2.2	Free energy of formation, melting point, boiling point data for fluoride salts used in molten salt electrolysis	43
2.3	Density and electrical conductance of molten fluoride salts	44
2.4	Vapor pressure data for some fluoride salts at 1473K	44
2.5	Overall cell reactions of uranium and theoretical potentials	46
3.1	Salient features of the furnace for fluoride salt bath preparation	62
3.2	List of impurities present in the fluoride salt mixtures	68
3.3	Melting points and weight loss of different fluoride electrolytes	72
3.4	Thermodynamic calculations of reaction between fluoride salts and different materials at 1500K	86
3.5	Reaction of uranium tetrafluoride with ceramic materials at 1500K	93
3.6	Specification of heating module for conducting fluoride salt compatibility studies	95
3.5	List of experiments conducted for compatibility studies with different electrolytes at 1473K	101
4.1	Matrix of the experiments conducted for UO <sub>2</sub> solubility in molten fluoride salts	117

<b>Table</b>	<b>Description</b>	<b>Page no</b>
4.2	Parametric study for microwave dissolution of fluoride samples for uranium analysis	119
4.3	Solubility of UO <sub>2</sub> in LiF-BaF <sub>2</sub> -LaF <sub>3</sub> melts	121
4.4	Solubility of UO <sub>2</sub> in mixed fluoride electrolytes	122
5.1	Peak potential and peak current at different sweep rate for cathodic peaks II <sub>c</sub> and III <sub>c</sub>	139
6.1	Commonly produced metals by the electrolysis of fused salts	155
6.2	Weight of individual salts used for preparation of different salt mixtures for electrolysis studies	160
6.3	Detailed comparison of different electrolytic cell designs for study of UO <sub>2</sub> reduction to uranium metal	168
6.4	List of UO <sub>2</sub> electrolytic reduction experiments conducted with different cell designs in phases	189
7.1	Materials of construction and their compatibility with liquid uranium	198
7.2	List of parametric studies conducted for plasma coating of yttria	204
7.3	Optimized yttria coating parameters by plasma spray	205
7.4.	Microhardness values of sintered blocks of yttria and yttria coated coupons	206
7.5	List of the liquid uranium corrosion study experiments conducted and observations	222

# CHAPTER I

## INTRODUCTION

---

Electrolytic reduction of uranium oxide to uranium in producing uranium metal has assumed importance because of the introduction of metallic nuclear fuels and Atomic Vapor Laser Isotope Separation (AVLIS) in the Indian nuclear fuel cycle. This chapter presents a general overview of different methods of uranium metal production and the basis for choosing electrolytic reduction of uranium oxide to uranium for producing uranium feed metal. The advantages of electrolytic reduction, existing knowledge gaps and the challenges are also outlined.

In the AVLIS method of uranium enrichment uranium atomic vapour is produced by evaporating uranium. A composite laser beam is used to excite and selectively ionize the desired uranium isotope in the atomic vapour. The ion is selectively removed by application of electromagnetic field. Uranium isotopic tailoring or enrichment is an intermediate step in the Indian nuclear fuel cycle, that increases the concentration of  $^{235}\text{U}$  in natural uranium during enrichment or reduces the concentration of  $^{232}\text{U}$  when used for cleanup of spent fuel from the thorium fuel cycle. Because of its very high separation factor in a single step AVLIS has great potential.

Thus, in addition to the use uranium metal as nuclear fuel, the requirement of uranium metal in AVLIS provide motivation to evaluate various uranium metal production processes and arrive at a suitable production technique for uranium metal.

## 1.1 Considerations for uranium feed metal production

A process with the following considerations, for the uranium feed metal preparation, can be advantageously integrated into the nuclear fuel cycle.

- a. Minimal number of steps or a single step process
- b. The least effluent and minimal radioactive waste generation
- c. Process amenable for operation in a radiochemical environment
- d. Low or nil potential for criticality hazard from the neutronic accident point of view
- e. A process capable of accepting any of following feed material directly
  - a. Oxides ( $\text{UO}_2$ ,  $\text{UO}_3$ ,  $\text{U}_3\text{O}_8$  etc.)
  - b. Partially oxidized metal
  - c. Recycled bath from polishing and stripping lines.
- f. Amenable for continuous or semi-continuous operation

Conventional method of large scale production of uranium metal is based on chemical reduction of uranium halide, usually by a metallic reductant, such as magnesium, calcium, zinc. These processes require production of  $\text{UCl}_3$  or  $\text{UF}_4$  from uranium oxide. For special requirements, high temperature reduction of uranium oxides by magnesium and carbon reductant has been employed, but in smaller batch sizes. Electrolytic reduction of  $\text{UCl}_3$  to uranium in chloride baths, or  $\text{UF}_4$  to uranium in fluoride baths have been deployed in the industrial scale. The electrolytic processes are reviewed in chapter 2 of the thesis. These processes also require an intermediate stage of production of  $\text{UCl}_3$  or  $\text{UF}_4$ .

Direct cathodic electrolytic reduction of  $\text{UO}_2$  by FFC route is in principle feasible, but will be difficult to implement due to the problems of handling the unconverted oxide feed material. Direct reduction of uranium oxide in fluoride baths with uranium deposition in molten form has the potential of dealing and easy integration to the nuclear fuel cycle using metallic fuels. The process is safer in a radioactive environment than the metallothermic reduction process. The last mentioned process is addressed in the thesis. A comparison of different uranium metal production techniques reported in the literature with the starting raw material as uranium oxide has been provided in Table 1.1.

## **1.2 Electrolytic reduction process**

The process for preparing uranium metal from uranium oxide is given in figure 1.1, a process capable of reducing uranium oxide directly to metal would offer a considerable advantage since the oxide is obtained directly from the nitrate. Pyro-electrochemical reduction of the oxide promises to be such a process, which offers the additional attraction of being amenable to continuous operation when run at temperatures higher than the melting point of uranium metal. It is considered that the pyro-electrochemical process is the most efficient way to recover uranium metal from oxides in the spent fuel. This process is capable of accepting the feed material in all forms of oxides of uranium, fluorides of uranium and partially oxidized metal. Being a single step low pressure process, it is also amenable for operation in the hot cell environment. Dry processing (non-aqueous) is especially notable because of following advantages.

- a. Single step process
- b. Compact process

Table 1.1 Comparison of different uranium metal production techniques.

S.no	Description of technique and temperature of operation	Feed material	Reducing agent	The stages involved from uranium oxide to uranium metal	Waste generated
1.	<p>Metallothermic reduction of UF<sub>4</sub> [1.1]</p> <p>923K starting, 1673K maximum</p>	UF <sub>4</sub>	Ca or Mg metal	<p>a. Reduction of other oxides of uranium to UO<sub>2</sub></p> <p>b. Hydro-fluorination of UO<sub>2</sub> to UF<sub>4</sub></p> <p>c. Charging</p> <p>d. Metallothermic reduction by Ca or Mg</p> <p>e. Waste treatment for uranium recovery</p> <p>f. Melting</p> <p>g. Casting</p> <p><u>Auxiliary processes</u></p> <ul style="list-style-type: none"> <li>• HF gas plant</li> <li>• Magnesium supply</li> </ul>	<p>0.53 kg MgF<sub>2</sub> or 0.65 kg CaF<sub>2</sub> per kg of uranium with some uranium trapped</p> <p>Secondary waste generated by uranium recovery operation</p>
2.	<p>Pyrometallurgical Mg-Zn reduction of uranium trichloride [1.2]</p> <p>1073K</p>	UCl <sub>3</sub>	Mg and Zn metal	<p>a. Chlorination of uranium oxides</p> <p>b. Feed mixture preparation</p> <p>c. Charging</p> <p>d. Reduction</p> <p>e. Distillation</p> <p>f. Melting</p> <p>g. Casting</p> <p><u>Auxiliary processes</u></p> <ul style="list-style-type: none"> <li>• HCl gas plant</li> <li>• Magnesium supply</li> </ul>	<p>MgCl<sub>2</sub> which is recycled by electrolysis to Mg metal.</p> <p>Secondary waste generated in the Mg electrolysis process</p>

S.no	Description of technique and temperature of operation	Feed material	Reducing agent	The stages involved from uranium oxide to uranium metal	Waste generated
3.	Carbothermic hydrogen reduction [1.2]  >2200K	UO <sub>3</sub>	Carbon & hydrogen	a. Feed mixture preparation b. Charging c. Reduction d. Melting e. Casting <u>Auxiliary processes</u> • Hydrogen generators	Waste generated during charge preparation and removing unconverted oxides
4.	Hydrogen plasma reduction [1.3]  >2400K	UO <sub>2</sub> , U <sub>3</sub> O <sub>8</sub>	Carbon	a. Feed preparation b. Introducing the feed into plasma c. Reduction d. Melting and casting <u>Auxiliary processes</u> • Hydrogen generators • Plasma flame reactor	Gaseous waste generated carries uranium dust, which has to be recovered, leading to secondary waste generation.
5.	Direct reduction of U <sub>3</sub> O <sub>8</sub> with magnesium and MgO recycle [1.2]  1073K	U <sub>3</sub> O <sub>8</sub>	Mg metal	a. Feed mixture preparation b. Charging c. Reduction d. Separation of MgO e. Distillation f. Melting g. Casting <u>Auxiliary processes</u> • Conversion of MgO to anhydrous MgCl <sub>2</sub> • Magnesium supply	MgO which is recycled to generate Mg metal.  Secondary waste generation by uranium recovery operations

S.no	Description of technique and temperature of operation	Feed material	Reducing agent	The stages involved from uranium oxide to uranium metal	Waste generated
6.	Electro-deoxidation of uranium oxide [1.4]  1173K	Uranium oxide pellets	Electrons	a. Preparation of pellets with optimized parameters b. Deoxidation of uranium oxide pellets c. Removing unconverted oxide d. Melting e. Casting	Waste generated during pellet preparation and removing unconverted oxides
7.	Electrolytic reduction of uranium oxide in chloride melts below melting point of uranium [1.5,1.6]  723K to 1173K	Uranium oxide in any form, partially oxidized metal, UCl <sub>3</sub> , UCl <sub>4</sub> ,	Electrons	a. Hydro-chlorination of uranium oxides to get seed UCl <sub>4</sub> /UCl <sub>3</sub> b. Feed mixture preparation with UCl <sub>4</sub> / UCl <sub>3</sub> c. Charging d. Electrolytic reduction e. Continuous/intermittent addition of uranium oxide and replenishment of UCl <sub>4</sub> / UCl <sub>3</sub> f. Cleaning of dendritic deposits to remove trapped electrolyte g. Melting h. Casting <u><b>Auxiliary processes</b></u> <ul style="list-style-type: none"> <li>• HCl generator</li> <li>• Chlorine off gas treatment plate</li> </ul>	Ideally zero waste process.  Only secondary waste generation during cleaning and melting of dendritic deposits.

S.no	Description of technique and temperature of operation	Feed material	Reducing agent	The stages involved from uranium oxide to uranium metal	Waste generated
8.	Electrolytic reduction of uranium oxide with UF <sub>4</sub> additive above melting point of uranium [1.7-1.10]  1443K to 1523K	Uranium oxide in any form, partially oxidized metal, UF <sub>3</sub> , UF <sub>4</sub> , UF <sub>6</sub> gas	Electrons	a. Hydro-fluorination of uranium oxides to get seed UF <sub>4</sub> b. Feed mixture preparation with UF <sub>4</sub> c. Charging d. Electrolytic reduction e. Continuous/intermittent addition of uranium oxide and replenishment of UF <sub>4</sub> f. Casting <u>Auxiliary processes</u> • HF synthesis	Ideally zero waste process.  Secondary waste generation during refurbishment.
9.	Electrolytic reduction of uranium oxide with LaF <sub>3</sub> additive above melting point of uranium 1473K <u>(In this work)</u>	Uranium oxide in any form, partially oxidized metal, UF <sub>3</sub> , UF <sub>4</sub> , UF <sub>6</sub> gas	Electrons	a. Charging of non uranium containing electrolyte b. Electrolytic reduction c. Continuous/intermittent addition of uranium oxide d. Casting	Ideally zero waste process.  Secondary waste generation during lifecycle refurbishment only

- c. Reduction in generation of secondary waste; electrons are replacing chemicals as reducing agents.
- d. Suitability of process for adaptation to radiochemical environment with remote handling
- e. Neutronic safety

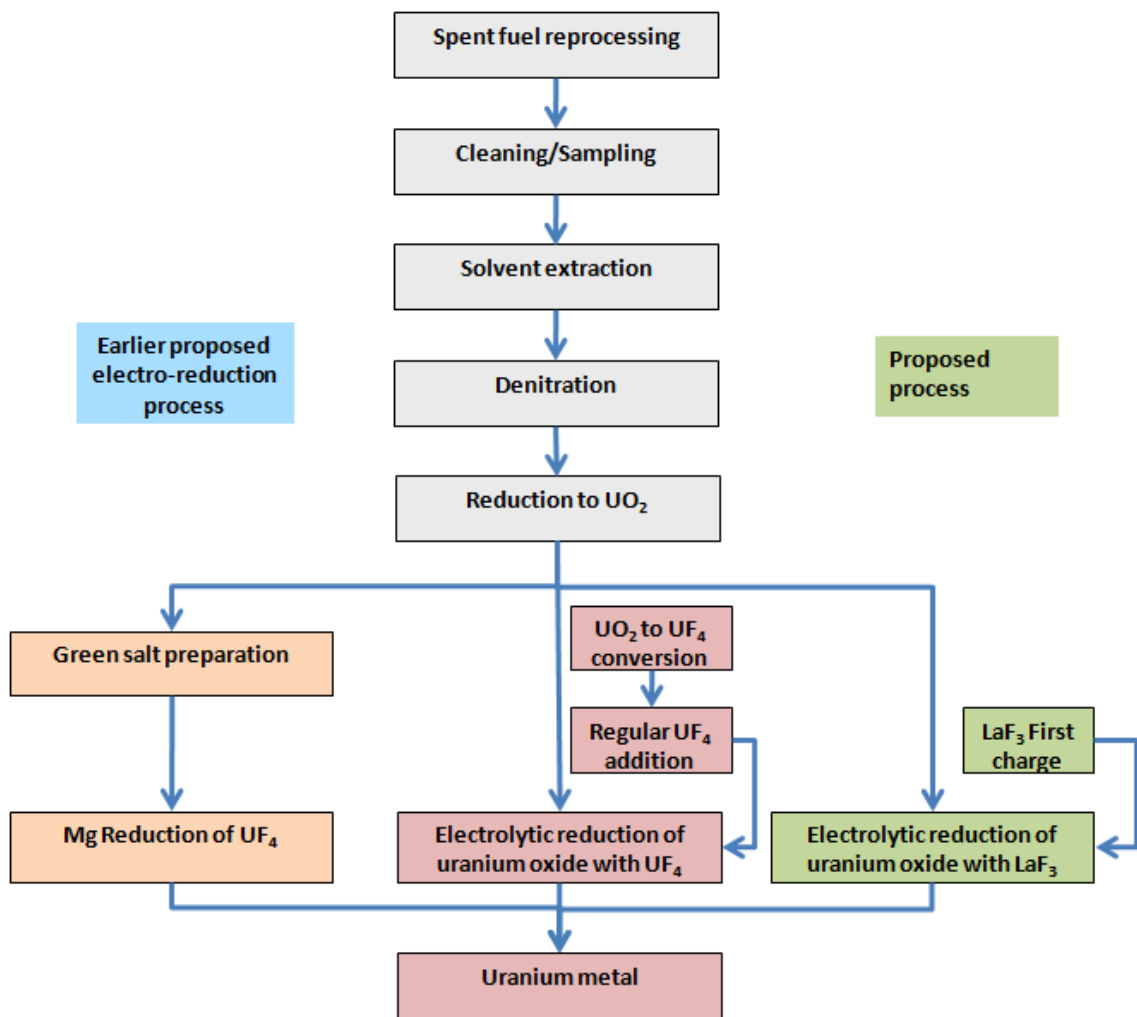


Figure 1.1. Block diagram of different routes for preparing uranium metal from oxides

The electrolytic reduction process operating above the melting point of uranium is very similar to the Hall - Heroult process of reduction of  $Al_2O_3$  to aluminum metal. The uranium oxide feed dissolves in the molten fluoride. The electrolyte is composed of

fluorides of Li, Ba, Ca etc which provides the desired electrochemical window of operation. The addition of  $\text{UF}_4$  enhances dissolution of  $\text{UO}_2$  and its decomposition to  $\text{U}^{4+}$  and  $\text{O}^{2-}$  ions. The tetravalent uranium ions migrate to the cathode, and first get converted to trivalent ion and then to uranium metal at the cathode. Solid dendrite deposits of uranium are formed in the lower temperature bath electrolytic process where the cell needs to be operated in batch mode. Liquid uranium is deposited in the cell operating above the melting point of uranium. These cells usually have fluoride electrolyte and operate in continuous mode, where liquid uranium is tapped intermittently. Oxygen ion migrates to the graphite anode and gets converted to CO and leaves the cell. Other complications in high temperature electrolytic reduction process are parasitic processes due to multi-valency of uranium, and handling of the reactant.

When this electrolytic reduction process is to be integrated with nuclear fuel cycle, which involves handling different isotopes of uranium,  $\text{UF}_4$  as the solvent poses definite problems, particularly with the uranium isotopes generated in the thorium fuel cycle. There will be a need to follow additional steps with  $\text{UF}_4$  solvent (a) Synthesis of  $\text{UF}_4$  by hydro-fluorination of uranium oxide with the isotopic composition of interest (b) periodic makeup of  $\text{UF}_4$  with the isotopic composition of the feed metal to continue the electrolysis. Both uranium and fluorine get depleted in the bath during electrolysis due to the conditions of electrolysis. These additional steps in the electrolytic reduction defeat the very advantage of being a single step process for uranium oxide conversion to metal.

Thus, an electrolytic reduction process where there is no need to add  $\text{UF}_4$  as an additive in molten salt electrolyte, can prove advantageous for the following reasons: (i) it can be

utilized for electrolytic reduction for any isotope of uranium (ii) Steps required for conversion of desired isotope of uranium oxide to  $UF_4$  by hydro-fluorination are totally avoided (iii) Periodic make of  $UF_4$  of the isotope of interest is not required as  $UF_4$  is not used as solvent (iv) possibility of achieving higher cathode current efficiency with an electrolyte with low solubility of uranium metal. In principle, the electrolyte can be fully decontaminated to remove the uranium and reduce secondary waste. It is worth noting that, reduction in the number of steps involved in the processes from spent fuel reprocessing to the uranium metal product, would result in a corresponding reduction in the man-rem consumption.

While choosing a new molten salt electrolyte may be based on the thermodynamic considerations, one has to address the various gaps in the data and knowledge, namely, their melting points, high temperature behavior, stability at operational temperature etc. Following data pertaining to the new proposed electrolyte are also to be determined for the electrolytic reduction process: (a) solubility behavior of oxides of uranium in the new electrolyte, (b) deposition potential of uranium ions (c) formation of stable phase which will prevent uranium deposition (d) selection of compatible materials for containment of the electrolyte as well as the liquid metal. Additional challenges in the electrolytic reduction process are related to the liquid product collection, tapping of liquid uranium, holding of liquid uranium for extended duration during the electrolysis and intermediate holding points before sending to fuel processing plant. These have to be designed for the high temperature of operation (1473K), the extremely corrosive nature of both the molten uranium and the molten fluoride electrolyte, and very high reactivity of molten uranium. Reported data on electrolytic reduction processes indicate that there are only a few materials other than graphite which satisfactorily withstand the

corrosive effects in contact with molten uranium and molten fluoride salts. Most ceramic materials are severely attacked by molten fluoride electrolyte and most metallic materials are attacked by liquid uranium. To demonstrate a workable electrolytic reduction process, engineering components have to be developed and tested, for handling both molten fluoride electrolytes and molten uranium. As many of the engineering components used in the electrolytic reduction process are complex in nature, due emphasis has to be given to the fabrication methods. Protective barrier coatings on the conventional metallic materials or ceramic materials may prove advantageous for fabricating engineering components. This becomes an essential requirement of the deployment of the metal production process. All the above areas need to be studied in detail for effective control and improvement in efficiency of the electrolyte reduction process. This forms the motivation of the PhD research.

It goes without saying that safety assumes utmost importance in all high temperature operations that involve handling of radioactive materials. All the experimental setups have to qualify the leak tightness requirement ( $1\text{E-}9$  mbar.l/s or better) for handling highly reactive liquid uranium and molten fluoride electrolyte at 1473K. All the experimental assemblies used have to go through formal safety audit, and safety clearance has to be obtained prior to the commencement of experiments. Detailed HAZOP analysis has to be carried out and engineered safety features have to be incorporated into the experimental assemblies to prevent any accidental release of radioactivity. These aspects have to be addressed in the Ph.D research work.

### 1.3 Objectives and scope

The objective of this research work is to develop a molten salt electrochemical process operating at 1473K by studying the performance of molten fluoride LiF-BaF<sub>2</sub> baths with a new proposed fluorine donating additive, understand the mechanism of uranium reduction in fluoride baths, investigate the feasibility of uranium metal production with new solvents such as rare earth fluoride electrolytes, with due emphasis on development of materials and components for handling liquid uranium and electrolyte at high temperature.

LiF-BaF<sub>2</sub> eutectic supporting electrolyte is chosen due to its relatively low melting point (1094K) and as it offers a wide electrochemical window for deposition of uranium metal at the cathode and evolution of CO at the anode. LaF<sub>3</sub> was chosen as the solvent for UO<sub>2</sub> among other rare earths as it is easily available and deposition potential is higher than uranium. There are no reported data on the use of LaF<sub>3</sub> containing electrolytes for uranium oxide to metal conversion, hence this work will make an original contribution.

The scope of this doctoral program is divided into the following specific areas of study:

- a) Thermo-physical characterization of electrolytes,
- b) Solubility studies of UO<sub>2</sub> in the LaF<sub>3</sub> electrolyte baths,
- c) Electrochemical studies in the LiF-BaF<sub>2</sub> electrolytes with UF<sub>4</sub> or LaF<sub>3</sub> additive,
- d) Electrolysis of UO<sub>2</sub> to U metal and
- e) Development of compatible materials for handling of electrolyte and liquid uranium.

These also involve the design and development of experimental setups, particularly taking into account the hazards associated with handling of radiotoxic materials in powder form and operations at 1473K and conducting the experiments in a safe manner with adequate precaution, and safety clearance from the regulators.

#### **1.4 Organization of the thesis**

While chapter I provides an introduction to the Ph.D research work, Chapter II presents briefly the literature survey of electrolytic reduction of uranium oxide, solubility of uranium oxides in molten fluoride salts and the thermo-chemistry of the electrolytic reduction process in molten fluoride baths. An abstract is also presented in a tabular form enumerating the salient results reported to date in the literature.

Chapter III deals with the studies conducted on the development of a preconditioning procedure, the preparation of fluoride salt mixtures, the determination of melting points of different fluoride salt mixtures and the selection of materials for the electrolytic reduction. This study forms the basis for design of all the subsequent experiments which involve salt preparation and handling.

Chapter IV provides an overview of methods of measurement of saturation solubility of uranium oxide in molten salt electrolyte and describes the solubility studies of uranium oxide in LiF-BaF<sub>2</sub> with varying amounts of solvent in the temperature range of 1423K to 1523K. The procedure adopted for measuring the solubility, results and analytical techniques are also presented.

Chapter V focuses on the determination of deposition potential of uranium ions by electrochemical studies of uranium in molten fluoride melts at the nominal temperature of 1473K. The reaction mechanism and behavior with oxide addition are also described. Based on the deposition potential, cell voltages have been chosen for the electrolysis studies.

Chapter VI presents the work on the feasibility of electrolytic reduction of uranium oxide to uranium metal in LiF-BaF<sub>2</sub>-LaF<sub>3</sub> melts at nominal temperature of 1473K, by a methodical approach of establishing the cell configuration that leads to deposition of uranium metal in reported electrolyte compositions and study the new electrolyte for deposition of uranium metal in the same cell. The effect of different forms of uranium oxide (powder, sintered pellet, UO<sub>2</sub>+C composite pellet) on the electrolytic reduction process also forms a part of the study, along with different liquid cathode materials for uranium deposition.

Chapter VII deals with the development of engineering components for various applications in the electrolytic cell. The basis for choice of refractory metals with protective coating, selection of protective coating, development of coatings, thermal stability testing and compatibility of these coated components against liquid uranium is presented.

Chapter VIII summarizes the major conclusions of the research work, the major contributions to science and some possible future work.

References directly related to the chapter are provided at the end of each chapter.

## References

- 1.1 C.D. Harrington, A.E. Ruehle, "Uranium Production Technology", 1959.
- 1.2 R. S. Hargrove, J. B. Knighton, R. S. Eby, J. H. Pashley, R. E. Norman, INTEGRATION OF THE AVLIS PROCESS INTO THE NUCLEAR FUEL CYCLE, Summer Meeting of the AIChE August 24-27, 1986, Boston, Massachusetts
- 1.3 I. N. Toumanov, Plasma and High Frequency Processes for Obtaining and Processing Materials in the Nuclear Fuel Cycle, Nova Publishers, 2003.
- 1.4 K.S. Mohandas, L. Shakila, N. Sanil, D. Sri Maha Vishnu, K. Nagarajan, Studies on the electrochemical deoxidation of uranium oxide in molten calcium chloride, in: Fray International Symposium, Cancun, Mexico, 27 November–01 December, 2011.
- 1.5 Driggs F.H., Lilliendahl W.D., "The preparation of metal powders by electrolysis of fused salts I-Ductile uranium", Ind Engg. Chemistry, Vol 22, pp 516-519, 1930.
- 1.6 M. Kolodney, "Preparation of first electrolytic plutonium and uranium from fused chlorides", Journal of Electrochemical society, vol 129, pp 2438-2442, 1982.
- 1.7 Niedarch L.W. & Dearing B.E., Jour of the Electrochemical society, Vol 105, No. 6, pp 353-358, 1958.
- 1.8 Piper R. D., "Process development quarterly progress report", Mallinckrodt Chemical Works, Rep No. MCW-1480, 1963.
- 1.9 Henrie T. A, "Electrowinning rare-earth and uranium metals from their oxides", Journal of Metals, pp 978-981, 1964.

1.10 Haas P.A, Adcock P.W, Coroneos A.C. and Hendrix D.E, *Met & Mat transactions B.*, Vol 25B, pp 505-518, 1994.

# **CHAPTER II**

## **LITERATURE REVIEW**

### **AND THERMO-CHEMISTRY OF**

### **ELECTROLYTIC REDUCTION PROCESS**

---

This chapter presents the literature survey for electrolytic reduction of uranium oxide and the thermo-chemistry of the electrolytic reduction process.

#### **2.1 Electrolytic Reduction of Uranium oxides to Uranium**

This literature survey is separated into two major sections; electrolytic reduction in chloride electrolytes and electrolytic reduction in fluoride electrolytes. Separate sections are presented for the following: Summary of the data available in literature, solubility studies in fluoride electrolytes, and the associated problems in the electrolytic reduction process.

##### **2.1.1 Electrolytic Reduction of Uranium oxides in Chloride Electrolytes**

Peligot [2.1] in 1842 made the first attempt to produce metallic uranium by reduction of uranium chloride by sodium in a porcelain crucible. A mixture of sodium, KCl and  $UCl_3$  was heated in a crucible to commence the reduction reaction. Pierle and Kahlenberg [2.2] in 1923 attempted to uranium metal production by electrolysis below 1407K in a double sodium uranium chloride electrolyte using carbon

electrodes. They obtained small uranium metallic crystals embedded in spongy mass. They found that potassium, sodium uranate, potassium uranous fluoride, mixtures of potassium nitrate and uranyl nitrate, and silver nitrate and uranyl nitrate were unsatisfactory for the production of uranium metal.

### **Studies by Driggs and Lilliendahl [2.3]**

Driggs and Lilliendahl [2.3] in 1930 reported the deposition of metallic uranium by electrolysis of a molten chloride electrolyte. NaCl-KCl base electrolyte with  $KUF_5$  and  $UCl_4$  was used to produce metallic uranium. When uranyl chloride ( $UO_2Cl_2$ ) or uranium trioxide ( $UO_3$ ) was used as the source of uranium black shining crystals of uranium dioxide ( $UO_2$ ) were deposited on a molybdenum cathode, which they described it as treelike. The cell operation temperature was 1048K with cell voltage of 5V which provided a cathode current density of  $\sim 1.5 \text{ A/cm}^2$ . Uranium deposited from  $UCl_4$  was extremely pure with only trace amounts of carbon (600 ppm), iron (500 ppm), and silicon (100 ppm) as impurities.

### **Studies by Kolodney [2.4]**

During the Manhattan project, Kolodney [2.4] electrodeposited uranium from an electrolyte with 48%  $BaCl_2$ -31%  $KCl$  -15%  $NaCl$  by weight and added  $UCl_3$  as a source of uranium. Electrolytic cells of 11mm diameter, equipped with tungsten cathodes 1mm diameter and 10 mm long were used. The anodes were 3 mm graphite rods separated from the cathodes by 3mm. The total electrolyte weight was held constant at 10g and the operating temperature at 923K. The cells were operated at a cathode current density of 1 to 4  $\text{A/cm}^2$ , with recoveries between 40 and 70%, the higher yields corresponding to higher concentrations of uranium in the electrolyte. In his study  $UCl_3$  was varied between 5 wt% to 75 Wt %. He reported that  $UCl_3$  concentration in the range of 25 to 35% provided the best results with respect to yield

and purity. The uranium metal was found in the form of small, bright crystals. He described the uranium deposit as silvery, bright, dendritic and malleable. Major impurities in the uranium deposit were carbon (100-180 ppm), oxygen (24-400 ppm), and chlorine (410 ppm).

### **Studies by Marzano and Noland [2.5]**

Marzano and Noland [2.5] examined the fundamental aspects of uranium electrodeposition from molten salts in KCl-BaCl<sub>2</sub> electrolytes. Their initial experiments were with low-purity UCl<sub>3</sub> which was added to the KCl-BaCl<sub>2</sub>. They reported large initial over potential (8 to 9 V) for deposition, which was attributed to trace level impurities of water and oxygen in the cell. As the impurities reduced after initial electrolysis, they could continue the electrolysis with 2-3 V and current efficiencies of the order of 50-60%. They analyzed the metal deposited and the impurities were found to be coming from UCl<sub>3</sub> starting material. High-purity UCl<sub>3</sub> synthesized on their own led to significant improvement in the purity of the final product. They also found LiCl-KCl eutectic could substitute for KCl-BaCl<sub>2</sub> electrolyte without compromising on the yield or the quality of the deposit. It should also be pointed out that in all their experiments, they never observed a smooth coherent deposit more than a few microns thick. As deposits grew thicker, they always became dendritic. To alter the nature of the final product, they tried rotating the cathode, periodical reversal of current, operating the electrolyte near the freezing point of the melt, addition of nucleation impurities, and imposing an alternating current field around the cathode. All the attempts failed to alter the dendritic nature of the deposit. Subsequently, Blumenthal [2.6] attempted melting of uranium deposited by Marzano and Noland. He cast ingots from washing electrodeposited uranium, which were better than 99.993% pure and were found to be free from impurities.

### **Studies by Kantan et al. [2.7]**

In 1955 Kantan et al. [2.7] reported uranium electrodeposition from molten salts from NaCl-KCl salt, which was the same base electrolyte used by Driggs and Lilliendahl [2.3]. They reported better current efficiency with  $\text{UF}_4$  rather than as  $\text{KUF}_5$  as the source of uranium. In the same year, Niedrach and Glam [2.8] reported the use of reactive nickel cathodes for electrodeposition of uranium. The deposited uranium formed a low-melting U-Ni alloy at the nickel cathode, which dripped off the cathode surface. Thus, liquid uranium alloy was collected at a cell temperature below the melting point of pure uranium.

### **Studies by Inman et al. [2.9]**

During the study of electrochemistry of uranium in the molten LiCl-KCl- $\text{UCl}_3$  electrolyte, Inman et al. [2.9] observed dendritic deposits of uranium. They suggested a three electron single step reduction of uranium ion to uranium metal in molten LiCl-KCl- $\text{UCl}_3$ , which was controlled by the diffusion rate. They observed finer and more powdery deposits with increase in cathode current density. They attributed the formation of the powdery portion of the deposit to the chemical reduction of  $\text{UCl}_3$  by metallic lithium which deposited on the electrode surface.

### **Studies by Hill et al. [2.10]**

Electrochemical studies of uranium in LiCl-KCl and  $\text{MgCl}_2$ -NaCl-KCl electrolytes were reported by Hill, Perano, and Osteryoung [2.10]. Standard potentials of uranium ions in LiCl-KCl and  $\text{MgCl}_2$ -NaCl-KCl electrolytes versus a  $\text{Pt}^{2+} / \text{Pt}$  reference electrode at 723K were compared.  $\text{U}^{4+} / \text{U}^{3+}$  standard potential in LiCl-KCl and  $\text{MgCl}_2$ -NaCl-KCl electrolyte was observed to be -1.25 V and -1.30 V respectively. They also determined the  $\text{UO}_2^{2+} / \text{UO}_2$  standard potential to be -0.285 V in the LiCl-KCl eutectic. The reduction of  $\text{U}^{4+}$  to uranium metal was found to occur in two steps,

a reversible one-electron reduction to  $U^{3+}$  followed the three-electron reduction to uranium metal. No other uranium oxidation states were observed. An extensive review article on electrorefining of uranium and plutonium is has been reported by Willet et al.[2.11].

### **2.1.2 Electrolytic Reduction of Uranium oxides in Fluoride electrolytes**

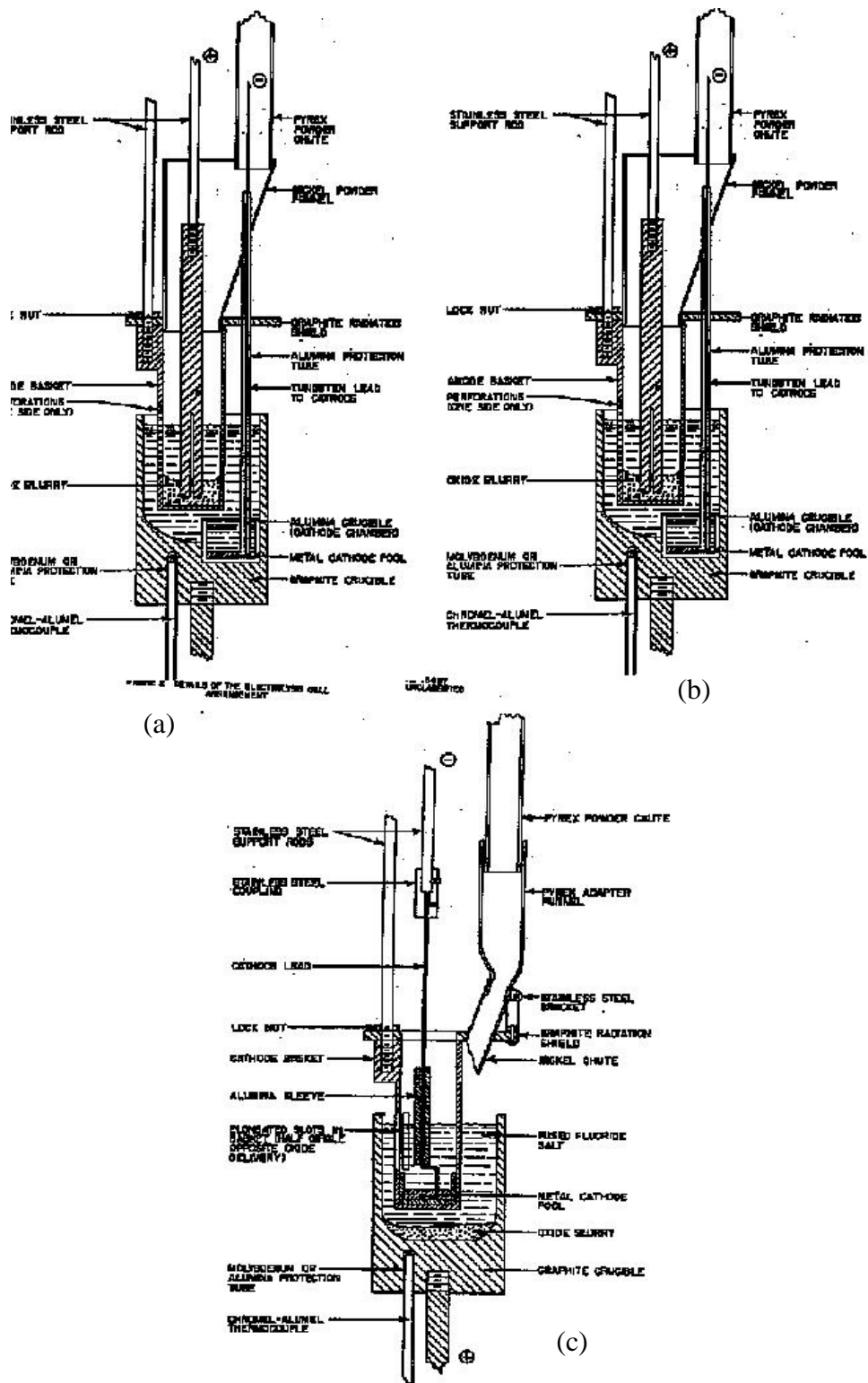
In all the work reported till this point, chloride salts have been employed to produce the uranium metal with the operating temperatures being below the melting point of uranium. The bulky, dendritic deposits formed by such processes, trap large quantities of the salt bath, and a series of steps is required before the metal can be separated from the salt and compacted. These steps are inherently labor expensive, and result in losses as well as considerable recycle of material to the electrolysis cell. However a process which would give pure uranium as the product with minimal steps would be of great advantage. This requires the cell to be operated at temperatures above the melting point of uranium with an electrolyte, which is stable at high temperatures.

#### **Studies by Knolls Atomic Power Laboratories, Niedrach et al. [2.12-2.16]**

Niedrach et.al [2.12-2.16] published several reports describing a process for the electrolytic reduction of  $UO_2$ ,  $UO_3$  and  $U_3O_8$  to uranium metal. The experimental setups they made use of are shown in figures 2.1a, 2.1b and 2.1c. The cell was operated at 1523K with a graphite anode and a liquid cathode of uranium or copper. In some of the preliminary runs oxide was fed to the cells intermittently, but in most of the work continuous-feed mechanism was used for controlled addition of uranium oxide. Due to the difficulty in severity of the operating conditions imposed by higher melting point and chemical reactivity of the uranium, they limited their studies to the effect of current, dissolved uranium in the bath and the properties of the oxide feed.

Their primary salt composition was 50:50 mole % mixture of  $\text{MgF}_2$  and  $\text{BaF}_2$  with varying quantities of  $\text{UF}_4$  ranging from 10 mole % to 40 mole %, but most of their results were for 20 mole %  $\text{UF}_4$  which was found to be the optimum. Lower concentrations of  $\text{UF}_4$  resulted in polarization effects at the anode, and higher concentrations of  $\text{UF}_4$  resulted in lower efficiencies. With the 20 mole %  $\text{UF}_4$  bath an anode current density of  $3.6 \text{ Amp/cm}^2$  was used without difficulty. Lower solubility of  $\text{UO}_2$  in the salt baths was observed as the greatest difficulty. Solubilities of the order of 2 wt% were measured in two widely different baths containing 9 and 84 wt %  $\text{UF}_4$  respectively. Coupled with low solubility, the high density of the oxide resulted in rapid settling, forming a dense sludge at the bottom of the cell, which interfered with the coagulation of the product metal. In spite of the slow addition, the oxides settled at the bottom of the cell, resulting in a mixture of uranium particles embedded in the salt and oxide matrix.

To circumvent the oxide settling problem, suspended basket anode was used or a graphite basket acting as cathode was used to collect the metal (Figure 2.1 c). Their observation was that any of the uranium oxide  $\text{UO}_2$ ,  $\text{UO}_3$  and  $\text{U}_3\text{O}_8$  could be used, and forms of oxide do not influence the efficiency. The product metal was pure with low concentrations of oxygen (4-6 ppm), barium (<200 ppm), magnesium (7-20 ppm) and hydrogen (<1ppm). A design for the conceptual cell was provided by the authors to produce metal at 1000 Kg/day [2.13, 2.16].



Figures 2.1 Different Cell designs by KAPL [2.11-2.15]

### **Studies at Bureau of Mines by T.A. Henrie et al. [2.17]**

Although the KAPL study was an excellent start for electrolytic reduction of uranium oxides to uranium above the melting point of uranium, the research and development work was almost untouched in the areas of solubility of electrolytes, current densities and different electrolytes. Almost simultaneously, work was started in Weldon Spring and at the Bureau of Mines in 1958. As part of a broad rare-earth electrowinning program, Henrie and coworkers [2.17] studied the preparation of liquid uranium, by direct electrolysis of  $\text{UO}_2$  dissolved in fluoride melts. The electrolyte composition was 35 wt%  $\text{UF}_4$ , 5 Wt %  $\text{LiF}$ , and 60 Wt %  $\text{BaF}_2$ . Several cell designs were tried to obtain better coalescence of metal produced, to have a zone of metal collection considerably above the melting point of uranium and to limit the oxide sludge material. Though good coalescence was obtained with basket anode, it did not lend itself to practical operations of extended duration. This led them to develop a compartment cell as shown in figure 2.2 with 8 inches in inside diameter with two rod-type anodes and a single cathode. This kind of set up could achieve almost complete utilization of  $\text{UO}_2$  added. The cell was operated at 15-17 Volts with current ranging from 300-400 Amps with the anode and cathode current densities being  $2.29 \text{ Amp/cm}^2$  and  $17.1 \text{ Amp/cm}^2$  respectively. The oxide was fed continuously at a rate of 5 g/min. The authors were able to produce uranium metal weighing 2200 g with current efficiency of 38%. The metal obtained was 99.8% pure with major impurities being Carbon (~700 ppm), Aluminum (~300 ppm) and Iron (~200 ppm). Low current efficiency and poor coalescence have been reported as the major problems of electrowinning of uranium. The authors attributed the poor efficiency to poor coalescence. Fine nodules formed had much higher surface area and reacted more rapidly with the electrolyte constituents, which resulted in the redissolution of metal. Oxidation of anode rods during electrolysis, with the resultant decrease in

surface area, caused a gradual increase in anode current density upto the limit imposed by the anode effect. They did not conduct any solubility studies.

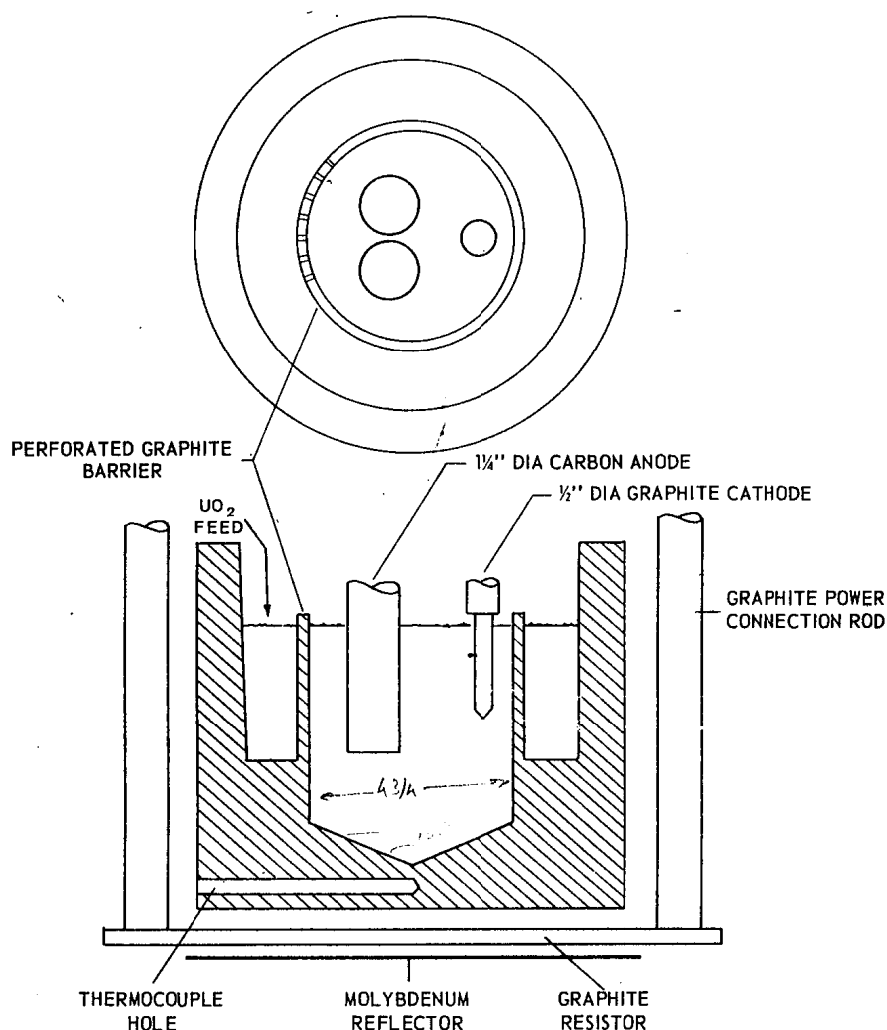


**Figure 2.2** Conceptual compartmental cell design for reduction of uranium oxides [2.17]

**Studies at Mallinckrodt Chemical Works by Piper et.al [2.18-2.25]**

At Mallinckrodt chemical works, Piper et al. [2.18-2.25] reported investigations on the electrolytic production of uranium metal from uranium oxides. Adopting an electrolytic process similar to the Hall process for the production of aluminum, they recovered nearly 100% of the uranium metal from different uranium oxides. To avoid oxide contamination in the product metal, they fabricated  $\text{UO}_2$ -carbon consumable anode

pellets by mixing  $\text{UO}_2$  powders and coal tar pitch, and carbonized the tar by heating. On the basis of experiments the authors have suggested that, the  $\text{UO}_2$ -carbon anodes should contain close to the stoichiometric 8.2% carbon for optimum performance. Two cell arrangements, differing in the type of anode used, were used for most of their work. The basket anode cell, shown in figure 2.3 essentially consisted of a perforated cylindrical graphite crucible containing crushed lumps of  $\text{UO}_2$ -carbon mixture, which served as the anode and another graphite crucible for containment of molten salt and molten metal acted as the cathode.

The second type of cell, the “bare anode” cell, was essentially similar to basket anode arrangement, except that in place of a basket, a block of  $\text{UO}_2$ -carbon mixture served as the anode. The anode pellet or basket was placed in the molten salt (65%  $\text{BaF}_2$ -10%  $\text{LiF}$ -25%  $\text{UF}_4$  by weight), and the cell that kept hot at 1423K. The graphite cell crucible served as the cathode. The highest cell current used was 300 Amp corresponding to 1.2  $\text{Amp/cm}^2$  cathode current density. The cell operation at 300 Amp and 1423K resulted in a collection rate of 0.21 kg/h of liquid uranium metal with a current efficiency of 35%. All the uranium in the feed was transferred to the product.

The authors conducted experiments with other cell designs also, more specifically with different variations of the anode; perforated plate anode, slotted anode, neutral basket, rod-type anode, vertical plate anode, tapered anode and anode basket were used. Electrolyte with  $\text{BaF}_2$ - $\text{LiF}$  (1:1) molar ratio with 15 Wt %  $\text{UF}_4$ , operating at 0.5  $\text{Amp/cm}^2$  with the perforated graphite anode and at 1443K gave the highest cathode current efficiency of 44%. During this experiment, there was intermittent addition of  $\text{UO}_2$ - $\text{UF}_4$ . Apart from the above, in the very extensive work carried out by the

investigators at the Mallinckrodt Chemical Works [17-23], they studied the effect of other variables that included electrolyte composition, frozen crust, current density, composition of  $\text{UO}_2$ -Carbon pellet and anode geometry.

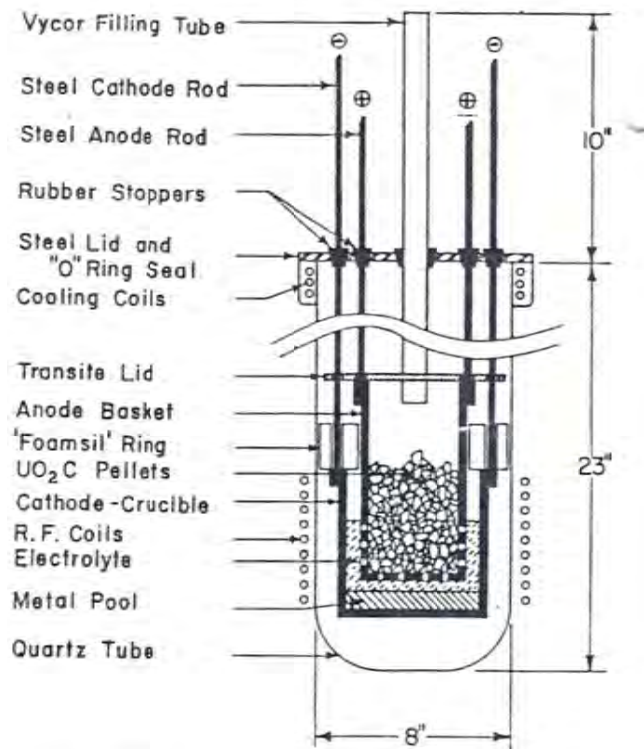


Figure 3. Basket anode-container cathode cell

**Figure 2.3** Cell with basket anode used by Piper [2.23]

After conducting more than 500 experiments in the laboratory, a pilot plant [2.23] was designed for continuous operation, operated at 10000 Amp and 3 V which produced more than 22.7 tons of uranium metal. The  $\text{UF}_4$  content in the electrolyte varied between 9-16%, and the cathode current efficiencies varied between 25-70%. In all the pilot plant runs, although it was targeted to produce low impurity metal, but high aluminum content was observed, which was attributed to be coming from the lid of the furnace.

It was hypothesized that the cyclic reaction mechanism accounted for the relatively low current efficiency obtained in the laboratory cells. To get optimum efficiency it has been

suggested that the supply of uranium ions should be larger than the supply of electrons. In some cases when the cell was operated for more than eight hours, the formation of carbon scum (called 'crud') was reported. Crud is essentially a mixture of carbon with trapped electrolyte and small amounts of uranium oxide, uranium metal and uranium carbide. This crud resulted in loss of current efficiency.

### **Studies at Oak Ridge National Laboratories by Haas and coworkers [2.26-2.27]**

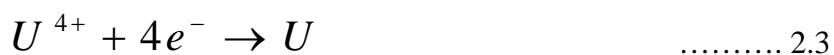
There was no significant addition to the research results for almost 25 years, till in the year 1993, Haas et al.[ 2.26-2.27] at the Oak Ridge National Laboratories verified the work that was reported by conducting the experiments already reported by others [2.18-2.25] with more data in the areas of optimization of current efficiencies, current densities, bath composition, composition, generation of cell gases and solubility of feed materials. The design of the apparatus used by the authors was closest to that of Piper [2.18-2.25]. Most of the work was done in a cell with frozen crust. The thermal gradients required to get a frozen side ledge was controlled by induction heating of the base. The electrolytic cell was fed for ~12-15 hours at typical feed rates of 3-8 g of the  $\text{UO}_2\text{-UF}_4$  mixture per minute. Many variations of the electrolytic cells were also tried, namely, different liquid electrolytes, frozen crust approach, boron nitride insulating sleeve and liner. The anodes used were either perforated anode, slab anode, plate anode or composite anode. Few runs were also reported with top-entry carbon cathode. The feeding was either continuous or intermittent, and varied from  $\text{UF}_4$  alone and  $\text{UO}_2$  feed only. Their results showed cathode current efficiency of 42%, which is the best achieved by them with a graphite plate anode and frozen side ledge operation. The uranium feed was intermittent and the cell was operated just above the melting point of uranium at 1423K and produced 1.6 kg of metal. But the experiments with the composite anodes showed behavior which were contrary to the composite anode results reported by MCW

with a cathode current efficiency of 44%. This work concluded that the three important factors are, (a) high availability of dissolved  $\text{UO}_2$  at anode (b) high anode current density nearest to maximum as possible without anode effect (c) coalescence of the liquid uranium metal. A specific combination of these factors gives good production of coalesced uranium. The authors also did solubility studies which are reviewed in the section of this chapter on the solubility of uranium oxides in the electrolyte.

#### **Studies by Takeshi Shimada and coworkers [2.28, 2.29]**

Takeshi Shimada et.al. [2.28, 2.29] had carried out research work for the development of new reprocessing technique/process for direct electrolysis of oxide in the spent fuel for the integral fast reactor. Their experiments were primarily with two different compositions of salts and both with 25 Wt%  $\text{UF}_4$ . The diluent salts used were  $\text{LiF-BaF}_2$  and  $\text{CaF}_2\text{-BaF}_2$ . Unlike the experiments that were reported with the graphite crucible made as cathode, they made the graphite crucible as the anode with oxide added at the bottom, which has high surface area and Tantalum rod as the cathode with a boron nitride crucible acting as an electrically isolated reservoir for liquid uranium metal below the tantalum rod.  $\text{CaF}_2\text{-BaF}_2$  salt resulted in better cathode current efficiency and purity than  $\text{LiF-BaF}_2$  electrolyte in their experiments. When compared to the cathode current efficiencies that had been reported, their values indicate very low value of 5% maximum. The low current efficiency was attributed to the redissolution of uranium metal; the authors confirmed the redissolution of the uranium metal formed in the fluoride salt by the XPS studies, by determining the valence of uranium in different parts of the solidified salt. The current density-potential curves for the electrolysis of uranium oxide in a molten fluoride mixture containing  $\text{BaF}_2\text{-CaF}_2\text{-LiF-UF}_4$ , at 1473K and 1523K were investigated to determine the electrochemical reaction during electrolysis of

uranium oxide in the molten fluoride bath. Three kinds of reactions were found to occur at the cathode at different potentials.



The reduction of  $U^{3+}$  to U was found to be relatively fast from the analysis of the current density vs potential curves, and from XPS analysis of uranium species present in the solidified salts. The sequence of the cathodic reactions of uranium ions is Eq. 2.1, Eq 2.2 and Eq. 2.3. They could not measure the standard electrode potential of the reactions.

## 2.2 Summary of the literature reviewed

The literature reviewed on direct electrolytic reduction of uranium oxide in molten fluoride electrolyte above the melting point of uranium has been summarized in terms of main variables of the process in Table 2.1 for ready reference. The cells have been operated at a nominal temperature of 1433K or 1473K. The basic fluoride salt used so far are LiF-BaF<sub>2</sub>, LiF-CaF<sub>2</sub>. In all the baths UF<sub>4</sub> has been used as an additive for dissolution of uranium oxide. The anode and cathode configurations have been varied, depending on the design adopted by various workers (a) to prevent contamination of liquid metal by uranium oxide powder, (b) allowing coalescence of liquid metal at the cathode and (c) minimizing the re-dissolution of uranium metal. The widest range of response variable is seen in the cathode current efficiency, 1.5% to 44%. Thus, there is a scope in investigating the contributions of various phenomena in the electrolysis to the cathode current efficiency.

Table 2.1 Brief details of the reported fluoride electrolytes used, operating temperature and efficiencies reported for uranium metal production

S.no	Electrolyte	Uranium feed	Cathode	Anode	Operating temperature	Cathode current efficiency, %	Reference
1.	65% BaF <sub>2</sub> , 10% LiF <sub>2</sub> 25% UF <sub>4</sub> (Wt %)	UO <sub>2</sub>	Tantalum in BN crucible	Graphite crucible	1473K	1.5	Takeshi Shimda et al. 1994
2.	45.5% BaF <sub>2</sub> , 10% LiF <sub>2</sub> 19.5 %CaF <sub>2</sub> , 25% UF <sub>4</sub> (Wt %)	UO <sub>2</sub>	Tantalum in BN crucible	Graphite crucible	1473K	5	Takeshi Shimda et al. 1994
3.	CaF <sub>2</sub> – LiF (7:1) Weight ratio	UO <sub>2</sub> and UF <sub>4</sub> continuous feeding	Graphite crucible with BN sieve	Graphite plate	1473K	32	Haas et al. 1994
4.	CaF <sub>2</sub> – LiF (7:1) base electrolyte with UF <sub>4</sub>	UO <sub>2</sub> and UF <sub>4</sub> intermittent feeding	Graphite crucible with BN liner	Graphite plate	1473K	42	Haas et al. 1994
5.	CaF <sub>2</sub> – LiF (1:1) base electrolyte with UF <sub>4</sub>	UO <sub>2</sub> and UF <sub>4</sub>	Graphite crucible with frozen side ledge	Graphite plate	1473K	28	Haas et al. 1994
6.	CaF <sub>2</sub> – LiF (1:1) base electrolyte with UF <sub>4</sub>	UO <sub>2</sub> and UF <sub>4</sub>	Graphite crucible	Graphite plate	1473K	27	Haas et al. 1994
7.	CaF <sub>2</sub> – LiF (4.1:1) base electrolyte with UF <sub>4</sub>	UO <sub>2</sub> and UF <sub>4</sub>	Graphite crucible	Graphite plate	1473K	24	Haas et al. 1994
8.	CaF <sub>2</sub> – LiF (4.7:1) base electrolyte with UF <sub>4</sub>	UO <sub>2</sub> and UF <sub>4</sub>	Graphite crucible	Graphite plate	1473K	11	Haas et al. 1994

S.no	Electrolyte	Uranium feed	Cathode	Anode	Operating temperature	Cathode current efficiency, %	Reference
9.	CaF <sub>2</sub> – LiF (7:1) base electrolyte with UF <sub>4</sub>	UO <sub>2</sub> and UF <sub>4</sub>	Graphite crucible	Graphite slab anode with annulus feed	1473K	19	Haas et al. 1994
10.	CaF <sub>2</sub> – LiF (7:1) base electrolyte with UF <sub>4</sub>	UO <sub>2</sub> and UF <sub>4</sub>	Iron plate cathode	Graphite Plate anode	<1473K	35	Haas et al. 1994
11.	CaF <sub>2</sub> – LiF (1:1) base electrolyte with UF <sub>4</sub>	UO <sub>2</sub> and UF <sub>4</sub>	Top entry carbon cathode	Graphite crucible	1473K	5	Haas et al. 1994
12.	CaF <sub>2</sub> – LiF (7:1) base electrolyte with UF <sub>4</sub>	UO <sub>2</sub> and UF <sub>4</sub>	Graphite crucible	Composite UO <sub>2</sub> -C Anode	1473K	No deposition	Haas et al. 1994
13.	CaF <sub>2</sub> – LiF (7:1) base electrolyte with UF <sub>4</sub>	UO <sub>2</sub> and UF <sub>4</sub>	Graphite crucible	Composite UO <sub>2</sub> -C Anode	1473K	No deposition	Haas et al. 1994
14.	CaF <sub>2</sub> – LiF (7:1) Cryolite bath without UF <sub>4</sub>	UO <sub>2</sub> and UF <sub>4</sub>	Graphite crucible	Graphite Plate anode	1473K	No deposition	Haas et al. 1994
15.	BaF <sub>2</sub> -LiF (1:1) base electrolyte with UF <sub>4</sub>	UO <sub>2</sub> and UF <sub>4</sub>	Graphite crucible without frozen side ledge	Graphite Plate anode	1473K	22	Haas et al. 1994
16.	BaF <sub>2</sub> -LiF (1:1) base electrolyte with UF <sub>4</sub>	UO <sub>2</sub> and UF <sub>4</sub>	Graphite crucible without frozen side ledge	Graphite slab anode	1473K	7	Haas et al. 1994

S.no	Electrolyte	Uranium feed	Cathode	Anode	Operating temperature	Cathode current efficiency, %	Reference
17.	BaF <sub>2</sub> -LiF (1:1) base electrolyte with UF <sub>4</sub>	UO <sub>2</sub> and UF <sub>4</sub> low rate of feed	Graphite crucible without frozen side ledge	Graphite slab anode	1473K	23	Haas et al. 1994
18.	BaF <sub>2</sub> -LiF (1:1) base electrolyte with UF <sub>4</sub>	UO <sub>2</sub> and UF <sub>4</sub> medium rate of Intermittent feed	Graphite crucible without frozen side ledge	Graphite slab anode	1473K	3	Haas et al. 1994
19.	BaF <sub>2</sub> -LiF (1:1) base electrolyte with UF <sub>4</sub>	UF <sub>4</sub> only Intermittent feed	Graphite crucible without frozen side ledge	Graphite slab anode	1473K	No deposition	Haas et al. 1994
20.	74% BaF <sub>2</sub> , 11% LiF, 15 % UF <sub>4</sub> (Wt %)	UO <sub>2</sub>	Graphite crucible 10" ID	8" diameter, 1" thick Plate graphite	1443K	Not specified	Piper R. D, 1966
21.	83% BaF <sub>2</sub> , 12% LiF, 15 % UF <sub>4</sub> (Wt %)	UO <sub>2</sub>	Graphite crucible 10.7" ID	8" diameter, 1" thick Plate graphite	1423K	Not specified	Piper R. D, 1966
22.	BaF <sub>2</sub> -LiF (1:1) Molar Ratio, 25 wt % UF <sub>4</sub>	UO <sub>2</sub>	Graphite crucible 4.25" ID	Graphite basket	1443K	11	Piper R. D, 1966
23.	BaF <sub>2</sub> -LiF (1:1) Molar Ratio, 14 wt % UF <sub>4</sub>	UO <sub>2</sub>	Graphite crucible 4.25" ID	Graphite neutral basket and cylindrical anode	1443K	14	Piper R. D, 1966
24.	BaF <sub>2</sub> -LiF (1:1) Molar Ratio, 30 wt % UF <sub>4</sub>	UO <sub>2</sub>	Graphite crucible 4.25" ID	3" diameter graphite rod	1443K	11	Piper R. D, 1966
25.	BaF <sub>2</sub> -LiF (1:1) Molar Ratio, 25 wt % UF <sub>4</sub>	UO <sub>2</sub>	Graphite crucible 7" ID	Taped graphite rod	1443K	33	Piper R. D, 1966
26.	BaF <sub>2</sub> -LiF (1:1) Molar Ratio, 15 wt % UF <sub>4</sub>	UO <sub>2</sub>	Graphite crucible 10" ID	Perforated plate graphite anode	1443K	44	Piper R. D, 1966

S.no	Electrolyte	Uranium feed	Cathode	Anode	Operating temperature	Cathode current efficiency, %	Reference
27.	BaF <sub>2</sub> -LiF (1:1) Molar Ratio, 21 wt % UF <sub>4</sub>	UO <sub>2</sub>	Graphite crucible 10" ID	Perforated plate graphite anode	1443K	30	Piper R. D, 1966
28.	BaF <sub>2</sub> -LiF (1:1) Molar Ratio, 16 wt % UF <sub>4</sub>	UO <sub>2</sub>	Graphite crucible 10" ID	Perforated plate graphite anode	1443K	44	Piper R. D, 1966
29.	65% BaF <sub>2</sub> , 10% MgF <sub>2</sub> 25% UF <sub>4</sub>	UO <sub>2</sub> +C	Graphite crucible	UO <sub>2</sub> + C pellet in a Basket	1443	39	Piper R. D, 1966
30.	46% BaF <sub>2</sub> , 44% MgF <sub>2</sub> 30% UF <sub>4</sub> (Mol %)	UO <sub>2</sub> feed	Graphite crucible	Graphite 1 in diameter Cylindrical Rod	1523K	Not specified	Niedarch et al. 1957
31.	46% BaF <sub>2</sub> , 44% MgF <sub>2</sub> 40% UF <sub>4</sub> (Mol %)	UO <sub>2</sub> feed	Graphite crucible	Graphite 1 in diameter Cylindrical Rod	1473K	Not specified	Niedarch et al. 1957
32.	10% LiF, 70% BaF <sub>2</sub> 20% UF <sub>4</sub> (wt %)	Micronised UO <sub>2</sub>	Alumina lined Graphite	Graphite 1 in diameter Cylindrical Rod	1523K	Not specified	Niedarch et al. 1957
33.	20% MgF <sub>2</sub> , 60% BaF <sub>2</sub> 20% UF <sub>4</sub> (wt %)	Micronised UO <sub>3</sub>	Alumina lined Graphite	Graphite 1 in diameter Cylindrical Rod	1473K	Not specified	Niedarch et al. 1957
34.	41% BaF <sub>2</sub> , 39% MgF <sub>2</sub> 20% UF <sub>4</sub> (Mol %)	UO <sub>3</sub> from Ammonium Uranite	Alumina lined Graphite	Graphite 1 in diameter Cylindrical Rod	1523K	Not specified	Niedarch et al. 1957
35.	41% BaF <sub>2</sub> , 39% MgF <sub>2</sub> 20% UF <sub>4</sub> (Mol %)	UO <sub>3</sub> from UO <sub>4</sub>	Alumina lined Graphite	Graphite 1 in diameter Cylindrical Rod	1473K	Not specified	Niedarch et al. 1957

### 2.3 UO<sub>2</sub> Solubility studies

In the electrolytic production of uranium by electrolytic reduction of its oxide, the first step in the cell reaction is evidently the dissolution of UO<sub>2</sub> in the molten fluoride bath. This dissolution step gives a uranium fluoride complex ion and two oxygen ions. The oxide ions then migrate to the graphite anode and combine with carbon to form CO. The uranium fluoride complex ion migrates to the cathode where the uranium ion is reduced to metal. The diffusive flux of uranium ion becomes the rate controlling step in the entire process when the concentration of uranium is low, resulting from slow dissolution of the oxide in molten electrolyte. Therefore the UO<sub>2</sub> solubility values and dissolution rates in the molten fluoride electrolytes are important to understand the electrolytic cell behavior. A study of the parameters affecting the solubility and kinetics of dissolution will help in increasing the solubility and also in optimizing the cell performance.

L.W. Niedrach and B.E. Dearing [2.12-2.16] reported that the solubility of UO<sub>2</sub> in the electrolyte with high and low concentrations of UF<sub>4</sub> vary only slightly. The solubility of UO<sub>2</sub> was measured by them at 1473K. The melts were sampled from upper portion of the molten mixture well separated from the oxide sludge in the bottom of the container. One electrolyte of LiF-BaF<sub>2</sub> with low concentration of, namely LiF-BaF<sub>2</sub>-9wt % UF<sub>4</sub>, and another with high concentration of UF<sub>4</sub> namely LiF-BaF<sub>2</sub>-82 Wt % UF<sub>4</sub> showed approximately the same uranium oxide solubilities, of about 2 Wt %. Oxygen analysis was performed by treatment with BrF<sub>3</sub>+KBrF<sub>3</sub> and measurement of oxygen released manometrically. The results of oxide solubility studies are also reported by a Bureau of Mines Study [2.30]. They used the stick sampling technique in which the equilibrated salt-UO<sub>2</sub> mixture was sampled by drawing the molten salt through a porous graphite disc, to remove any suspended UO<sub>2</sub> particles. The sample was analyzed by the inert gas

atmosphere fusion method. All the experiments were done at 1523K with three salt composition in weight % (i) 55% UF<sub>4</sub>-40% BaF<sub>2</sub>-5% SrF<sub>2</sub> (ii) 40% UF<sub>4</sub>-45% BaF<sub>2</sub>-15% CaF<sub>2</sub>, and (iii) 40% UF<sub>4</sub>-57% BaF<sub>2</sub>-5% LiF, which showed UO<sub>2</sub> solubility of 4 %, 3.0 % and 3.0% respectively.

### **Solubility studies by Varwig J.W [2.25]**

In 1964, Varwig J. W [2.25] at the MCW investigated the solubility of uranium oxides in the molten salt containing various diluent salt mixtures with different mole ratios. The first attempts of UO<sub>2</sub> dissolution were made in a number of non-uranium containing salts. Na<sub>3</sub>AlF<sub>6</sub> showed the highest solubility of UO<sub>2</sub> ~10 Wt % and NaF and MgF-CaF<sub>2</sub> eutectic showed <1% solubility. They did not continue with cryolite as an electrolyte constituent as aluminum would co-deposit with uranium. Analysis of the sample for oxygen in UO<sub>2</sub> was carried out by vacuum fusion. The salt pellet was dropped into a crucible at ~1900°C. The salt vaporized and the oxygen in the salt reacted with the graphite crucible to give carbon monoxide and CO<sub>2</sub>. A mass spectrometer head was incorporated in the equipment to accurately measure the quantities of these two gases formed.

Varwig et al. reported a series of equilibrations at 1423K by using LiF-BaF<sub>2</sub> in a 1:1 mole ratio base salt and with various percentages of UF<sub>4</sub>. The ratio of LiF-BaF<sub>2</sub> was found to have no effect on the solubility values with the same UF<sub>4</sub> content. Though extensive work has been reported, only some important conclusions of their work are reviewed here. The UO<sub>2</sub> solubility is a function of UF<sub>4</sub> content, varying from 0.1 Wt% of UO<sub>2</sub> at 0% UF<sub>4</sub> to ~2.3 Wt % UO<sub>2</sub> at 45 Wt % UF<sub>4</sub>. No difference was observed on the solubility values with either micronized UO<sub>2</sub> or fluidized bed reduced UO<sub>2</sub>. The diluent salt mixtures LiF: BaF<sub>2</sub>, MgF<sub>2</sub>:BaF<sub>2</sub>, LiF-YF<sub>3</sub>, and LiF:BaF+ 9Wt % ThF<sub>4</sub> gave

similar  $\text{UO}_2$  solubilities for similar quantities of  $\text{UF}_4$ . The diluent salt  $\text{LiF}:\text{SrF}_2$  gave a lower solubility and  $\text{LiF}:\text{CeF}_3$  exhibited a higher solubility. The results of their investigations are shown in the figure 2.4.

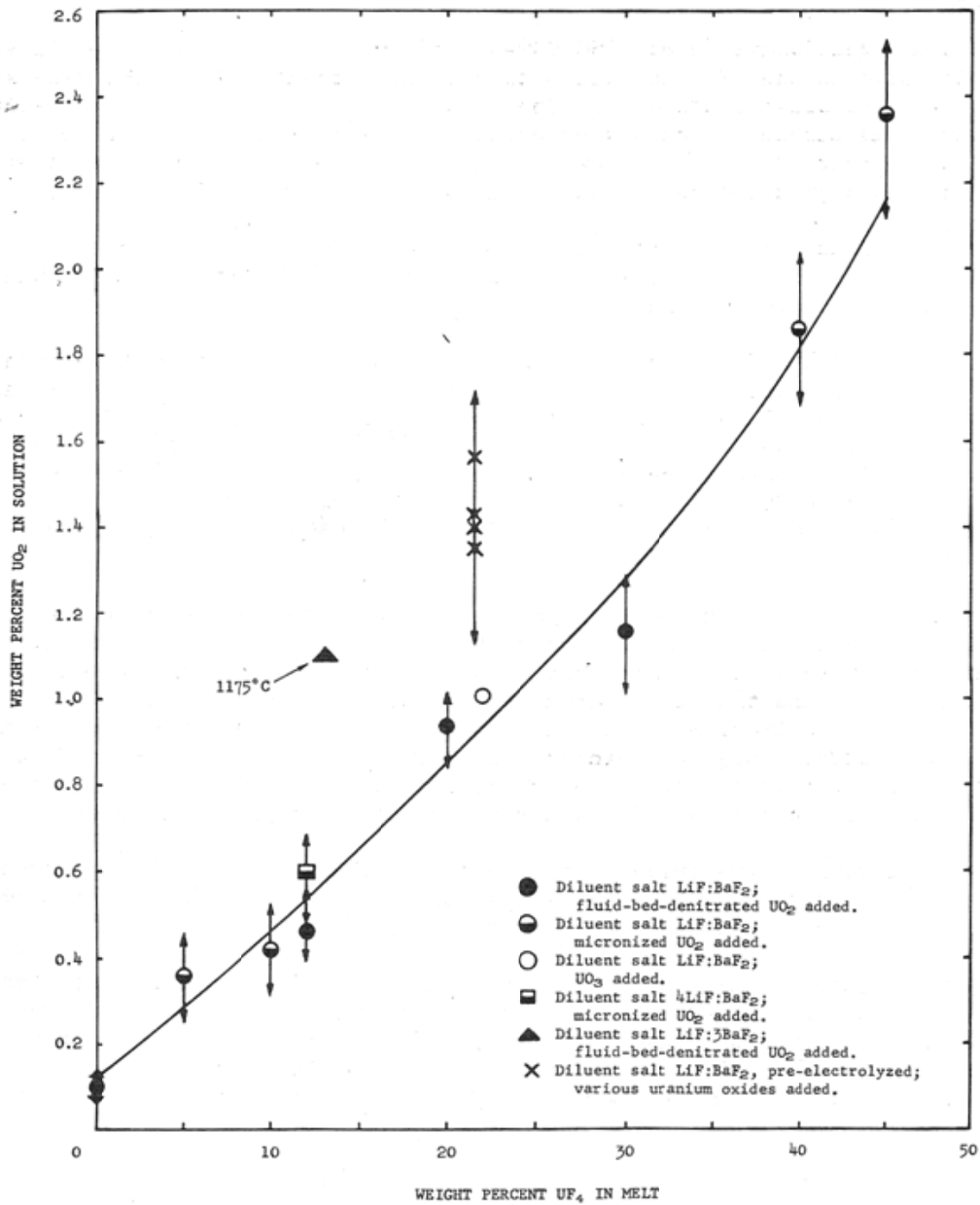


Figure 2.4.  $\text{UO}_2$  Solubility at 1423K in  $\text{LiF}-\text{BaF}_2$  by Varwig [2.25]

### Solubility studies by Greenfield B.F and Hyde K.R [2.31]

Some preliminary work on  $\text{UO}_2$  solubility was reported to have been done earlier by Greenfield B.F and K. R. Hyde [2.31] which was later published in 1983. Their investigation involved the determination of equilibrium solubility and the rate of solubility of  $\text{UO}_2$  in various binary and ternary melts containing  $\text{UF}_4$ . The solubility of  $\text{UO}_2$  was determined by inert gas fusion technique, namely, by analyzing the amount of oxygen present in the salt. The solubility of  $\text{UO}_2$  in two binary mixtures  $\text{LiF}+\text{UF}_4$  and  $\text{BaF}_2+\text{UF}_4$  over the range of compositions reported are shown in figures 2.5 and 2.6 where increase in both temperature and  $\text{UF}_4$  concentration in binary mixture contribute to higher solubility. Contrary to the observations by Varwig [2.25], the authors found that the solubility is related to both the charge and the radius of the cation of the diluent fluoride; the smaller the cation and the greater its charge, the more is the solubility of  $\text{UO}_2$  in  $\text{UF}_4$  with the same amount of  $\text{UF}_4$ . This was true in both binary and ternary mixtures for a given mole fraction of  $\text{UF}_4$ . They also reported that the solidified melts showed no solid solubility of  $\text{UO}_2$  in the fluorides.

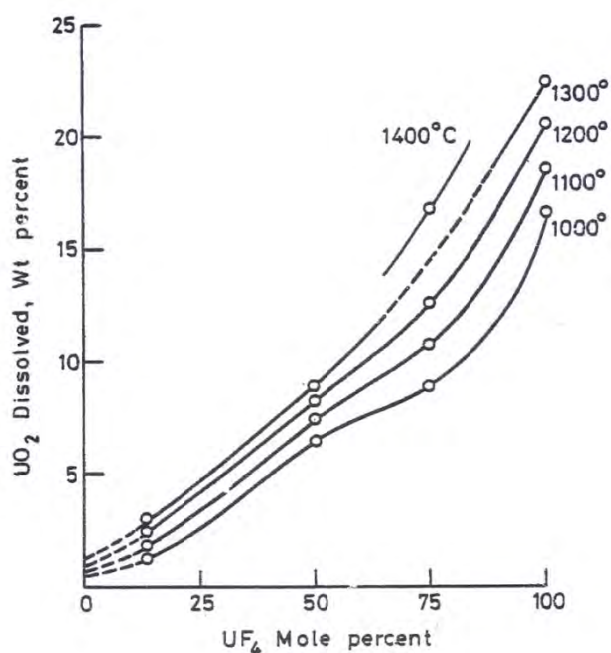


Figure 2.5 Solubility of  $\text{UO}_2$  in  $\text{LiF}/\text{UF}_4$  melts by Greenfield and Hyde [2.31]

The measurements of the rate of solubility in a few ternary melts indicated that the rates were higher in the melts with the highest equilibrium solubility. The melt of 66 mol% BaF<sub>2</sub> – 14 mol% LiF and 20 mole % UF<sub>4</sub> was saturated with UO<sub>2</sub> in less than 2 minutes at 1473K in comparison with other melts. There was an oxygen surge observed by Varwig [2.25] immediately (30 sec) after the addition of UO<sub>2</sub> to the melt. The same effect was also observed by Greenhyde [2.31] who explained that this could be resulting from the rapid dissolution of all the finer particles to produce a super-saturated solution, but was probably more due to passage of fine undissolved particles of UO<sub>2</sub> through the filter before they would settle down.

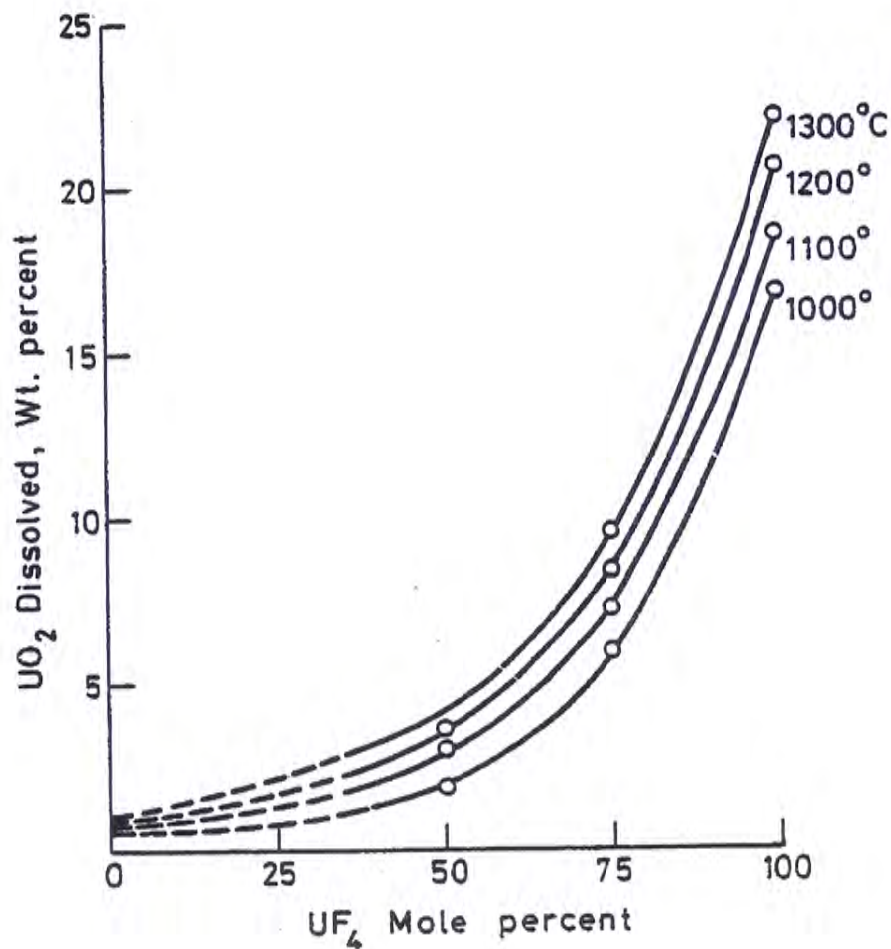


Figure 2.6 Solubility of UO<sub>2</sub> in BaF<sub>2</sub>/UF<sub>4</sub> melts by Greenfield and Hyde [2.31]

### **Solubility studies by Haas and coworkers [2.27]**

Again for more than 20 years there were no reports on the solubility studies until Haas [2.27] at Oak Ridge National laboratories reported the results by verifying the ones that were already reported in the literature and supplementing them with some more experimental investigations. His investigations included equilibrating the fluoride salt with excess of  $\text{UO}_2$  for 1 hour at 1473K and taking a sample by a hot filtering technique using a porous graphite filter, and analyzing the salt for total uranium. This is different from the work of the other groups where the dissolved oxygen in the melt was used as a measure of  $\text{UO}_2$  solubility. The powder used was with a nominal size of  $3\mu\text{m}$  and a surface area of  $7\text{ m}^2/\text{g}$ . The major experimental variables included the composition of the bath before addition of  $\text{UF}_4$ , amount of  $\text{UF}_4$ , temperature and the characteristics of  $\text{UO}_2$  added in the fluoride melts. The chemical composition and the physical form of the uranium oxide were found to have no effect on the solubility values. All other forms of oxide added to melt converted to  $\text{UO}_2$  in the molten bath.  $\text{UO}_2$  of finer particle size was found to rapidly recrystallize to a coarser and denser form of  $\text{UO}_2$ . Solubility of  $\text{UO}_2$  in the absence of  $\text{UF}_4$  was reported to be only 0.0003 mol fraction and increased linearly with the increase of  $\text{UF}_4$  upto 0.5 mole fraction of  $\text{UF}_4$  [2.26]. Thereafter, the solubility value rose above the linear curve. MCW had reported an increase in the solubility of  $\text{UO}_2$  with a decrease in  $\text{UF}_4$ , however, this trend was not observed in these investigations. This was attributed to the 0.3 mass % of  $\text{O}_2$ , which was present as an impurity in the melts investigated by MCW.

The effect of  $\text{LiF}:\text{CaF}_2$  ratios on the solubility were small or insignificant, which agrees with the result reported by Varwig [2.25]. The values reported by the authors were higher than those reported in the literature for  $\text{BaF}_2+\text{LiF}$  mixtures. Haas et al [2.27] had

mentioned qualitative result of higher solubilities of  $\text{UO}_2$  in  $\text{ThF}_4$  and  $\text{LaF}_3$  than in  $\text{UF}_4$ ; however, no data was reported by them.

#### 2.4 Thermo-chemistry of the electrolytic reduction process

The thermochemistry of uranium in molten salt baths containing fluorides and oxides is quite involved as uranium ions are multivalent and tend to form complexes. The electrolyte is a single liquid phase at 1473K. At the anode gaseous  $\text{CO}$  and  $\text{CF}_4$ , solid  $\text{UO}_2$  which is not dissolved and graphite anode are present as separate phases and at the cathode liquid uranium metal or alloy and graphite cathode are present as separate phases. The electrolytic cell essentially consists of a graphite container acting as the cathode and contains the electrolyte and molten metal product formed. Graphite blocks are used as anodes and  $\text{UO}_2$  additions are made from the top. As the uranium metal formed is denser than the electrolyte, it settles down at the bottom, which can be tapped at periodic intervals. The  $\text{CO}/\text{CF}_4$  gas formed is taken out as off gas. A schematic of the electrolytic reduction cell is shown in figure 2.7.

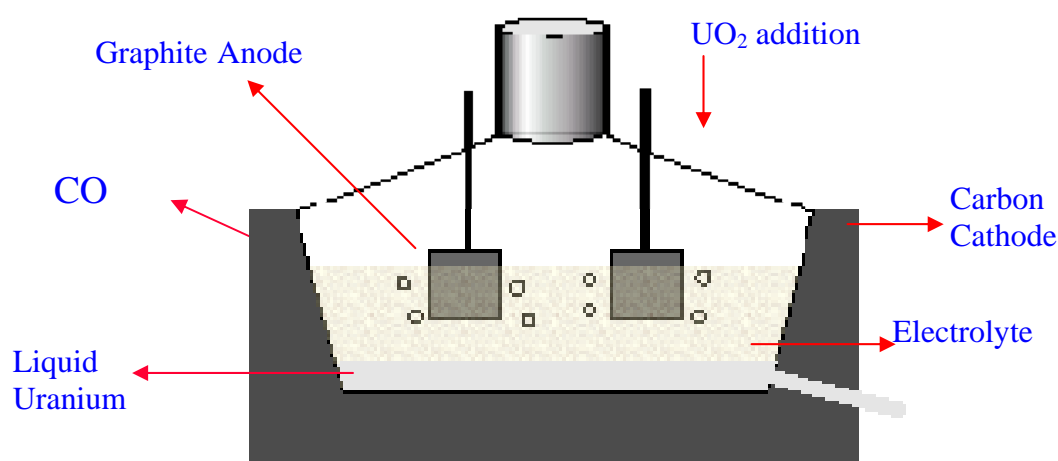


Figure 2.7 Schematic of Electrolytic reduction cell.

The molten salt properties that are important to the electrolytic cell operation, as reported in the literature [2.3, 2.12-2.16, 2.18-2.24, 2.26], are enumerated below.

1. The cations in the electrolyte should be more difficult to reduce than uranium.
2. The anions should not be easily oxidized at the graphite anode in preference to the formation of CO from the oxygen in the feed.
3. The melting points should be low enough for the formation of molten mixtures at a convenient temperature of operation.
4. The salt should have low vapor pressure to prevent excessive losses at the operating temperature
5. Ideally, the molten electrolyte should have adequate solubility for the feed uranium oxide

Alkaline, alkaline-earth, and rare-earth compounds in the fluoride melts have higher deposition potential for respective cations than that for uranium and hence are suitable as cations in the electrolyte. The other criteria of anions which allow formation of CO are best satisfied by the fluoride salts of the alkaline, alkaline-earth, and rare-earth. Chloride salts have been used. However, their high vapour pressure leads to loss of electrolyte. Also, at the cell operating temperatures of 1473K chloride salts lead to formation of  $\text{Cl}_2$  as a product in addition to CO. Although individual melting points of some of the fluorides electrolytes used such as  $\text{BaF}_2$ ,  $\text{CaF}_2$  are higher than 1473K, binary mixtures and the ternary mixtures of  $\text{BaF}_2$  with  $\text{LiF}$  as the supporting electrolyte and  $\text{UF}_4$  as the functional electrolyte, are well below the cell operating temperature.

Most of the authors have found that the solubility of the uranium oxide feed in the molten fluoride salt requires  $\text{UF}_4$  as the major component [2.10-2.29]. The solubility of

UO<sub>2</sub> is reported to be proportional to UF<sub>4</sub> concentration upto 50 mol% of UF<sub>4</sub>, and the effects of other fluoride salts in the supporting electrolyte were shown to be small [2.27, 2.30].

While UF<sub>4</sub>, is the primary solvent for the uranium dioxide, the fluoride of the light element, such as Li (or Mg) raises the electrical conductivity of the melt and the fluoride of a heavier element, such as barium or calcium, raises the melting point while simultaneously lowering the volatility of the melt. The thermophysical properties such as melting points, boiling points,  $\Delta G$  of formation and decomposition potentials of various fluoride salts of interest are given in Table 2.2. the electrical conductance, density in Table 2.3 and vapour pressure in Table 2.4.

**Table 2.2** Free energy of formation, melting point, boiling point data for fluoride salts used in molten salt electrolysis [2.32]

S.no	Compound	Melting point (K)	Boiling point (K)	Free energy of formation $-\Delta G^\circ$ at 1473K, kJ	Decomposition potential, V
1	CaF <sub>2</sub>	1691	2809	978	5.07
2	LiF	1121	1950	475	4.92
3	BaF <sub>2</sub>	1641	2410	953	4.94
4	UF <sub>4</sub>	1233	1690	1501	3.89
5	LaF <sub>3</sub>	1750	2327	1339	4.63
6	MgF <sub>2</sub>	1536	2512	869	4.50
7	NaF	1269	1968	422	4.37
8	KF	1131	1778	421	4.36

**Table 2.3** Density and electrical conductance of molten fluoride salts [2.32].Density:  $\rho = a - bT$ Specific Conductance:  $\kappa = a + bT + cT^2$ 

Compound	Electrical conductance x 10E-2 (ohm <sup>-1</sup> m <sup>-1</sup> )			Density x 10E3(kg/m <sup>3</sup> )	
	a	b	c	a	B
LiF	-15.0389	3.5354E-2	-1.2814E-5	2.3581	-0.4902E-3
BaF <sub>2</sub>	-	-	-	5.775	-9.99E-4
UF <sub>4</sub>	-2.023	2.803E-3	-	7.784	-9.920E-4
LaF <sub>3</sub>	-13.538	22.487E-3	-8.167E-6	5.793	-6.82E-4
CaF <sub>2</sub>	-	-	-	3.179	-3.91E-4
MgF <sub>2</sub>	-	-	-	3.235	-5.24E-4
NaF	1.4605	2.7374E-3	-	2.655	-0.54E-3
KF	9.9728E-2	3.0628E-3	-	2.6464	-0.6515E-3

**Table 2.4** Vapor pressure data for some fluoride salts at 1473K [2.34]

Compound	Vapour pressure (Pa)
LiF	1.16E+03
BaF <sub>2</sub>	2.67E+00
CaF <sub>2</sub>	9.91E-02
UF <sub>4</sub>	1.27E+04
LaF <sub>3</sub>	1.33E+02
LiCl	2.41E+04
CaCl <sub>2</sub>	1.35E+02
KCl	1.60E+04
NaCl	1.10E+04
UCl <sub>4</sub>	2.56E+06
MgCl <sub>2</sub>	2.28E+04

The uranium compounds in the melt give the following ionic species:



The reactions at the cathode are [2.26] given by Eq (2.1), (2.2) and (2.3)



The reactions at the anode are [2.26]:



All these reactions above are given in terms of simple anions and cations, but complexes of uranium, fluorine and oxygen are the predominant forms in actual cells. The uranium feed compounds would react to give the complexes instead of simple ionizations shown by the equations [2.1 to 2.12]. The net effect of complex formation is to make the cathodic reactions more difficult in comparison to the simple cation.

For overall reactions, the free energy change and the equilibrium voltages have been calculated and listed in Table 2.5. In the calculations, Carbon, uranium metal,  $\text{UO}_2$  and  $\text{CO}$  are considered to be in their standard states. It is to be noted that the reaction shown in equation 2.21 represents a cyclic reaction of  $\text{U}^{3+}$  and  $\text{U}^{4+}$  and has the same species on both the sides of the equation, and the theoretical voltage is the result of the concentration differences [2.26]

**Table 2.5** Overall cell reactions of uranium and theoretical potentials.

Eq no	Overall reaction	Value of n	$\Delta G^\circ$ kJ at 1500K [*1]	$-E = \Delta G^\circ/nF$ (V) [*1]	$\Delta G^\circ$ kJ at 1473K [*2]	$-E = \Delta G^\circ/nF$ (V) [*2]
2.13	$\text{UO}_2 + 2\text{C} \rightarrow \text{U} + 2\text{CO}$	4	343	0.89	348	0.90
2.14	$\text{UF}_4 + \text{C} \rightarrow \text{U} + \text{CF}_4$	4	754	1.95	791	2.05
2.15	$\text{UCl}_4 \rightarrow \text{U} + 2\text{Cl}_2$	4	740	1.92	684	1.77
2.16	$\text{UO}_2 \rightarrow \text{U} + \text{O}_2$	4	830	2.15	831	2.15
2.17	$\text{UF}_4 \rightarrow \text{U} + 2\text{F}_2$	4	1460	3.78	1501	3.89
2.18	$\text{UO}_2 + 3\text{UF}_4 + 2\text{C} \rightarrow 4\text{UF}_3 + 2\text{CO}$	4	283	0.73	230	0.60
2.19	$4\text{UF}_4 + \text{C} \rightarrow 4\text{UF}_3 + \text{CF}_4$	4	694	1.80	557	1.44
2.20	$4\text{UF}_3 + 3\text{C} \rightarrow 4\text{U} + 3\text{CF}_4$	12	2323	2.01	2608	2.25
2.21	$\text{U}^{4+} + \text{U}^{3+} \rightarrow \text{U}^{3+} + \text{U}^{4+}$	1	0	0	0	0
2.22	$\text{U} + 3\text{UF}_4 \rightarrow 4\text{UF}_3$	1	-	-	-234	-2.43

\*1. Reference [2.26]

\*2. Computed value in this work with ASTD Version 2.0 [2.32]

The calculations in the table provide theoretical minimum possible voltage required at equilibrium and does not include any consideration for the rates of reactions. Besides the thermodynamic feasibility, the kinetics of the reaction is also very important. The voltage across the electrodes in an operating electrolytic cell is the summation of the

minimum theoretical voltage, the voltage drop across the electrolyte, over potentials of both cathode and anode. The lead resistance to the electrodes may also be significant and should be considered while calculating the practical cell potential.

The back reaction of uranium metal formed with UF<sub>4</sub> containing electrolyte is also possible by the following chemical reaction



This reaction is independent of the electrolysis in the cell, and represents the redissolution of the uranium metal. The problem associated with the product of this reaction is that, if UF<sub>3</sub> is not immediately removed from the system, a cyclic reaction will be set up. This causes parasitic current to be setup, involving oxidation of UF<sub>3</sub> at the anode and reduction of UF<sub>4</sub> at the cathode. This cyclic reaction evidently results in loss of efficiency of the cell. This behavior can be represented as half cell reactions.

At the anode



at the cathode:



The dissolution of metallic uranium formed and the cyclic reaction have been identified by various authors to be the main problems for low current efficiency and poor uranium metal yield [2.10-2.29]. The formation of particular gaseous product does not prove which reactions are occurring. Carbon monoxide formation is not generally observed

below 2-2.5 V, and the rate of reaction of equation 2.16 to form CO by electrolysis may be small initially, and becomes faster only at higher voltages.

## **2.5 Associated Problems in electrolytic reduction of uranium oxides**

The general problems reported in the electrolytic reduction of uranium oxides to uranium metal are

- a. The redissolution and the cyclic reaction setup by the formation of  $\text{UF}_3$  leading to loss in current efficiency. (discussed in section 2.4)
- b. Settling of oxide in the interface between the molten metal at the cathode and the electrolyte which hinders coalescence of the metal formed.
- c. Lack of solubility of uranium oxides in the electrolyte not allowing to operate at higher current densities
- d. Formation of crud

Production of liquid uranium in an electrolytic cell implies that it is recovered from oxide in a coalesced form; any uranium metal re-dispersed or re-dissolved in the salt bath or otherwise not recovered makes the process inefficient. The most important factor for higher efficiency is the high availability of dissolved  $\text{UO}_2$  at the anode. The main factors which influence the solubility are the amount of  $\text{UF}_4$ , the temperature of the melt and rate of dissolution by the viscosity of the melt. Rare-earth fluorides show a higher capacity to dissolve  $\text{UO}_2$  than  $\text{UF}_4$  salt mixtures, but the experiments so far have been very limited. A melt with low dissolved  $\text{UO}_2$  concentrations will allow low anode current densities which gets limited by anode effect. A schematic picture showing the anode effect is shown in figure 2.8, where the gas evolving at the anode envelops the anode, leading to drastic reduction of the cell current.

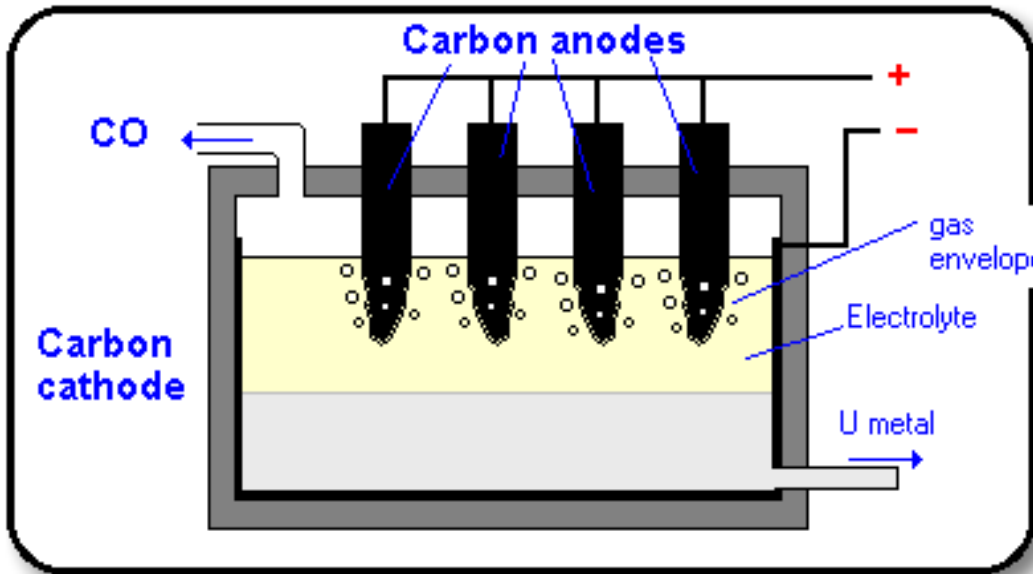


Figure 2.8 Pictorial representation of anode effect in electrolytic cells.

The oxide settling problem during the experiment proved to be the greatest difficulty that was encountered by many investigators [2.10-2.29]. It is a problem not only because it is a loss of oxide to the electrolytic process, but also the settled material forms a dense oxide sludge at the electrolyte liquid metal cathode interface of the cell which prevents the coagulation of the product metal. As a result, many investigators could not produce massive agglomerate of product metal, except in instances where care had been taken to avoid the sludge formation by (i) changing the design of the electrolytic cell and (ii) intermittent addition of  $UO_2$  to get complete solubility before the powder reaches the bottom.

From the Stoke's law the velocity of settling of particles is given by

$$v = \frac{2}{9} g \frac{(\rho - \rho') r^2}{\eta} \dots\dots\dots 2.26$$

Where  $\rho$  and  $\rho'$  are the densities of the oxide and the salt respectively in g/cc,  $\eta$ - viscosity of the electrolyte in centipoise, r- radius of the oxide particle in cm, and g-

acceleration due to gravity in  $\text{cm}^2/\text{s}$ . The density of the oxide is  $\sim 10.82 \text{ g/cc}$ , the electrolyte is  $\sim 3\text{-}4 \text{ g/cc}$  where as for uranium it is  $\sim 18 \text{ g/cc}$ . The velocity of a  $44 \mu\text{m}$  particle is around  $0.8 \text{ cm/min}$  in the electrolyte with viscosity approximately  $0.01 \text{ poise}$ . With this low velocity, the powder dissolves before it sinks to the bottom in a large electrolytic cell.

Another problem that was reported by Piper R. D [2.23] is the formation of crud, which is the formation of a carbon scum with the electrolyte, a small amount of uranium oxide, uranium metal and uranium carbide on the electrolyte surface when the cell was operated either for more than eight hours or at high temperatures. The mechanism for the formation of crud is that, the carbon particles floating on the electrolyte surface get bonded to the crucible wall with a thin layer of uranium and uranium carbide. This crud becomes cathodic. The usual result of this effect is loss in current efficiency due to increased current flow to the crud, and occurrence of extensive back reactions. Some success has been reported in burning off the carbon particles by purging of  $\text{CO}_2$ . But the sure cure was removal of the crud by skimming.

## References

- 2.1 Peligot, Ann. Chim. Phys., [3],5,5,(1842).
- 2.2 Pierle and Kahlenberg, "Journal of Phys. Chem.", Vol 23, pp 317, 1923.
- 2.3 Driggs F.H., Lilliendahl W.D., "The preparation of metal powders by electrolysis of fused salts I-Ductile uranium", Ind Engg. Chemistry, Vol 22, pp 516-519, 1930.

- 2.4 M. Kolodney, "Preparation of first electrolytic plutonium and uranium from fused chlorides", *Journal of Electrochemical society*, vol 129, pp 2438-2442, 1982.
- 2.5 Marzano C. and Noland R. A., "The electrolytic refining of uranium", Argonne National laboratory Report, ANL-5102, 1953.
- 2.6 Blumenthal B., "Melting of high purity uranium", *Journal of Metals*, pp 1199-1205, 1955.
- 2.7 Kantan S.K., Srinivasan N. and Tendolkar G. S., "Electrolytic preparation of uranium from a fluoride bath", *Chem Engg progress Symposium*, Ser 50, No. 12, pp 63-66, 1954.
- 2.8 Niedarch L. W. and Glamm A.C., "Uranium purification by electrorefining", *Journal of the Electrochemical society*, Vol 103, No. 9, pp 521-528, 1958.
- 2.9 D. Inman, G.J. Hills, L. Young and J. O'M. Bockris, *Trans Faraday soc.* 55, pp 1904, 1959.
- 2.10 D.L. Hill, J. Perano and R.A. Osteryoung, "An electrochemical study of uranium in fused chlorides", *Journal of electrochemical society*, Vol 107, No. 8, pp 698-705, 1960.
- 2.11 J L Willit, W E Miller and J E Battles, "Electrorefining of uranium and plutonium – A literature review", *Journal of nuclear materials*, 195, 229-249, 1992.
- 2.12 Niedarch L. W. and Dearing B. E., "The preparation of uranium metal by the electrolytic reduction of its oxides", *Journal of the Electrochemical society*, Vol 105, No. 6, pp 353-358, 1958.
- 2.13 Niedarch L. W., "New approach to electrolytic uranium", *Nucleonics*, Vol. 16, No 1, pp 64-65, 1958.

- 2.14 Niedarch L. W. and Glamm A.C., "Uranium purification by electrorefining", Journal of the Electrochemical society, Vol 103, No. 9, pp 521-528, 1958.
- 2.15 Niedarch L. W. and Dearing B. E., "Electrowinning of uranium from its oxides", Knolls Atomic Power Laboratory, Rep No KAPL-1761, 1957.
- 2.16 Niedarch L. W. and Schafer A. C., "Electrowinning of uranium from its oxides II A preliminary Engineering evaluation", Knolls Atomic Power Laboratory, Rep No KAPL-1668, 1957.
- 2.17 Henrie T. A., "Electrowinning rare-earth and uranium metals from their oxides", Journal of Metals, pp 978-981, 1964.
- 2.18 Piper R. D., and R.F. Leifield, "Electroreduction of uranium oxides to massive uranium metal", Mallinckrodt Chemical Works, Rep No. MCW-1447, 1960.
- 2.19 Piper R. D., and R.F. Leifield, "Electrolytic reduction of uranium metal from uranium oxides", I & EC Process Design and development, Vol 1, No. 3, pp 208-212, 1962.
- 2.20 Piper R. D., and Gay. E. C, "Process development quarterly progress report", Mallinckrodt Chemical Works, Rep No. MCW-1479, 1962.
- 2.21 Piper R. D., "Process development quarterly progress report", Mallinckrodt Chemical Works, Rep No. MCW-1480, 1963.
- 2.22 Piper R. D., Vie J.D., Reyland J.N., Kornfeld R.J., and D.E. Treadway, "Methods for tapping molten uranium from an electrolytic cell", Mallinckrodt Chemical Works, Rep No. MCW-1481, 1963.
- 2.23 Piper R. D., "Laboratory report of the uranium Electroreduction process", Mallinckrodt Chemical Works, Rep No. MCW-1500, 1966.

- 2.24 Stevenson J.W., "Electrolytic uranium project: Cell operation, terminal progress report", Mallinckrodt Chemical Works, Rep No. MCW-1514, 1966.
- 2.25 Varwig J.W., "Solubility of  $UO_2$  in molten salt", Mallinckrodt Chemical Works, Rep No. MCW-1490, 1964.
- 2.26 Haas P.A, Adcock P.W, Coroneos A.C. and Hendrix D.E, "Small cell experiments for electrolytic reduction of uranium oxides to uranium metal using fluoride salts", Metallurgical and Material transactions B., Vol 25B, pp 505-518, 1994.
- 2.27 Haas P.A and Stanley P. Cooper, "Solubility of uranium oxides in fluoride salts at  $1200^{\circ}C$ ", American chemical society, Vol 38, No. 1, pp 26-30, 1993.
- 2.28 Takeshi Shimda, Nobuo Tedzuka, Yuzo Shimizu and Masanobu Miyake, "Electrochemical reduction of uranium oxide in molten fluoride mixture", Journal of Alloys and compounds, 204, pp 1-4, 1994.
- 2.29 Takeshi Shimda, Nobuo Tedzuka, Yuzo Shimizu and Masanobu Miyake, "Electrode reactions of Uranium during electrolysis of its oxide in a molten fluoride bath", Journal of Alloys and compounds, 206, pp 249-253, 1994.
- 2.30 Porter B., and Brown E.A., "Determination of oxide solubility in the Molten fluorides", Bureau of Mines Report of investigation 5878, U.S. Department of interior, Bureau of Mines,(1961).
- 2.31 Greenfield B.F, and Hyde K.R., "The solubility of uranium Dioxide in Fluoride melts", AERE Harwell, AERE-R6343, 1983.
- 2.32 Belov G V, Trusov B G, ASTD Version 2.0, 1995
- 2.33 G.J. Janz, W. Dampier, G.R. Lakshminarayanan, P.K. Lorenz and R. P. T. Tomkins , "Molten Salts", Vol 1. Electrical conductivity, Density and viscosity data, NSRDS-NBS 15, 1968.

2.34 W F Gale and T C Totemeier, Smithells metals reference book, 8th ed,  
ISBN: 978-0-7506-7509-3

# CHAPTER III

## THERMO-PHYSICAL CHARACTERIZATION AND MATERIALS FOR ELECTROLYTE HANDLING

---

This chapter deals with the studies conducted and the work done in (1) preparation of fluoride salt mixtures (2) preconditioning of the fluoride salt mixtures (3) and determination of their melting points of fluoride salt mixtures. Apart from the above, compatibility studies of different materials with various electrolyte mixtures are also reported in this chapter.

### 3.1 Introduction

There are only a few inorganic fluoride salt mixtures, namely, LiF, BaF<sub>2</sub>, CaF<sub>2</sub> and MgF<sub>2</sub> along with the solvent for fluoride additives such as UF<sub>4</sub>, rare earth fluorides etc., which meet the requirements of melting point, vapor pressure and electrochemical deposition potential for the electrolytic reduction of uranium oxide to uranium metal. These fluoride salt mixtures are very hygroscopic, reactive with oxygen and highly corrosive in their molten form. The challenges involve their handling and mixing, purification and containment materials to prepare salt baths. The salt mixtures proposed for the work have either UF<sub>4</sub> or LaF<sub>3</sub> as the solvent and LiF:BaF<sub>2</sub> with 1:1 mole ratio is used as the diluent salt. The properties of LiF-BaF<sub>2</sub>[3.1], LiF-CaF<sub>2</sub>[3.2], BaF<sub>2</sub>-CaF<sub>2</sub>-LiF [3.3], LiF-UF<sub>4</sub> [3.4], CaF<sub>2</sub>-UF<sub>4</sub> [3.5], LiF-LaF<sub>3</sub> [3.6], BaF<sub>2</sub>-LaF<sub>3</sub> [3.7] systems have been sparsely reported in the literature.

Data on the ternary eutectic mixtures of LiF- BaF<sub>2</sub>, LiF-CaF<sub>2</sub> with UF<sub>4</sub> is scanty. Further, there is practically no information available in literature about LiF- BaF<sub>2</sub>-LaF<sub>3</sub> system phase diagram.

### **3.1.1 Importance of purity of the molten salt**

For a molten salt mixture to function as the electrolyte in molten salt electrolysis of uranium oxide, it should possess the desired electrochemical range, that is, the potential range in which an electrode can be polarized in a solution without the passage of substantial Faradaic current. Hence, the amount of current passing in the salt mixture below the decomposition voltage of the salts can be directly attributed to the impurity in the salt mixture. In molten salts, there is always a background current present and its magnitude is determined by the impurities of multivalent elements, which undergo electron transfer reactions at the electrodes, and the transport between the anode and cathode by the conducting electrons. The impurities in the molten salt, limit the electrochemical range of electrolyte. Other reasons that make the purification step unavoidable are as follows

1. Formation of oxy-fluorides in the electrolyte due to the presence of moisture and oxygen impurities
2. Occurrence of secondary reactions during the electrolysis process due to the impurities
3. Unwanted co-deposition at the cathode affects the purity of metal
4. The purity of the electrolyte mixture has a strong influence on the corrosion behaviour of the electrolyte with various materials

Several procedures for the purification of salt melts and conditioning procedures have been reported in the literature [3.8-3.17]. Moisture removal by vacuum drying was

demonstrated to remove  $\text{Br}^-$ ,  $\text{OH}^-$ ,  $\text{CO}_3^-$  ions from the fluoride melts [3.16]. Purification of fluoride and chloride melts by purging hydrogen chloride or hydrogen fluoride gas has been reported by Liu et al. [3.17]. Melt purification by pre-electrolysis technique has been employed by various authors [3.8-15, 3.16, 3.17]. However, a detailed procedure for purification of molten fluoride salts and a systematic evaluation of the conditioning process procedure has not been provided by any of the authors. Although analytical techniques can be used for assessment of the quality of the electrolyte by sampling, the process is laborious and time consuming. An in-situ online assessment method like LSV has a definite advantage to study the quality of the electrolyte. The possibility of using Linear Sweep Voltammetry (LSV) as a measure of the extent of purification has also not been explored by the previous authors. The use of LSV to measure purity in this work has been discussed in section 3.3.

### **3.1.2 Selection of materials for the components of the electrolytic cell**

In an electrolytic cell, the materials used for different components have diverse functionalities and each has its own chemical resistance requirements. In case of the cathode containment vessel, the material has to withstand the chemical corrosion effects of the electrolyte as well as the liquid metal cathode (pure uranium, copper, tin, U-Sn alloy, U-Cu alloy). The requirements of the anode are that it should withstand the electrolyte and must have corrosion resistance against carbon monoxide ( $\text{CO}$ ), carbon tetrafluoride ( $\text{CF}_4$ ), oxygen ( $\text{O}_2$ ) and fluorine ( $\text{F}_2$ ) gases which evolve during the electrolysis process. Along with the above requirements, the anode also has to withstand the oxidizing conditions prevailing near the anode due the presence of  $\text{O}^{2-}$  ions. The container for the electrolyte, has to withstand various chemical

effects of the catholyte and anolyte. It is to be noted that the body of the containment vessel may also attain different potentials (both anodic and cathodic) due to dissimilar compositions present at various locations of the container. It goes without saying that all the materials that are being exposed to both the electrolyte and the product metal should not add any impurities to the electrolyte which may alter the chemistry of the molten fluoride system; it will then disturb the conditions of deposition and eventually introduce impurities in the product metal. The other structural components that are not directly exposed to the electrolyte and liquid metal have to withstand the vapors of fluoride salts which are transported to various parts by the argon purge gas used for purification and providing an inert cover to the electrolyte.

The oxygen impurity in the purge gas also has a strong influence on the electrochemical range of the salt and the corrosion behavior. In all the experiments, argon gas having  $<0.1$ ppm oxygen is required during the complete run. The desired level of  $<0.1$ ppm of oxygen was achieved by passing argon gas in an in-house developed argon purification system; this equipment has been designed, fabricated and tested and also productionised. It contains a  $\sim 350$ mm height copper mesh bed maintained at 673K, over which cylinder inert argon ( $\sim 10$ -100ppm oxygen) flows through a rate of 8-10 l/h. The capacity of the bed is  $\sim 3000$  litres. The photograph of the apparatus is shown in figure 3.1.

Corrosion of alloys in molten fluoride has been extensively studied for numerous nuclear reactor applications, particularly in the molten salt reactor application. Studies on LiF-BeF<sub>2</sub>, FLINAK base salts with the addition of UF<sub>4</sub>, ZrF<sub>4</sub> and ThF<sub>4</sub> upto 1073K have extensively been reported by various authors [3.7-3.15]. However

reported data on corrosion aspects of LiF-BaF<sub>2</sub> with UF<sub>4</sub> as additive at 1473K is scanty. Data pertaining to LiF-BaF<sub>2</sub> with LaF<sub>3</sub> additive is not available till date.



Figure 3.1 (a) Photograph of the argon purifier to generate argon with < 0.1ppm oxygen (b) Copper mesh roll absorber used in purifier

The objectives of the work was to

1. Determine the melting point of different LaF<sub>3</sub> salt mixtures

2. Determine the losses from LiF- BaF<sub>2</sub>-LaF<sub>3</sub> mixtures at high temperature of 1473K
3. Develop the preconditioning procedure to obtain suitable electrochemical window
4. Conduct a compatibility study of multi-component fluorides systems with different materials to select suitable materials for electrolytic cell components.

As no standard apparatus or equipment was available for all the studies, separate experimental setups were required to be made in house for each study. For generating first level data, thermodynamic calculations were necessary to determine the reaction of electrolyte and uranium with different materials and the effect of oxygen and moisture on the corrosion behavior of the materials.

### **3.2 Melting point determination**

The determination of melting points of various electrolyte mixtures involves the following steps

- a. Preparation of salt mixtures
- b. Melting and crushing of frozen salt mixtures to remove stratification effects, and
- c. Melting point determination in thermogravimetry and differential thermal analysis (TG-DTA) apparatus

#### **3.2.1 Experimental setup for salt mixture preparation**

Preparation of the salt mixtures mainly requires a muffle to provide an inert gas cover for the crucible and a heating system to achieve the desired temperature. The experimental setup for salt bath preparation was designed from first principles. The

components were fabricated according to the design and assembled. Material selection was based on functionality, thermo-mechanical properties of the materials, ease of fabrication and cost. The design considerations for the systems are as follows:

#### Considerations for the experimental setup

1. All the experiments require inert gas cover to prevent any reaction between oxygen and the electrolyte, and oxidation of the structural components.
2. Maximum temperature to be attained is 1323K (~200K above the eutectic temperature of LiF:BaF<sub>2</sub> 1:1 mole ratio). Thus, all the materials used in the experimental setup should have suitable strength at 1323K.
3. Container materials should be compatible with the molten electrolyte
4. All the other structural materials should be compatible with vapors of LiF, BaF<sub>2</sub>, CaF<sub>2</sub>, etc.
5. All the seals used in the experimental setup should be leak tight to a sensitivity of 1E-9 mbar.l/s to prevent oxygen leak into the system.
6. The setup should have a uniform hot zone of atleast 100mm length, at any given temperature.
7. Maximum design temperature accordingly should be 1368K, 50K above the desired temperature.
8. The microprocessor controlled and programmable system should achieve the desired heating rate and holding times required for operation.
9. The system should have safety features for over temperature and over heater current trip to prevent any accident.
10. The furnace should have multi-layered insulation to keep the external surfaces of heater below 333K.

Based on the above design considerations, the specifications were prepared with 4kW KANTHAL heating element, vertical split architecture type muffle furnace and a maximum temperature of 1368K. Salient features of the heater are as shown in Table 3.1.

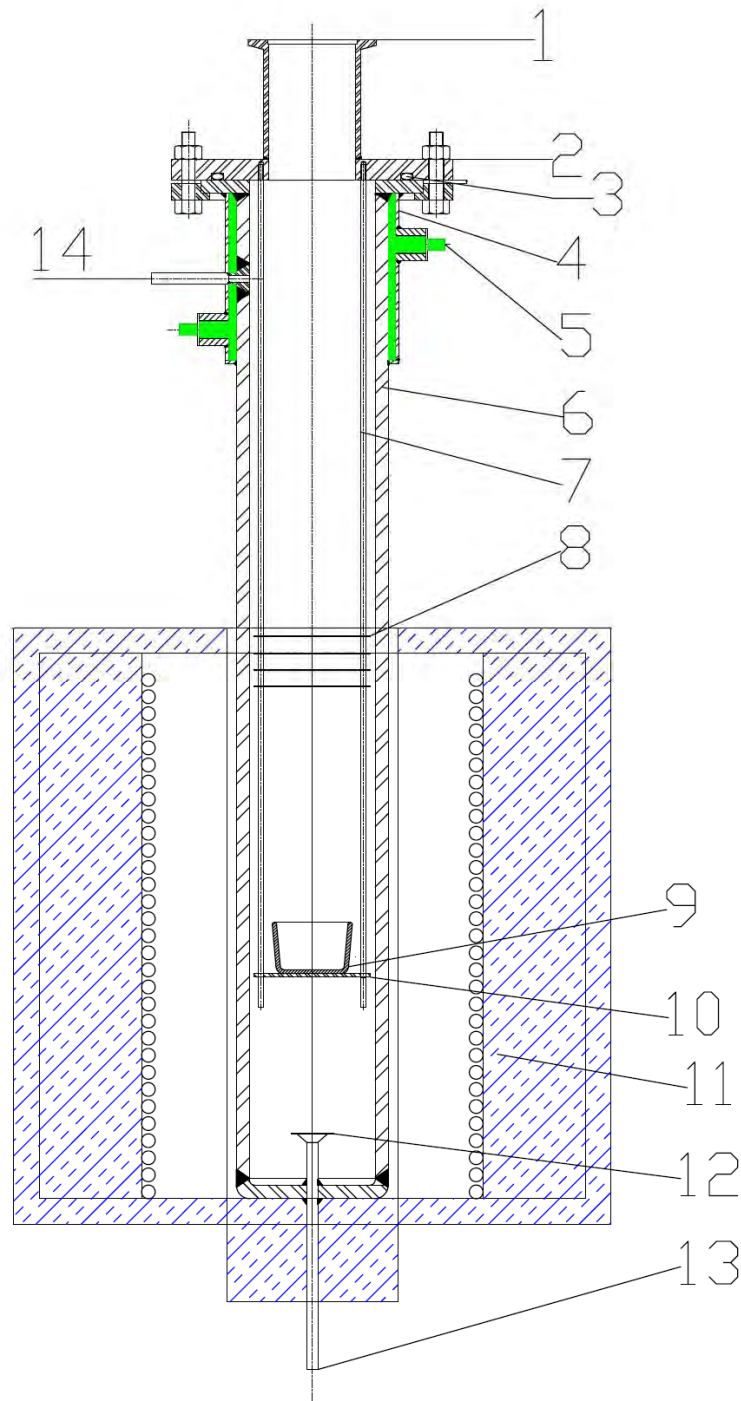
Table 3.1 Salient features of the furnace for fluoride salt bath preparation

<b>S.no</b>	<b>Specification</b>	<b>Required value</b>
1.	Furnace type	Vertical muffle, Split design
2.	Power rating	4kW
3.	Process Temperature	1368K maximum, Accuracy $\pm 5K$
4.	Uniform temperature zone	At least 100mm
5.	Diameter Inner	100mm
6.	Diameter outer (Including casing)	350mm
7.	Heated Length	275mm
8.	Control panel	Single phase SSR based power supply, with PID Controller and microprocessor based temperature controller-cum-Indicator,

Inconel 600 material (UNS N06600) was chosen from the available standard engineering materials, as it exhibits excellent mechanical properties at high temperature and presents the desirable combination of high strength and good workability. The high nickel content provides the alloy with good corrosion resistance against molten fluoride vapors. Chromium present in inconel imparts resistance to high temperature oxidation of the muffle on the outer surface which is exposed to air.

A 73.5mm ID, 88.9mm OD pipe was chosen to accommodate 50.8mm OD graphite crucible, and wall thickness of 7.6mm was provided to compensate for any reduction in thickness occurring over a period of time. A cylindrical pipe of inconel was chosen

keeping in view the fabrication and ease in availability. A SS304 flange of 150mm OD 12mm thickness with an O-ring groove, was welded at one end of the pipe and the other end of the pipe was closed by welding a 10mm thick Inconel plate. The muffle at the flange end had a welded cooling jacket to cool the O-ring joint. The length of the inconel tube was 600mm and was based on the consideration that water cooling at 2lpm should be sufficient to maintain the temperature of the flange below 333K, which is below the setting temperature of Viton O-ring. A gas inlet was provided at the bottom of the vessel and an outlet at the top to ensure complete displacement of the air with argon gas. The flange had a provision for fastening three 3mm dia inconel rods which support an inconel plate of 68mm dia 2mm thickness. The graphite crucible rested on this inconel plate with an alumina disc of 50mm dia 5mm thickness as separator between the graphite and the inconel plate; this prevented reaction between them. The mating flange for the open end of the muffle had a KF 50 flange, which was used to connect a leak tight feed through. Separate KF 50 flanges were fabricated for insertion of thermocouples for characterization of the setup such as thermal profiling and also to insert a thermowell for measuring temperature during the experiments. The schematic of the experimental setup and fabrication drawing of the inconel muffle are shown in figures 3.2 and 3.3 respectively.



- |                                   |                                  |
|-----------------------------------|----------------------------------|
| 1. KF opening on top flange       | 2. SS flange with O ring groove  |
| 3. Viton O ring seal              | 4. Water cooling jacket          |
| 5. Water inlet connection         | 6. Inconel 600 muffle            |
| 7. 3mm dia inconel hanging rods   | 8. Inconel 600 radiation shields |
| 9. High density graphite crucible | 10. 3mm thk alumina base plate   |
| 11. Resistive heating furnace     | 12. Inconel gas diffuser         |
| 13. Argon gas inlet               | 14. Argon gas outlet             |

Figure 3.2 Schematic of experimental assembly used for salt mixture preparation

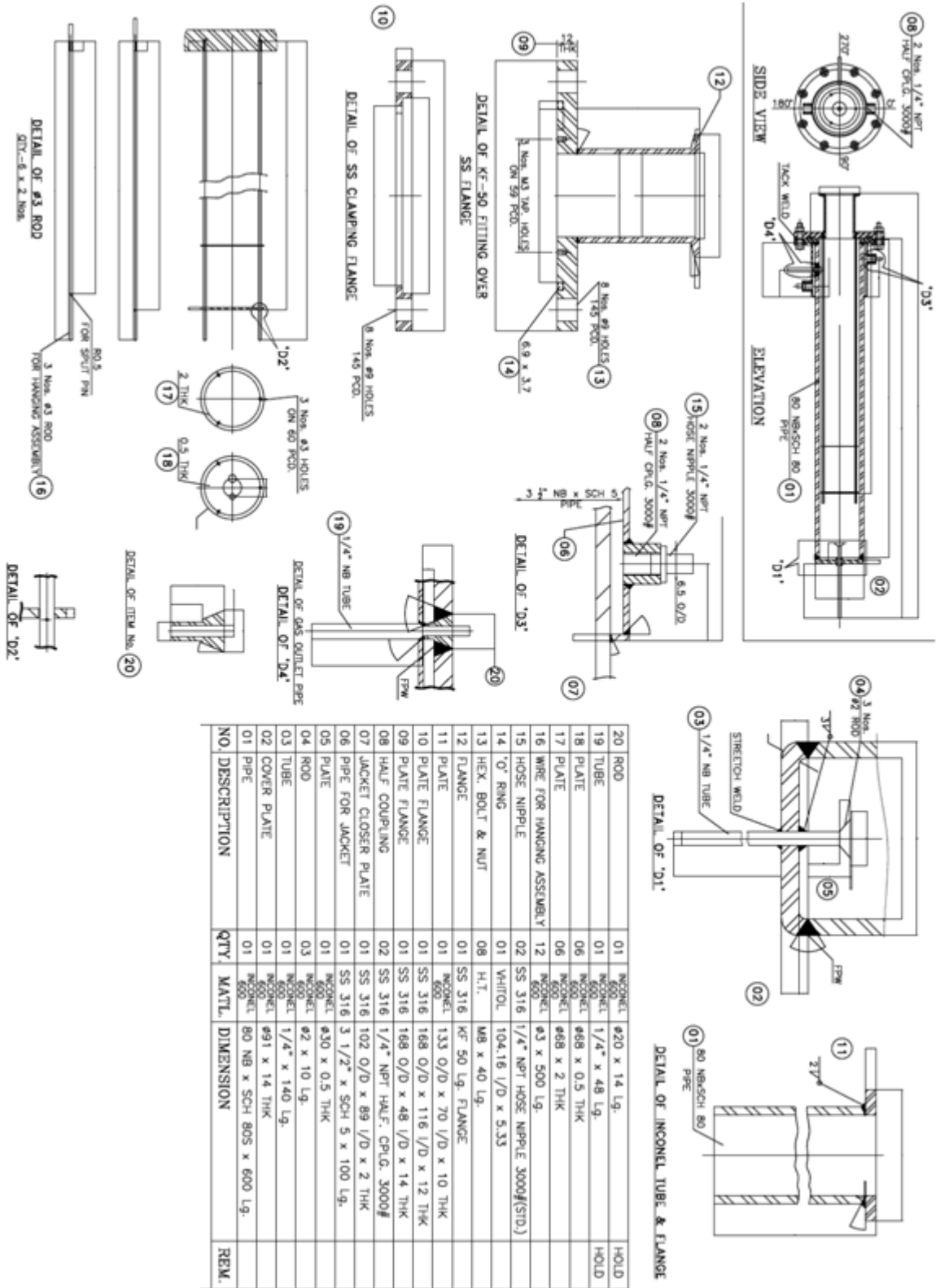
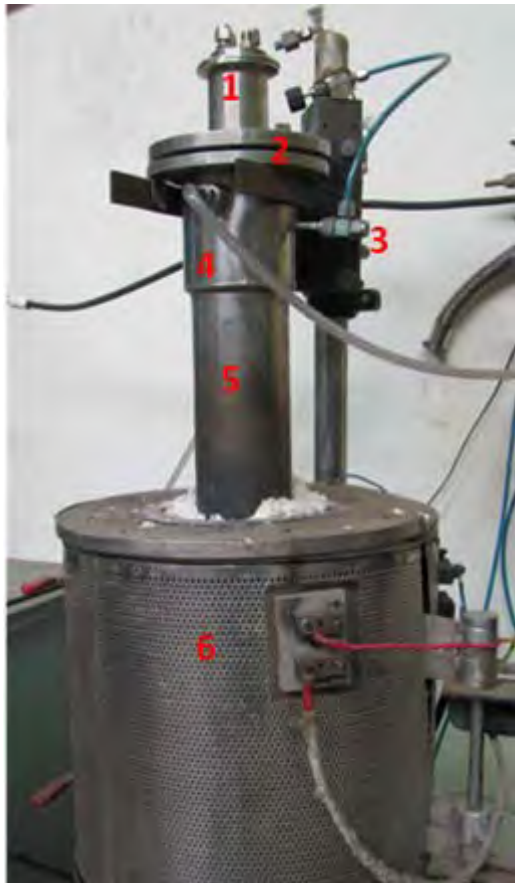


Figure 3.3 Fabrication drawing of inconel 600 muffle of salt mixture preparation assembly

### **3.2.2 Testing and performance evaluation of experimental setup**

All the weld joints in the fabricated setup were tested for weld defects by liquid dye penetrant test and it was ensured that no visible defects were present. The performance of the experimental setup was evaluated for its leak tightness. The setup was assembled with the argon inlet and outlet connections closed with a 1/4" needle valve and the system was evacuated through KF-50 nozzle. The leak tightness of the assembled setup was ensured by leak testing with an Alcatel Helium Mass Spectrometer Leak Detector (He-MSLD) to a sensitivity of  $1\text{E-}9$  mbar.l/s. Figure 3.4 shows a photograph of the experimental setup. The setup was characterized for the maximum attainable temperature, heating rate and uniform zone temperature. Figure 3.5 shows variation of temperature with a ramp rate of 600K/hr and figure 3.6 temperature variation inside the muffle. The tests show that the system was capable of delivering a heating rate of 600K/hr and a uniform temperature zone of 100mm was obtained within  $\pm 5\text{K}$ . The temperature difference measured between the inside of the inconel muffle and its outside surface of the inconel muffle and was found to be around 20K in the range of 1173K to 1323K. In all the subsequent experiments, the control of the furnace was based on the thermocouple in contact with the outer surface of the inconel muffle, thus the setpoint of the furnace was always set 20K above the desired value of the experiment.



1. KF 50 nozzle
2. Flange assembly
3. Argon outlet
4. Water cooling jacket
5. Inconel muffle
6. Heating system

Figure 3.4 Photograph of the experimental setup for salt mixture with heating system.

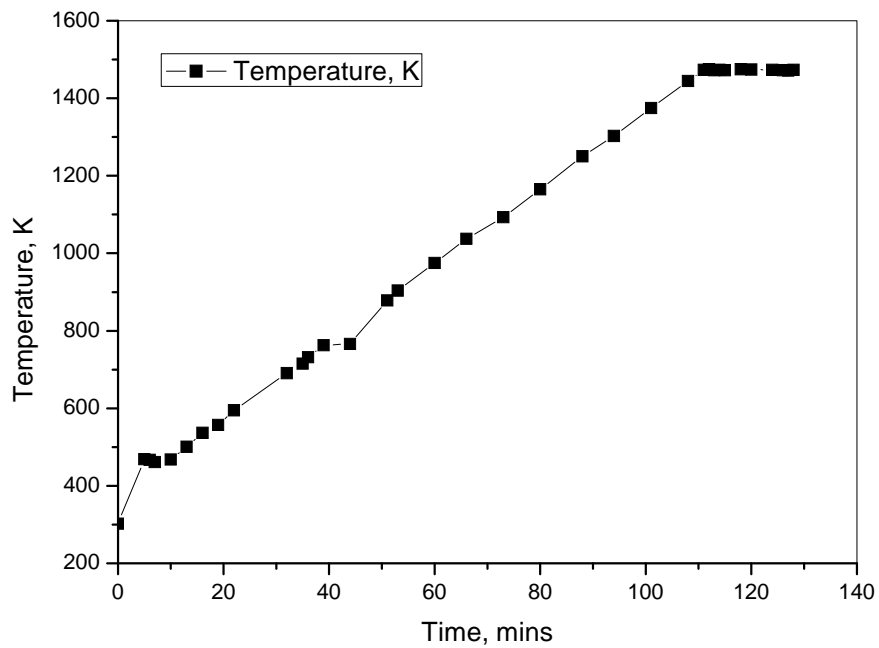


Figure 3.5 Temperature time characteristics of tubular furnace for ramp of 600K/hr

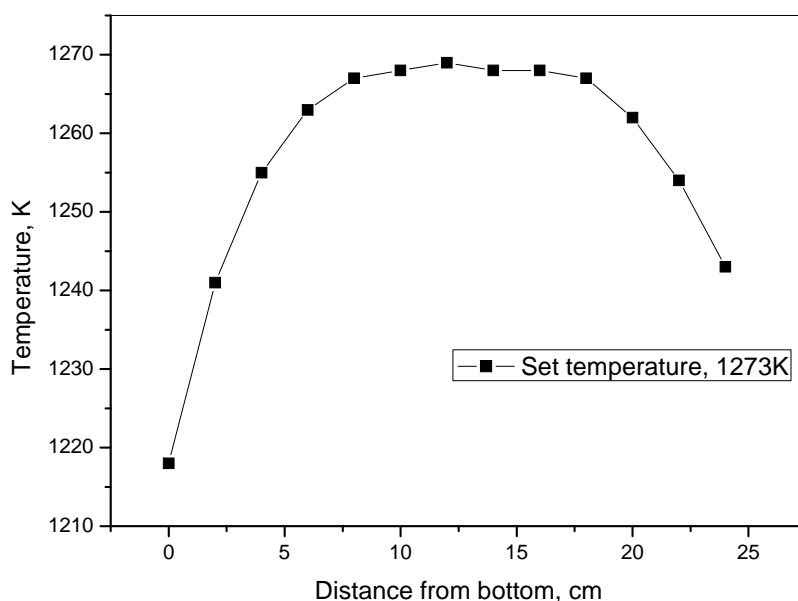


Figure 3.6 Temperature profile at the centre of the furnace at 1273K set point

### 3.2.3 Salt mixture preparation

Both LiF and BaF<sub>2</sub> were of reagent grade with minimum assay of 99% and were sourced from M/s Sigma Aldrich with CAS No. 7789-24-4 and 7787-32-8 respectively. LaF<sub>3</sub> was sourced from M/s Prabhat chemicals with CAS No. 13709-38-1 and had minimum purity of 99.5%. UF<sub>4</sub> was procured from Uranium Extraction Division, BARC which was of nuclear grade and had a minimum assay of 99%. The list of impurities present in different salt mixtures were as shown in Table 3.2

Table 3.2 list of impurities present in the fluoride salt mixtures

#### a. Impurities in LiF salt

Cl <0.01%, SO<sub>4</sub> <0.01%, Al <0.02%, Ba <0.07%, Ca <0.002%, Cd <0.05%, Co <0.0005%, Cr <0.0005%, Cu <0.0005%, Fe <0.01%, K <0.005%, Mg <0.01%, Mn <0.005%, Mo <0.0005%, Na <0.01%, Ni <0.01%, Pb <0.0005%, Sr <0.01%, Zn <0.001%

b. Impurities in LaF<sub>3</sub> salt

CeO<sub>2</sub> <0.05%, Pr<sub>6</sub>O<sub>11</sub> <0.05%, Nd<sub>2</sub>O<sub>3</sub> <0.05%, Sm<sub>2</sub>O<sub>3</sub> <0.05%, Gd<sub>2</sub>O<sub>3</sub> <0.01%, CaO <0.05%, Fe<sub>2</sub>O<sub>3</sub> <0.05%, PbO <0.05%, SiO<sub>2</sub> <0.05%

c. Impurities in BaF<sub>2</sub> salt

Co <0.0005%, B <0.0005%, Mn <0.0005%, Fe <0.0005%, Pb <0.0015%, Mg <0.0025%, Ni <0.0005%, Cr <0.0005%, Sn <0.0005%, Al <0.0003%, Ca <0.0005%, V BDL, Mo <0.0005%, Ti BDL, Na <0.01%

d. Impurities in CaF<sub>2</sub> salt

Co <0.0005%, B <0.0005%, Mn <0.0005%, Fe <0.0005%, Pb <0.0005%, Mg <0.005%, Ni <0.0005%, Cr <0.0005%, Sn <0.0005%, Al <0.0003%, Ca <0.0005%, V <.0015%, Mo <0.0005%, Ti BDL, Na <0.01%

*BDL-Below detectable limits*

In TG-DTA studies, several batches of 50g base salt mixture of LiF-BaF<sub>2</sub> 1:1 mole ratio was prepared. 43.55g of BaF<sub>2</sub> and 6.45g of LiF were weighed in a Mettler Toledo make, Model No. AX205 balance with 0.01mg accuracy. Weighed salt mixtures were then hand mixed in a 100mm dia agate mortar and pestle for approximately 45 minutes for uniform mixing. These premixed salts were carefully transferred to a high density graphite crucible (~1.98 g/cc) of 50.8mm OD at the top and 27mm OD at the bottom with a uniform wall thickness of 2.4mm. Compaction of powders was done with a pestle to accommodate the powder in the graphite crucible, and the crucible was transferred to a desiccator. For melting, the crucible was placed on the alumina plate in the setup and the plate was lowered into the inconel muffle.

After tightening all the fasteners, the system was leak tested by soap bubble test for any obvious leaks. Before commencement of heating, the inconel muffle was evacuated to  $1\text{E-}2$  mbar and back filled with high purity argon having  $<0.1\text{ppm}$  of oxygen. The evacuation and back filling operation was done 9-10 times before start of heating the salt mixture. Continuous flow of argon purge gas was maintained during heating and cooling of the salt mixture. The assembly was heated at a rate of  $5\text{K}/\text{min}$  to  $673\text{K}$  and was soaked for 24hrs to remove any volatile impurities and moisture. Thereafter, the temperature was increased to  $1273\text{K}$  at the rate of  $5\text{K}/\text{min}$  and held for 4 hours. Cooling was done at  $10\text{K}/\text{min}$  to room temperature. The assembly was opened and the entire contents of the crucible was ground in a  $100\text{mm}$  dia mortar and pestle for around 45 mins to remove the inhomogeneity that might have developed by stratification during the cooling cycle. The ground mixture was transferred to airtight containers and stored in a desiccator. Samples were taken from this prepared stock for TG-DTA analysis. Identical procedure was followed in preparation of all the other salt mixtures of  $\text{LiF-CaF}_2$ ,  $\text{LiF-CaF}_2\text{-LaF}_3$  and  $\text{LiF-BaF}_2\text{-LaF}_3$  for TG-DTA analysis.

### **3.2.4 TG-DTA experiments**

TG-DTA experiments were conducted in a SETARAM make TG-DTA apparatus model number D17. Simultaneous thermogravimetry and DTA curves were followed with temperature and recorded using a data acquisition system connected to a computer. The temperature was controlled by a PID controller within limits of  $\pm 1\text{K}$ , and the heating rates employed were  $10\text{ K}/\text{min}$ . The facility was available in the model to program the thermal cycle, soaking and cooling rates. After the sample was loaded argon was purged for 45 minutes continuously. Argon purging was continued during the experiment. The weight loss was recorded with a sensitivity of  $0.01\text{ mg}$

and the sensitivity of heat flow measurement in the DTA experiments was 0.01 mW. All the reported data were recorded while heating the sample.

Approximately 80 mg of salt sample was taken in either a platinum or a graphite crucible. Standard alumina powder reference was taken in another crucible. These crucibles (one containing the sample and another containing the reference) were loaded into the TG/DTA system (SETARAM). The sample was heated at the rate of 10 K/min to 1473K. It was held at 1473K for 2 hours, followed by cooling at the rate of 10K/min up to 873K. Afterwards, the temperature was brought down by natural cooling. Three samples were base salt LiF:CaF<sub>2</sub> with 5%, 10%, and 15% LaF<sub>3</sub>. 3 samples were of LiF-BaF<sub>2</sub> base salt with 5%, 20% and 30% UF<sub>4</sub> and three more samples were of LiF-BaF<sub>2</sub> base salt with 5%, 20% and 30% LaF<sub>3</sub> respectively. The melting points and the evaporation losses observed in the experiments are listed in Table 3.3. It is seen that the melting points of all the salt mixtures are below 1100K. During the electrolysis process, the salt mixtures are heated to more than 300K above the melting point, where the viscosity is lower. Although lower viscosity is desirable for better mixing due to convective currents, leading to increase in the rate of dissolution of uranium oxide, it may pose a problem of mixing the anolyte with the catholyte.

Table 3.3 Melting points and weight loss of different fluoride electrolytes

S.no	Salt Composition	Melting peaks (K)	Weight loss, % in 2hrs
1	LiF:CaF <sub>2</sub> (6:4)-5 Wt % LaF <sub>3</sub>	974 1018	0.8
2	LiF:CaF <sub>2</sub> (6:4)-10 Wt % LaF <sub>3</sub>	974 1017.8	0.76
3	LiF:CaF <sub>2</sub> (6:4)-20 Wt % LaF <sub>3</sub>	974 1017	0.75
4	LiF:BaF <sub>2</sub> (1:1)-5 Wt % UF <sub>4</sub>	1094.6	0.625
5	LiF:BaF <sub>2</sub> (1:1)-20 Wt % UF <sub>4</sub>	1071.27	1.314
6	LiF:BaF <sub>2</sub> (1:1)-30 Wt % UF <sub>4</sub>	1071.98	1.023
7	LiF:BaF <sub>2</sub> (1:1)-5 Wt % LaF <sub>3</sub>	1054.33 1094.17	0.409
8	LiF:BaF <sub>2</sub> (1:1)-20 Wt % LaF <sub>3</sub>	984.7 1018.14	0.469
9	LiF:BaF <sub>2</sub> (1:1)-30 Wt % LaF <sub>3</sub>	984.78 1018.55	0.351

It can be seen from the data that the melting peaks of LiF:CaF<sub>2</sub>(6:4)-LaF<sub>3</sub> mixtures were not influenced by the concentration of LaF<sub>3</sub>. In LiF:BaF<sub>2</sub> base salts, addition of UF<sub>4</sub> and LaF<sub>3</sub> resulted in lowering of the melting point upto 20% and further increase of UF<sub>4</sub> or LaF<sub>3</sub> concentration had no effect on the melting peaks. Phases present at room temperature were investigated by XRD to determine the stable phases present. A typical XRD pattern of a salt mixture, LiF: BaF<sub>2</sub> (1:1 mole ratio) and 20 Wt % LaF<sub>3</sub> salt mixture was as shown in figure 3.7. This shows the presence of two compounds

in the salt mixture. Peaks marked 'A' correspond to the compound  $\text{LiBaF}_3$  and peaks marked 'B' correspond to compound  $\text{Ba}_2\text{LaF}_7$ . Other than these compounds no individual lines of the salts present were found. Figure 3.8 shows the XRD pattern of  $\text{LiF}:\text{BaF}_2$  (1:1 mole ratio) and 20 Wt %  $\text{UF}_4$  salt mixture. The peaks marked 'A' correspond to the phase  $\text{LiBaF}_3$  and peaks marked 'B' correspond to the  $\text{BaF}_2\text{-UF}_4$  solid solution.

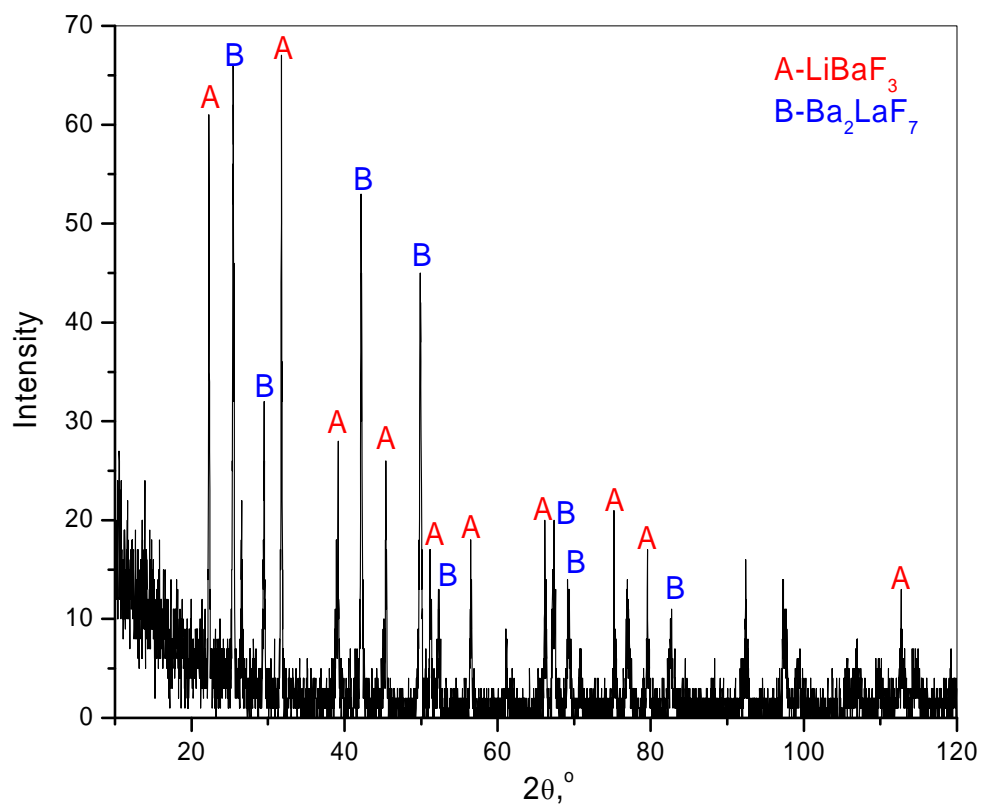


Figure 3.7 XRD pattern of  $\text{LiF}:\text{BaF}_2$  (1:1 mole ratio) and 20 Wt %  $\text{LaF}_3$  frozen salt mixture

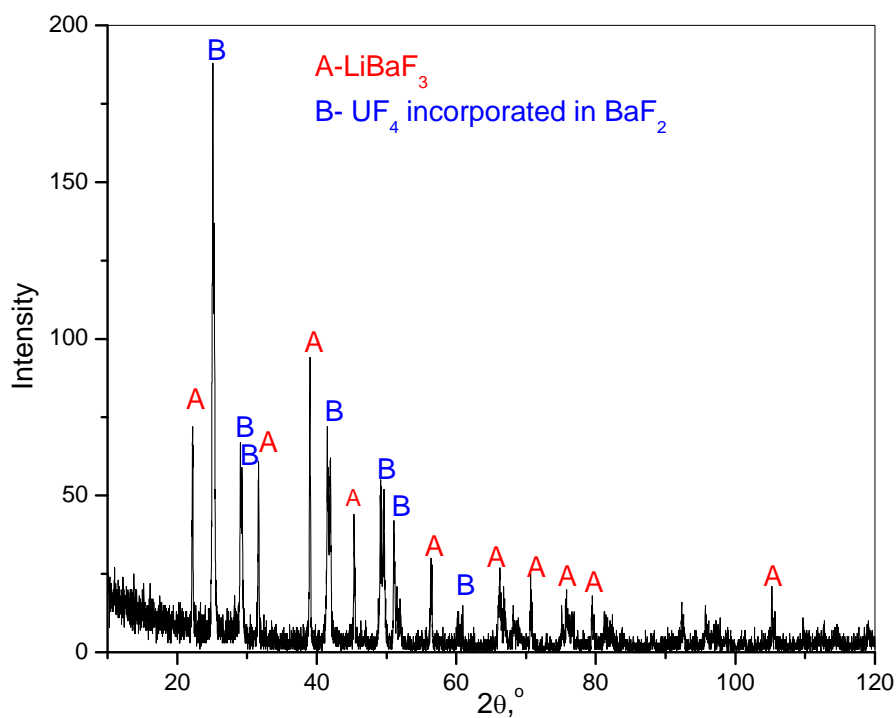


Figure 3.8 XRD pattern of LiF: BaF<sub>2</sub> (1:1 mole ratio) and 20 Wt % UF<sub>4</sub> frozen salt mixture

### 3.3 Conditioning procedure for electrolyte

Several procedures for the purification of salt melts and conditioning were studied to select a suitable one for this work. They are outlined below.

#### a. Removing moisture by vacuum drying

Water is readily removed from salts that are not strongly hydrated, by heating in vacuum. Vacuum drying at above ambient temperatures around 393K is effective in removing free moisture. However, in certain salt systems, gradual increase in temperature is required while heating because of possibility of occurrence of other reactions with the moisture. Most fluoride melts available from the suppliers are seldom free of traces of moisture.

### **b. Purification of chloride and fluoride melts by hydrogen chloride or hydrogen fluoride gas**

One of the techniques prevalent in purification of chloride and fluoride melts is to pass anhydrous hydrogen chloride gas in case of chloride melts through the mixture for sufficient length of time to displace air. The salt mixture is slowly heated, while continuing the flow of chloride gas until the mixture melts. After hydrogen chloride gas had been passed through the melt for a pre-determined time, it is replaced by a pure argon stream, to remove the dissolved hydrogen chloride gas. The procedure is identical with the fluoride salts, except that instead of hydrogen chloride gas, hydrogen fluoride gas is used in the process.

### **c. Melt purification by pre-electrolysis**

Melt purification of the molten salt by electrolysis involves in dissociating the oxygen containing impurities electrolytically. The process comprises of passing a current through a molten salt electrolyte, thereby electrolyzing a portion of the oxygen containing impurities at the anode. Care is taken that the cell voltage is well below the decomposition voltage of the principal constituent of the electrolyte. In molten salt water, oxygen and even carbon dioxide are electro active under the experimental conditions. In molten fluorides, the species  $\text{OH}^-$ ,  $\text{HF}$ ,  $\text{O}^{2-}$ ,  $\text{O}_2^{2-}$ ,  $\text{H}_2$  are derived from the atmospheric contaminants, either by chemical or electrochemical reactions. These species may themselves be reduced or oxidized at appropriate potentials. Both reduction and oxidation reactions take place simultaneously.

Factors affecting the purification process by pre-electrolysis are numerous; they include, the amount of current, the time of passage of current and the temperature of the molten salt bath. In fact, electrochemical technique has emerged as the most

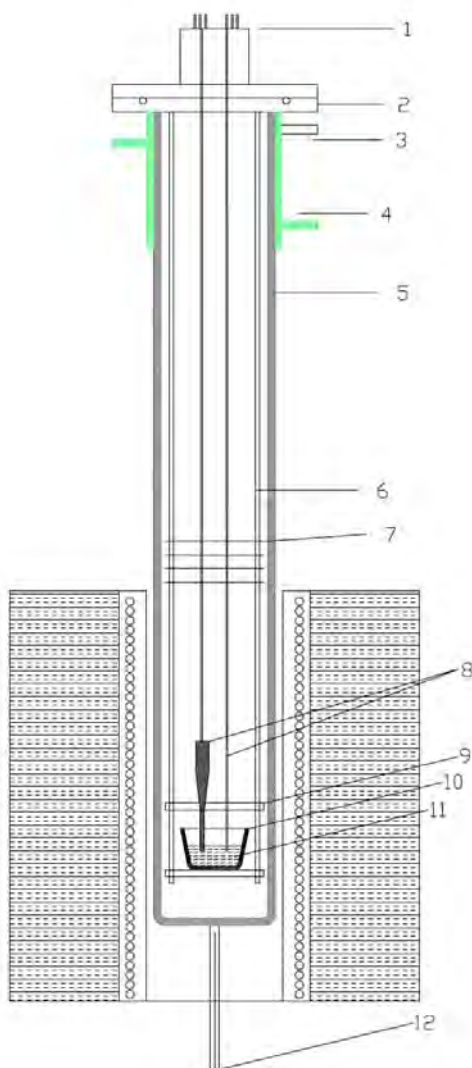
effective method for removing any kind of ionic impurities as it does not induce other undesirable elements into the salt system and it is a single step method as well as is easily operable.

### **3.3.1 Chemicals and Electrodes**

An electrode system is necessary to evaluate the effectiveness of conditioning by voltammetry. It was also used to carry out conditioning experiments by pre-electrolysis. LiF and BaF<sub>2</sub> salts used for preparation of the salt mixture were of reagent grade and the source was as described in section 3.2.3. A high density graphite electrode (density  $\geq 1.95$  g/cc, 3mm diameter) was used as the working electrode in all the experiments. A reliable reference electrode was a pre-requisite to conduct electrochemical investigations in the molten salt system. However, no reference electrode to date is available in the molten fluoride salt system to work in the range of 1200K-1500K. Hence all the experiments were conducted with a pseudo reference electrode, which was useful to compare molten salts of similar composition. When used in a different salt system, a change in its potential makes the pseudo reference electrode unfit to compare multiple salt systems. In two electrode configuration, the high density graphite crucible containing the electrolyte served both as the counter electrode and the reference electrode. In a few three electrode configuration experiments the high density graphite crucible containing the electrolyte served as the counter electrode and a 1mm dia platinum wire was used as a pseudo- reference electrode. An AUTOLAB PGSTAT 30 electrochemical workstation was used for recording the voltammograms. GPES software supplied with PGSTAT 30 was used for analysis of the voltammograms.

### 3.3.2 Apparatus and methods

All the experiments were conducted at 1173K in an inconel 600 muffle made for preparation of salt mixture. The apparatus which has been described in detail in section 3.2.1 was modified to include following additional features. In the first modification, a provision for electrical feed through was made in the flange to make connections for recording voltammograms. 4 platinum wires of 1 mm diameter and ~650mm long were brazed to the feed throughs to make the electrical connections. One platinum wire from the electrical feed through was crimped to the high density graphite electrode (density  $\geq 1.95$  g/cc, 3mm diameter) to serve as the working electrode and another platinum wire was twisted and linked to the crucible to serve as the counter electrode. The second modification was to introduce platinum wire as a pseudo reference electrode, where the wire was directly immersed 5-6mm deep into the electrolyte. The high density graphite electrode was of 8mm dia, which had a tapered section ending in 3mm dia cylinder for immersion. The electrode was supported at the tapered section by an alumina disc with 5mm dia holes. The centre to centre distance between the holes also maintained the inter-electrode distance. ~60g salt mixture prepared using the procedure described in section 3.2.3 was taken in each experiment. Before the commencement of heating, the inconel muffle was evacuated to  $1E-2$  mbar and back filled with high purity argon having  $<0.1$ ppm of oxygen. The evacuation and back filling operation were done 9-10 times before the start of heating the salt mixture. Heating to 673K (for soaking period at A) and 1173K (for soaking period at B) was at 5K/min whereas the cooling rate was 10K/min. The soaking periods A and B as shown in the plot were varied between 4 hrs and 24hrs.



- |  |   |
|--|---|
| 1. Flange with electrical feedthrough      | 2. Flange connecting Inconel 600 muffle |
| 3. Argon gas outlet                        | 4. Water cooling jacket arrangement     |
| 5. Inconel 600 muffle                      | 6. Inconel 600 hanging rods             |
| 7. Inconel 600 radiation shields           | 8. Electrodes used for voltammetry      |
| 9. Alumina electrode holder                | 10. High density graphite crucible      |
| 11. LiF-BaF <sub>2</sub> (1:1) electrolyte | 12. Argon inlet tube                    |

Figure 3.9. Schematic of experimental assembly for preconditioning of molten salt

Voltammograms were recorded during soaking at B. The heating cycle adopted is given in figure 3.10. Purified argon gas (<0.1ppm of oxygen) was purged continuously through out the experiment at 6 lph. The oxygen concentration in the

inlet gas was continuously monitored by an online oxygen gas analyzer (Systech 800 Series analyzer).

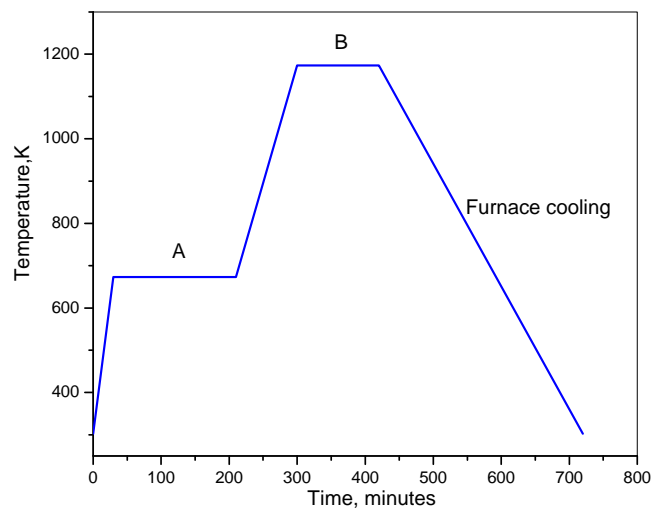


Figure 3.10. Heating cycle adopted for pre-conditioning the salt mixture

### 3.3.3 Results of experiments and selection of conditioning procedure

Figures 3.11 and 3.12 show the voltammograms at 1173K with two electrode configuration, for 4hr conditioning and 24 hour long conditioning cycles respectively.

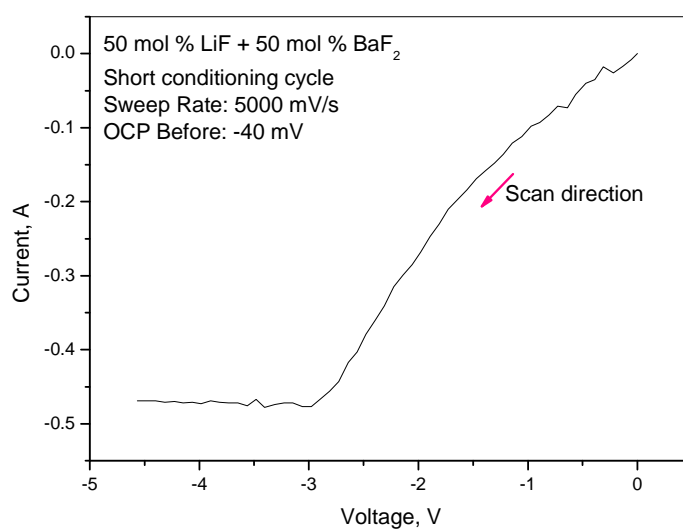


Figure 3.11 Voltammogram of LiF:BaF<sub>2</sub>(1:1) mixture, with short conditioning cycle, both graphite electrodes, at 1173K.

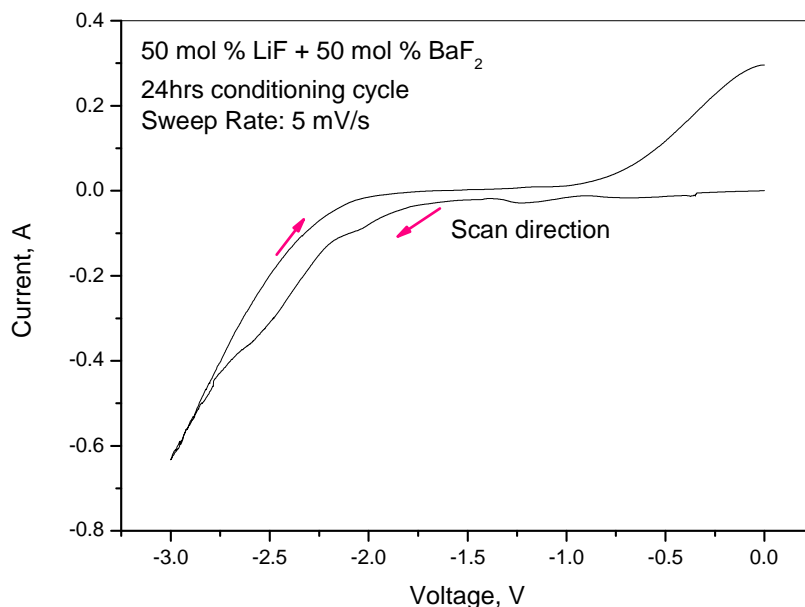


Figure 3.12 Voltammogram of LiF:BaF<sub>2</sub>(1:1) mixture, with 24hr conditioning cycle, both graphite electrodes, at 1173K.

In the plot with the 4 hours conditioning cycle, it is observed that the current linearly increased from 0mA to 475mA when the voltage was increased from 0V to 3.0V and thereafter it was almost constant at ~475mA. On the contrary, the voltammogram recorded with 24hrs conditioning cycle showed a maximum current of 110mA at 2.0V, thereafter sharply increased reaching a maximum of 800mA at 3.0V.

In both the cases beyond 2.0V lithium deposition reaction occurred on the graphite electrode. However, below 2.0V the presence of electroactive species contributed to the total current, which was much reduced in the case of the 24hrs conditioning cycle, indicating the removal of electroactive species by the long duration conditioning.

An experiment was conducted to compare the 2 electrode configuration and three electrode configuration with a pseudo reference electrode in LiF:BaF<sub>2</sub> (1:1) mixture. The sample after the 24hrs conditioning cycle was studied with a 3mm graphite electrode as the working electrode, the graphite crucible as the counter electrode and a platinum wire as the pseudo reference electrode. Figure 3.13 shows the voltammogram comparing the 2 electrode configuration and 3 electrode configurations.

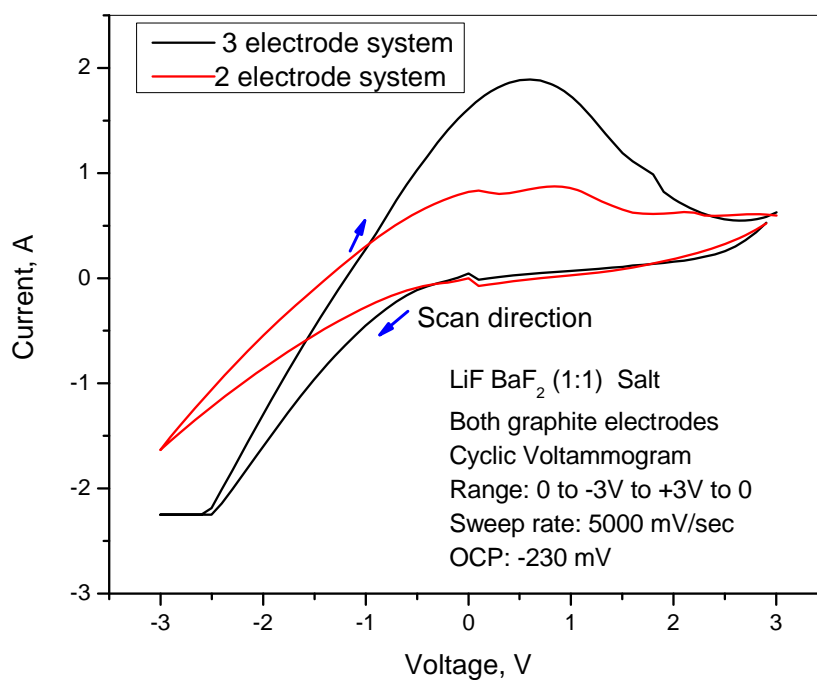


Figure 3.13. Voltammogram comparing 2 electrode configuration and 3 electrode configuration in LiF:BaF<sub>2</sub>(1:1) electrolyte at 1173K.

There were no additional reactions observed in the voltammogram of the 3 electrode system in comparison with that of the 2 electrode system. In case of the two electrode configuration, to maintain a potential of 3V on the working electrode, the potentiostat

imposed a voltage of  $\sim 4.8\text{V}$  between the counter and the working electrodes (measured with a  $1\text{E}14$  ohms impedance voltmeter). In case of the 3 electrode configuration the voltage between the counter and working electrode was measured by the voltmeter to be  $\sim 8.9\text{V}$ . The maximum currents observed at  $3\text{V}$  working electrode potential were  $1.63\text{A}$  and  $2.25\text{A}$  for 2 electrode and 3 electrode configurations respectively. Due to this additional voltage of  $\sim 4.1\text{V}$ , the current observed in the 3 electrode configuration was  $0.62\text{A}$  higher than that in the 2 electrode configuration. The peak anodic current was observed as  $1.89\text{A}$  at  $0.6\text{V}$  in the 3 electrode configuration and  $0.87\text{A}$  at  $0.9\text{V}$  in a 2 electrode configuration. With the 3 electrode configuration  $\sim 1.0\text{A}$  higher anodic current was present due to which higher current densities were reached.

LSV investigations in the as received salts and salt mixtures without any detailed conditioning procedure showed a high current flow even at very low voltages. The behavior was attributed to the presence of impurities from the salts and original salt specifications were checked. The AR grade salt composition specified by the manufacturer did not reveal any major impurities which can give rise to the huge current. The salt purity was cross checked with ICP-MS and salt was found to be relatively free of impurities which can give rise to high deposition currents at low temperatures. The crucible and electrode materials were also analyzed for the impurities present and found to be relatively free of impurities that could contribute to high deposition current. This analysis indicated that the current observed in LSV was possibly due to the impurities picked up from the environment. Impurities can be both volatile and non-volatile in nature, and by thermal conditioning of the electrolyte only volatile impurities could be removed. Volatile impurities if not removed from the salt,

can react to form non-volatile impurities. The major impurity that can be picked up from the environment is moisture, which in turn can lead to the formation of hydrogen fluoride, hydroxide or other oxy-fluoride complexes. The presence of dissolved oxygen also leads to formation of oxy-fluoride complexes, which in subsequent reduction of cations at the cathode introduces oxygen into the deposit, that is, leads to oxidation of the deposited metal. The carbon impurity in the bath seen in some of the experiments is usually from the organic impurities present in the salt. This was confirmed in the experiments when a low density graphite crucible was used which resulted in accumulation of fine particles in the electrolyte. The fine carbon particles cannot be tolerated in the process as they tend to produce large stray currents in the molten salt electrolyte.

### **3.4 Selection of materials for electrolytic cells**

The importance of selection of suitable materials for the components of the electrolytic cell has been discussed earlier in this chapter(sec 3.1.2). It is essential to generate experimental corrosion data for the materials by simulating the given conditions of the electrolytic cell, and study of the possible reactions; and their feasibility to select the targeted materials. To determine the feasibility of the reaction of the electrolyte with different materials thermodynamic calculations were performed. The free energy change for a chemical reaction is given by

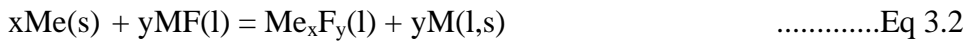
$$\Delta G = \Delta H - T\Delta S \quad \text{..... Eq 3.1}$$

where  $\Delta G$  is the free energy change in kJ/mole,  $\Delta H$  is the enthalpy in kJ/mole,  $T$  temperature in K and  $\Delta S$  is the entropy change in J/mole.K. The reaction is considered feasible if the free energy change is negative. Table 3.5 provides the free energy change, enthalpy, entropy for different reactions at 1500K [3.19].

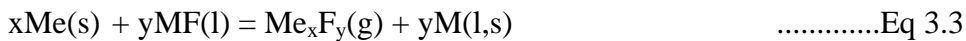
Calculations are made by ASTD ver 2.0 [3.19] based on the assumption of ideal solution behavior in the melt, as the data of activity coefficients are difficult to obtain experimentally.

### 3.4.1 Reactions of molten fluoride with metallic materials

In the absence of moisture and oxygen in the surrounding environment, corrosion reaction of a pure metal Me (Me = Fe, Ni, Cr) with fluoride ion of alkali, alkaline earth, actinide or rare earth compound MF (MF where M = Li, Ba, Ca, U, La) can be represented by



where l and s denote the liquid phase or solid phase respectively. For Ni, Cr and Fe, the corresponding compounds are NiF<sub>2</sub>, CrF<sub>2</sub>/CrF<sub>3</sub>, FeF<sub>2</sub>/FeF<sub>3</sub> respectively. In case of the refractory materials like Nb, Mo, W and Ta between 1000-1500K gaseous fluorides are the most stable phases formed and there are no stable condensed fluoride salts. The reaction with Me (Me = Nb, Mo, W, Ta) with fluoride ion of alkali, alkaline earth, actinide or rare earth compound MF (MF where M = Li, Ba, Ca, U, La) is represented by



Although the thermodynamic analysis provides the feasibility of the reaction, the extent of reaction has to be taken into consideration to evaluate the extent of corrosion. The equilibrium concentration of the respective fluorides is to be considered before the assessment of corrosion resistance of a metal against metal fluoride. Thus, when a metallic fluoride has a very low equilibrium concentration in the melt, the metal is generally expected to be corrosion resistant.

### 3.4.2 Effect of moisture

Moisture is a very common impurity in the fluoride and chloride salts and leads to deleterious effects; it is also very difficult to remove. Elaborate conditioning procedures are required to get a mixture with a very low moisture content. The presence of moisture and its reaction with fluoride salts leads to release of hydrogen fluoride gas which itself is very corrosive in nature . The possible reactions are given below



Corrosion in the electrolyte is often enhanced due to the presence of dissolved hydrogen fluoride gas, which is generated by the above reaction. Hydrogen fluoride gas leads to serious corrosion problems of metallic materials and in some cases can lead to hydrogen generation as shown by the reaction



From the above analysis, it is clear that the moisture content in the fluoride salts should be reduced to as low a level as possible for longer life of the container and structural components.

### 3.4.3 Reaction of molten fluoride salts with ceramic materials

Molten fluoride salts have fluxing properties which help in removing protective oxide scales that are generally formed on metal surfaces. The general corrosion mechanism is primarily of oxidation followed by dissolution of oxides in the melt. Presence of

oxygen and moisture aggravates the corrosion by either generation of corrosive hydrogen fluoride or formation of oxy-fluoride complexes. Due to the high temperature operation, thermal gradients are possible within the containment vessel. Natural convection between the hot and cold areas coupled with differential solubility can also lead to corrosion by dissolution in hot areas and deposition in cold areas. This type of corrosion is strongly dependent on the temperature of operation and also on the velocity of the electrolyte.

LiF, BaF<sub>2</sub>, UF<sub>4</sub> and LaF<sub>3</sub> are thermodynamically more stable than fluorides of iron, copper, nickel, and tin at 1500K. Similarly, there are no stable compounds of tantalum, molybdenum, and tungsten which can form by reaction with LiF, BaF<sub>2</sub>, UF<sub>4</sub> and LaF<sub>3</sub> at 1500K. However, ceramic oxides are found to react with UF<sub>4</sub>. The thermodynamic calculations of reaction between fluoride salts and different materials at 1500K is presented in Table 3.4.

Table 3.4 Thermodynamic calculations of reaction between fluoride salts and different materials at 1500K ('c' denotes condensed phase, and 'g' denotes gaseous phase)

S.no	Reaction	$\Delta S$ , J/mole K	$\Delta H$ , kJ/mole	$\Delta G$ , kJ/mole
1.	$4\text{LiF(c)}+2\text{Fe(c)}=4\text{Li(c)}+\text{Fe}_2\text{F}_4\text{(g)}$	1.59E+02	1.25E+03	1.01E+03
2.	$6\text{LiF(c)}+2\text{Fe(c)}=6\text{Li(c)}+\text{Fe}_2\text{F}_6\text{(g)}$	1.62E+02	1.83E+03	1.59E+03
3.	$\text{LiF(c)}+\text{Fe(c)}=\text{Li(c)}+\text{FeF(g)}$	1.57E+02	5.84E+02	3.48E+02
4.	$2\text{LiF(c)}+\text{Fe(c)}=2\text{Li(c)}+\text{FeF}_2\text{(g)}$	1.56E+02	7.14E+02	4.80E+02
5.	$2\text{LiF(c)}+\text{Fe(c)}=2\text{Li(c)}+\text{FeF}_2\text{(c)}$	2.73E+01	4.95E+02	4.54E+02
6.	$3\text{LiF(c)}+\text{Fe(c)}=3\text{Li(c)}+\text{FeF}_3\text{(c)}$	-5.30E+00	7.66E+02	7.74E+02
7.	$3\text{LiF(c)}+\text{Fe(c)}=3\text{Li(c)}+\text{FeF}_3\text{(g)}$	1.56E+02	1.01E+03	7.76E+02
8.	$3\text{BaF}_2\text{(c)}+2\text{Fe(c)}=3\text{Ba(c)}+2\text{FeF}_3\text{(g)}$	3.61E+02	2.04E+03	1.49E+03

S.no	Reaction	$\Delta S$ , J/mole K	$\Delta H$ , kJ/mole	$\Delta G$ , kJ/mole
9.	$3\text{BaF}_2(\text{c})+2\text{Fe}(\text{c})=3\text{Ba}(\text{c})+2\text{FeF}_3(\text{c})$	3.87E+01	1.55E+03	1.49E+03
10.	$\text{BaF}_2(\text{c})+\text{Fe}(\text{c})=\text{Ba}(\text{c})+\text{FeF}_2(\text{c})$	4.37E+01	5.00E+02	4.35E+02
11.	$\text{BaF}_2(\text{c})+\text{Fe}(\text{c})=\text{Ba}(\text{c})+\text{FeF}_2(\text{g})$	1.72E+02	7.19E+02	4.61E+02
12.	$\text{BaF}_2(\text{c})+2\text{Fe}(\text{c})=\text{Ba}(\text{c})+2\text{FeF}(\text{g})$	3.31E+02	1.17E+03	6.76E+02
13.	$2\text{BaF}_2(\text{c})+2\text{Fe}(\text{c})=2\text{Ba}(\text{c})+\text{Fe}_2\text{F}_4(\text{g})$	1.92E+02	1.26E+03	9.69E+02
14.	$3\text{BaF}_2(\text{c})+2\text{Fe}(\text{c})=3\text{Ba}(\text{c})+\text{Fe}_2\text{F}_6(\text{g})$	2.11E+02	1.85E+03	1.53E+03
15.	$\text{UF}_4(\text{c})+2\text{Fe}(\text{c})=\text{U}(\text{c})+\text{Fe}_2\text{F}_4(\text{g})$	1.40E+02	7.75E+02	5.65E+02
16.	$3\text{UF}_4(\text{c})+4\text{Fe}(\text{c})=3\text{U}(\text{c})+2\text{Fe}_2\text{F}_6(\text{g})$	2.66E+02	2.25E+03	1.85E+03
17.	$\text{UF}_4(\text{c})+4\text{Fe}(\text{c})=\text{U}(\text{c})+4\text{FeF}(\text{g})$	6.10E+02	1.86E+03	9.49E+02
18.	$\text{UF}_4(\text{c})+2\text{Fe}(\text{c})=\text{U}(\text{c})+2\text{FeF}_2(\text{c})$	3.56E+01	5.19E+02	4.66E+02
19.	$\text{UF}_4(\text{c})+2\text{Fe}(\text{c})=\text{U}(\text{c})+2\text{FeF}_2(\text{g})$	2.92E+02	9.57E+02	5.18E+02
20.	$3\text{UF}_4(\text{c})+4\text{Fe}(\text{c})=3\text{U}(\text{c})+4\text{FeF}_3(\text{g})$	5.66E+02	2.63E+03	1.78E+03
21.	$3\text{UF}_4(\text{c})+4\text{Fe}(\text{c})=3\text{U}(\text{c})+4\text{FeF}_3(\text{c})$	-7.81E+01	1.65E+03	1.77E+03
22.	$4\text{LaF}_3(\text{c})+6\text{Fe}(\text{c})=4\text{La}(\text{c})+3\text{Fe}_2\text{F}_4(\text{g})$	6.14E+02	3.59E+03	2.67E+03
23.	$2\text{LaF}_3(\text{c})+2\text{Fe}(\text{c})=2\text{La}(\text{c})+\text{Fe}_2\text{F}_6(\text{g})$	2.30E+02	1.76E+03	1.42E+03
24.	$\text{LaF}_3(\text{c})+3\text{Fe}(\text{c})=\text{La}(\text{c})+3\text{FeF}(\text{g})$	5.06E+02	1.72E+03	9.56E+02
25.	$2\text{LaF}_3(\text{c})+3\text{Fe}(\text{c})=2\text{La}(\text{c})+3\text{FeF}_2(\text{g})$	1.503E+02	1.413E+03	1.187E+03
26.	$\text{LaF}_3(\text{c})+\text{Fe}(\text{c})=\text{La}(\text{c})+\text{FeF}_3(\text{c})$	2.89E+01	7.30E+02	6.87E+02
27.	$\text{LaF}_3(\text{c})+\text{Fe}(\text{c})=\text{La}(\text{c})+\text{FeF}_3(\text{g})$	1.90E+02	9.73E+02	6.89E+02
28.	$\text{LiF}(\text{c})+\text{Ni}(\text{c})=\text{Li}(\text{c})+\text{NiF}(\text{g})$	1.54E+02	6.54E+02	4.24E+02
29.	$2\text{LiF}(\text{c})+\text{Ni}(\text{c})=2\text{Li}(\text{c})+\text{NiF}_2(\text{g})$	1.57E+02	8.17E+02	5.81E+02
30.	$2\text{LiF}(\text{c})+\text{Ni}(\text{c})=2\text{Li}(\text{c})+\text{NiF}_2(\text{c})$	-1.47E+01	5.19E+02	5.41E+02
31.	$\text{BaF}_2(\text{c})+\text{Ni}(\text{c})=\text{Ba}(\text{c})+\text{NiF}_2(\text{c})$	1.79E+00	5.24E+02	5.22E+02
32.	$\text{BaF}_2(\text{c})+\text{Ni}(\text{c})=\text{Ba}(\text{c})+\text{NiF}_2(\text{g})$	1.74E+02	8.22E+02	5.62E+02
33.	$\text{BaF}_2(\text{c})+2\text{Ni}(\text{c})=\text{Ba}(\text{c})+2\text{NiF}(\text{g})$	3.24E+02	1.31E+03	8.28E+02
34.	$\text{UF}_4(\text{c})+4\text{Ni}(\text{c})=\text{U}(\text{c})+4\text{NiF}(\text{g})$	5.96E+02	2.15E+03	1.25E+03
35.	$\text{UF}_4(\text{c})+2\text{Ni}(\text{c})=\text{U}(\text{c})+2\text{NiF}_2(\text{g})$	2.96E+02	1.16E+03	7.20E+02
36.	$\text{UF}_4(\text{c})+2\text{Ni}(\text{c})=\text{U}(\text{c})+2\text{NiF}_2(\text{c})$	-4.83E+01	5.68E+02	6.40E+02
37.	$2\text{LaF}_3(\text{c})+3\text{Ni}(\text{c})=2\text{La}(\text{c})+3\text{NiF}_2(\text{c})$	2.45E+01	1.49E+03	1.45E+03
38.	$2\text{LaF}_3(\text{c})+3\text{Ni}(\text{c})=2\text{La}(\text{c})+3\text{NiF}_2(\text{g})$	5.41E+02	2.38E+03	1.57E+03
39.	$\text{LaF}_3(\text{c})+3\text{Ni}(\text{c})=\text{La}(\text{c})+3\text{NiF}(\text{g})$	4.95E+02	1.93E+03	1.18E+03

S.no	Reaction	$\Delta S$ , J/mole K	$\Delta H$ , kJ/mole	$\Delta G$ , kJ/mole
40.	$\text{LiF(c)}+\text{Mo(c)}=\text{Li(c)}+\text{MoF(g)}$	1.68E+02	8.41E+02	5.89E+02
41.	$2\text{LiF(c)}+\text{Mo(c)}=2\text{Li(c)}+\text{MoF}_2\text{(g)}$	1.63E+02	9.89E+02	7.45E+02
42.	$3\text{LiF(c)}+\text{Mo(c)}=3\text{Li(c)}+\text{MoF}_3\text{(g)}$	1.62E+02	1.15E+03	9.10E+02
43.	$4\text{LiF(c)}+\text{Mo(c)}=4\text{Li(c)}+\text{MoF}_4\text{(g)}$	1.82E+02	1.39E+03	1.11E+03
44.	$6\text{LiF(c)}+\text{Mo(c)}=6\text{Li(c)}+\text{MoF}_6\text{(g)}$	1.26E+02	1.95E+03	1.76E+03
45.	$6\text{LiF(c)}+\text{Mo(c)}=6\text{Li(c)}+\text{MoF}_6\text{(c)}$	1.23E+02	1.99E+03	1.81E+03
46.	$5\text{LiF(c)}+\text{Mo(c)}=5\text{Li(c)}+\text{MoF}_5\text{(c)}$	2.67E+01	1.59E+03	1.55E+03
47.	$3\text{LiF(c)}+\text{Mo(c)}=3\text{Li(c)}+\text{MoF}_3\text{(c)}$	-2.80E+00	8.68E+02	8.72E+02
48.	$\text{BaF}_2\text{(c)}+2\text{Mo(c)}=\text{Ba(c)}+2\text{MoF(g)}$	3.52E+02	1.69E+03	1.16E+03
49.	$\text{BaF}_2\text{(c)}+\text{Mo(c)}=\text{Ba(c)}+\text{MoF}_2\text{(g)}$	1.79E+02	9.95E+02	7.26E+02
50.	$3\text{BaF}_2\text{(c)}+2\text{Mo(c)}=3\text{Ba(c)}+2\text{MoF}_3\text{(g)}$	3.73E+02	2.32E+03	1.76E+03
51.	$2\text{BaF}_2\text{(c)}+\text{Mo(c)}=2\text{Ba(c)}+\text{MoF}_4\text{(g)}$	2.15E+02	1.40E+03	1.07E+03
52.	$3\text{BaF}_2\text{(c)}+\text{Mo(c)}=3\text{Ba(c)}+\text{MoF}_6\text{(g)}$	1.75E+02	1.97E+03	1.71E+03
53.	$3\text{BaF}_2\text{(c)}+\text{Mo(c)}=3\text{Ba(c)}+\text{MoF}_6\text{(c)}$	1.72E+02	2.00E+03	1.75E+03
54.	$5\text{BaF}_2\text{(c)}+2\text{Mo(c)}=5\text{Ba(c)}+2\text{MoF}_5\text{(c)}$	1.36E+02	3.20E+03	3.00E+03
55.	$3\text{BaF}_2\text{(c)}+2\text{Mo(c)}=3\text{Ba(c)}+2\text{MoF}_3\text{(c)}$	4.37E+01	1.75E+03	1.69E+03
56.	$\text{UF}_4\text{(c)}+4\text{Mo(c)}=\text{U(c)}+4\text{MoF(g)}$	6.52E+02	2.89E+03	1.92E+03
57.	$\text{UF}_4\text{(c)}+2\text{Mo(c)}=\text{U(c)}+2\text{MoF}_2\text{(g)}$	3.07E+02	1.51E+03	1.05E+03
58.	$\text{UF}_4\text{(c)}+2\text{Mo(c)}=\text{U(c)}+2\text{MoF}_3\text{(g)}$	5.91E+02	3.20E+03	2.31E+03
59.	$\text{UF}_4\text{(c)}+\text{Mo(c)}=\text{U(c)}+\text{MoF}_4\text{(g)}$	1.63E+02	9.14E+02	6.69E+02
60.	$3\text{UF}_4\text{(c)}+2\text{Mo(c)}=3\text{U(c)}+2\text{MoF}_6\text{(g)}$	1.94E+02	2.49E+03	2.20E+03
61.	$3\text{UF}_4\text{(c)}+2\text{Mo(c)}=3\text{U(c)}+2\text{MoF}_6\text{(c)}$	1.88E+02	2.56E+03	2.28E+03
62.	$5\text{UF}_4\text{(c)}+4\text{Mo(c)}=5\text{U(c)}+4\text{MoF}_5\text{(c)}$	5.57E+02	2.90E+03	2.06E+03
63.	$\text{LaF}_3\text{(c)}+\text{Mo(c)}=\text{La(c)}+\text{MoF}_3\text{(g)}$	1.96E+02	1.12E+03	8.23E+02
64.	$4\text{LaF}_3\text{(c)}+3\text{Mo(c)}=4\text{La(c)}+3\text{MoF}_4\text{(g)}$	6.82E+02	4.01E+03	2.99E+03
65.	$2\text{LaF}_3\text{(c)}+\text{Mo(c)}=2\text{La(c)}+\text{MoF}_6\text{(g)}$	1.94E+02	1.88E+03	1.59E+03
66.	$2\text{LaF}_3\text{(c)}+\text{Mo(c)}=2\text{La(c)}+\text{MoF}_6\text{(c)}$	1.91E+02	1.92E+03	1.63E+03
67.	$5\text{LaF}_3\text{(c)}+3\text{Mo(c)}=5\text{La(c)}+3\text{MoF}_5\text{(c)}$	2.51E+02	4.58E+03	4.20E+03
68.	$\text{LaF}_3\text{(c)}+\text{Mo(c)}=\text{La(c)}+\text{MoF}_3\text{(c)}$	3.14E+01	8.32E+02	7.85E+02
69.	$\text{LiF(c)}+\text{Ta(c)}=\text{Li(c)}+\text{TaF(g)}$	1.58E+02	8.30E+02	5.93E+02
70.	$2\text{LiF(c)}+\text{Ta(c)}=2\text{Li(c)}+\text{TaF}_2\text{(g)}$	1.65E+02	8.92E+02	6.45E+02

S.no	Reaction	$\Delta S$ , J/mole K	$\Delta H$ , kJ/mole	$\Delta G$ , kJ/mole
71.	$3\text{LiF(c)}+\text{Ta(c)}=3\text{Li(c)}+\text{TaF3(g)}$	1.35E+02	9.55E+02	7.53E+02
72.	$4\text{LiF(c)}+\text{Ta(c)}=4\text{Li(c)}+\text{TaF4(g)}$	1.43E+02	1.02E+03	8.09E+02
73.	$5\text{LiF(c)}+\text{Ta(c)}=5\text{Li(c)}+\text{TaF5(g)}$	1.38E+02	1.15E+03	9.39E+02
74.	$5\text{LiF(c)}+\text{Ta(c)}=5\text{Li(c)}+\text{TaF5(c)}$	4.75E+01	1.07E+03	9.94E+02
75.	$3\text{LiF(c)}+\text{Ta(c)}=3\text{Li(c)}+\text{TaF3(c)}$	2.26E+01	4.43E+02	4.09E+02
76.	$\text{BaF2(c)}+2\text{Ta(c)}=\text{Ba(c)}+2\text{TaF(g)}$	3.33E+02	1.67E+03	1.17E+03
77.	$\text{BaF2(c)}+\text{Ta(c)}=\text{Ba(c)}+\text{TaF2(g)}$	1.81E+02	8.97E+02	6.26E+02
78.	$3\text{BaF2(c)}+2\text{Ta(c)}=3\text{Ba(c)}+2\text{TaF3(g)}$	3.19E+02	1.93E+03	1.45E+03
79.	$2\text{BaF2(c)}+\text{Ta(c)}=2\text{Ba(c)}+\text{TaF4(g)}$	1.75E+02	1.03E+03	7.70E+02
80.	$5\text{BaF2(c)}+2\text{Ta(c)}=5\text{Ba(c)}+2\text{TaF5(g)}$	3.58E+02	2.32E+03	1.78E+03
81.	$5\text{BaF2(c)}+2\text{Ta(c)}=5\text{Ba(c)}+2\text{TaF5(c)}$	1.77E+02	2.16E+03	1.89E+03
82.	$3\text{BaF2(c)}+2\text{Ta(c)}=3\text{Ba(c)}+2\text{TaF3(c)}$	9.35E+01	1.44E+03	1.30E+03
83.	$\text{BaF2(c)}+\text{Ta(c)}=\text{Ba(c)}+\text{TaF2(c)}$	3.90E+01	4.48E+02	3.89E+02
84.	$\text{UF4(c)}+4\text{Ta(c)}=\text{U(c)}+4\text{TaF(g)}$	6.14E+02	2.85E+03	1.93E+03
85.	$\text{UF4(c)}+2\text{Ta(c)}=\text{U(c)}+2\text{TaF2(g)}$	3.10E+02	1.31E+03	8.48E+02
86.	$3\text{UF4(c)}+4\text{Ta(c)}=3\text{U(c)}+4\text{TaF3(g)}$	4.82E+02	2.41E+03	1.69E+03
87.	$\text{UF4(c)}+\text{Ta(c)}=\text{U(c)}+\text{TaF4(g)}$	1.24E+02	5.51E+02	3.66E+02
88.	$5\text{UF4(c)}+4\text{Ta(c)}=5\text{U(c)}+4\text{TaF5(g)}$	4.56E+02	2.23E+03	1.54E+03
89.	$5\text{UF4(c)}+4\text{Ta(c)}=5\text{U(c)}+4\text{TaF5(c)}$	9.52E+01	1.91E+03	1.76E+03
90.	$3\text{UF4(c)}+4\text{Ta(c)}=3\text{U(c)}+4\text{TaF3(c)}$	3.14E+01	1.44E+03	1.39E+03
91.	$\text{UF4(c)}+2\text{Ta(c)}=\text{U(c)}+2\text{TaF2(c)}$	2.62E+01	4.14E+02	3.75E+02
92.	$\text{LaF3(c)}+3\text{Ta(c)}=\text{La(c)}+3\text{TaF(g)}$	5.09E+02	2.46E+03	1.69E+03
93.	$2\text{LaF3(c)}+3\text{Ta(c)}=2\text{La(c)}+3\text{TaF2(g)}$	5.62E+02	2.60E+03	1.76E+03
94.	$\text{LaF3(c)}+\text{Ta(c)}=\text{La(c)}+\text{TaF3(g)}$	1.69E+02	9.19E+02	6.66E+02
95.	$4\text{LaF3(c)}+3\text{Ta(c)}=4\text{La(c)}+3\text{TaF4(g)}$	5.64E+02	2.92E+03	2.08E+03
96.	$5\text{LaF3(c)}+3\text{Ta(c)}=5\text{La(c)}+3\text{TaF5(g)}$	5.85E+02	3.26E+03	2.38E+03
97.	$5\text{LaF3(c)}+3\text{Ta(c)}=5\text{La(c)}+3\text{TaF5(c)}$	3.14E+02	3.01E+03	2.54E+03
98.	$\text{LaF3(c)}+\text{Ta(c)}=\text{La(c)}+\text{TaF3(c)}$	5.63E+01	6.76E+02	5.92E+02
99.	$2\text{LaF3(c)}+3\text{Ta(c)}=2\text{La(c)}+3\text{TaF2(c)}$	1.36E+02	1.26E+03	1.05E+03
100.	$\text{LiF(c)}+\text{W(c)}=\text{Li(c)}+\text{WF(g)}$	1.74E+02	9.61E+02	6.99E+02
101.	$2\text{LiF(c)}+\text{W(c)}=2\text{Li(c)}+\text{WF2(g)}$	1.66E+02	1.07E+03	8.26E+02

S.no	Reaction	$\Delta S$ , J/mole K	$\Delta H$ , kJ/mole	$\Delta G$ , kJ/mole
102.	$3\text{LiF(c)}+\text{W(c)}=3\text{Li(c)}+\text{WF3(g)}$	1.65E+02	1.24E+03	9.90E+02
103.	$4\text{LiF(c)}+\text{W(c)}=4\text{Li(c)}+\text{WF4(g)}$	1.78E+02	1.41E+03	1.14E+03
104.	$5\text{LiF(c)}+\text{W(c)}=5\text{Li(c)}+\text{WF5(g)}$	1.71E+02	1.63E+03	1.38E+03
105.	$6\text{LiF(c)}+\text{W(c)}=6\text{Li(c)}+\text{WF6(g)}$	1.12E+02	1.79E+03	1.62E+03
106.	$6\text{LiF(c)}+\text{W(c)}=6\text{Li(c)}+\text{WF6(c)}$	7.97E+01	1.79E+03	1.67E+03
107.	$5\text{LiF(c)}+\text{W(c)}=5\text{Li(c)}+\text{WF5(c)}$	2.96E+01	1.53E+03	1.48E+03
108.	$4\text{LiF(c)}+\text{W(c)}=4\text{Li(c)}+\text{WF4(c)}$	2.18E+01	1.14E+03	1.11E+03
109.	$\text{BaF2(c)}+2\text{W(c)}=\text{Ba(c)}+2\text{WF(g)}$	3.65E+02	1.93E+03	1.38E+03
110.	$\text{BaF2(c)}+\text{W(c)}=\text{Ba(c)}+\text{WF2(g)}$	1.82E+02	1.08E+03	8.06E+02
111.	$3\text{BaF2(c)}+2\text{W(c)}=3\text{Ba(c)}+2\text{WF3(g)}$	3.80E+02	2.49E+03	1.92E+03
112.	$2\text{BaF2(c)}+\text{W(c)}=2\text{Ba(c)}+\text{WF4(g)}$	2.11E+02	1.42E+03	1.10E+03
113.	$5\text{BaF2(c)}+2\text{W(c)}=5\text{Ba(c)}+2\text{WF5(g)}$	4.24E+02	3.29E+03	2.66E+03
114.	$3\text{BaF2(c)}+\text{W(c)}=3\text{Ba(c)}+\text{WF6(g)}$	1.61E+02	1.80E+03	1.56E+03
115.	$3\text{BaF2(c)}+\text{W(c)}=3\text{Ba(c)}+\text{WF6(c)}$	1.29E+02	1.80E+03	1.61E+03
116.	$5\text{BaF2(c)}+2\text{W(c)}=5\text{Ba(c)}+2\text{WF5(c)}$	1.41E+02	3.08E+03	2.87E+03
117.	$2\text{BaF2(c)}+\text{W(c)}=2\text{Ba(c)}+\text{WF4(c)}$	5.47E+01	1.15E+03	1.07E+03
118.	$\text{UF4(c)}+4\text{W(c)}=\text{U(c)}+4\text{WF(g)}$	6.79E+02	3.37E+03	2.35E+03
119.	$\text{UF4(c)}+2\text{W(c)}=\text{U(c)}+2\text{WF2(g)}$	3.12E+02	1.68E+03	1.21E+03
120.	$3\text{UF4(c)}+4\text{W(c)}=3\text{U(c)}+4\text{WF3(g)}$	6.04E+02	3.54E+03	2.63E+03
121.	$\text{UF4(c)}+\text{W(c)}=\text{U(c)}+\text{WF4(g)}$	1.59E+02	9.38E+02	6.99E+02
122.	$5\text{UF4(c)}+4\text{W(c)}=5\text{U(c)}+4\text{WF5(g)}$	5.89E+02	4.18E+03	3.30E+03
123.	$3\text{UF4(c)}+2\text{W(c)}=3\text{U(c)}+2\text{WF6(g)}$	1.67E+02	2.16E+03	1.91E+03
124.	$3\text{UF4(c)}+2\text{W(c)}=3\text{U(c)}+2\text{WF6(c)}$	1.03E+02	2.16E+03	2.01E+03
125.	$5\text{UF4(c)}+4\text{W(c)}=5\text{U(c)}+4\text{WF5(c)}$	2.35E+01	3.76E+03	3.72E+03
126.	$\text{UF4(c)}+\text{W(c)}=\text{U(c)}+\text{WF4(c)}$	2.82E+00	6.68E+02	6.63E+02
127.	$\text{LaF3(c)}+3\text{W(c)}=\text{La(c)}+3\text{WF(g)}$	5.57E+02	2.85E+03	2.01E+03
128.	$2\text{LaF3(c)}+3\text{W(c)}=2\text{La(c)}+3\text{WF2(g)}$	5.65E+02	3.15E+03	2.30E+03
129.	$\text{LaF3(c)}+\text{W(c)}=\text{La(c)}+\text{WF3(g)}$	1.99E+02	1.20E+03	9.02E+02
130.	$4\text{LaF3(c)}+3\text{W(c)}=4\text{La(c)}+3\text{WF4(g)}$	6.71E+02	4.08E+03	3.08E+03
131.	$5\text{LaF3(c)}+3\text{W(c)}=5\text{La(c)}+3\text{WF5(g)}$	6.84E+02	4.72E+03	3.69E+03
132.	$2\text{LaF3(c)}+\text{W(c)}=2\text{La(c)}+\text{WF6(g)}$	1.80E+02	1.72E+03	1.45E+03

S.no	Reaction	$\Delta S$ , J/mole K	$\Delta H$ , kJ/mole	$\Delta G$ , kJ/mole
133.	$2\text{LaF}_3(\text{c})+\text{W}(\text{c})=2\text{La}(\text{c})+\text{WF}_6(\text{c})$	1.48E+02	1.72E+03	1.49E+03
134.	$5\text{LaF}_3(\text{c})+3\text{W}(\text{c})=5\text{La}(\text{c})+3\text{WF}_5(\text{c})$	2.60E+02	4.40E+03	4.01E+03
135.	$4\text{LaF}_3(\text{c})+3\text{W}(\text{c})=4\text{La}(\text{c})+3\text{WF}_4(\text{c})$	2.02E+02	3.27E+03	2.97E+03
136.	$\text{LiF}(\text{c})+\text{Cu}(\text{c})=\text{Li}(\text{c})+\text{CuF}(\text{g})$	1.33E+02	5.51E+02	3.51E+02
137.	$2\text{LiF}(\text{c})+\text{Cu}(\text{c})=2\text{Li}(\text{c})+\text{CuF}_2(\text{g})$	1.35E+02	8.70E+02	6.67E+02
138.	$2\text{LiF}(\text{c})+2\text{Cu}(\text{c})=2\text{Li}(\text{c})+\text{Cu}_2\text{F}_2(\text{g})$	1.36E+02	8.85E+02	6.81E+02
139.	$3\text{LiF}(\text{c})+3\text{Cu}(\text{c})=3\text{Li}(\text{c})+\text{Cu}_3\text{F}_3(\text{g})$	1.25E+02	1.18E+03	9.92E+02
140.	$2\text{LiF}(\text{c})+\text{Cu}(\text{c})=2\text{Li}(\text{c})+\text{CuF}_2(\text{c})$	5.12E+01	7.00E+02	6.24E+02
141.	$\text{LiF}(\text{c})+\text{Cu}(\text{c})=\text{Li}(\text{c})+\text{CuF}(\text{c})$	1.05E+01	3.02E+02	2.86E+02
142.	$\text{BaF}_2(\text{c})+2\text{Cu}(\text{c})=\text{Ba}(\text{c})+2\text{CuF}(\text{g})$	2.83E+02	1.11E+03	6.82E+02
143.	$\text{BaF}_2(\text{c})+\text{Cu}(\text{c})=\text{Ba}(\text{c})+\text{CuF}_2(\text{g})$	1.52E+02	8.75E+02	6.48E+02
144.	$\text{BaF}_2(\text{c})+2\text{Cu}(\text{c})=\text{Ba}(\text{c})+\text{Cu}_2\text{F}_2(\text{g})$	1.53E+02	8.90E+02	6.61E+02
145.	$3\text{BaF}_2(\text{c})+6\text{Cu}(\text{c})=3\text{Ba}(\text{c})+2\text{Cu}_3\text{F}_3(\text{g})$	3.00E+02	2.38E+03	1.93E+03
146.	$\text{BaF}_2(\text{c})+\text{Cu}(\text{c})=\text{Ba}(\text{c})+\text{CuF}_2(\text{c})$	6.76E+01	7.06E+02	6.04E+02
147.	$\text{BaF}_2(\text{c})+2\text{Cu}(\text{c})=\text{Ba}(\text{c})+2\text{CuF}(\text{c})$	3.75E+01	6.09E+02	5.53E+02
148.	$\text{UF}_4(\text{c})+4\text{Cu}(\text{c})=\text{U}(\text{c})+4\text{CuF}(\text{g})$	5.15E+02	1.73E+03	9.61E+02
149.	$\text{UF}_4(\text{c})+2\text{Cu}(\text{c})=\text{U}(\text{c})+2\text{CuF}_2(\text{g})$	2.51E+02	1.27E+03	8.92E+02
150.	$\text{UF}_4(\text{c})+4\text{Cu}(\text{c})=\text{U}(\text{c})+2\text{Cu}_2\text{F}_2(\text{g})$	2.54E+02	1.30E+03	9.19E+02
151.	$3\text{UF}_4(\text{c})+12\text{Cu}(\text{c})=3\text{U}(\text{c})+4\text{Cu}_3\text{F}_3(\text{g})$	4.45E+02	3.31E+03	2.64E+03
152.	$\text{UF}_4(\text{c})+2\text{Cu}(\text{c})=\text{U}(\text{c})+2\text{CuF}_2(\text{c})$	8.34E+01	9.30E+02	8.05E+02
153.	$\text{UF}_4(\text{c})+4\text{Cu}(\text{c})=\text{U}(\text{c})+4\text{CuF}(\text{c})$	2.31E+01	7.37E+02	7.03E+02
154.	$\text{LaF}_3(\text{c})+3\text{Cu}(\text{c})=\text{La}(\text{c})+3\text{CuF}(\text{g})$	4.35E+02	1.62E+03	9.65E+02
155.	$2\text{LaF}_3(\text{c})+3\text{Cu}(\text{c})=2\text{La}(\text{c})+3\text{CuF}_2(\text{g})$	4.74E+02	2.54E+03	1.83E+03
156.	$2\text{LaF}_3(\text{c})+6\text{Cu}(\text{c})=2\text{La}(\text{c})+3\text{Cu}_2\text{F}_2(\text{g})$	4.77E+02	2.58E+03	1.87E+03
157.	$\text{LaF}_3(\text{c})+3\text{Cu}(\text{c})=\text{La}(\text{c})+\text{Cu}_3\text{F}_3(\text{g})$	1.60E+02	1.14E+03	9.05E+02
158.	$2\text{LaF}_3(\text{c})+3\text{Cu}(\text{c})=2\text{La}(\text{c})+3\text{CuF}_2(\text{c})$	2.22E+02	2.03E+03	1.70E+03
159.	$\text{LaF}_3(\text{c})+3\text{Cu}(\text{c})=\text{La}(\text{c})+3\text{CuF}(\text{c})$	6.58E+01	8.70E+02	7.71E+02
160.	$\text{LiF}(\text{c})+\text{Sn}(\text{c})=\text{Li}(\text{c})+\text{SnF}(\text{g})$	1.27E+02	4.71E+02	2.81E+02
161.	$2\text{LiF}(\text{c})+\text{Sn}(\text{c})=2\text{Li}(\text{c})+\text{SnF}_2(\text{g})$	1.31E+02	6.64E+02	4.67E+02
162.	$3\text{LiF}(\text{c})+\text{Sn}(\text{c})=3\text{Li}(\text{c})+\text{SnF}_3(\text{g})$	1.30E+02	1.11E+03	9.09E+02
163.	$4\text{LiF}(\text{c})+\text{Sn}(\text{c})=4\text{Li}(\text{c})+\text{SnF}_4(\text{g})$	1.13E+02	1.30E+03	1.13E+03

S.no	Reaction	$\Delta S$ , J/mole K	$\Delta H$ , kJ/mole	$\Delta G$ , kJ/mole
164.	$4\text{LiF(c)}+\text{Sn(c)}=4\text{Li(c)}+\text{SnF4(c)}$	3.44E+01	1.17E+03	1.12E+03
165.	$2\text{LiF(c)}+\text{Sn(c)}=2\text{Li(c)}+\text{SnF2(c)}$	2.81E+01	5.57E+02	5.15E+02
166.	$\text{BaF2(c)}+2\text{Sn(c)}=\text{Ba(c)}+2\text{SnF(g)}$	2.71E+02	9.48E+02	5.42E+02
167.	$\text{BaF2(c)}+\text{Sn(c)}=\text{Ba(c)}+\text{SnF2(g)}$	1.48E+02	6.69E+02	4.48E+02
168.	$3\text{BaF2(c)}+2\text{Sn(c)}=3\text{Ba(c)}+2\text{SnF3(g)}$	3.10E+02	2.23E+03	1.76E+03
169.	$2\text{BaF2(c)}+\text{Sn(c)}=2\text{Ba(c)}+\text{SnF4(g)}$	1.46E+02	1.31E+03	1.09E+03
170.	$2\text{BaF2(c)}+\text{Sn(c)}=2\text{Ba(c)}+\text{SnF4(c)}$	6.73E+01	1.18E+03	1.08E+03
171.	$\text{BaF2(c)}+\text{Sn(c)}=\text{Ba(c)}+\text{SnF2(c)}$	4.45E+01	5.62E+02	4.95E+02
172.	$\text{UF4(c)}+4\text{Sn(c)}=\text{U(c)}+4\text{SnF(g)}$	4.89E+02	1.41E+03	6.81E+02
173.	$\text{UF4(c)}+2\text{Sn(c)}=\text{U(c)}+2\text{SnF2(g)}$	2.43E+02	8.57E+02	4.92E+02
174.	$3\text{UF4(c)}+4\text{Sn(c)}=3\text{U(c)}+4\text{SnF3(g)}$	4.65E+02	3.01E+03	2.31E+03
175.	$\text{UF4(c)}+\text{Sn(c)}=\text{U(c)}+\text{SnF4(g)}$	9.38E+01	8.31E+02	6.90E+02
176.	$\text{UF4(c)}+\text{Sn(c)}=\text{U(c)}+\text{SnF4(c)}$	1.55E+01	7.00E+02	6.77E+02
177.	$\text{UF4(c)}+2\text{Sn(c)}=\text{U(c)}+2\text{SnF2(c)}$	3.73E+01	6.43E+02	5.87E+02
178.	$\text{LaF3(c)}+3\text{Sn(c)}=\text{La(c)}+3\text{SnF(g)}$	4.15E+02	1.38E+03	7.55E+02
179.	$2\text{LaF3(c)}+3\text{Sn(c)}=2\text{La(c)}+3\text{SnF2(g)}$	4.62E+02	1.92E+03	1.23E+03
180.	$\text{LaF3(c)}+\text{Sn(c)}=\text{La(c)}+\text{SnF3(g)}$	1.65E+02	1.07E+03	8.22E+02
181.	$4\text{LaF3(c)}+3\text{Sn(c)}=4\text{La(c)}+3\text{SnF4(g)}$	4.75E+02	3.76E+03	3.05E+03
182.	$4\text{LaF3(c)}+3\text{Sn(c)}=4\text{La(c)}+3\text{SnF4(c)}$	2.40E+02	3.37E+03	3.01E+03
183.	$2\text{LaF3(c)}+3\text{Sn(c)}=2\text{La(c)}+3\text{SnF2(c)}$	1.53E+02	1.60E+03	1.37E+03
184.	$6\text{LiF(c)}+\text{Al2O3(c)}=3\text{Li2O(c)}+2\text{AlF3(g)}$	1.79E+02	9.54E+02	6.85E+02
185.	$6\text{LiF(c)}+\text{Al2O3(c)}=3\text{Li2O(c)}+2\text{AlF3(c)}$	-1.73E+02	4.06E+02	6.65E+02
186.	$3\text{BaF2(c)}+\text{Al2O3(c)}=3\text{BaO(c)}+2\text{AlF3(c)}$	-4.77E+01	5.22E+02	5.93E+02
187.	$3\text{BaF2(c)}+\text{Al2O3(c)}=3\text{BaO(c)}+2\text{AlF3(g)}$	3.04E+02	1.07E+03	6.13E+02
188.	$3\text{UF4(c)}+2\text{Al2O3(c)}=3\text{UO2(c)}+4\text{AlF3(c)}$	-1.61E+02	-3.29E+02	-8.72E+01
189.	$3\text{UF4(c)}+2\text{Al2O3(c)}=3\text{UO2(c)}+4\text{AlF3(g)}$	5.43E+02	7.67E+02	-4.74E+01
190.	$2\text{LaF3(c)}+\text{Al2O3(c)}=\text{La2O3(c)}+2\text{AlF3(c)}$	-3.81E+00	3.11E+02	3.17E+02
191.	$2\text{LaF3(c)}+\text{Al2O3(c)}=\text{La2O3(c)}+2\text{AlF3(g)}$	3.48E+02	8.59E+02	3.37E+02
192.	$4\text{LiF(c)}+\text{ZrO2(c)}=2\text{Li2O(c)}+\text{ZrF4(g)}$	5.99E+01	5.62E+02	4.72E+02
193.	$4\text{LiF(c)}+\text{ZrO2(c)}=2\text{Li2O(c)}+\text{ZrF4(c)}$	-6.30E+01	4.19E+02	5.13E+02
194.	$2\text{BaF2(c)}+\text{ZrO2(c)}=2\text{BaO(c)}+\text{ZrF4(c)}$	2.05E+01	4.96E+02	4.65E+02

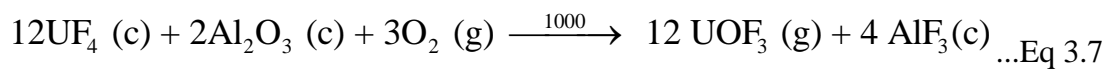
S.no	Reaction	$\Delta S$ , J/mole K	$\Delta H$ , kJ/mole	$\Delta G$ , kJ/mole
195.	$62\text{BaF}_2(\text{c})+\text{ZrO}_2(\text{c})=2\text{BaO}(\text{c})+\text{ZrF}_4(\text{c})$	2.05E+01	4.96E+02	4.65E+02
196.	$\text{UF}_4(\text{c})+\text{ZrO}_2(\text{c})=\text{UO}_2(\text{c})+\text{ZrF}_4(\text{c})$	-1.43E+00	3.86E+01	4.07E+01
197.	$\text{UF}_4(\text{c})+\text{ZrO}_2(\text{c})=\text{UO}_2(\text{c})+\text{ZrF}_4(\text{g})$	1.22E+02	1.81E+02	-8.56E-01
198.	$4\text{LaF}_3(\text{c})+3\text{ZrO}_2(\text{c})=2\text{La}_2\text{O}_3(\text{c})+3\text{ZrF}_4(\text{c})$	1.49E+02	1.07E+03	8.43E+02
199.	$4\text{LaF}_3(\text{c})+3\text{ZrO}_2(\text{c})=2\text{La}_2\text{O}_3(\text{c})+3\text{ZrF}_4(\text{g})$	5.18E+02	1.50E+03	7.18E+02
200.	$2\text{LiF}(\text{c})+\text{MgO}(\text{c})=\text{Li}_2\text{O}(\text{c})+\text{MgF}_2(\text{c})$	-5.17E+01	6.37E+01	1.41E+02
201.	$2\text{LiF}(\text{c})+\text{MgO}(\text{c})=\text{Li}_2\text{O}(\text{c})+\text{MgF}_2(\text{g})$	1.11E+02	4.30E+02	2.63E+02
202.	$\text{BaF}_2(\text{c})+\text{MgO}(\text{c})=\text{BaO}(\text{c})+\text{MgF}_2(\text{c})$	-1.00E+01	1.02E+02	1.17E+02
203.	$\text{BaF}_2(\text{c})+\text{MgO}(\text{c})=\text{BaO}(\text{c})+\text{MgF}_2(\text{g})$	1.53E+02	4.68E+02	2.39E+02
204.	$\text{UF}_4(\text{c})+2\text{MgO}(\text{c})=\text{UO}_2(\text{c})+2\text{MgF}_2(\text{g})$	2.84E+02	4.79E+02	5.34E+01
205.	$\text{UF}_4(\text{c})+2\text{MgO}(\text{c})=\text{UO}_2(\text{c})+2\text{MgF}_2(\text{c})$	-4.19E+01	-2.53E+02	-1.90E+02
206.	$2\text{LaF}_3(\text{c})+3\text{MgO}(\text{c})=\text{La}_2\text{O}_3(\text{c})+3\text{MgF}_2(\text{c})$	1.39E+01	9.62E+01	7.54E+01
207.	$2\text{LaF}_3(\text{c})+3\text{MgO}(\text{c})=\text{La}_2\text{O}_3(\text{c})+3\text{MgF}_2(\text{g})$	5.02E+02	1.19E+03	4.40E+02
208.	$\text{UF}_4(\text{c})+\text{SiO}_2(\text{c})=\text{UO}_2(\text{c})+\text{SiF}_4(\text{g})$	9.34E+01	5.30E+01	-8.72E+01
209.	$2\text{BaF}_2(\text{c})+\text{SiO}_2(\text{c})=2\text{BaO}(\text{c})+\text{SiF}_4(\text{g})$	1.15E+02	5.11E+02	3.38E+02
210.	$4\text{LiF}(\text{c})+\text{SiO}_2(\text{c})=2\text{Li}_2\text{O}(\text{c})+\text{SiF}_4(\text{g})$	3.19E+01	4.33E+02	3.85E+02

A few representative feasible reactions of alumina, zirconia, magnesia and quartz with uranium tetrafluoride are extracted from the Table 3.4 and presented in Table 3.5.

Table 3.5 Reaction of uranium tetrafluoride with ceramic materials at 1500K

S.no	Reaction	$\Delta G$ , kJ/mole
1.	$3\text{UF}_4(\text{c})+2\text{Al}_2\text{O}_3(\text{c})=3\text{UO}_2(\text{c})+4\text{AlF}_3(\text{c})$	-8.72E+01
2.	$\text{UF}_4(\text{c})+\text{ZrO}_2(\text{c})=\text{UO}_2(\text{c})+\text{ZrF}_4(\text{g})$	-8.56E-01
3.	$\text{UF}_4(\text{c})+2\text{MgO}(\text{c})=\text{UO}_2(\text{c})+2\text{MgF}_2(\text{c})$	-1.90E+02
4.	$\text{UF}_4(\text{c})+\text{SiO}_2(\text{c})=\text{UO}_2(\text{c})+\text{SiF}_4(\text{g})$	-8.72E+01

The presence of oxygen was found to assist the corrosion of alumina. Eq 3.7 shows the reaction which was found to be highly feasible for decomposition of UF<sub>4</sub> in oxygen that might be present in the furnace. The change in free energy for this reaction, is  $\Delta G = -117.45$  KJ/mole at 1273K.



### **3.5 Experimental study for selection of materials for electrolytic cells**

As the list of materials for testing was long, and the number of molten salt compositions were many, only a visual observation of the effects of corrosion could be performed. Sufficiently long hours of exposure, similar to the duration of the experiment was used to select the suitable material combination for the setup. The experimental method involved in melting and soaking above the melting point, a chosen electrolyte for a period of 48hrs in the container made of the material being investigated.

#### **3.5.1 Experimental setup for testing compatibility of materials for electrolytic cells**

The design considerations discussed for salt mixture preparation (section 3.2.1) are valid for the experimental setup for testing compatibility of materials for electrolytic cells. However, for the compatibility studies the following major changes in size and heating capacity were required. The inert gas hot zone was made from a 90mm diameter alumina tube. The temperature for materials testing was chosen as 1473K, the nominal temperature of electrolysis operation. Therefore the design temperature of the heating system was kept at 1573K. A Kanthal Fibrothal 6kW heater element of

appropriate size (specifications indicated in Table 3.6) was used. The top loading, resistance heated fibrothal tubular heating module was configured for vertical operation, designed to heat ceramic tube of diameter upto 150 mm diameter to a temperature of around 1573K. As before the heating element made of APM Kanthal material was surrounded by vacuum formed high-grade ceramic fiber enclosure for heat insulation, which could maintain the skin temperature at 333K.

Table 3.6 Specification of heating module for conducting fluoride salt compatibility studies

<b>S.no</b>	<b>Specification</b>	<b>Required value</b>
1.	Heating module type	Kanthal Fibrothal Tube module, Type B
2.	Heating module designation	RAC 150/200
3.	Process Temperature	1573K maximum
4.	Uniform temperature zone	150mm
5.	Diameter Inner	150mm
6.	Diameter outer	350mm
7.	Heated Length	220mm
8.	Power	5955W maximum

The control panel with the microprocessor based Eurotherm make 3216 PID temperature controller and Eurotherm 7100A power controller integrated with the fibrothal heating module.

The service temperature of most of the metallic materials in air is limited to 1373K. Hence for experiments in the range of 1473K-1573K metallic muffle materials was

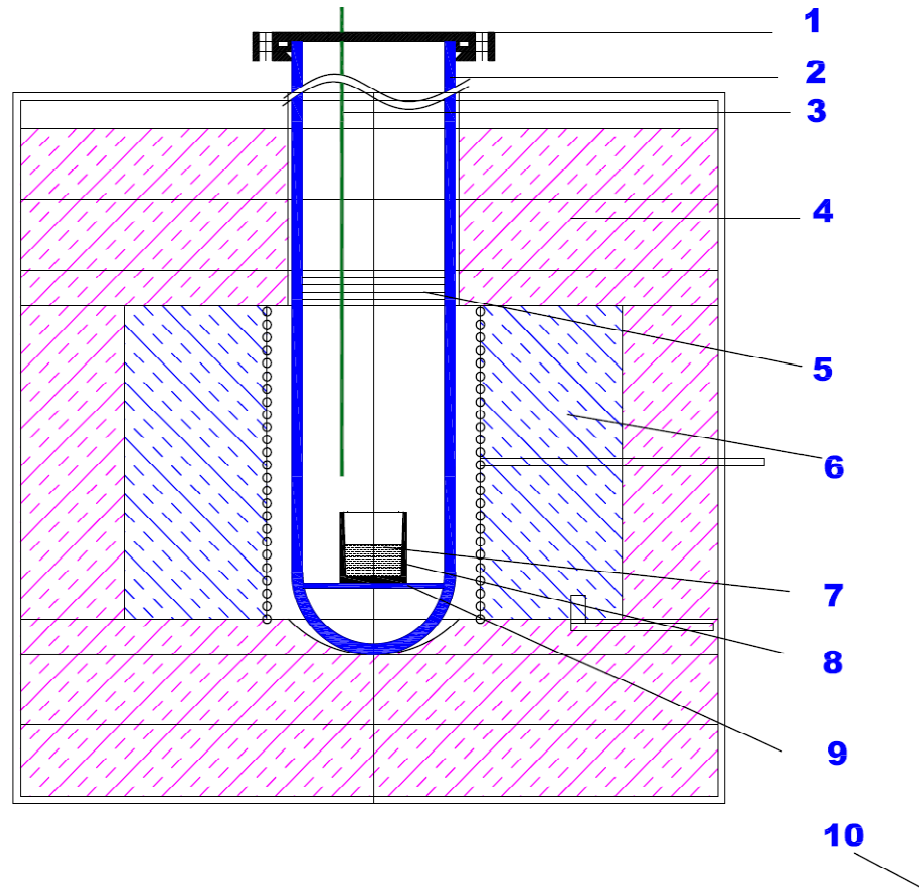
replaced with an alumina ceramic tube as the maximum service temperature of the alumina tube is 2173K and tubular sections are readily available from a number of suppliers. Alumina ware exhibits good resistance to corrosion, stability in oxidizing and reducing atmospheres and exhibits very low out gassing property in high vacuum. Unlike metallic materials, fabrication and joining of ceramic materials is difficult and also they have poor thermal shock resistance in comparison to metallic materials. Hence, the heating and cooling rates were limited to 200K/hr to protect the alumina tube. Degussit AL-23 grade recrystallized alumina tube was procured from M/s Friatec, Germany. Tube had dimensions of 80mm ID, 90 mm OD and 800 mm length and one end was closed with a hemispherical dished end.

Initially a tube with both ends open was planned for the experiments. As both the ends of the tube have to fitted with O ring sealed flanges which are water cooled, the tube length became too long to maintain thermal gradients for safe operation. Hence one end closed alumina tube of 800mm long with a hemispherical end was considered safe for the required thermal gradients. It has to be emphasized that the surface finish and ovality of the alumina tube played a very important role in the final leak tightness of the system achieved. Diametric tolerances of the tube were in the range of  $\pm 0.1$ mm and the sealing surface free of any surface defects.

The schematic of the experimental assembly used is shown in figure 3.14. All the experiments were conducted at 1473K in recrystallized alumina tube closed at one end. The open end of the tube was sealed by a stainless steel flange assembly consisting of three SS304 flanges with O ring grooves. Water cooling channels were provided on the flanges with O rings grooves to maintain the temperature of O-rings

below 333K. An alumina plate of 95mm diameter and 5mm thick placed inside at the closed end of the tube served as base for resting the crucibles. The crucible with the sample was lowered into the tube with the help of tongs. Purified argon gas (<0.1ppm of oxygen) was purged continuously through out the experiment at 6-8 lph. The oxygen concentration in the inlet gas was continuously monitored by online oxygen gas analyzer (Systech 800 Series analyzer). Heating of the alumina tube was done by the 6kW resistive heating furnace with an accuracy of  $\pm 5^{\circ}\text{C}$ . The furnace was housed inside a fumehood and the purge gas released into the fumehood was exhausted through HEPA filters to remove any radioactive particulate and through a water scrubber to absorb fluoride vapour if any. The process and instrumentation diagram of the experimental setup is as shown in figure 3.15.

# Fumehood



- |   |                                      |
|---|--------------------------------------|
| 1. Water cooled stainless steel flanges | 6. Fibrothal heating module          |
| 2. Alumina tube                         | 7. Electrolyte studied               |
| 3. Thermocouple                         | 8. Crucible of material being tested |
| 4. Furnace for heating                  | 9. Alumina base support plate.       |
| 5. Pack of radiation shields            | 10. Fumehood                         |

Figure 3.14 Schematic of experimental assembly for material compatibility studies

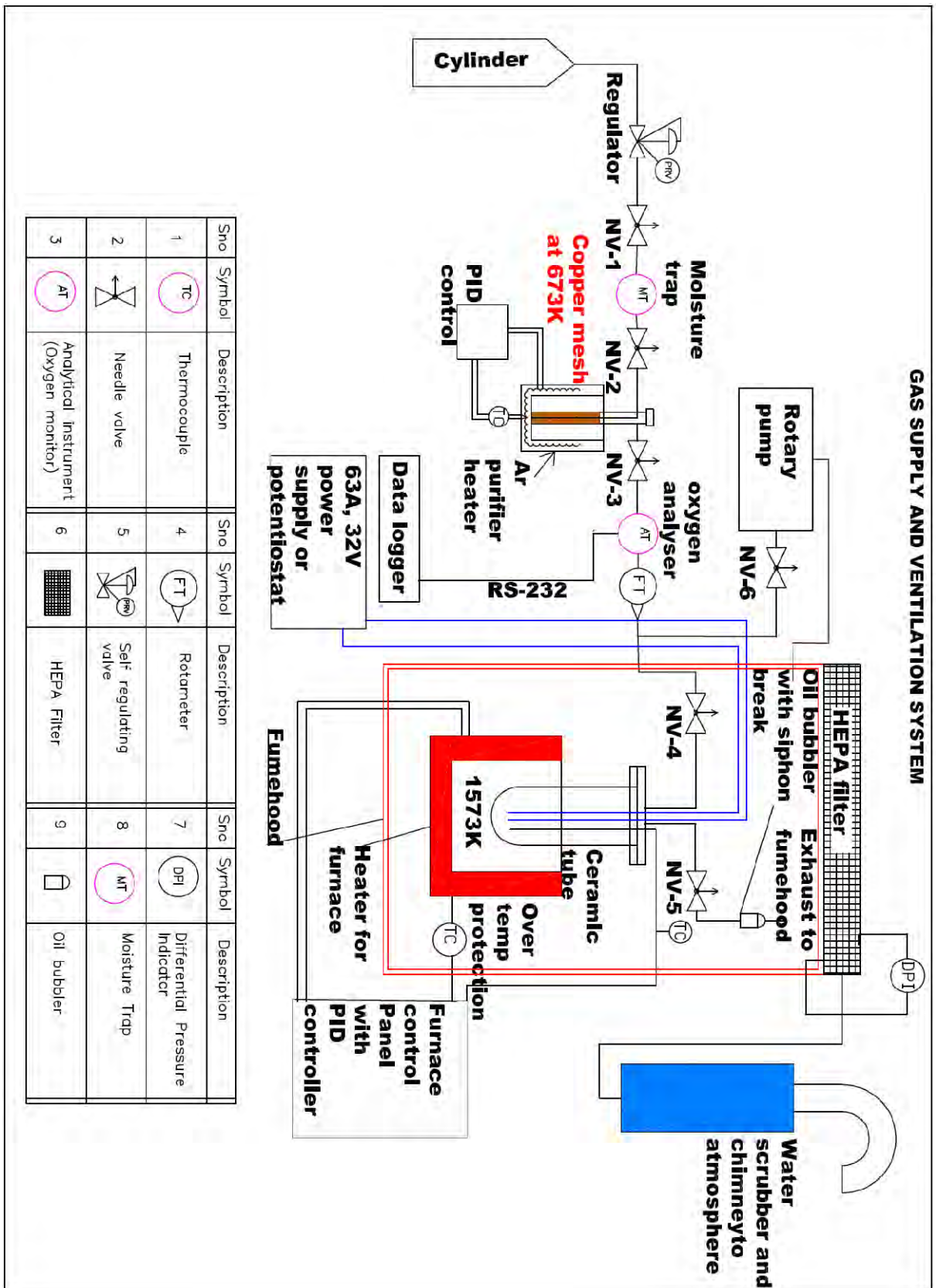


Figure 3.15 Process and Instrumentation diagram of the typical fumehood experimental setup

### 3.5.2 Tests conducted

LiF, BaF<sub>2</sub>, UF<sub>4</sub> and LaF<sub>3</sub> used for preparation of the salt mixtures were of reagent grade as mentioned in the earlier section. The salt preparation procedure used for studies on compatible materials for electrolytes was as discussed in section 3.2.3 for salt mixture preparation. Around 30g salt was taken in each experiment. Containers were fabricated according to the availability of the shapes and sizes of ceramic materials. In case of high density graphite, a crucible of 50mm OD, 27mm height with 15° draft angle was used for testing corrosion resistance against electrolytes. In case of hexagonal boron nitride, small cups of 25mm OD, 15mm height with 3° draft angle were fabricated and used for testing. Alumina crucibles of 15mm diameter 20mm height were used for compatibility studies. The detailed list of materials tested against the electrolyte and the outcome of the study are presented in Table 3.5. Detailed SEM analysis and other metallographic investigations of the test samples were not conducted if any visible attack was observed.

It was found that high density graphite is the best suited material for containment of any type of fluoride electrolyte. LaPO<sub>4</sub> and YPO<sub>4</sub> have demonstrated promising results which can also be used for cathode containment that hold liquid uranium or U-alloy. Although hexagonal boron nitride has been decided to be used for most of the electrolysis experiments in this research work, in practical applications it may be eventually be replaced with LaPO<sub>4</sub> as boron contamination may not be tolerable for nuclear grade metal produced by electrolytic reduction.

Table 3.5 List of experiments conducted for compatibility studies with different electrolytes at 1473K

S.no	Salt composition	Furnace atmosphere	Material of construction	Observations of experiments
1	LiF:BaF <sub>2</sub> (1:1) Mixture	Air	Alumina	<b>No attack observed</b>
2	LiF:BaF <sub>2</sub> (1:1)-5Wt% UF <sub>4</sub>	Air	Alumina	Mild attack noticed
3	LiF:BaF <sub>2</sub> (1:1)-5Wt% UF <sub>4</sub>	Vacuum	Alumina	Mild attack noticed
4	LiF:BaF <sub>2</sub> (1:1)-20Wt% UF <sub>4</sub>	Helium	Alumina	Severely attacked
5	LiF:BaF <sub>2</sub> (1:1)-20Wt% UF <sub>4</sub> (Dry)	Vacuum	Alumina	Mild attack noticed
6	LiF:BaF <sub>2</sub> (1:1)-20Wt% UF <sub>4</sub>	Air	Alumina	Severely attacked
7	LiF:BaF <sub>2</sub> (1:1)-20Wt% UF <sub>4</sub>	Air	Quartz	Severely attacked
8	All electrolytes	Argon	Graphite	<b>No attack, fine powders seen</b>
9	LiF:BaF <sub>2</sub> (1:1)-25Wt% UF <sub>4</sub>	Argon	Y <sub>2</sub> O <sub>3</sub>	Attacked
10	LiF:BaF <sub>2</sub> (1:1)-25Wt% LaF <sub>3</sub>	Argon	Y <sub>2</sub> O <sub>3</sub>	Attacked

<b>S.no</b>	<b>Salt composition</b>	<b>Furnace atmosphere</b>	<b>Material of construction</b>	<b>Observations of experiments</b>
11	LiF:BaF <sub>2</sub> (1:1)-25Wt% UF <sub>4</sub>	Argon	LaPO <sub>4</sub>	<b>No attack observed</b>
12	LiF:BaF <sub>2</sub> (1:1)-25Wt% LaF <sub>3</sub>	Argon	LaPO <sub>4</sub>	<b>No attack observed</b>
13	LiF:BaF <sub>2</sub> (1:1)-25Wt% UF <sub>4</sub>	Argon	YPO <sub>4</sub>	<b>No attack observed</b>
14	LiF:BaF <sub>2</sub> (1:1)-25Wt% LaF <sub>3</sub>	Argon	YPO <sub>4</sub>	<b>No attack observed</b>
15	LiF:BaF <sub>2</sub> (1:1)-25Wt% UF <sub>4</sub>	Argon	Hex BN	<b>No attack observed</b>
16	LiF:BaF <sub>2</sub> (1:1)-25Wt% LaF <sub>3</sub>	Argon	Hex BN	<b>No attack observed</b>
17	All electrolytes	Argon	HD Graphite	<b>No attack observed</b>

### 3.6 Conclusions

A number of multi-component fluoride salt mixtures LiF:BaF<sub>2</sub>(1:1)- with 5 wt % to 30 wt% UF<sub>4</sub> , LiF:BaF<sub>2</sub>(1:1)- 5 wt % to 30 wt% LaF<sub>3</sub>, and LiF:CaF<sub>2</sub>(6:4) with 5 wt % to 30 wt% UF<sub>4</sub> which are planned for use in the development of electrochemical process for uranium oxide to uranium metal conversion at 1473K were characterized for their melting temperature and room temperature phases after melting. The melting points of the eutectic compounds of LiF-BaF<sub>2</sub> and LiF-CaF<sub>2</sub> were verified with the data reported in literature validated the experimental facility and the techniques which were adopted for characterization.

This study has shown that the conditioning procedure has a strong influence on the behavior of the electrolyte. The purity of the electrolyte was assessed by linear sweep voltammetry. Although the nature of the electroactive species present was not identified, the current flowing in the electrolyte indicated the total amount of electroactive species. The concentration of the contaminant reduced by conditioning over 24hrs. The pre-treatment procedure established for LiF:BaF<sub>2</sub>(1:1) systems can be adapted and implemented for large scale practical systems. Pre-treatment time can be reduced by improving the surface area of exposure to the atmosphere such as falling film outgassing in counter current flow of argon gas.

Thermodynamic feasibility of reaction between different fluoride salt mixtures and various materials for use in the research work was verified first by thermodynamic considerations, and then by actual compatibility experiments at 1473K. Moisture and oxygen were found to have a deleterious effect in so far as enhancement of corrosion is concerned.

## References

- 3.1. A. I. Agulyanskii and V. A. Bessonova, *Zh. Neorg. Khim.*, **27** [4] 1029-1032, 1982. *Russ. J. Inorg. Chem. (Engl. Transl.)*, **27** [4] 579-581, 1982.
- 3.2. W. E. Roake, *J. Electrochem. Soc.*, **104** [11] 661-662, 1957.
- 3.3. G. A. Bukhalova and V. T. Berezhnaya, *Zh. Neorg. Khim.*, *Russ. J. Inorg. Chem. (Engl. Transl.)*, **2** [6] 1408-1412, 1957.
- 3.4. C. J. Barton, H. A. Friedman, W. R. Grimes, H. Insley, R. E. Moore, and R. E. Thoma, *J. Am. Ceram. Soc.*, **41**, 63-69, 1958.
- 3.5. N. P. Nekrasova, E. N. Oblomeev, V. N. Golovanova, and A. V. Beznosikova, *At. Energ.*, **22** [4] 293-297 (1967); *Sov. At. Energy (Engl. Transl.)*, **22** 367-371, 1967.
- 3.6. A. I. Agulyanskii and V. A. Bessonova, *Zh. Neorg. Khim.*, *Russ. J. Inorg. Chem. (Engl. Transl.)*, **27** [4] 1029-1032, 1982.
- 3.7. B. P. Sobolev and N. L. Tkachenko, *J. Less-Common Met.*, **85**, 155-170, 1982.
- 3.8. Doron Orbakh, *Nonaqueous electrochemistry*, CRC Press, 1999.
- 3.9. Piper R. D., MCW, Rep No. MCW-1480, 1963.
- 3.10. Niedarch L.W. & Dearing B.E., *Jour of the Electrochemical society*, Vol 105, No. 6, pp 353-358, 1958.
- 3.11. Henrie T. A, *Journal of Metals*, pp 978-981, 1964.
- 3.12. Haas P.A, Adcock P.W, Coroneos A.C. and Hendrix D.E, *Met & Mat transactions B.*, Vol 25B, pp 505-518, 1994.
- 3.13. Haas P.A and Stanley P. Cooper, *American chemical society*, Vol 38, No. 1, pp 26-30, 1993.
- 3.14. Takeshi Shimada, Nobuo Tedzuka, Yuza Shimizu and Masanobu Miyake, *Journal of Alloys and Compounds*, 204, pp 1-4, 1994.
- 3.15. D. L. Hill, J. Perano, and R. A. Osteryoung, *J. Electrochem. Soc.* 107, pp 698, 1960.
- 3.16. H. A. Laitinen and W. S. Ferguson, *Anal. Chem. Techniques and Principles*, **29**, 4, 1957.
- 3.17. C.H. Liu, K.E. Johnson and H.A. Laitinen, *Electroanalytical Chemistry of molten salt*, in L. Meties, ed., *Handbook of Analytical Chemistry*, McGraw- Hill, New York, 1963.
- 3.18. FactSage thermochemical software, FactSage 2013
- 3.19. Belov G V, Trusov B G, *ASTD Version 2.0*, 1995.

## CHAPTER IV

### SOLUBILITY OF $\text{UO}_2$ IN FLUORIDE MELTS

---

This chapter deals with the solubility studies of uranium oxide in  $\text{LiF-BaF}_2$  with varying amounts of  $\text{LaF}_3$  and  $\text{UF}_4$  in the range of 1423K to 1523K. The procedure adopted for measuring the solubility, results and analytical techniques are also presented.

#### 4.1 Introduction

The solubility of uranium oxide in the molten fluoride electrolyte is one of the important parameters for operating an electrolytic cell at 1473K for electrolytic reduction of uranium oxide to uranium metal. It is widely accepted that only the dissolved oxide in the electrolyte is available for electrolysis. The investigation was undertaken to measure the solubility of uranium oxide in the  $\text{LiF-BaF}_2$  supporting electrolyte with  $\text{UF}_4$  and  $\text{LaF}_3$  additives as solvents for  $\text{UO}_2$ . Molten fluorides, in general, have very limited solubility for oxides and an outstanding exception being the cryolite for alumina which exhibits a much higher solubility. To enhance the solubility of a particular oxide a fluoride solvent of the same metal oxide is added to the electrolyte. In case of  $\text{UO}_2$ , in the studies reported in the literature till now  $\text{UF}_4$  has been used as the solvent. The solubility of  $\text{UO}_2$  in different compositions of electrolytes with  $\text{UF}_4$  has been reported by some authors [4.1-4.7]. Marden et al. have reported the use of a mixture of double fluorides, such as,  $\text{KUF}_5$  as solvent for low temperature cell operation [4.7]. When the process is adapted to uranium metal

production for isotope separation of uranium or recycling metallic fuel with different isotopic composition,  $\text{UF}_4$  of the specific isotopic composition has to be used as additive; this will be a difficult proposition. Hence, alternatively,  $\text{LaF}_3$  was chosen as an alternative solvent for  $\text{UO}_2$  for the research work. Among other rare earths  $\text{LaF}_3$  is easily available and the deposition potential of lanthanum is higher than that of uranium in fluoride melt. Although other rare earth fluorides may have potential for use as solvent for  $\text{UO}_2$ , in this research work, only  $\text{LaF}_3$  has been studied.

The variation of uranium oxide solubility with  $\text{UF}_4$  as the solvent in different supporting electrolyte mixtures is reported in the literature [4.1-4.7]. A survey of literature shows that extensive data on the solubility of  $\text{UO}_2$  in  $\text{UF}_4$  in  $\text{LiF-BaF}_2$  and  $\text{LiF-CaF}_2$  melts have been reported by Knolls Atomic power Laboratories (KAPL), United States Bureau of Mines (USBM), Mallinckrodt Chemical Works (MCW) [4.1-4.7]. A consolidated review of all the existing data and additional new set of data on  $\text{UO}_2$  solubility in  $\text{UF}_4$  till the time of review is reported by Oak Ridge National Laboratory (ORNL) [4.7]. The main experimental variables published in the literature are the supporting electrolyte, temperature, concentration of functional electrolyte  $\text{UF}_4$  and characteristics of  $\text{UO}_2$  solute. Greenfield and Hyde had found that the physical form of oxide and chemical composition did not affect the solubility after equilibration [4.6]. Various data clearly indicate that  $\text{UF}_4$  concentration is the most important parameter for solubility of  $\text{UO}_2$  other than the temperature of the bath. The effect of temperature on  $\text{UO}_2$  solubility for a number of binary mixtures of fluoride salts with solvents are reported by various authors [4.1-4.7]. Their data show increasing solubility of  $\text{UO}_2$  with increasing temperature. The effect of surface area of

UO<sub>2</sub> on the time required for saturation concentration has been reported by Bernard [4.5].

The LiF-BaF<sub>2</sub>-LaF<sub>3</sub> system taken up in this work has not been studied by any author; except for a qualitative data with mixed LaF<sub>3</sub> +UF<sub>4</sub> by Haas et al. [4.6] and that too based on a single experiment. Therefore, one of the objectives of this study is to generate for the first time data on solubility of UO<sub>2</sub> in LiF-BaF<sub>2</sub> - LaF<sub>3</sub> salt mixtures and a range mixed electrolytes of LaF<sub>3</sub>+UF<sub>4</sub>. The solubility data above the melting point of uranium would be of importance to both the designers and operators of electrolytic cells.

Hardacre has reported the use of extended X-Ray Absorption Fine Structure (EXAFS), and other spectroscopic techniques to investigate both the structure of ionic liquids or molten salts as well as the species dissolved in the ionic liquids [4.8]. The structure of low temperature molten salts has been studied in more detail using EXAFS. Structural and species investigation by EXAFS is still in a development stage for fluoride media at high temperature. Since, this study has focused on the extent of UO<sub>2</sub> going into the electrolyte, no separate effort was directed to determine the exact form of the oxide complex formed by dissolution in the range of temperature studied.

In addition, to the solubility limit of uranium oxide, the rate at which the oxide dissolves in the electrolyte is equally important. The electrolytic cell can be operated with an electrolyte even with a low solubility limit if the oxide dissolves at a rate sufficient to maintain the minimum requisite concentration without depletion of the

active ions, which would eventually lead to undesirable anodic reactions. In the electrolytic reduction process it can produce  $\text{CF}_4$  in place of CO when the concentrations fall below the desired level. The parameters of the electrochemical cell are optimized to suite the actual rate of dissolution. No separate rate measurement studies were planned. However, in the work the rate of dissolution of oxide has been addressed in so far as it affects the duration of the experiment and measurement of the limit of solubility of total oxide.

#### **4.1.1 Methods of determination of saturation solubility**

The saturation solubility of the oxide in an electrolyte bath can be determined in numerous ways listed below. The criteria for selection of the method of determination are also discussed.

1. Oxide can be added to the electrolyte and laser based visual techniques can be used to determine the point beyond which oxide is not soluble. This technique demands a transparent container like quartz for the electrolyte at high temperature, which is not available for the corrosive fluoride medium. It was found that the electrolyte attacks quartz and makes it translucent; hence it was not pursued.
2. The second method involves equilibrating the electrolyte with different amounts of oxide, quenching quickly and observing the undissolved oxide metallographically to determine the limit of solubility. Quenching the salt mixtures was avoided in this work as it involves potential release of radioactive powders and vapors.
3. The third method consists of observing the changes in freezing or melting point of the electrolyte with oxide addition and the point beyond which there

is no significant change is taken as the limit. Measurement of electrode potentials with oxide addition by potentiometry and the point beyond which potential remains constant may be considered as the limit. Electrode potential measurement is possible with fluoride media, however reliable high temperature reference electrode was not available to adopt this method here.

4. A transient electrochemical technique like linear sweep voltammetry(LSV) can be used to determine the potential at which the onset of anode effect and treat that potential as a measure of the solubility; the higher the anode effect potential the higher is the concentration. In this technique, a known quantity of uranium oxide powder is added and dissolved and the anode effect potential is determined. The point beyond which the anode effect potential does not vary is considered the limit of solubility. Here too, the non availability of a reference electrode causes problems, and therefore, it was not pursued.
5. In the fifth method, a solid shape of the oxide is immersed in the electrolyte and after sufficient time has elapsed, the weight change can be taken as the limit of solubility. Weight change measurement of the sintered  $\text{UO}_2$  pellet immersed in the electrolyte was attempted, however the mechanical operation to remove adhering electrolyte led to chipping of the pellets and introduced errors. Similar problem of electrolyte adhesion with solid rods have been reported by the Greenfield and Hyde [4.6]. Hence this technique could not be adopted.
6. The next method involves, collecting a sample of electrolyte that has been saturated with oxide and conduct chemical analysis to determine the extent of solubility, with due precaution of sampling the liquid through a filter such that it separates suspended undissolved oxide fully. Several attempts of

equilibrating the electrolyte with  $\text{UO}_2$  powder and collecting a sample through the porous graphite filter from the surface of electrolyte again did not yield reliable results. Therefore, a more reliable method was explored.

7. In this method of sampling in cold conditions, it involved equilibrating the electrolyte bath with the sintered pellet of uranium oxide and collecting the solidified electrolyte sample by carefully separating the pellet after cooling the electrolyte to room temperature. Adhered salt to the  $\text{UO}_2$  pellet was removed separately and was not mixed with the electrolyte sample. This last approach has several advantages; a) the electrolyte bath does not have to be free from any dissolved oxide at the start of determination, b) the oxide does not have to remain in solution in the solid form as there are no suspended oxide particles in the liquid sample coming from the powder and c) visibility of the experimental crucible is not required at high temperature operation. This method was, therefore, adopted.

The main steps in conducting the experiments on uranium oxide solubility in  $\text{LaF}_3$  containing salt mixtures are enumerated below.

- a. Salt mixture preparation
- b. Purification of the electrolyte
- c. Dissolving the solute to saturation in the intended electrolyte at the temperature of study
- d. Sample collection and preparation
- e. Analysis for total uranium

## 4.2 Salt mixture preparation and their purification

All the individual salts used in the experiment were dried in vacuum at 1073K for 3hrs in a graphite crucible and then transferred into the desiccators and retained as stock. ~30g electrolyte mixture was prepared by weighing and mixing the individual salts of LiF, BaF<sub>2</sub> and LaF<sub>3</sub> in the desired proportions in a mortar and pestle and transferred to a graphite crucible. The procedure developed in this work for preparation of salt mixture has been described in chapter 3 (section 3.2.3). UO<sub>2</sub> powder and sintered UO<sub>2</sub> pellets were obtained from Nuclear Fuel Complex, Hyderabad and were of nuclear grade used in reactor applications. The conditioning procedure involved first equilibrating the electrolyte mixture for pretreatment at 673K for 24hrs and another 24hrs at 1473K in a continuous stream of high purity argon gas having <0.1ppm of oxygen, the procedure is described in detail also in chapter 3 (section 3.3). The composition of salt mixtures prepared and characterized were LiF: BaF<sub>2</sub>(1:1) base salt with 10, 30 and 50 Wt % LaF<sub>3</sub>. In a few experiments 8.1 wt%LaF<sub>3</sub>-1.9 wt% UF<sub>4</sub> and 28.1 wt%LaF<sub>3</sub>-1.9 wt% UF<sub>4</sub> mixture was used instead of 10% LaF<sub>3</sub> and 30% LaF<sub>3</sub> respectively.

## 4.3 Experimental setup for solubility studies

### *Design and fabrication of the experimental setup*

The experimental setup consists of a muffle to provide an inert gas cover and a heating system to achieve the desired temperature. The experimental setup for solubility studies was designed from first principles for heat transfer aspects to arrive at the final length of the muffle. The material selection was based on thermodynamic considerations, functionality, properties of the materials, cost considerations and ease of fabrication. The design considerations for this experimental setup related to the

inert gas requirement, structural and containment materials, hot zone uniformity, leak tightness, sealing O ring are similar to the ones for preparation of all the mixtures for thermo-physical characterization described in Chapter 3 (sec 3.2.4). Additional considerations for this experimental setup for uranium oxide solubility studies for safety and internal arrangement are as follows

1. The maximum design temperature should be 1673K, 50K above the desired temperature.
2. All the experiments need to be conducted in a fume hood to prevent spread of radioactive powders and vapours.
3. The air drawn through the fume hood should be filtered through a HEPA filter with a particulate removal efficiency of  $>99.97\%$  for  $0.3\mu\text{m}$  size particle, to prevent discharge of radioactive particles into the atmosphere
4. After the HEPA filtration, the air should be passed through a water scrubber to removal fluoride vapours present.
5. Detailed HAZOP analysis should be carried out and engineered safety features should be incorporated in the experimental assembly to prevent any accidental release of radioactivity. The experimental assembly shall have to go through formal safety audit, and safety clearance from regulatory authorities has to be obtained prior to commencement of experiments.
6. Movement of the internals should be through an O ring sealed shaft seal arrangement or through a Teflon ferrule, for leak free operation. The movement should also be guided for accuracy.
7. The cross-section of the connecting members should be such that they have sufficient strength at high temperature and yet minimize heat losses by conduction.

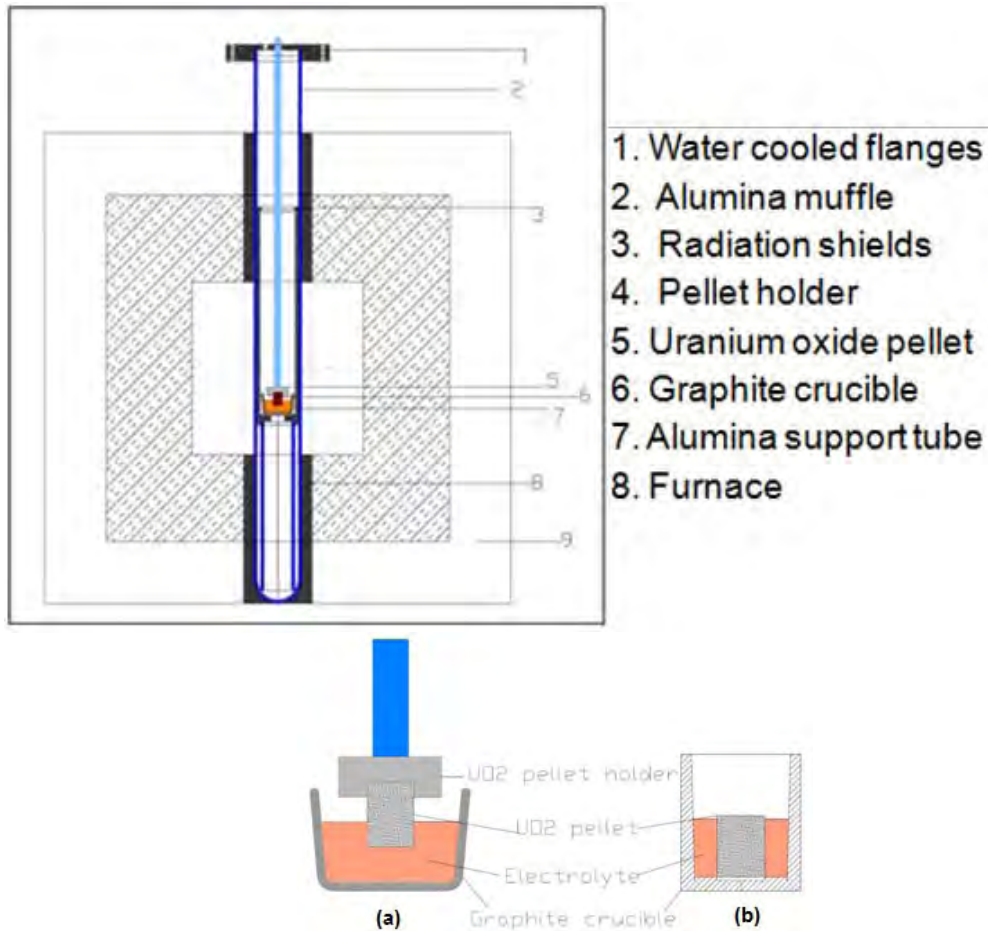


Figure 4.1 Schematic of the experimental setup for solubility study



- |                           |  |
|---------------------------|--|
| 1 Fumehood                | 4 Experimental setup with alumina tube |
| 2 Furnace inside fumehood | 5 Fumehood sash                        |
| 3 Thermocouple            | 6 Control panel for furnace            |

Figure 4.2 Photograph of the solubility study experimental setup inside fumehood

A recrystallized alumina tube of 80mm ID and 90mm OD 800mm long, closed at one end was used as the muffle. Viton O ring sealed water cooled stainless steel flanges were used on the open end of the alumina tube. The flange had openings for gas inlet and outlet connections, and the other feed throughs for pellet holder and thermocouple. Heating of the alumina tube was done by a 6kW resistive heating furnace controlled by a PID controller within the range of  $\pm 3\text{K}$ . A pack of radiation shields of 78mm diameter was used to prevent heat losses and to maintain a uniform temperature zone; the pack of shields was supported from the flange. A high density graphite crucible of ~50mm diameter was used to contain the salt mixture. The crucible containing the electrolyte rested on an alumina support tube of 45mm OD in the uniform temperature zone, which has in turn rested on the bottom of the alumina tube. The  $\text{UO}_2$  pellet holder was made out of high density graphite, and had a provision to hold the  $\text{UO}_2$  pellet of ~13mm diameter and ~19mm height on one end. The other end of the pellet holder had a provision to fasten an 8mm diameter molybdenum rod. All the other high temperature structural members were made of either graphite or molybdenum. High purity argon with <0.1ppm of oxygen was purged continuously during the experiment. The oxygen concentration in the inlet gas was continuously monitored by an online oxygen gas analyzer (Systech 800 Series analyzer). The furnace was housed inside a fumehood and the purge gas released into the fumehood was passed through HEPA filters and a water scrubber to remove radioactive particulate and fluoride vapour respectively before exhausting to the environment. The schematic diagram of the experimental setup is shown in Fig.4.1 and the photograph in figure 4.2. Safety clearance was obtained from the Regulatory authorities before carrying out the experiments with radioactive materials.

#### 4.4 Experimental procedure

Electrolyte mixtures of LiF: BaF<sub>2</sub>(1:1) with 10, 30 and 50 Wt % LaF<sub>3</sub>, 8.1 wt%LaF<sub>3</sub>-1.9 wt% UF<sub>4</sub>, 28.1 wt%LaF<sub>3</sub>-1.9 wt% UF<sub>4</sub> were prepared in batches of 30g with the salt mixture preparation procedure which has been developed (chapter 3). The preconditioning procedure used in the setup of experiments also was as developed in this work (Para 3.3). Two experimental methods were used in the solubility studies. In the first method, a pre-weighed sintered UO<sub>2</sub> pellet was held in a graphite pellet holder, and after the preconditioning of the electrolyte the pellet was immersed in the electrolyte in molten condition and removed before cooling of the electrolyte (as shown in figure 4.1a). In the second method sintered UO<sub>2</sub> pellet was weighed and placed in the high density graphite crucible. The electrolyte mixture was added to the annular gap between the crucible and the pellet. The graphite crucible had a draft angle of 3° to remove the solidified salt mixture easily. The pellet was immersed fully without a holder and was allowed to cool down along with the electrolyte (figure 1b) after equilibration. As the total surface area available was higher with UO<sub>2</sub> pellet fully immersed in the electrolyte, this procedure was adopted for all the experiments. After the equilibration of the molten electrolyte with UO<sub>2</sub> the setup was cooled. Before commencing flow of the argon purge gas, the complete system was evacuated to 1E-2 mbar and back filled with argon at least 8-10 times to remove the trapped air.

The next step involved in equilibrating the electrolyte and the sintered UO<sub>2</sub> pellets for 48hrs at the temperature of study. Initially the time required for reaching saturation was determined by conducting different experiments with immersion duration of 12, 24, 36 and 48 hrs. It was observed that the concentration reached saturation after 24hrs of immersion of the pellet. In all the data generation experiments the sintered

UO<sub>2</sub> pellets were equilibrated with the electrolyte for 48hrs at the temperature of the study; this ensured saturation even with the experimental uncertainties. In an attempt to study the effect of increase in the surface area available for dissolution, in one of the experiments equilibrating a UO<sub>2</sub>+C pellet with the electrolyte was tried. It was observed that the UO<sub>2</sub>+C pellet had disintegrated and no meaningful determination of solubility limit was possible. Hence using UO<sub>2</sub>+C pellet was not continued. The molten fluoride salt mixture solvent was equilibrated with a sintered uranium oxide pellet at 1473K, 1523K and 1573K. The samples and the experiments with their nomenclature are presented in Table 4.1.

After cooling to room temperature the salt mixture was separated from the pellet, the entire sample was ground for homogenizing and analysis of total uranium concentration. All the uranium in the sample is assumed to be obtained from the dissolved UO<sub>2</sub>. The complete matrix of the experiments conducted is shown in Table 4.1. Around 45 experiments were conducted and several experiments were repeated more than one or two times to obtain more accurate estimate.

Table 4.1 Matrix of the experiments conducted for UO<sub>2</sub> solubility in molten fluoride salts

	UO <sub>2</sub> Pellet			UO <sub>2</sub> Pellet, Mixed electrolyte						UO <sub>2</sub> +C Pellet			UO <sub>2</sub> +C Anodic
%LaF <sub>3</sub>	10Wt%	30Wt%	50Wt%	8.1% LaF <sub>3</sub> 1.9% UF <sub>4</sub>	28.1% LaF <sub>3</sub> 1.9% UF <sub>4</sub>	48.1% LaF <sub>3</sub> 1.9% UF <sub>4</sub>	9.4% LaF <sub>3</sub> 0.6% UF <sub>4</sub>	29.4% LaF <sub>3</sub> 0.6% UF <sub>4</sub>	49.4% LaF <sub>3</sub> 0.6% UF <sub>4</sub>	10Wt%	30Wt%	50Wt%	10Wt%
1423K	√ SS20A	√ SS20B	√ SS20C	-	-	-	-	-	-	-	-	-	-
1473K	√ SS21A	√ SS21B	√ SS21C	√ SS28A	√ SS28B	√ SS28C	√ SS28D	√ SS28E	√ SS28F	√ SS26A	√ SS26B	√ SS26C	√ SS25 SS27 SS29 SS30
1523K	√ SS22A	√ SS22B	√ SS22C	-	-	-	-	-	-	-	-	-	-

## **4.5 Sample dissolution and uranium analysis methods**

Sample dissolution is one of the biggest challenges faced by the analytical chemist while analyzing the mixture of fluoride samples. There are three main techniques for sample dissolution/decomposition a) fusion; b) acid leaching or acid dissolution; and c) complete microwave digestion. Fusion technique is used individually or in combination with acid leaching to dissolve samples analyzed in radioanalytical laboratories, when total sample dissolution of a difficult sample matrix is required. Leaching technique is used to determine only the soluble fraction of the radionuclide of interest under specific conditions. However, recent advances in microwave vessel design allow use of higher temperature (upto 500K) and pressure (upto 100bar) along with higher quantity of samples. The advantages of microwave digestion are that it is faster, cleaner, more reproducible, and more accurate than traditional hotplate digestion. Hence, microwave dissolution was used for dissolving all the samples generated in the study. A detailed list of solutions tried for dissolution are presented in Table 4.2. Inductively coupled plasma mass spectrometry (ICP-MS) was used for the determination of the total uranium present in the dissolved sample.

## **4.6 Results and discussions**

### **4.6.1 Uncertainties and errors**

Due to several difficulties in conducting solubility measurements in molten fluoride electrolytes at high temperature, there is an unavoidable scatter in the results. The individual solubility data presented in Table 4.3 is the mean of at least 3 observations and the uranium oxide solubility data reproducibility is of the order of  $\pm 5\%$  of the value reported. This limit also includes the error in obtaining samples for analysis and also the uncertainties in the analytical instrumentation technique.

Table 4.2 Parametric study for microwave dissolution of fluoride samples for uranium analysis

Salt and Solvent	A		B		C		D	E			
Quantity	50mg	100mg	50mg	100mg	50mg	100mg	100mg	50mg	100mg	200mg	>300mg
LiF	√	√	√	√	<b>X</b>	<b>X</b>	<b>X</b>	-	-	-	-
CaF <sub>2</sub>	√	√	√	√	<b>X</b>	<b>X</b>	<b>X</b>	-	-	-	-
LiF-CaF <sub>2</sub>	√	√	√	√	<b>X</b>	<b>X</b>	<b>X</b>	√	√	√	√ <sup>#</sup>
LiF-BaF <sub>2</sub>	<b>X</b>	√	√	√	√ <sup>#</sup>						
LiF-BaF <sub>2</sub> -10%UF <sub>4</sub>	<b>X</b>	√	√	√	√ <sup>#</sup>						
LiF-BaF <sub>2</sub> -25%UF <sub>4</sub>	<b>X</b>	√	√	√	√ <sup>#</sup>						
LiF-BaF <sub>2</sub> -10%LaF <sub>3</sub>	<b>X</b>	√	√	√	√ <sup>#</sup>						
LiF-BaF <sub>2</sub> -20%LaF <sub>3</sub>	<b>X</b>	√	√	√	√ <sup>#</sup>						
UO <sub>2</sub>	-	-	-	-	-	-	-	√	√	√	√ <sup>#</sup>

A: 7ml Conc HCl, 1ml Conc HNO<sub>3</sub> solvent, for 20min at 220°C.

B: 7ml Conc HCl, 1ml Conc HNO<sub>3</sub> solvent, for 30min at 220°C.

C: 5ml Conc HCl, 5ml Conc HNO<sub>3</sub> solvent, for 30min at 220°C.

D: 8.7ml Conc HCl, 1.3ml Conc HNO<sub>3</sub>, 0.5g H<sub>3</sub>BO<sub>3</sub> solvent, for 40min at 220°C.

E: 6ml Conc HCl, 6ml H<sub>3</sub>BO<sub>3</sub> solution (0.7M), for 20min at 220°C.

#-with proportionate increase of solution required for dissolution of 200mg.

#### 4.6.2 Effect of LaF<sub>3</sub> concentration

Studies were conducted with 10%, 30% and 50% LaF<sub>3</sub> additions in the LiF-BaF<sub>2</sub> base electrolyte. The solubility of UO<sub>2</sub> increased with increase in LaF<sub>3</sub> in the electrolyte in the range of 1423K-1523K. The solubility variation for 30% LaF<sub>3</sub> and 50% LaF<sub>3</sub> bearing solvents remained in a similar range within the standard deviation of analysis. The solubility of oxides in uranium fluoride melts is predominantly due to the formation of complexes of uranium, fluorine and oxygen. Similar kinds of complexes are probably formed by addition of LaF<sub>3</sub>. Although a number of uranium oxy fluoride complexes exist, such a complex prevailing at high temperature has never been proven in the molten fluoride system. Greenfield and Hyde have reported compound formation of UF<sub>4</sub> with diluent salt, K<sub>2</sub>UF<sub>6</sub> or 2KFUF<sub>4</sub> in KF containing electrolytes and 4LiF.UF<sub>4</sub>, 7LiF.6UF<sub>4</sub> in LiF rich electrolytes; which reduce the total availability of free UF<sub>4</sub> which associates with UO<sub>2</sub> to increase its solubility [4.6]. In a similar fashion, Ba<sub>2</sub>LaF<sub>7</sub> phase has been observed at room temperature by XRD of samples from solubility studies. This probably explains the reason for not having a large variation of UO<sub>2</sub> solubility in melts containing 30 Wt% LaF<sub>3</sub> and 50% LaF<sub>3</sub>. At 1523K probably the compound is unstable thereby freeing LaF<sub>3</sub> which increases the solubility of UO<sub>2</sub> at that temperature. However, no obvious correlation between the room temperature phases present and the UO<sub>2</sub> solubility could be derived from the results. The oxide solubility of a molten fluoride mixture under equilibrium condition of a fixed bath composition and temperature is not dependent on the total surface area of oxide per unit mass of electrolyte, as observed in the experiment with LiF-BaF<sub>2</sub>-10 wt%LaF<sub>3</sub>. However, the time required for reaching saturation or equilibrium will be less as the surface area for dissolution is higher.

Table 4.3 Solubility of UO<sub>2</sub> in LiF-BaF<sub>2</sub>-LaF<sub>3</sub> melts

S.no	Sample No and % LaF <sub>3</sub>	% UO <sub>2</sub> solubility at 1423K	% UO <sub>2</sub> solubility at 1473K	% UO <sub>2</sub> solubility at 1523K
1	SS20 10% LaF <sub>3</sub>	0.11	0.415	0.76
2	SS21 30% LaF <sub>3</sub>	0.2	0.57	0.8
3	SS22 50% LaF <sub>3</sub>	0.19	0.56	0.984

#### 4.6.3 Effect of temperature

Information of UO<sub>2</sub> solubility as a function of temperature in different electrolytes is important as the temperature of electrolysis plays an important role. Studies conducted with 10%, 30% and 50% LaF<sub>3</sub> additions in LiF-BaF<sub>2</sub> base electrolyte in the range of 1423K-1523K are analyzed. As anticipated intuitively at a given percentage of LaF<sub>3</sub> with molten fluoride mixture the UO<sub>2</sub> solubility increased with increase in temperature of the molten salt. In the LiF-BaF<sub>2</sub> 1:1- 10% LaF<sub>3</sub> electrolyte the solubility of UO<sub>2</sub> was 0.11 wt% at 1423K, which increased to 0.145 wt% at 1473K and further increased to 0.76% at 1523K. Similar increasing trend with temperature was observed for LiF-BaF<sub>2</sub> 1:1- 30% LaF<sub>3</sub> and LiF-BaF<sub>2</sub> 1:1- 50% LaF<sub>3</sub> electrolytes as shown in figure 4.4. The maximum solubility of UO<sub>2</sub> in LaF<sub>3</sub> containing electrolytes observed at 1523K in LiF-BaF<sub>2</sub> 1:1- 50% LaF<sub>3</sub> electrolyte, was 0.984%.

#### 4.6.4 Effect of addition of UF<sub>4</sub> to LaF<sub>3</sub> (mixed electrolyte)

1.9 wt% of UF<sub>4</sub> has been added as a replacement of LaF<sub>3</sub> in the experiments conducted with LiF-BaF<sub>2</sub>- 8.1 wt%LaF<sub>3</sub>-1.9 wt% UF<sub>4</sub> (Sample No. SS28A) and LiF-BaF<sub>2</sub>-28.1 wt%LaF<sub>3</sub>-1.9 wt% UF<sub>4</sub> (Sample No. SS28B) at 1473K. With the addition of 1.9% UF<sub>4</sub> to the LaF<sub>3</sub>, the combined effect of the mixed electrolyte resulted in a higher UO<sub>2</sub> solubility in comparison to the UF<sub>4</sub> free electrolyte. Total uranium in the electrolyte was

analyzed and the contribution from UF<sub>4</sub> has been subtracted to arrive at the solubility of UO<sub>2</sub>.

Table 4.4 Solubility of UO<sub>2</sub> in mixed electrolytes

Electrolyte	% UO <sub>2</sub> solubility at 1473K
LiF-BaF <sub>2</sub> - 9.4 wt%LaF <sub>3</sub> -0.6 wt% UF <sub>4</sub>	0.46
LiF-BaF <sub>2</sub> - 8.1 wt%LaF <sub>3</sub> -1.9 wt% UF <sub>4</sub>	1.04
LiF-BaF <sub>2</sub> -28.1 wt%LaF <sub>3</sub> -1.9 wt% UF <sub>4</sub>	0.92

The effect of UF<sub>4</sub> addition resulted in a higher dissolution as shown in figure 4.5. This could be due to a complex formation between UO<sub>2</sub> and UF<sub>4</sub>. The UO<sub>2</sub> solubility at 1473K in LiF-BaF<sub>2</sub>- 8.1 wt%LaF<sub>3</sub>-1.9 wt% UF<sub>4</sub> and LiF-BaF<sub>2</sub>-28.1 wt%LaF<sub>3</sub>-1.9 wt% UF<sub>4</sub> electrolyte was 1.04% and 0.92% respectively.

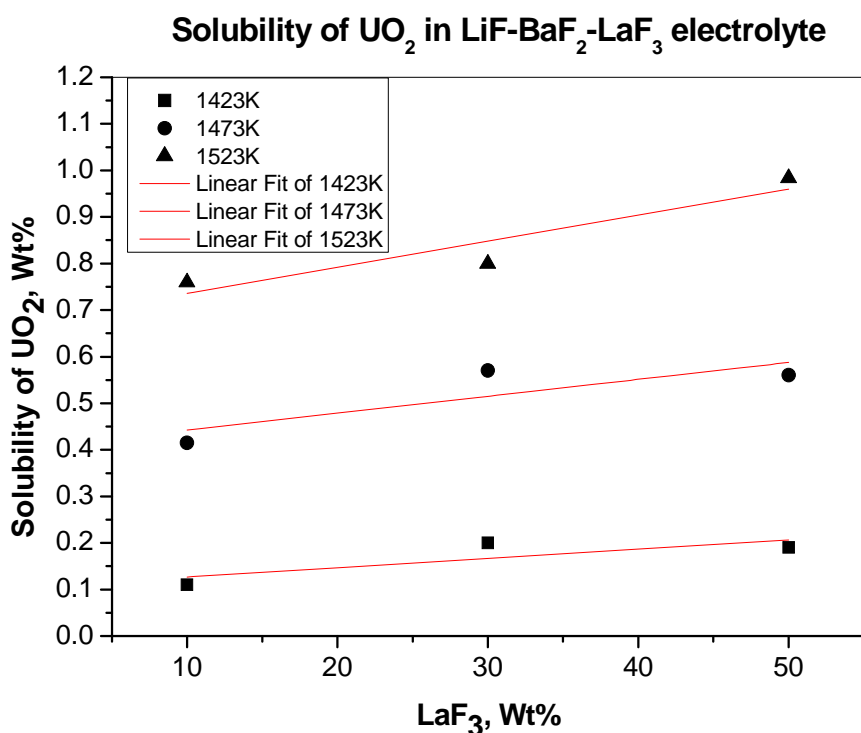


Figure 4.3 Variation of solubility of UO<sub>2</sub> with LaF<sub>3</sub> concentration in electrolytes

Effect of temperature on the solubility of  $\text{UO}_2$  in  $\text{LiF-BaF}_2\text{-LaF}_3$  electrolyte

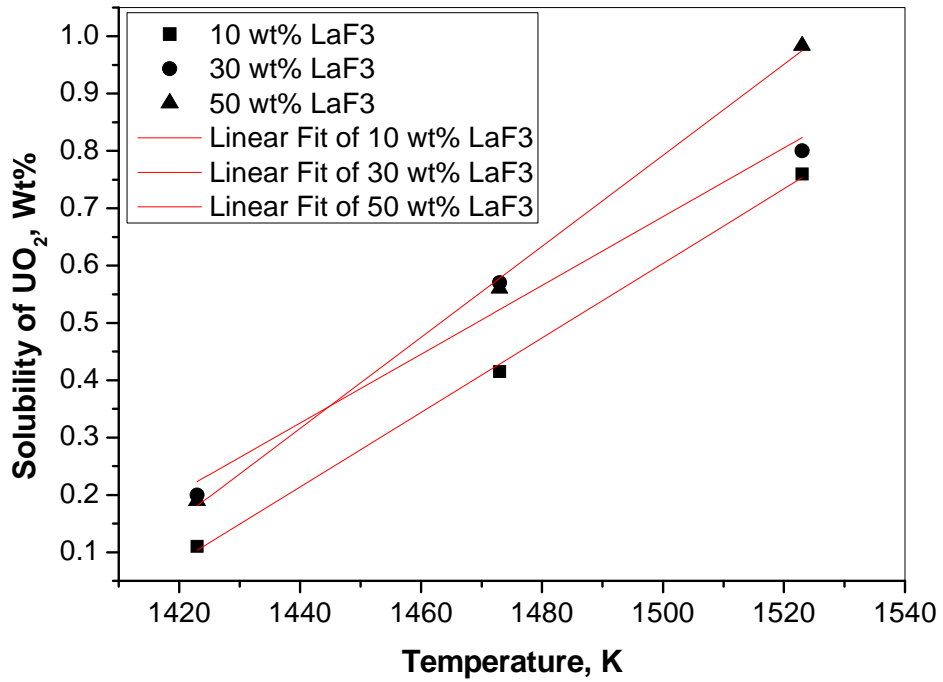


Figure 4.4 Variation of solubility of uranium oxide with temperature

Effect of  $\text{UF}_4$  on the solubility of  $\text{UO}_2$  in  $\text{LiF-BaF}_2\text{-LaF}_3$  electrolyte at 1473K

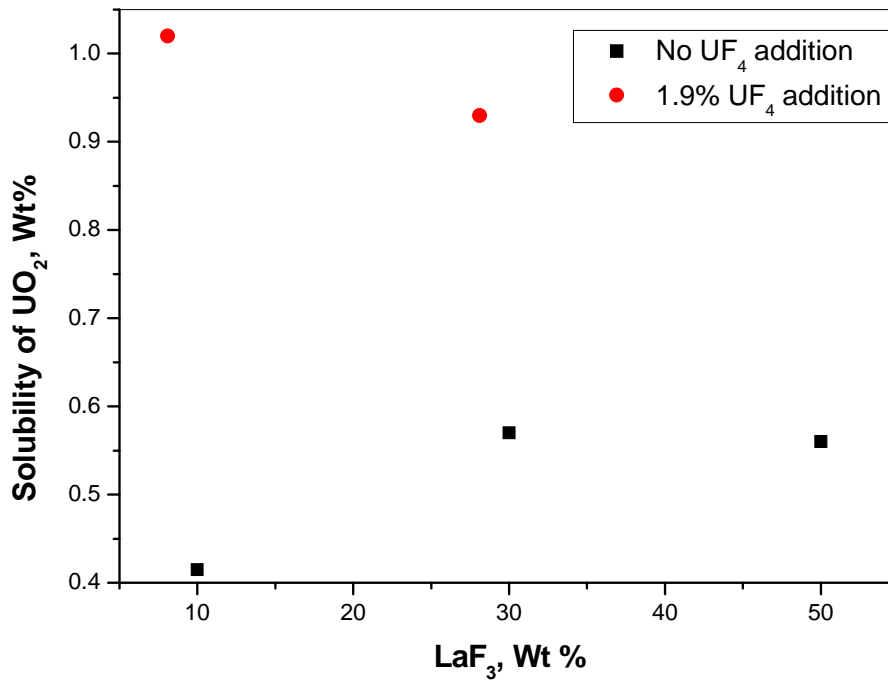
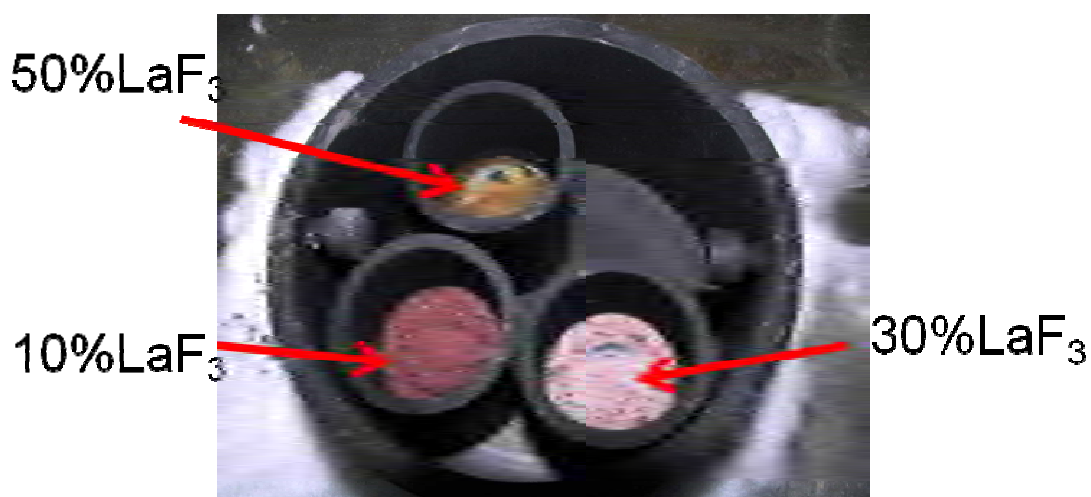


Figure 4.5 Solubility of uranium oxide in mixed electrolytes



**Pellet holder and pellet used for solubility studies**



**Colours developed in different electrolytes**

Figure 4.6 Photographs of pellet holder, pellet and colors developed after the experiment.

#### **4.7 Conclusions**

The solubility of UO<sub>2</sub> in ternary mixtures of LiF-BaF<sub>2</sub>-LaF<sub>3</sub> was determined over a range of composition at temperatures from 1423K to 1523K. The measurement confirmed that the LaF<sub>3</sub> is a reasonably good solvent for UO<sub>2</sub> and its solubility increases with an increase in the LaF<sub>3</sub> quantity. The UO<sub>2</sub> solubility was also found to increase with an increase in the temperature at a given concentration of LaF<sub>3</sub>. Replacing a small amount of LaF<sub>3</sub> with UF<sub>4</sub> had a net positive effect and was found to enhance the

solubility in mixed electrolytes. These results provide guidance for the selection of solvent for the electrolytic cells to produce liquid uranium, which can be utilized for different isotopes of uranium without a separate synthesis step for UF<sub>4</sub> for that particular isotope.

## References

- 4.1. Greenfield, B. F.; Hyde, K. R. The Solubility of Uranium Dioxide in Fluoride Melts. United Kingdom Atomic Energy Authority Report AERE, R-6463; 1983.
- 4.2. Niedrach, L. W.; Dearing, B. E. Electrowining of Uranium from Its Oxides - I. Laboratory Studies. Knolls Atomic Power Laboratory, Rep No KAPL-1761, 1957.
- 4.3. Haas, P. A.; Cooper, P. Solubility of Uranium Oxide in Fluoride Salt at 1200<sup>o</sup>C. U.S. Department of Energy Report K/AIS-243, November 1989.
- 4.4. Varwig J.W., "Solubility of UO<sub>2</sub> in molten salt", Mallinckrodt Chemical Works, Rep No. MCW-1490, 1964.
- 4.5. Porter B., and Brown E.A., "Determination of oxide solubility in the Molten fluorides", Bureau of Mines Report of investigation 5878, U.S. Department of interior, 1961.
- 4.6. Haas P.A and Stanley P. Cooper, "Solubility of uranium oxides in fluoride salts at 1200<sup>o</sup> C", American chemical society, Vol 38, No. 1, pp 26-30, 1993.
- 4.7. Marden J W et. al. "The electrolytic process for the manufacture of uranium, AECD-3687, 1946

- 4.8. Christopher Hardacre, "APPLICATION OF EXAFS TO MOLTEN SALTS AND IONIC LIQUID TECHNOLOGY" *Annu. Rev. Mater. Res.*35:29–49, 2005.

## CHAPTER V

# ELECTROCHEMICAL STUDIES OF URANIUM IN FLUORIDE MELTS

---

This chapter describes the electrochemical studies of uranium in fluoride melts at 1473K.

### 5.1 Introduction

In the pyro electrochemical process for electrolytic reduction of uranium oxide to uranium metal operating at 1473K, uranium oxide is dissolved at the anode and uranium is deposited as liquid metal at the cathode in the electrolyte containing LiF-BaF<sub>2</sub> with UF<sub>4</sub> as the solvent for UO<sub>2</sub> (Chapter II). Many electrochemical studies have been conducted and reported on the electrochemical reactions of U<sup>4+</sup>→U<sup>3+</sup> and U<sup>3+</sup>→U in molten chloride electrolytes by voltammetric studies, chronopotentiometry and potentiostatic measurements as a part of pyro electrochemical reprocessing of spent fuel [5.1-5.16]. Recent interest in the molten salt reactor technology has led to electrochemical investigations of uranium in molten fluoride salt mixtures by Chamelot and Hamel et al. [5.3-5.4]. All the reported data on electrochemistry of uranium in molten fluoride and chloride are below 1000K. As the electrolytic reduction process of uranium oxide to uranium metal is being developed for nominal temperature of 1473K, meaningful application of the published data to the requirements of current work is difficult because of the temperature, difference in reference electrode and working electrode. In the open literature, no electrochemical

studies have been published related to uranium ion electrochemical behavior in LiF-BaF<sub>2</sub> melts; also data related to deposition potentials of uranium ions in melts containing UF<sub>4</sub> at 1473K is not available. In this work, to overcome the difficulty of preparing UF<sub>4</sub> with specific isotopic composition of uranium, LaF<sub>3</sub> has been proposed as a solvent (as described in chapter IV). The electrochemical data for LiF-BaF<sub>2</sub> melt also with LaF<sub>3</sub> solvent have to be generated for the first time. This electrochemical study forms the basis for the development of the UO<sub>2</sub> electroreduction process. Voltammetry is a powerful transient electrochemical technique for not only understanding the dynamic features of electrochemical redox reaction, but also the energetics, and hence, is preferred by most authors. In the present study of electrochemical reduction of uranium ions in LiF-BaF<sub>2</sub>- UF<sub>4</sub> and LiF-BaF<sub>2</sub>- LaF<sub>3</sub> melts, voltammetric investigations supplemented by chronopotentiometry were planned. The investigations were planned with and without addition of UO<sub>2</sub> in the fluoride melt.

## **5.2 Experimental setup for electrochemical studies**

Similar to the experimental setup for solubility studies, the experimental setup for electrochemical experiments also consisted of a muffle to provide an inert gas cover and a heating system to achieve the desired temperature. It was thus a modified design of the solubility study setup. The design of the experimental setup kept in view the following: (a) uniform high temperature zone of 100mm length for operation, (b) required temperature gradient at the cold end to be maintained by the water circulation in the jacketed flange, (c) compatible material of construction that would not deteriorate by metal carbide formation, (d) making a leak tight joint to maintain an oxygen free atmosphere with leak tightness of 1E-9 mbar.l/s or better at the

temperature of operation, (e) provision of insulated electrical feed throughs. Other aspects, such as movement of internals, safety aspects of handling radioactive materials, fumehood requirement for handling radioactive powders (as discussed in section 4.3 of chapter IV for UO<sub>2</sub> solubility studies) were also valid for this experimental setup.

The length of the hotzone, the distance between the cover flanges and the hot zone, the radiation shielding pack and its location, the gas connections and the instrumentation (temperature, pressure and oxygen concentration) for this setup were also designed from the first principles. The system was built according to the design, which was validated by testing. Minor modifications, such as, increase in the total number of disks in the radiation shields and relocating it for reduction of heat losses, were carried out. The system was characterized for leak tightness of 1E-9 mbar.l/s in hot and cold conditions; the temperature profile with the desired size of the uniform temperature zone was established.

All the experiments were conducted at 1473K in a recrystallized alumina tube (80mm ID, 90mm OD and 800mm long) which is closed at one end. The open end was sealed by a pair of stainless steel flanges with O rings between the flange and alumina tube and between the flanges. The flange had provision for electrical feed throughs to make connections to the electrodes for voltammetry. The SS flange had a built in water cooling jacket to cool the O ring seals. Molybdenum rods which were threaded to the top cover stainless steel flange held a threaded graphite crucible holder of 68mm diameter 15mm height. It had an internal thread (50mm diameter x 15mm height) to fasten the crucible of 50mm diameter near the rim; 50mm height and a

uniform wall thickness of 5mm. The electrodes were 50mm long, 0.5mm diameter in case of working electrode and 1mm diameter in case of reference electrode. Electrodes were fastened to a tantalum electrode holder of 6mm diameter and 50mm long, which had a provision to fix the electrode on one end and a 3mm diameter 500mm long tantalum rod at the other end. This tantalum rod was in turn connected to a 5mm diameter 150mm long, stainless steel rod, which was led out of the water cooled flanges through a Teflon sealed electrical feed through. Three such electrodes were taken out of the flange; they served as the counter electrode, the reference electrode and the working electrode, respectively. The schematic of the experimental assembly is shown in figure 5. Figures 5.2a and 5.2b show the photograph of the furnace inside the fumehood and the components of the system.

Purified argon gas with  $<0.1$ ppm of oxygen was purged continuously at 6-8 lph throughout the experiment. The oxygen concentration in the inlet gas was continuously monitored by an online Systech 800 Series oxygen analyzer. Heating of the alumina tube was done by a 6kW resistive heating furnace controlled by a PID controller within the range of  $\pm 3$ K. The process and instrumentation diagram for the electrochemical experiments was identical to that shown in section 3.5.1 of chapter III for development of materials for electrolyte handling.

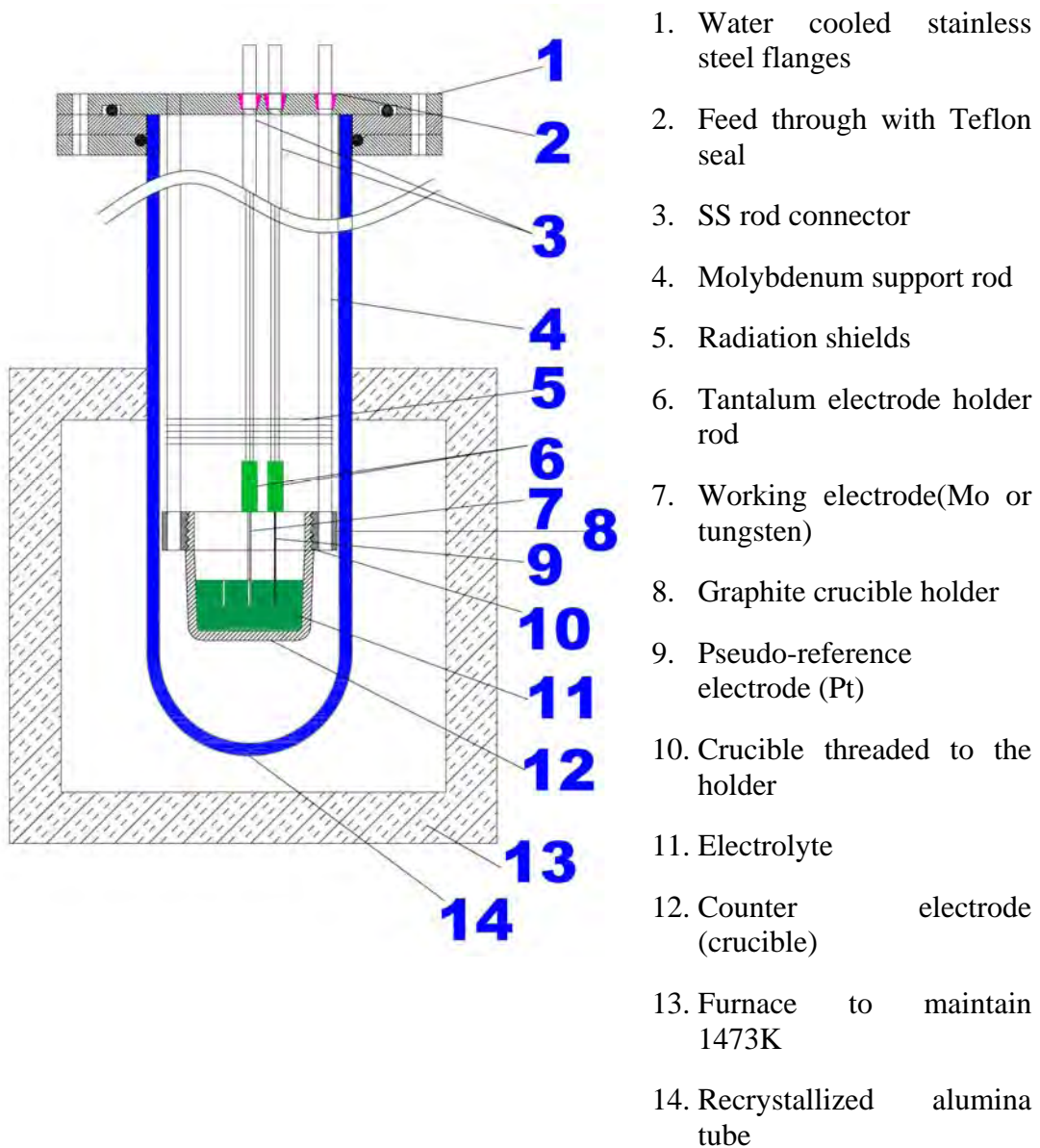


Figure 5.1 Schematic of setup for electrochemical studies



Figure 5.2a Photograph of the setup inside fumehood for electrochemical studies



Figure 5.2b Photograph of the components used for electrochemical studies

### 5.3 Experimental materials and methods

As done in case of the experiments discussed in earlier chapter, LiF and BaF<sub>2</sub> (minimum assay of 99%) were procured from M/s Sigma Aldrich with CAS No. 7789-24-4 and 7787-32-8 respectively. LaF<sub>3</sub> (CAS No. 13709-38-1) was procured from M/s Prabhat chemicals with minimum purity of 99.5%. Nuclear grade UF<sub>4</sub> (>99% assay) was procured from Uranium Extraction Division, BARC. UO<sub>2</sub> powder was obtained from Nuclear Fuel Complex, Hyderabad and was of nuclear grade used for reactor applications. All the salts were dried in vacuum at 1173K for 3hrs in a graphite crucible and then transferred into the desiccators as stock. These pre-dried and pre-weighed salts were used in preparing salt mixtures. Around 60g electrolyte mixture was prepared by weighing the individual salts of LiF, BaF<sub>2</sub> and UF<sub>4</sub> or LaF<sub>3</sub> in the desired proportions and mixing in a mortar and pestle. The mixture was transferred to the graphite crucible. The conditioning procedure involved first equilibrating the electrolyte mixture in the graphite crucible for pretreatment at 673K for 24hrs and another 24hrs at 1473K in a continuous stream of high purity argon gas having <0.1ppm of oxygen as described earlier. The compositions of salt mixtures prepared were LiF: BaF<sub>2</sub>(1:1)-25Wt% UF<sub>4</sub> and LiF-BaF<sub>2</sub>(1:1)-25Wt% LaF<sub>3</sub>. Where voltammograms were recorded with uranium oxide addition uranium oxide powder (4 to 8g) was taken at the bottom of the crucible and then the prepared salt mixture was added.

The electrochemical studies on UF<sub>4</sub> in LiF-BaF<sub>2</sub> eutectic were carried out with and without UO<sub>2</sub> at 1473K by cyclic voltammetry followed by chronopotentiometry. Tungsten or molybdenum wire 0.5mm in diameter and 50mm long were used as the working electrode. The high density graphite crucible served as the counter electrode

and the potentials were referred to a 1mm diameter 50mm long platinum wire acting as a quasi-reference electrode (QRE). The inter-electrode distance was maintained by extent of immersion in the crucible which was calibrated prior to the experiment. AUTOLAB PGSTAT 30 electrochemical workstation was used for recording the voltammograms. GPES software supplied with PGSTAT 30 was used for analyzing the voltammograms. Several trials were taken to establish the suitable sweep rates for voltammetry and also the useful current ranges for chronopotentiometry. These experiments also helped to arrive at the time interval of 1hr required between the tests to equilibrate the mixture. The sweep rate was varied from 50mV/s to 1000mV/s in all the voltammogram recordings. For all the chronopotentiometric experiments, the current was varied from 50mA to 300 mA to study the chronopotentiometric wave. All the electrochemical measurements such as voltammetry and chronopotentiometry were repeated with same sample as well as different sample for each study. The experiments were repeated with different sample of the same composition to obtain conclusive data.

#### **5.4 Results and discussions**

The electrochemical window of the pure LiF-BaF<sub>2</sub> electrolyte was determined without any additives. It was observed that during the cathodic sweep that there was no significant peak before the deposition of lithium at -1.2V and in the anodic sweep anodic dissolution of tungsten electrode at 0.9V. Both the voltages were referred to the platinum pseudo reference electrode immersed in the electrolyte. As can be seen in the voltammogram of LiF-BaF<sub>2</sub> (1:1) electrolyte (figure 5.3), there is a crossover between the cathodic current branch at -1.6V which is characteristic of the nucleation and growth process, in this case the nucleation and growth of lithium. At -2.2V, the

current limit of potentiostat is reached, and thus it was not possible to exceed this voltage. During the scan towards the positive direction, an anodic peak was observed at -0.85V as shown by a well defined peak; this extended up to 0.9V where complete dissolution of the lithium, which was deposited during the cathodic scan, occurs and the onset of dissolution of tungsten takes place.

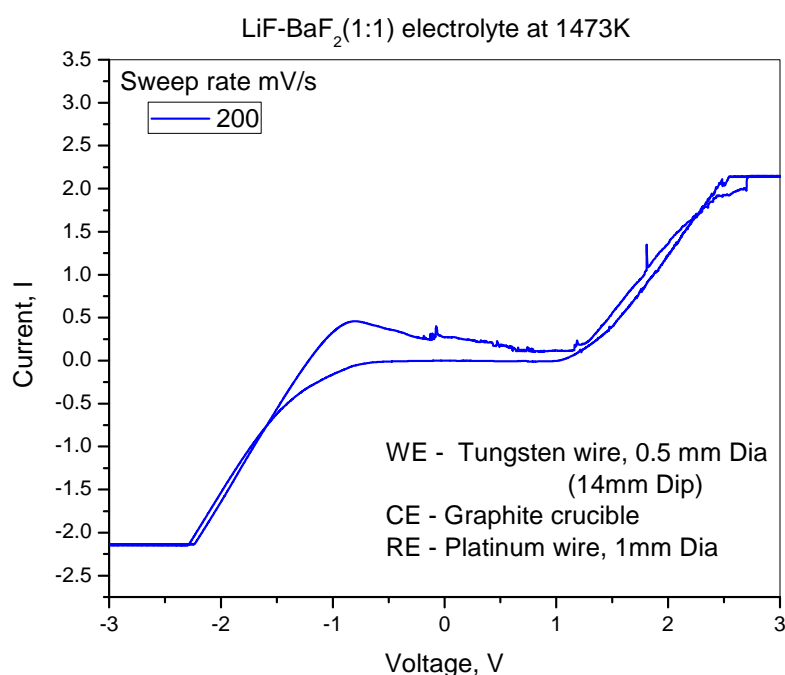


Figure 5.3 Voltammogram of LiF-BaF<sub>2</sub> equimolar electrolyte at 1473K

Figure 5.4 shows a typical cyclic voltammogram obtained with LiF-BaF<sub>2</sub>-25 wt% UF<sub>4</sub> with tungsten as the working electrode and graphite crucible as the counter electrode at 1473K against a platinum pseudo reference electrode immersed in the electrolyte. The cathodic peak I<sub>c</sub> at -1.245V corresponds to lithium deposition and the anodic peak at 0.55V corresponds to lithium dissolution. Two more cathode peaks, II<sub>c</sub> and III<sub>c</sub> and two more anodic peaks, II<sub>a</sub> and III<sub>a</sub> are also observed. They are discussed below.

### 5.4.1 Analysis of cathodic peak IIc and anodic peak IIa

The shape of the cathodic peak IIc and the resulting anode peak IIa suggest that the cathodic reaction corresponds to the reduction of an ion to the corresponding metal, which is followed by oxidation of the deposited metal during the anodic sweep. For a reversible electrochemical reaction which is controlled by diffusion of ions, the cathodic peak current is expressed by Randels-Sevcick equation [5.17]

$$i_p = 0.4463.nFA \left( \frac{nF}{RT} \right)^{1/2} D^{1/2} C_o \nu^{1/2} \dots\dots\dots \text{Eq 5.1}$$

where  $i_p$  is the peak current in amperes,  $C_o$  is the bulk concentration in mol/cm<sup>3</sup>,  $n$  is the number of electrons involved in eq/mol,  $F$  the Faraday constant in C/mol,  $A$  the electrode area in cm<sup>2</sup>,  $D$  the diffusion coefficient in cm<sup>2</sup>/s,  $t$  the time in seconds,  $\nu$  the sweep rate in V/s,  $T$  the temperature in Kelvin and  $R$  the universal gas constant in consistent units.

For a soluble-insoluble ( $U^{3+} \rightarrow U$  metal) system the potential difference between the anodic and cathodic peaks is given by

$$\Delta E_p = 2.3RT/nF \dots\dots\dots \text{Eq 5.2}$$

where  $n$  is the number of electrons involved in eq/mol,  $F$  the Faraday constant in C/mol,  $T$  the temperature in Kelvin,  $R$  universal gas constant, and  $\Delta E_p = (E_{pc} - E_{pa})$ . At 1473K the theoretical separation between the anodic and cathodic peak works out to  $\Delta E_p = 0.292/n$  V where  $n$  is the number of electrons involved in eq/mol. For a  $U^{3+} \rightarrow U$  system the number of electrons participating in the reaction are 3, and the theoretical

separation between the anodic and cathodic peak  $\Delta E_p$  is 0.0973 V. The voltammogram in figure 5.4 shows a peak separation voltage between the cathodic and anodic peaks of 0.65V which is more than the minimum theoretical value possible of 0.0973V. Similar greater separation between the cathodic and anodic peaks was observed for 50mV/s, 200mV/s, 500mV/s, 800mV/s and 1000mV/s sweep rates.

For a reversible electrochemical reaction resulting in an insoluble product ( $U^{3+} \rightarrow U$  metal), the difference between the peak potential  $E_p$  and the half peak potential  $E_{p1/2}$  is related to the number of electrons involved in the reaction given by formula

$$E_{p1/2} = E_p + 0.7725(RT/nF) \quad \dots\dots\dots \text{Eq 5.3}$$

where n is the number of electrons involved in eq/mol, F the Faraday constant in C/mol, T the temperature in Kelvin and R the Universal gas constant [5.9]. Substituting the value of  $E_{p1/2}$  as -0.826V and  $E_p$  as -0.863V the values obtained with tungsten electrode at a scan rate of 0.1V/s, n was found to be approximately 2.65, which is close to the theoretical value of 3 electrons. Hence, it was concluded that the cathodic peak IIc corresponds to reduction of  $U^{3+} \rightarrow U$ .

It is seen that the anodic peak IIa is broad and also not smooth. It appears that smaller peaks are riding over the main peak. At 1473K, the solubility of uranium metal in tungsten is ~1% by weight, and probably an alloy had been formed during the reduction of  $U^{3+} \rightarrow U$ . During reoxidation in the anodic sweep, uranium dissolution occurred from U-W alloy instead of from a pure metal, giving rise to multiple anode

waves in the peak. This kind of behavior has also been observed by Chamelot et al. [5.3] when the nickel electrode was used as a reactive cathode for lanthanide electrochemical studies. This behavior also indicates that the tungsten electrode although expected to be an inert working electrode, is not behaving like one. As all the other refractory metals are inferior to tungsten in respect of liquid uranium solubility at 1473K, the experiments were continued with tungsten.

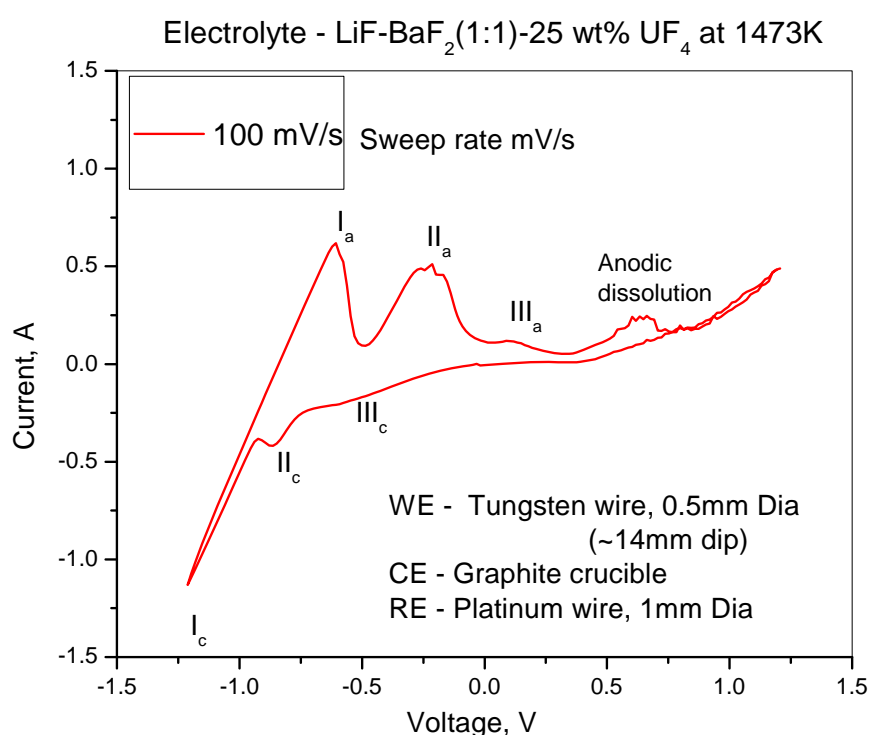


Figure 5.4 cyclic voltammogram in LiF-BaF<sub>2</sub> (1:1)25 wt% UF<sub>4</sub> electrolyte

Table 5.1 presents the data of peak potential and peak current at different sweep rates. As can be seen from the table, the cathodic peaks of  $U^{3+} \rightarrow U$  (peak II<sub>c</sub>) are shifted more cathodically from -0.818V to -1.04V when the scan rate was increased from 0.05V/s to 1V/s respectively. The plot of peak potential  $E_p^{IIc}$  vs the log of sweep rate,

log  $v$  shows a linear variation (figure 5.5). This behavior suggests that the reduction of peak II<sub>c</sub> is probably quasi-reversible.

In Table 5.1 listed are the sweep rates vs voltages and currents of cathodic peaks II<sub>c</sub> and III<sub>c</sub>. It is observed from Table 5.1 that the peak current of the peak II<sub>c</sub> increased from -0.265A to -1.0A with an increase in the scan rate from 0.05V/s to 1V/s. The plot of peak current  $I_p^{IIc}$  vs square root of sweep rate  $v^{1/2}$  also showed a linear variation as shown in figure 5.6, obeying Randels-Sevcick equation, which indicates that the process is diffusion controlled.

Table 5.1 Peak potential and peak current at different sweep rate for cathodic peaks II<sub>c</sub> and III<sub>c</sub>

Sweep rate	Square root of sweep rate	Log of sweep rate	Peak II <sub>c</sub> U <sup>3+</sup> → U	Peak II <sub>c</sub> U <sup>3+</sup> → U	Peak III <sub>c</sub> U <sup>4+</sup> → U <sup>3+</sup>	Peak III <sub>c</sub> U <sup>4+</sup> → U <sup>3+</sup>
$v, V/s$	$v^{1/2} (V/s)^{1/2}$	$\log v$	$E_p^{IIc}, V$	$I_p^{IIc}, A$	$E_p^{IIIc}, V$	$I_p^{IIIc}, A$
0.05	0.224	-1.3	-0.818	-0.265	-0.576	-0.169
0.1	0.316	-1	-0.863	-0.418	-0.591	-0.204
0.2	0.447	-0.69	-0.91	-0.582	-0.713	-0.562
0.5	0.707	-0.301	-0.98	-0.806	-0.757	-0.731
0.8	0.894	-0.097	-0.99	-0.815	-0.77	-0.780
1	1	0	-1.04	-1.0	-0.773	-0.804

Variation of peak potential  $E_p^{IIc}$  with log of sweep rate for peak IIc for reaction  $U^{3+}$  to U metal

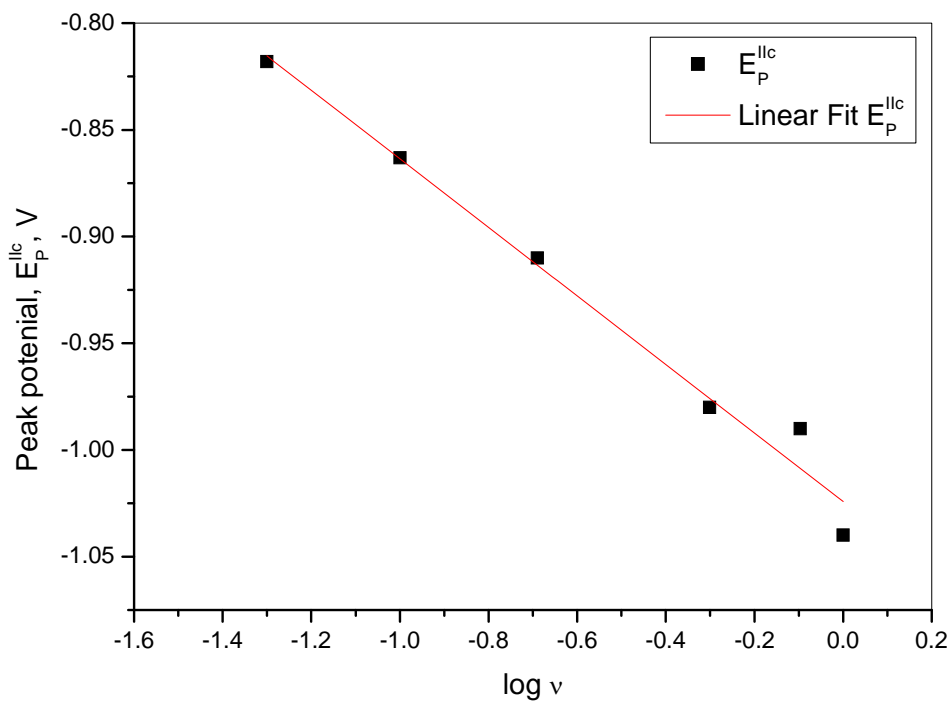


Figure 5.5 Linear variation of peak potential  $E_p^{IIc}$  with sweep rate for peak IIc

Variation of peak current  $I_p^{IIc}$  with square root of sweep rate for peak IIc for reaction  $U^{3+}$  to U metal

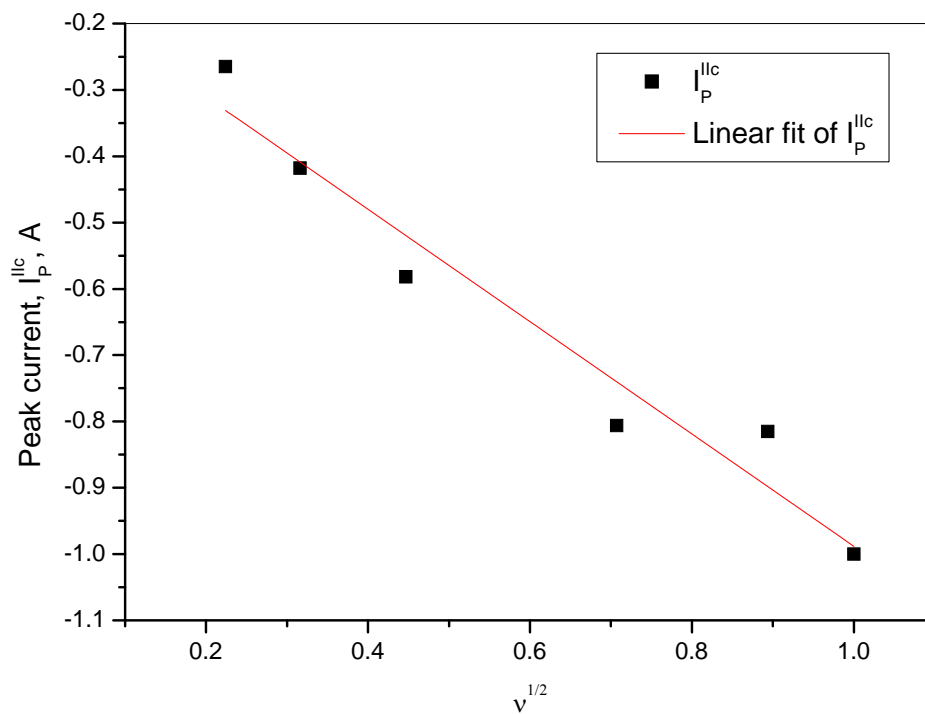


Figure 5.6 Linear variation of peak current  $I_p^{IIc}$  with square root of sweep rate for peak IIc

#### 5.4.2 Analysis of cathodic peak IIIc and anodic peak IIIa

Similarly the peak current for the peak III<sub>c</sub> increased with the sweep rate, from -0.169A at 0.05V/s to -0.804A at 1V/s. The plot of peak current  $I_p^{IIIc}$  vs square root of sweep rate  $v^{1/2}$  showed a linear variation as shown in figure 5.7, which indicates that the electrochemical reaction of peak III<sub>c</sub> is also diffusion controlled. The cathodic potentials of peak III<sub>c</sub> were shifted more cathodically with an increase in the scan rate varying from -0.576V at 0.05V/s sweep rate to -0.773V at 1V/s sweep rate. The plot of the peak potential  $E_p^{IIIc}$  vs log of sweep rate,  $\log v$  shows a linear variation as shown in figure 5.8. This behaviour again suggests that the reduction of peak IIIc is probably quasi-reversible. In an electrolyte containing UF<sub>4</sub> the possible ionic states of uranium are U<sup>4+</sup> and U<sup>3+</sup>. Reduction of U<sup>4+</sup> to U requires a higher potential when compared to U<sup>3+</sup>. Further, the cathodic peak IIc was already attributed to reduction reaction  $U^{3+} \rightarrow U$  based on the number of electrons involved. Hence, the most probable reaction is reduction of  $U^{4+} \rightarrow U^{3+}$ . The potential observed by Hamel et al. [5.4] for  $U^{4+} \rightarrow U^{3+}$  reaction was -0.64V. Thus, it is reasonable to attribute peaks IIIc and IIIa correspond to the redox couple represented by



Generally for a reversible redox couple with soluble-soluble reactant and product ( $U^{4+} \rightarrow U^{3+}$ ), the amplitude of the anodic and cathodic peak current are nearly the same as observed by Prabhakara Reddy et al. [5.9]. This kind of correspondence was not observed in IIIc and IIIa. For a soluble-soluble reversible system (Eq 5.2) the potential difference between the anodic and cathodic peak potential is given by expression

$$\Delta E_p = 2.2RT/nF \quad \dots\dots\dots \text{Eq 5.5}$$

where  $n$  is the number of electrons involved in eq/mol,  $F$  the Faraday constant in C/mol,  $T$  the temperature in Kelvin,  $R$  the universal gas constant in consistent units, and  $\Delta E_p = (E_{pc} - E_{pa})$ . At 1473K the theoretical peak separation between the anodic and cathodic peaks is  $\Delta E_p = 0.279/n$  V where  $n$  is the number of electrons involved in eq/mol. Theoretically for a reversible redox reaction of  $U^{4+} + e \rightleftharpoons U^{3+}$  the difference between the cathodic and anodic peaks is 0.279 V, whereas the observed difference between anodic and cathodic peaks was 0.51V at 0.1V/s sweep rate which differed from the theoretical value by 0.231V. As the peak potentials of the cathodic peak  $E_p^{IIIc}$  were found to shift more cathodically with increase in the sweep rate, the reduction reaction of  $U^{4+} \rightarrow U^{3+}$  indicated quasi reversibility. As there was also a linear dependence of the peak current with square root of the sweep rate, it is inferred that the reduction process  $U^{4+} \rightarrow U^{3+}$  is diffusion controlled.

Variation of peak potential  $E_p^{\text{IIIc}}$  with log of sweep rate for peak IIIc for reaction  $U^{4+}$  to  $U^{3+}$  metal

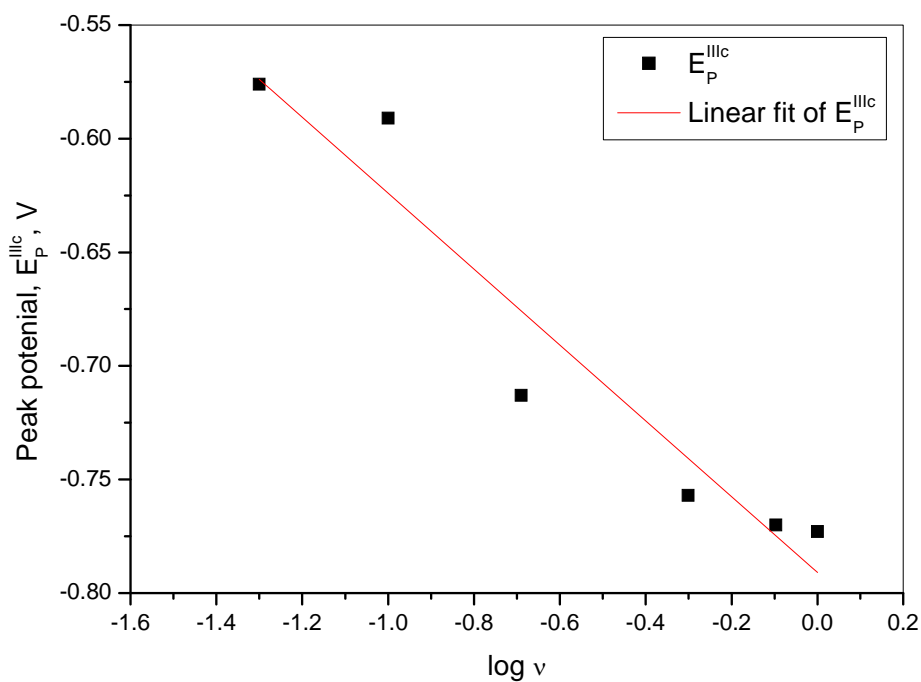


Figure 5.7 Linear variation of peak potential  $E_p^{\text{IIIc}}$  with log of sweep rate for Peak IIIc

Variation of peak current  $I_p^{\text{IIIc}}$  with square root of sweep rate for peak IIIc for reaction  $U^{4+}$  to  $U^{3+}$

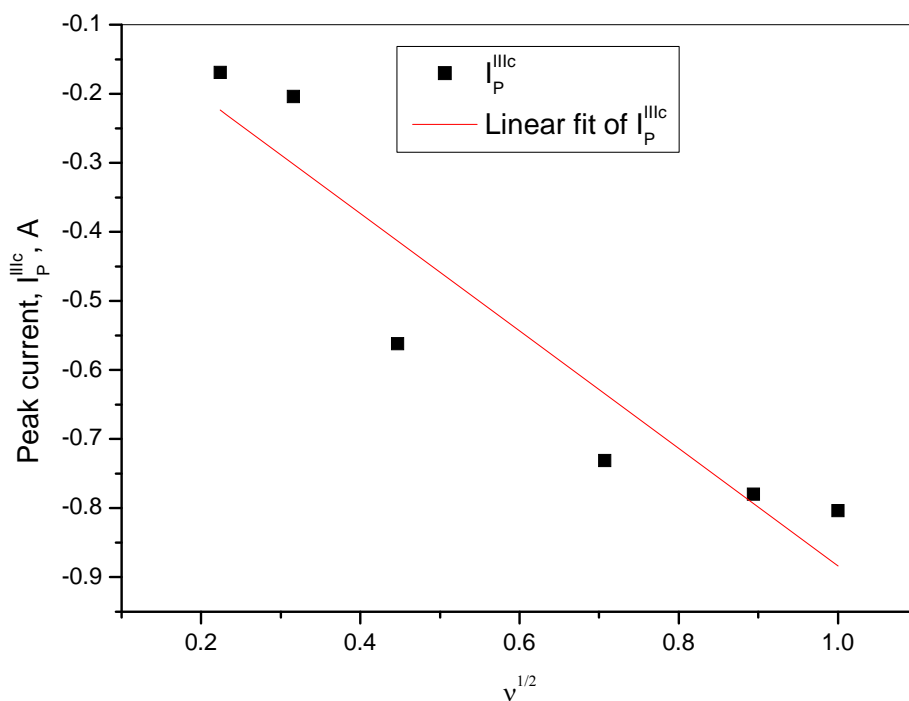


Figure 5.8 Linear variation of peak current  $I_p^{\text{IIIc}}$  with square root of sweep rate for Peak IIIc

### 5.4.3 Chronopotentiometry in LiF-BaF<sub>2</sub> (1:1)-25 wt% UF<sub>4</sub>

Chronopotentiograms were recorded at different currents to confirm the inference from voltammetry that the reduction processes are diffusion controlled in LiF-BaF<sub>2</sub> (1:1)-25 wt% UF<sub>4</sub>. A typical chronopotentiogram for reduction of uranium ions on a tungsten electrode with current of 175mA at 1473K is as shown in figure 5.9. The chronopotentiograms exhibited two reduction waves corresponding to the two reduction peaks as observed in the cyclic voltammogram. The first wave was at a potential of -0.7V and the second wave was at a potential of -0.87V which can be attributed to reduction of uranium ion from U<sup>4+</sup> + e → U<sup>3+</sup> and U<sup>3+</sup> → U metal respectively. Similarly, two reduction waves were observed in the chronopotentiograms recorded in the range of 125mA to 300mA. The relation between the current applied and the transition time τ for a constant current under a semi-infinite diffusion controlled reaction process is given by Sand's equation [5.18] as

$$\frac{i\tau^{1/2}}{C_o} = \frac{nFAD_o^{1/2} \pi^{1/2}}{2} \dots\dots\dots\text{Eq 5.6}$$

where i is the current in amperes, C<sub>o</sub> is the bulk concentration in mol/cm<sup>3</sup>, n is the number of electrons involved in eq/mol, F the Faraday constant in C/mol, A the electrode area in cm<sup>2</sup>, D<sub>o</sub> the diffusion coefficient in cm<sup>2</sup>/s, τ the transition time in seconds, T the temperature in Kelvin, and R Universal gas constant in consistent units.

The product of  $it^{1/2}$  for the reaction  $U^{4+} + e \rightarrow U^{3+}$  was found to be constant around 0.35 in the current range of 150 to 300mA as shown in figure 5.10. As the reaction  $U^{4+} + e \rightarrow U^{3+}$  obeys Sands equation, this confirms that the reduction process is indeed diffusion controlled.

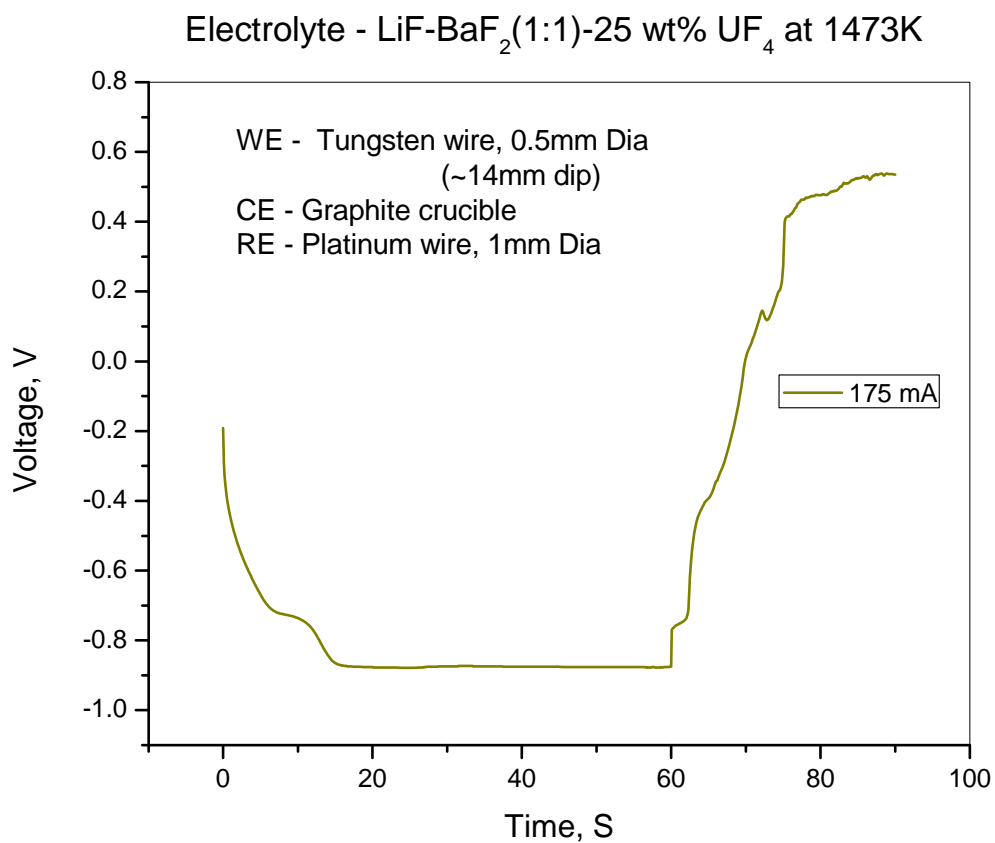


Figure 5.9 Chronopotentiogram in LiF-BaF<sub>2</sub> (1:1)25 wt% UF<sub>4</sub>

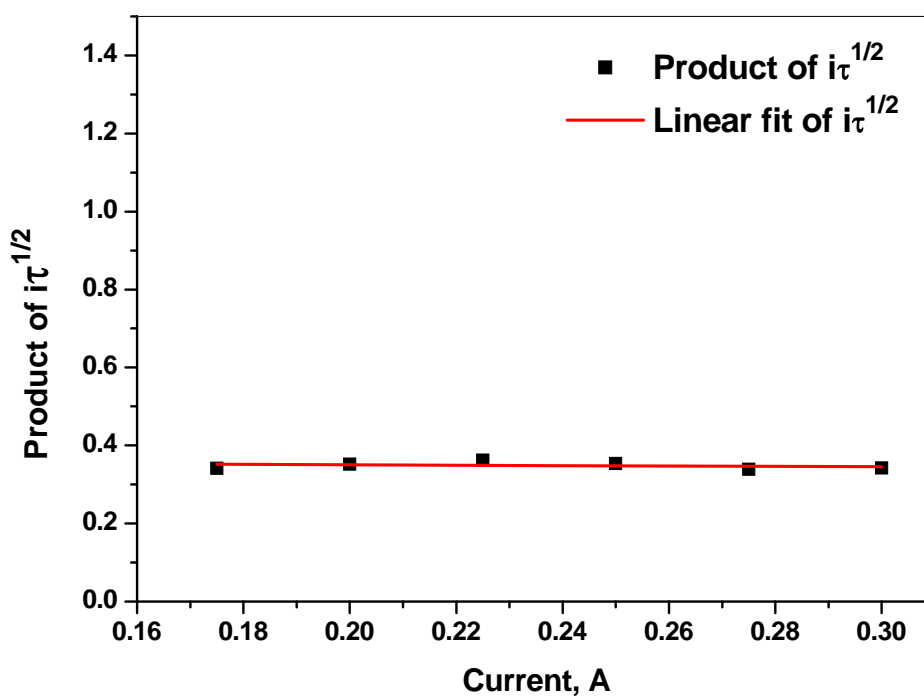


Figure 5.10 Product of  $i\tau^{1/2}$  for Chronopotentiogram in LiF-BaF<sub>2</sub> (1:1)25 wt% UF<sub>4</sub>

#### 5.4.4 Effect of UO<sub>2</sub> addition in LiF-BaF<sub>2</sub> (1:1)25 wt% UF<sub>4</sub>

To study the effect of UO<sub>2</sub> addition to the electrolyte, 4 g of UO<sub>2</sub> was added to 60 g LiF-BaF<sub>2</sub> (1:1)25 wt% UF<sub>4</sub> electrolyte and equilibrated for 24hrs. The UO<sub>2</sub> added was in excess of the quantity required for attaining saturation solubility of UO<sub>2</sub>. It was observed that the addition of UO<sub>2</sub> resulted in the formation of complex ions of uranium, oxygen and fluorine which is indicated by the absence of two distinct reduction peaks observed in voltammogram of LiF-BaF<sub>2</sub> (1:1)-25 wt% without any UO<sub>2</sub> addition. As shown in figure 5.11, a broad shallow peak has replaced the two reduction peaks corresponding to  $U^{4+} \rightarrow U^{3+}$  and  $U^{3+} \rightarrow U$ . The complex of uranium,

oxygen and fluorine may have distributed the energy levels and reduction of such complex can take place over a range of potential instead of a single potential. Such deposition over a range of potential results in a wider and shallower peak with low magnitude of peak current, but the total Coulombs consumed for a given amount of metal deposited remain equal in the electrolytes with and without uranium oxide.

The exact nature of the complex formed has neither been studied nor reported in the open literature. Figure 5.12 shows the chronopotentiogram recorded in LiF-BaF<sub>2</sub> (1:1)25 wt% UF<sub>4</sub> electrolyte with 4g UO<sub>2</sub> on tungsten electrode. Similar to the observation made in the voltammogram, only one reduction wave was observed corresponding to the complex. It was also observed that the potential at which the chronopotentiometric wave was observed was 0.11V more negative than that of the electrolyte without UO<sub>2</sub> addition. One can hypothesize that the net effect of any complexation is to increase the deposition potential of an ion to a more cathodic value.

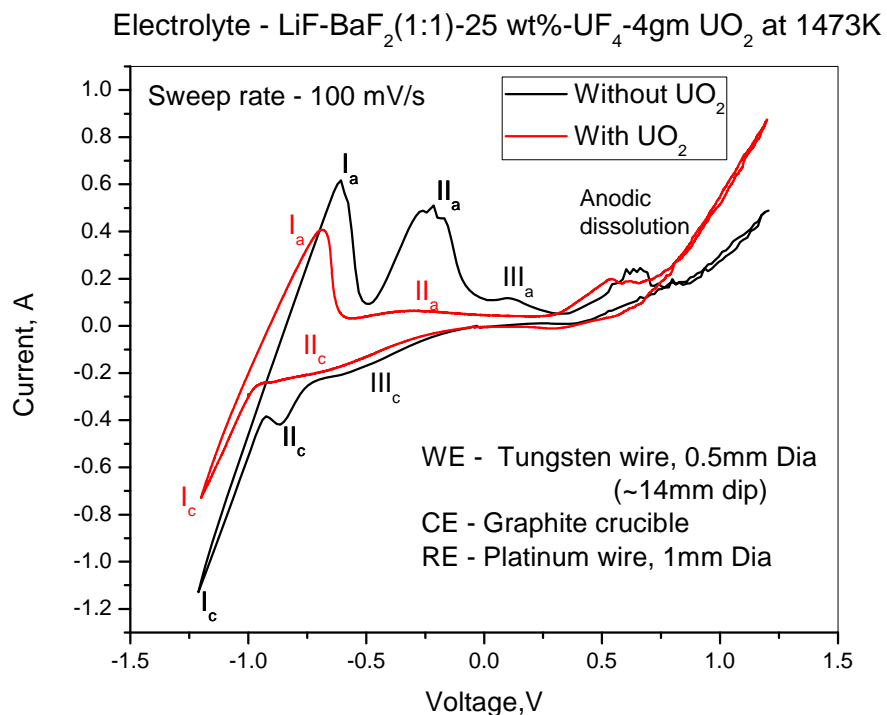


Figure 5.11 Cyclic voltammogram of LiF-BaF<sub>2</sub> (1:1)25 wt% UF<sub>4</sub> electrolyte with and without UO<sub>2</sub>

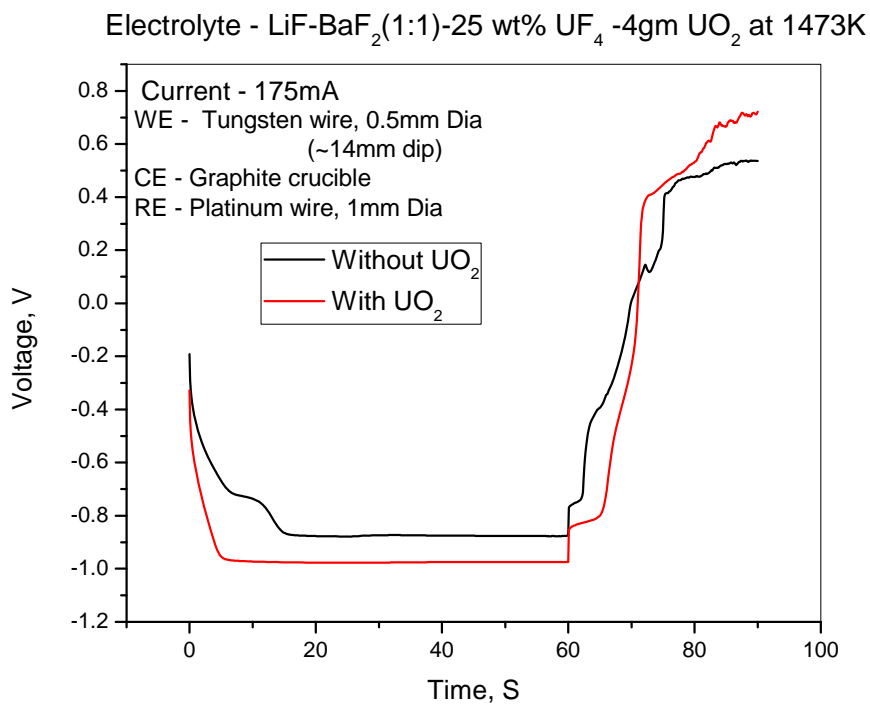


Figure 5.12 Chronopotentiogram of LiF-BaF<sub>2</sub> (1:1)25 wt% UF<sub>4</sub> electrolyte

#### **5.4.5 Electrochemical investigations in LiF-BaF<sub>2</sub> (1:1)-25 wt% LaF<sub>3</sub> melts with and without UO<sub>2</sub>**

Voltammograms and chronopotentiograms were recorded in LiF-BaF<sub>2</sub> (1:1)-25 wt% LaF<sub>3</sub> melts with and without the addition of UO<sub>2</sub> for studying the electrochemical range of LiF-BaF<sub>2</sub> (1:1)-25 wt% LaF<sub>3</sub> electrolyte and the effect of UO<sub>2</sub> addition to the LiF-BaF<sub>2</sub> (1:1)-25 wt% LaF<sub>3</sub>. A typical voltammogram in LiF-BaF<sub>2</sub> (1:1)-25 wt% LaF<sub>3</sub> electrolyte with and without uranium oxide is shown in figure 5.13. It was observed that in LiF-BaF<sub>2</sub> (1:1)-25 wt% LaF<sub>3</sub> there was no significant peak before the deposition of lithium at -1.23V during the cathodic sweep and the anodic dissolution of tungsten electrode at 0.54V in the anodic sweep. Both the voltages were referred to the platinum pseudo reference electrode immersed in the electrolyte. The electrochemical window in the cathode range was similar to the LiF-BaF<sub>2</sub>(1:1) electrolyte, however dissolution of tungsten in the LiF-BaF<sub>2</sub>(1:1)-25 wt% LaF<sub>3</sub> electrolyte during anodic sweep was found to occur at 0.54V, similar to LiF-BaF<sub>2</sub>(1:1)-25 wt% UF<sub>4</sub> which was lower by 0.36V in comparison to the LiF-BaF<sub>2</sub>(1:1). The experiments established that LiF-BaF<sub>2</sub> (1:1)-25 wt% LaF<sub>3</sub> has a suitable electrochemical range for deposition of uranium, which has a deposition potential of around -1V.

To study the effect of UO<sub>2</sub> to the electrolyte, 8g of UO<sub>2</sub> was added to a 60g mixture of LiF-BaF<sub>2</sub> (1:1)-25 wt% LaF<sub>3</sub> and equilibrated for 24hrs. The UO<sub>2</sub> added was again in excess of the quantity required for attaining saturation solubility of UO<sub>2</sub>, as determined in the solubility study with LiF-BaF<sub>2</sub>(1:1) 25 wt% LaF<sub>3</sub> melts (chapter IV). In the electrolyte with UO<sub>2</sub> dissolved in LiF-BaF<sub>2</sub> (1:1) 25 wt% LaF<sub>3</sub> melt, there

were no specific peaks corresponding to  $U^{4+} \rightarrow U^{3+}$  and  $U^{3+} \rightarrow U$ . A small shallow peak was observed at around -1.12V which is the only additional peak observed in the cathodic sweep, indicating that uranium may be present as a complex of uranium, oxygen and fluorine.

Figure 5.14 gives the comparison of chronopotentiograms with 175mA current in LiF-BaF<sub>2</sub> (1:1)-25 wt% UF<sub>4</sub>, LiF-BaF<sub>2</sub> (1:1)-25 wt% UF<sub>4</sub>-UO<sub>2</sub> mixture and LiF-BaF<sub>2</sub> (1:1)-25 wt% LaF<sub>3</sub>-UO<sub>2</sub> mixture at 1473K. It can be seen that with the addition of UO<sub>2</sub>, only a single chronopotentiometric wave was observed in both LiF-BaF<sub>2</sub>(1:1)-25 wt% UF<sub>4</sub>-UO<sub>2</sub> and LiF-BaF<sub>2</sub>(1:1)-25 wt% LaF<sub>3</sub>-UO<sub>2</sub> mixtures. The potential at which the wave occurs in LiF-BaF<sub>2</sub> (1:1)-25 wt% UF<sub>4</sub>-UO<sub>2</sub> mixture is -0.98V whereas in LiF-BaF<sub>2</sub> (1:1)-25 wt% LaF<sub>3</sub>-UO<sub>2</sub> mixture it is at -1.28V. This indicates that the complex of uranium with oxygen and fluorine is more stable in LiF-BaF<sub>2</sub> (1:1)-25 wt% LaF<sub>3</sub> melts in comparison to that in the LiF-BaF<sub>2</sub> (1:1)-25 wt% UF<sub>4</sub> melts, thus requiring an additional 0.3V for the reduction reaction to occur.

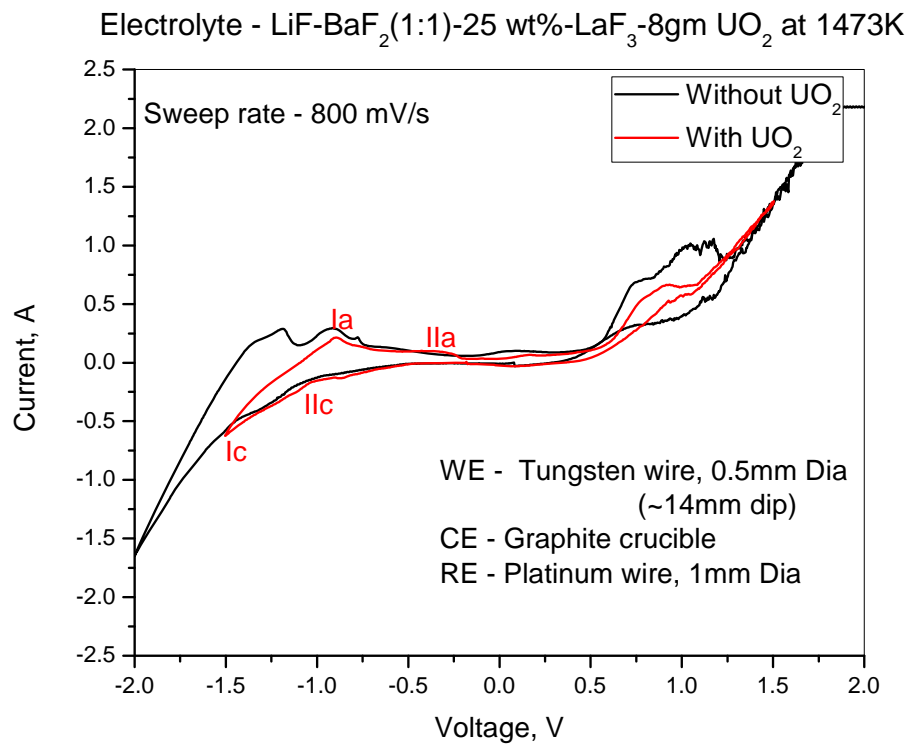


Figure 5.13 Voltammogram of  $\text{LiF-BaF}_2(1:1)25 \text{ wt\% LaF}_3$  electrolyte with and without uranium oxide

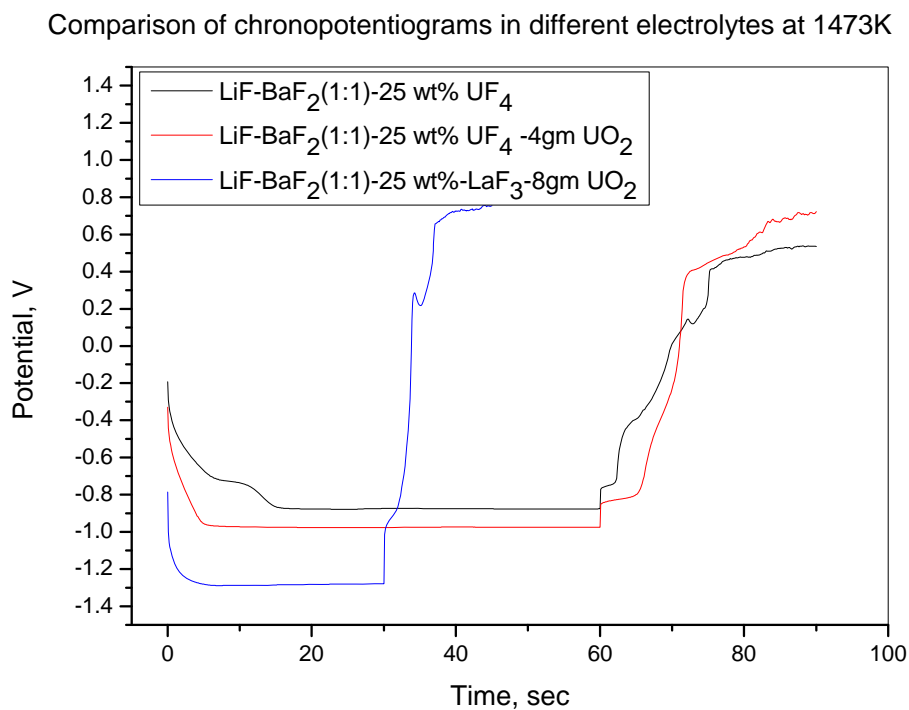


Figure 5.14 Comparison of chronopotentiograms of different electrolytes at 1473K

## 5.5 Conclusions

LiF-BaF<sub>2</sub> (1:1) melts and LiF-BaF<sub>2</sub> (1:1)-25 wt% LaF<sub>3</sub> without addition of any uranium bearing additive were found to have an electrochemical window suitable for the electrolytic deposition of uranium from the melts at 1473K. In the electrolyte LiF-BaF<sub>2</sub>(1:1)25 wt% UF<sub>4</sub>, two redox peaks were observed in the cyclic voltammograms, which were attributed to two redox reactions of U<sup>4+</sup> → U<sup>3+</sup> and U<sup>3+</sup> → U. The reduction potentials of U<sup>4+</sup> → U<sup>3+</sup> and U<sup>3+</sup> → U were -0.804V and -0.999V versus the Quasi Reference platinum Electrode (QRE) at 1473K. It was observed that the cathodic peak potentials shifted more cathodically with an increase in the scan rate, indicating an increasing shift away from reversibility. The linearity of peak current versus  $v^{1/2}$  shows that the electrochemical reduction process is a diffusion controlled process, as it obeys Randels-Sevcick equation.

The chronopotentiograms of UF<sub>4</sub> with the applied current on a tungsten working electrode exhibited two waves corresponding to the two peaks observed in the same potential range as observed in the cyclic voltammogram, which were associated to the two stage reduction of uranium ions, from U<sup>4+</sup> → U<sup>3+</sup> and U<sup>3+</sup> → U metal. The product of applied current and the transition time  $\tau^{1/2}$  in the chronopotentiogram was found to follow the Sand's law, confirming that the electrode process is indeed diffusion controlled.

It is observed that with the addition of UO<sub>2</sub> to the LiF-BaF<sub>2</sub> (1:1)-25 wt% UF<sub>4</sub> electrolyte, the two redox peaks, observed without UO<sub>2</sub>, disappeared and only a broad peak remained, which indicates that uranium may be present as an oxy fluoride complex. Similar behavior was also observed in LiF-BaF<sub>2</sub> (1:1)-25 wt% LaF<sub>3</sub>-UO<sub>2</sub>

mixture. The deposition potentials determined in these experiments were utilized for choosing the cell voltages for molten salt conditioning and electrolysis.

## References

- 5.1. K. Nagarajan, B. Prabhakara Reddy, Suddhasattwa Ghosh, G. Ravisankar, K.S. Mohandas, U. Kamachi Mudali, K.V.G. Kutty, K.V. Kasi Viswanathan, C. Anand Babu, P. Kalyanasundaram P.R. Vasudeva Rao and Baldev Raj, Development of Pyrochemical Reprocessing for Spent Metal Fuels, *Energy Procedia* 7 (2011) 431–436
- 5.2. Sylvie Delpech, *Molten Salts for Nuclear Applications, Molten Salts Chemistry*, 2013, Pages 497-520
- 5.3. P. Chamelot L Massot, C Hamel, C Nourry, P. Taxil, Feasibility of the electrochemical way in molten fluorides for separating thorium and lanthanides and extracting lanthanides from the solvent, *Journal of Nuclear Materials*, 360, 1, 2007.
- 5.4. C. Hamel, P. Chamelot, A. Laplace, E. Walle, O. Dugne, P. Taxil, Reduction process of uranium(IV) and uranium(III) in molten fluorides, *Electrochimica Acta*, Volume 52, Issue 12, 10 March 2007, Pages 3995-4003
- 5.5. Mathieu Gibilaro, Laurent Cassayre, Olivier Lemoine, Laurent Massot, Olivier Dugne, Rikard Malmbeck, Pierre Chamelot, Direct electrochemical reduction of solid uranium oxide in molten fluoride salts, *Journal of Nuclear Materials*, Volume 414, Issue 2, 15 July 2011, Pages 169-173
- 5.6. Takeshi Shimada, Nobuo Tedzuka, Yuzo Shimizu, Masanobu Miyake, Electrode reactions of uranium during electrolysis of its oxide in a molten fluoride mixture, *Journal of Alloys and Compounds*, Volume 206, Issue 2, May 1994, Pages 249-253
- 5.7. D.L. Manning, Gleb Mamantov, Current-voltage curves for zirconium and uranium in molten fluorides, *Journal of Electroanalytical Chemistry* (1959), Volume 6, Issue 4, October 1963, Pages 328-329.

- 5.8. D.L. Manning, G. Mamantov, Studies on the electroreduction of uranium(IV) in molten LiF-BeF<sub>2</sub>-ZrF<sub>4</sub> by square wave voltammetry, *Electrochimica Acta*, Volume 19, Issue 4, April 1974, Pages 177-179
- 5.9. Prabhakara Reddy, S. Vandarkuzhali, T. Subramanian, P. Venkatesh, Electrochemical studies on the redox mechanism of uranium chloride in molten LiCl KCl eutectic, *Electrochimica Acta*, 49, 15, 2004.
- 5.10. Shirai, Electrochemical behavior of actinide ions in LiCl KCl eutectic melts, *Journal of Alloys and Compounds*, 271 273, [issue], 1998.
- 5.11. S A Kuznetsov, H Hayashi, K Minaato, M. Gaune-Escard, Electrochemical transient techniques for determination of uranium and rare earth metal separation coefficients in molten salts, *Electrochimica Acta*, 51, 12, 2006.
- 5.12. S A Kuznetsov, and M. Gaune-Escard, Electrochemical transient techniques for study of the electrochemistry and thermodynamics of nuclear materials in molten salts, *Journal of Nuclear Materials*, 389, 1, 2009.
- 5.13. G. Mamantov, D.L. Manning, *Anal. Chem.* 38 (1966) 1494.
- 5.14. D.L. Manning, G. Mamantov, Electrochemical reduction of U(IV) in molten LiF-BeF<sub>2</sub>-ZrF<sub>4</sub> (65.6-29.4-5.0 MOLE %). Evidence for adsorption of U(IV), *J. Electroanal. Chem.* 17 (1968) 137.
- 5.15. D.L. Manning, Gleb Mamantov, Disproportionation of electrochemically-generated uranium(V) in molten LiF-BeF<sub>2</sub>-ZrF<sub>4</sub> AT 500°, *Journal of Electroanalytical Chemistry and Interfacial Electrochemistry*, Volume 18, Issues 1-2, July 1968, Pages 137-141
- 5.16. F.R. Clayton, G. Mamantov, *J. Electrochem. Soc.* 121 (1974) 86.
- 5.17. P Delahay, *New instrumental methods in electrochemistry*, Inter-science publishers, New York, 1954.
- 5.18. A J Bard, L R Faulkner, *Electrochemical methods, Fundamentals and Applications*, John Wiley and Sons Inc, New York, 1980, Chapter 9-11.

## CHAPTER VI

# ELECTROLYTIC REDUCTION OF URANIUM OXIDE TO URANIUM METAL

---

### 6.1 Introduction

Although many metals and alloys can be electrodeposited from molten salt systems, only a few metals are produced on an industrial scale. The most widely known application of molten salt of over a century is the use of fused cryolite ( $\text{Na}_3\text{AlF}_6$ ) which acts, as both the solvent for alumina and the electrolyte for electrowinning liquid aluminum in the Hall-Heroult cell. The nearly identical ionic radii of fluoride and oxide ions permit the dissolution of alumina with the formation of soluble oxyfluoride complex anions, and a favourable chemistry for which an improvement or replacement has not been found. Other examples are the electrodeposition of refractory metals, Mg, B, U, rare-earth metals, etc in fused fluorides and chlorides. Thermodynamically, electrowinning is the only route available for the production of metals from very stable compounds. In Table 6.1 are presented some metals that are electrowon from their fused salt mixtures.

**Table 6.1 Commonly produced metals by the electrolysis of fused salts [6.1]**

S.no	Metal	Electrolyte, Wt%	Cathode	Anode	Temp, °C	CE(%)
1.	Li	55%LiCl, 45% KCl	Carbon steel	Graphite	460	80-85
2.	Na	42%NaCl, 58% CaCl <sub>2</sub>	Copper Steel	Nickel Graphite	320 580-600	40-50 80-90
3.	Mg	KCl, NaCl	Steel	Graphite	700	75-90
4.	Al	$\text{Na}_3\text{AlF}_6$	Carbon	Carbon	960-1000	80-95%

Uranium metal production by electrolysis of  $\text{UO}_2$  above the melting point of uranium with  $\text{UF}_4$  as additive in  $\text{LiF-BaF}_2$  base electrolyte has been reported by various authors [6.2-6.19]. When the electrolytic reduction process is to be adopted for preparation of uranium feed metal of different isotopic composition for the nuclear fuel cycle using  $\text{UF}_4$  as an additive may be very difficult. In such a case, an electrolyte that does not contain any uranium initially would be highly advantageous. Attempts to use cryolite as a solvent by Haas [6.16] led to deposition of aluminum metal along with uranium. Haas et al. [6.17] have also qualitatively studied the solubility of uranium oxide in  $\text{ThF}_4$ ,  $\text{LaF}_3$ . However, they did not extend their investigations to molten salt electrolysis; hence the motivation for development of an electrolytic process for reduction of uranium oxide to uranium metal in  $\text{LiF-BaF}_2$  base electrolyte with a non-uranium additive replacing  $\text{UF}_4$ .

## **6.2 Selection of electrolyte**

In the present work,  $\text{LaF}_3$  was chosen among the other rare earth fluorides for the following reasons (a) it is easily available and abundant, (b) the cathodic deposition potential of lanthanum is higher than that of uranium (c)  $\text{LaF}_3$  does not form any highly stable complexes at operating temperatures which will interfere in the electrolysis process.

There is no reported data on the use of  $\text{LaF}_3$  containing electrolytes for uranium oxide to metal conversion by electrolytic reduction in molten salt. The objective of the present work was to study the feasibility of the electrolytic reduction of uranium oxide to uranium metal in  $\text{LiF-BaF}_2\text{-LaF}_3$  melts at 1473K, and also establishing a cell configuration that leads to deposition of uranium metal. The effect of different forms

of uranium oxide feed material (powder, sintered pellet,  $\text{UO}_2+\text{C}$  composite pellet) on the electrolytic reduction process needed to be studied and so also different liquid cathode materials for uranium deposition.

Current efficiency in electrolysis of uranium oxide from fused salt mixtures depends on the following factors

1. Dissolution of the metal deposited at the cathode in fused salt electrolyte
2. Dissolution of the anodic products (CO) in the fused salt electrolytes and leading to back reaction of the deposited metal with CO
3. Appearance of secondary cyclic reactions due to multivalence
4. Settling of the un-dissolved oxide on the liquid metal and reducing the cathode surface

As the primary objective of the study was to demonstrate the feasibility of the process of uranium oxide to uranium metal conversion, no separate effort was directed towards the determination and improvement of the cathode and anode current efficiencies. Thus, off gas analysis which provides information on the nature of the anodic reaction, was not included in the study.

Fused salt electrolysis is generally carried out at the lowest possible temperature to avoid evaporation of the electrolyte from the bath and reduce dissolution of the cathodic and anodic products back into the electrolyte. As the process is meant to produce liquid uranium directly, above the melting point of uranium, 1473K was chosen for the operation; at 70K above the melting point of uranium has better

flowability and coalescence. The viscosity of liquid uranium at 1473K is 5.8 N/(m.s) [6.20]. A lower temperature of operation would lead to solid dendritic deposit of the metal, and still higher temperature would lead to accelerated corrosion as well as a higher rate of dissolution of the deposited metal. The secondary reactions are generally circumvented by a careful cell design and appropriate choice of the electrode materials. The most significant decrease in the current efficiency is related to the  $U^{4+} \leftrightarrow U^{3+}$  cyclic reaction which is aided by re-dissolution of the deposited uranium metal, converting  $UF_4$  to  $UF_3$  and its diffusion into the bulk of electrolyte. Once uranium is dissolved,  $UF_3$  is generated and it sets up a cyclic reaction. Porter et al. [6.21] has reported a high rate of dissolution of uranium metal in the electrolyte (melting point 1129K) with 25 wt %  $UF_4$ , namely,  $16.7 \text{ g/cm}^2 \cdot \text{sec}$  at 1148K. Another problem is associated with the rate at which  $UO_2$  is added. Higher than the required rate of addition of  $UO_2$  would lead to an intermediate layer of undissolved  $UO_2$  which would reduce the cathode area, and at a lower rate of addition of oxide,  $UF_4$  would deplete leading to occurrence of the anode effect.

Purification of molten salt electrolyte melts is an important step in the operation. It depends on the nature of the molten salt system used in the process. Pre-electrolysis is another commonly used treatment technique for purification of melts supplementing the preconditioning procedure (described in Chapter III). Pre-electrolysis removes heavy metals and oxides and it is carefully carried out below the decomposition potential of the salt mixture to avoid undesirable side reactions. Deoxygenated and dried inert atmosphere is used in the cell in order to reduce oxidation and corrosion of the structural materials, and importantly to prevent the generation of electroactive oxygen containing species in the melts.

### **6.3 Materials used in the electrolysis and salt preparation**

99% pure LiF (CAS No. 7789-24-4) and BaF<sub>2</sub> (CAS No. 7787-32-8) of M/s Sigma Aldrich were used for the experiments. 99.5% pure LaF<sub>3</sub> (CAS No. 13709-38-1) made by M/s Prabhat chemicals was obtained. Nuclear grade UF<sub>4</sub> and UO<sub>2</sub> (powder and sintered pellet) were obtained from Uranium Extraction Division, BARC and Nuclear Fuel Complex, Hyderabad respectively. The list of impurities presented in Table 3.2 of Chapter III applies. All these salts were weighed and dried in vacuum at 1073K for 3hrs in a graphite crucible and then transferred into the desiccators, as stock.

The materials employed in the electrolytic cells are selected on the basis of the nature of the melt and the operating conditions. The cathode and anode materials are chosen such that the over potential is minimized and they are compatible with the anodic and cathodic products. The selection of materials in the cell for the experiments was based on the study conducted in this work which is reported in Chapter III (section 3.4). High density graphite (density >1.95 g/cc) components were used in all the experiments for the crucible and the anode compartment. For cathode compartment applications, electrically insulating hexagonal boron nitride was used which was found to have good corrosion resistance to liquid uranium, and U alloys and molten electrolytes of LiF-BaF<sub>2</sub> with UF<sub>4</sub> or LaF<sub>3</sub>. Al<sub>2</sub>O<sub>3</sub>, Y<sub>2</sub>O<sub>3</sub>, SiO<sub>2</sub>, low density graphite were found to be incompatible with the electrolyte. All the structural materials in high temperature zone, namely, radiation shields, anode and cathode connector rods which were not in contact with the electrolyte were made of either graphite or molybdenum.

All the connectors for the anode and the cathode that were in contact with the electrolyte were made of high density graphite.

The electrolyte mixture was prepared by weighing and mixing the individual salts of LiF, BaF<sub>2</sub> and UF<sub>4</sub> or LaF<sub>3</sub> in the desired proportions in a mortar and pestle and transferred to a graphite crucible (procedure described in section 3.2.3 of chapter III). Different quantities of electrolyte were used in different experiments, but the salt preparation procedure remained the same in all the experiments. The conditioning procedure (described in chapter III section 3.3) of the salt mixture involved in first equilibrating the electrolyte mixture for pretreatment at 673K for 24hrs and another 24hrs at 1473K in a continuous stream of high purity argon gas having <0.1ppm of oxygen. The individual weights of each salt used in the mixture are listed in Table 6.2 for different electrolytic cells. The total quantity of the salt mixture naturally depended on the size and shape of the cell.

Table 6.2 Weight of individual salts used for preparation of different salt mixtures for electrolysis studies

Salt	Cell S80	Cell S350	Cell S700	Cell S1400
LiF, g	7.7	33.8	67.6	135.2
BaF <sub>2</sub> , g	52.3	228.7	457.4	914.8
LaF <sub>3</sub> or UF <sub>4</sub> , g	20	87.5	175	350

### 6.3.1 Preparation of UO<sub>2</sub>+C pellets

Two kinds of UO<sub>2</sub>+C pellets were prepared and used in the experiments. To make the first kind of UO<sub>2</sub>+C pellets, the stoichiometric amount of carbon required for the reduction of UO<sub>2</sub> was added along with 1 wt% zinc behenate as the binder and 1 wt

% naphthalene as the lubricant. ~50g batches of powder were prepared and pellets of 13mm diameter, ~8mm height, weighing ~4g each were prepared by cold pelletization at  $5\text{T/cm}^2$  load. The green pellets were heated at 673K in vacuum of  $1\text{E}-2$  mbar to remove the binder and lubricant, and further heated to 1573K in high purity argon gas atmosphere at a rate of 100K/hr and soaked for 4 hours for graphitization and then cooled to room temperature.

In the second type of pellets carbon powder was mixed with a stoichiometric amount of  $\text{UO}_2$  and ~2 to 3 wt% biomass tar (obtained from pyrolysis of municipal waste) was added as a binder. Detailed chemical analysis of the tar was not conducted as the composition depended on the nature of the municipal waste. As biomass tar was used only as a binder and not as an explicit source of carbon small variation in composition was not expected to have any serious effect on chemistry of pellet. Pellets of 13mm diameter, ~8mm height were prepared at  $5\text{T/cm}^2$  load and weighed ~3.8g each. The pellets were heated to 1573K at 100K/hr in argon gas and soaked for 4 hrs for graphitization of tar.

No shrinkage of the pellets was observed after heating; therefore, a porosity measurement was not conducted. The density of the  $\text{UO}_2+\text{C}$  pellets varied between 3.5 and 3.6 g/cc. The sintered pellets had sufficient strength and remained intact during handling and assembling the electrolytic cell.

#### **6.4 Experimental setup for electrolysis studies**

As in the earlier experiments for solubility and electrochemical studies, the experimental setup for the electrolysis experiments also consisted of a muffle to

provide an inert gas cover and a heating system to achieve the desired temperature. The design calculations made from the first principles for the experimental setup for solubility studies were utilized for the present setup. The material selection was again based on thermodynamic considerations, functionality, properties of the materials, cost of the material, and ease of fabrication. The design considerations, namely, inert gas requirement, structural and containment materials, hot zone uniformity, leak tightness, design temperature, movement of internals, safety aspects, fumehood requirement, sealing O ring (as described in section 4.3 of chapter IV) were also valid for this experimental setup. Additional considerations for the experimental setup for electrolysis studies were as follows.

#### Additional considerations

1. Wherever possible, joints in the electrical connections are to be avoided to prevent voltage drop across the joints. Also, the joint should be at such a temperature that the materials does not react with each other and form a phase having low electrical conductivity.
2. Sufficient electrical insulation (of a few M $\Omega$ ) should be maintained between the electrodes used for electrochemical and electrolysis studies to reduce leakage currents practically to zero.

A recrystallized alumina tube of 100mm ID, 115mm OD and 800mm length, closed at one end, was used as the muffle. Viton O-ring sealed water cooled stainless steel flanges were used on the open end of the alumina tube. The flange had openings for gas inlet and outlet connections, and other feed throughs for electrode connections (anode and cathode) and thermocouple. The inert gas purge line and thermocouples were taken through the water cooled stainless steel flange assembly with Viton O-ring

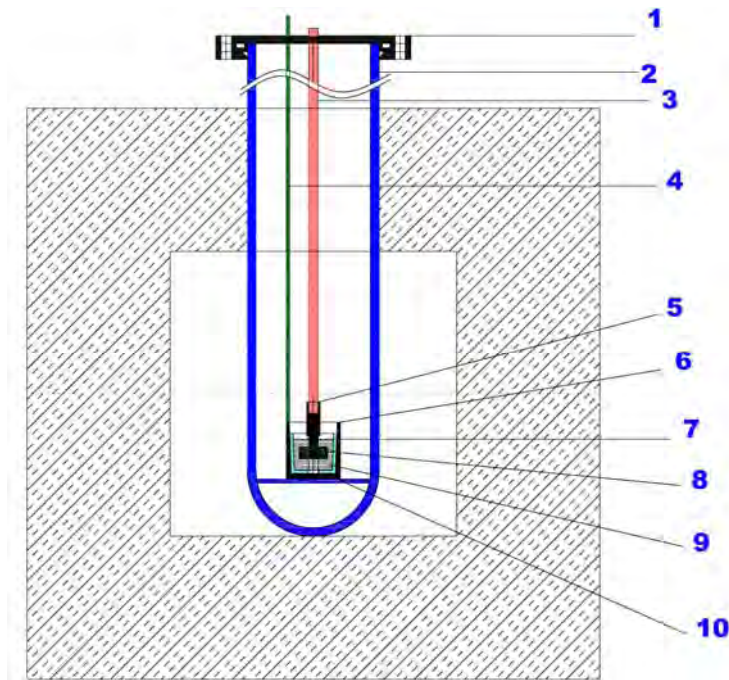
seals. The anode and cathode electrical connecting rods were taken through Teflon seals; both the anode and cathode connecting rods could be independently lifted or inserted to achieve the desired insertion depth in the molten salt bath. The inter-electrode distance was maintained by the extent of immersion in the crucible which was calibrated prior to the experiment. High purity argon with  $<0.1$ ppm of oxygen was purged continuously during the experiment. The oxygen concentration in the inlet gas was continuously monitored by an online oxygen gas analyzer (Systech 800 Series analyzer). Heating of the alumina tube was done by a 6kW resistive heating furnace controlled by a PID controller within the range of  $\pm 3$ K. A pack of radiation shields of 98mm diameter was used to prevent heat losses and to maintain a uniform temperature zone; the pack of shields was supported from the flange by 3 mm inconel 600 rods. A high density graphite crucible (of different sizes in different experiments) was used to contain the salt mixture. The crucible containing the electrolyte rested on an alumina plate of 98mm diameter and 5 mm thick, which in turn rested on the base of the alumina tube. The anode compartments to hold  $\text{UO}_2$  powder,  $\text{UO}_2$  pellet or  $\text{UO}_2 + \text{C}$  pellet were made out of high density graphite. The anode compartment had a provision to fasten an 8mm diameter threaded rod. A graphite rod of 10mm diameter with M8 internal threading was connected to the anode compartment and the end of the rod was connected to a graphite adapter, which had a provision to fasten a 6mm diameter molybdenum rod. A graphite rod was used to provide electrical connection to the cathode chamber, which had a provision to connect a 6mm diameter molybdenum rod similar to that in the anode. The desired cathode current density was attained by providing an insulating BN liner to the graphite crucible and exposing only the desired area of the graphite surface. All the other high temperature structural members were made of either graphite or molybdenum. The furnace was housed

inside fumehood. The purge gas was released into the fumehood. The exhaust of the fumehood was passed through HEPA filters and a water scrubber to remove radioactive particulate and fluoride vapour respectively before venting to the environment. A photograph of the experimental setup in the fumehood is shown in figure 6.1. And the schematic diagram of the experimental set-up in figure 6.2. Necessary safety clearance was obtained from the regulatory authorities before carrying out the experiments with radioactive materials.



1. SS Fume hood floor
2. Resistive furnace
3. Ceramic tube inside the furnace
4. Water cooled flange assembly
5. Molybdenum electrodes for electrolysis
6. Sash of fumehood

Figure 6.1 Photograph of experimental setup for electrolysis inside the fumehood



- |   |                                |
|---|--------------------------------|
| 1. Water cooled stainless steel flanges | 2. Recrystallized alumina tube |
| 3. Molybdenum rod anode connector       | 4. Nickel cathode connection   |
| 5. Graphite powder holder               | 6. Graphite crucible cathode   |
| 7. BN insulating liner                  | 8. Uranium oxide powder        |
| 9. Electrolyte                          | 10. Alumina base support plate |

Figure 6.2 Schematic of the electrolysis assembly with setup A

### 6.5 Experimental variables for electrolysis of $\text{UO}_2$ to U metal

Several electrolysis experiments were conducted to study the effects of the following

1. Variation of the size of the cell
2. Anode and cathode configurations
3. Cathode and liquid cathode materials
4. Anode materials
5. Different electrolytes

Four cell sizes S-80, S-350, S-700 and S-1400 were used in the full experimental plan which had electrolyte holding capacities of 80g, 350g, 700g and 1400g respectively.

Different anode and cathode design configurations were used in each cell size. The cathode area in different cell designs varied from  $0.785\text{cm}^2$  to  $11.43\text{cm}^2$ . Similarly the

polarity of the electrolyte container was anodic, cathodic or electrically floating. The configurations are shown in figures 6.3-6.4.

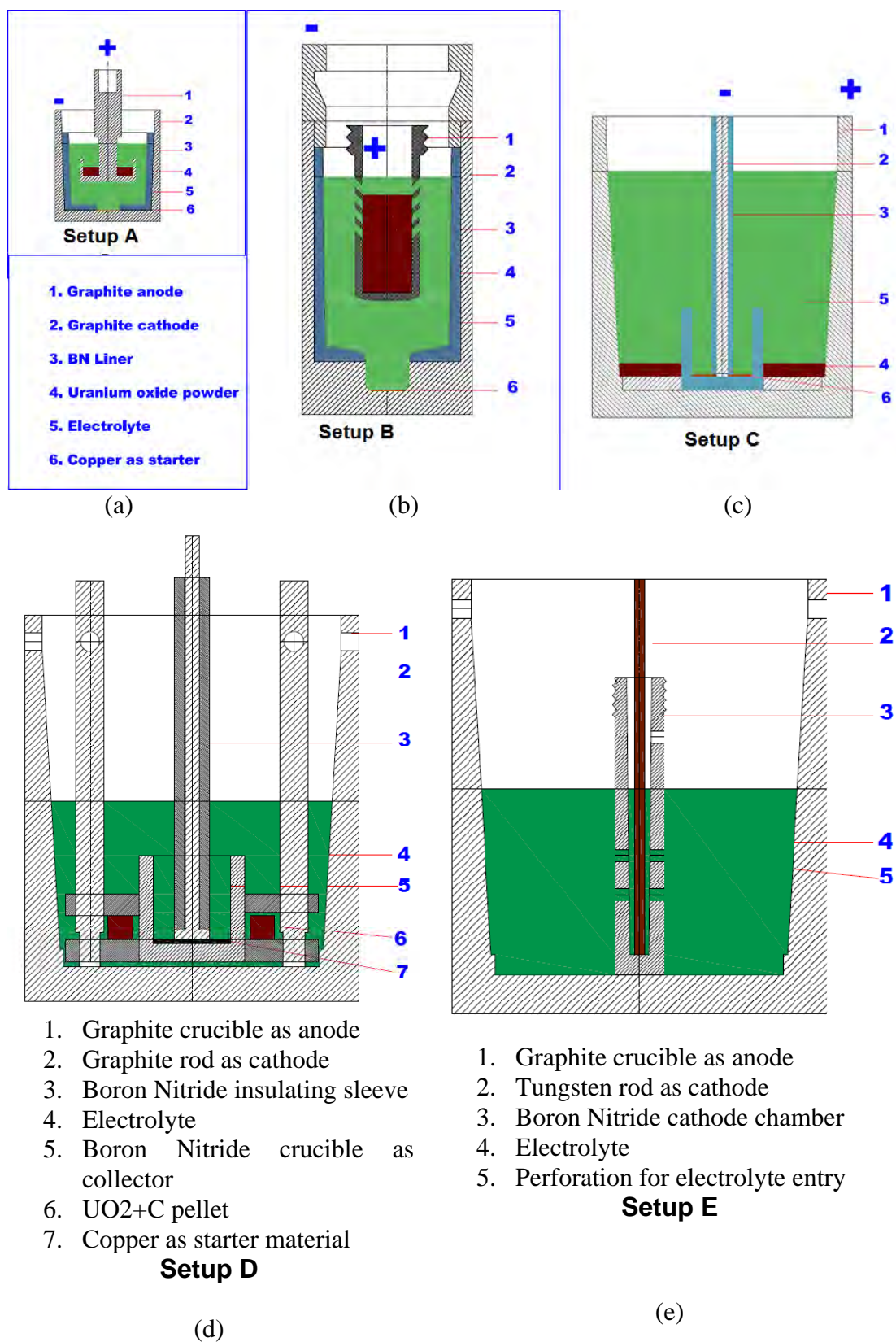


Figure 6.3 Schematic of setup A, B, C D and E the for electrolysis experiments



Table 6.3 Detailed comparison of different electrolytic cell designs for study of UO<sub>2</sub> reduction to uranium metal

	Setup A	Setup B	Setup C	Setup D	Setup E	Setup F	Setup G	Setup H
<b>Cell size</b>	S80	S350	S700	S700	S700	S1400	S1400	S1400
<b>capacity, g</b>	80g	350g	700g	700g	700g	1400g	1400g	1400g
<b>Graphite crucible dimensions</b>	47mm OD, 42mm ID, 50mm height	58mm OD, 50mm ID, 100mm height	95mm OD, 85mm ID, 110mm height	95mm OD, 85mm ID, 110mm height	95mm OD, 85mm ID, 110mm height	95mm OD, 85mm ID, 210mm height	95mm OD, 85mm ID, 210mm height	95mm OD, 85mm ID, 210mm height
<b>Polarity of crucible</b>	Cathodic	Cathodic	Anodic	Anodic	Cathodic	Electrically floating	Electrically floating	Electrically floating
<b>Anode</b>	Graphite bucket with UO <sub>2</sub>	UO <sub>2</sub> in graphite cylindrical bucket with perforations	Graphite crucible with UO <sub>2</sub> at the bottom	Graphite crucible, pellet holder and UO <sub>2</sub> +C	Graphite crucible	UO <sub>2</sub> +C in closed graphite compartment with perforations	UO <sub>2</sub> +C in closed graphite compartment with perforations	UO <sub>2</sub> pellets in open graphite compartment with perforations
<b>Cathode</b>	Graphite crucible	Graphite crucible	Copper in contact (initially) with graphite rod	Copper in (initially) contact with graphite rod	2.5mm diameter Tungsten rod	Liquid copper or tin	Liquid copper or tin	Liquid copper or tin
<b>Cathode area, cm<sup>2</sup></b>	0.785 cm <sup>2</sup>	3.18 cm <sup>2</sup>	1.25 cm <sup>2</sup>	1.25 cm <sup>2</sup>	2.1 cm <sup>2</sup>	11.43 cm <sup>2</sup>	11.43 cm <sup>2</sup>	11.43 cm <sup>2</sup>
<b>Source of uranium</b>	UO <sub>2</sub> powder	UO <sub>2</sub> powder	UO <sub>2</sub> powder	UO <sub>2</sub> +C pellets	UF <sub>4</sub> only	UO <sub>2</sub> +C pellets	UO <sub>2</sub> +C pellets	Sintered UO <sub>2</sub> pellets

In the electrolysis experiments with S-80 and S-350 cell sizes, four different anode designs were used. A bucket type anode (Figure 6.5a to hold ~5g of  $\text{UO}_2$  powder), a perforated anode cylinder (Figure 6.5b to hold ~10g  $\text{UO}_2$ ), floating BN powder holder (Figure 6.5c to hold ~25g  $\text{UO}_2$ ) and graphite powder holder anode (figure 6.5d to hold ~25g of  $\text{UO}_2$ ) anodes. Experiments were conducted with interelectrode distance varying from 10mm to 30mm.

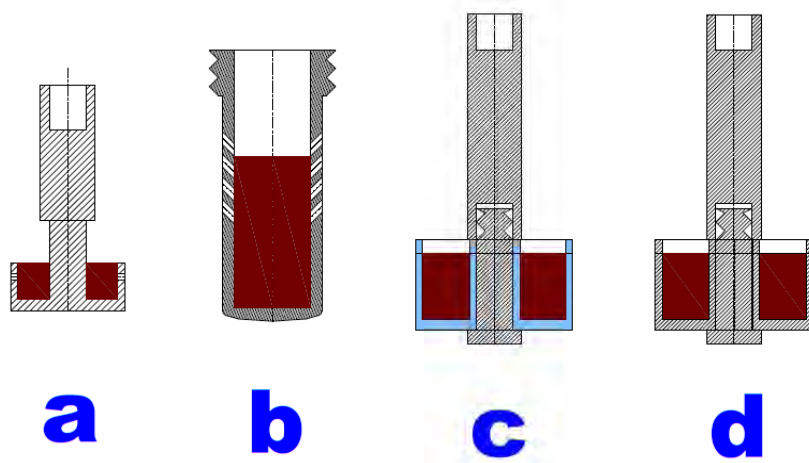


Figure 6.5 Different anode designs used in the electrolysis studies



Figure 6.6 Photograph of different anodes of graphite used in the electrolysis experiment



1. High density graphite crucible
2. High density graphite anode compartment with perforations
3. Graphite connector rod for anode compartment
4. Hexagonal boron nitride cathode containment
5. Graphite connector rod for cathode compartment

Figure 6.7 Photographs of the components in assembled condition of Setup F

## 6.6 Electrolysis experiments

Given the severity of the operational conditions imposed due to the operation above the melting point of uranium and the high temperature chemical reactivity of uranium metal with the electrolyte as well as the containment material, and additionally, the molten electrolyte reactivity with container material, scope was not available to vary large number of parameters. With a limited solubility of  $\text{UO}_2$ , ~2 wt% in  $\text{LiF-BaF}_2\text{-25Wt\% UF}_4$  and the small size of cell chosen for the experiments continuous addition of  $\text{UO}_2$  was not considered in this study. Thus, each experiment was always a batch process. A total of 62 experiments were conducted. All the graphite components were degassed at 1573K before use to removal all the volatile products. Pre-dried and pre-weighed salts were used in preparing salt mixtures and then transferred to a graphite crucible.

The methodology of the study was to first identify a cell configuration that leads to production of uranium with  $\text{LiF-BaF}_2\text{-25Wt\% UF}_4$ , successfully tried by the previous authors, and the utilize the validated cell design to study the effect of the source of uranium in the form of  $\text{UO}_2$  powder,  $\text{UO}_2\text{+C}$  pellets or sintered  $\text{UO}_2$  pellets and different liquid cathodes. An Identical cell was used to study the effect of  $\text{LaF}_3$  additive with various sources of uranium oxide and liquid cathodes for demonstration of feasibility of uranium metal production.

These experiments were conducted in 4 phases. The conclusion of each phase led to the selection of parameters of the next phase of the experiments. The experiments are enumerated below phase wise with a description of the objective, apparatus, procedure,

experiments conducted, results and discussions. Data is presented here only for representative experiments.

In every experiment, the post electrolysis step involved cooling the contents to room temperature. The contents of the crucible, the cathode or the anode compartments were examined and several samples were taken for analysis. In a few of the experiments, the crucible along with boron nitride liner was cut across the diameter to study stratification in the electrolyte and preferential settling of uranium oxide powder.

#### **6.6.1 Phase 1 electrolysis experiments (ES1-ES7a)**

The primary task in the Phase 1 electrolysis experiments was to arrive at the cell size and the configuration that could yield uranium with LiF-BaF<sub>2</sub>-25Wt% UF<sub>4</sub> which is the most widely reported composition for production of uranium. Hence small electrolytic cells were fabricated and used. A high density graphite crucible was used as containment for the electrolyte and to function as the cathode. A hexagonal boron nitride liner was used to reduce the total exposed area of graphite cathode. Around 0.5-1g copper disc was placed on the floor of the graphite crucible to serve as liquid cathode when it melted after reaching the operation temperature. Premixed electrolyte was charged into the crucible which was lowered into alumina ceramic tube. Pretreatment of the electrolyte was conducted at 673K for 24hrs and another 24hrs at 1473K. It was observed that after melting the height of the electrolyte reduced to ~1/3 of the powder fill level. High density graphite or a boron nitride anode compartment with UO<sub>2</sub> powder, thermally equilibrated while hanging inside the alumina tube and was slowly immersed into the electrolyte. After dissolution of UO<sub>2</sub> by

diffusion and natural convection, potential was applied across the electrodes and electrolysis was conducted for a duration of 200-300 mins. After the electrolysis, the anode compartment was lifted above the electrolyte and the furnace was cooled at a rate of 200K/hr in argon atmosphere. A photograph of S80 cell post experiment is shown in figure 6.8.



Figure 6.8 Photograph of S80 cell after the electrolysis with anode power holder embedded

In all the experiments of phase 1 the cell sizes of either S-80 or S-350 of setup A and B were employed.  $\text{UO}_2$  powder was used as source of  $\text{UO}_2$  and the anode designs as shown in figure 6.4 a, b, c and d were used. The experiments were conducted with and without liquid copper cathode. Given the quantity of electrolyte used in S-80 cells and S-350 cells, the inter electrode distance could not be increased beyond 20mm and 30mm respectively. The experiments in S-80 cells were conducted with constant current density of  $1.2\text{A}/\text{cm}^2$  and  $2.2\text{A}/\text{cm}^2$ . The electrolysis duration was varied between 200 and 400mins.

Liquid uranium product is possible when the uranium is deposited in liquid phase on the cathode surface coalesce. Recovery of liquid uranium requires coalescence of uranium. Molten uranium being the desired product the dispersed, re-oxidised uranium or the

dissolved in the electrolyte were not recoverable and hence was not considered as the product.

In all the experiments with S-80 and S-350 cells no coalesced liquid uranium was obtained after the experiment. A mixture of  $\text{UO}_2$  and electrolyte was always seen at the bottom of the crucible owing to settling of higher density of  $\text{UO}_2$ . It is a known fact that molten salt electrolytic cells scale down poorly. Due to the proximity of the anolyte and the catholyte, the transfer of  $\text{U}^{3+}$  generated at cathode to the anode was faster, where it oxidized to  $\text{U}^{4+}$ , thereby setting up a cyclic reaction which resulted in a huge parasitic current. Similar conditions might have prevailed in the cells of S-350 sizes. This was confirmed by the observation of green color near the anode (figure 6.8) and brown or red color at the cathode indicating a greater abundance of  $\text{U}^{4+}$  and  $\text{U}^{3+}$  respectively. The uranium dissolution rate of uranium in the electrolyte may have been much higher than  $16.7 \text{ g/cm}^2\cdot\text{s}$  at 1473K (the dissolution rate reported by Porter et al. at 1148K). Over the area of the cathode,  $0.785 \text{ cm}^2$ , the rate of deposition of uranium with a current density of  $1.2\text{A/cm}^2$  is  $5.8\text{E-}4 \text{ g/s}$  at 100% efficiency. This is much lower than the rate of dissolution. However, it is to be noted that during electrolysis due to cathodic polarization, the rate of dissolution would have been lower than plain chemical dissolution, but still it did not lead to collection of uranium. Also the insufficient amount of copper provided as liquid cathode might not have offered a uniform layer of the liquid cathode where uranium could have deposited and coalesced. Compounding this problem was the settling of the undissolved  $\text{UO}_2$  which had come out of anode bucket, which could have hindered the coalescence of uranium metal.

A few experiments with high current density of  $5.6\text{A}/\text{cm}^2$  also did not lead to any recoverable uranium production, which indicated that there was no limitation on account of critical current density to obtain uranium. The effect of the inter-electrode distance was studied with increasing the inter-electrode distance to 30mm in S-350 cells which also did not yield any better result.

Thus, the combination of chemical dissolution at the cathode, transfer of dissolved uranium ions to anode to setup the cyclic reaction, inadequacy of the liquid cathode provision and  $\text{UO}_2$  settling on the cathode, contributed to non-deposition of liquid uranium product. As there was no success in a uranium deposition in S-80 and S-350 cells, they were discontinued and new bigger size cells were fabricated.

#### **6.6.2 Phase 2 electrolysis experiments (ES8-ES9)**

The objective of the phase 2 experiments in the bigger size cells (S-700) was to obtain uranium in  $\text{LiF-BaF}_2\text{-}25\text{Wt}\% \text{UF}_4$ . The improvement from the earlier small cells (S-80 and S-350) was the provision of a separate boron nitride compartment for cathode which increased the distance between the anolyte and catholyte. Elaborate arrangements were made to prevent settling of uranium oxide powder on the liquid by placing  $\text{UO}_2$  below the boron nitride compartment top surface.

In this phase of experiments, a high density graphite crucible was used as the container for the crucible as well as to function as the anode compartment. A boron nitride cup of 25mm diameter and 25mm height served as the cathode compartment with ~1g of copper as the

liquid cathode. This boron nitride crucible was fixed at the bottom by threading it to the graphite crucible. A graphite electrode of 10mm diameter with an insulating boron nitride sleeve with an exposed length of 3mm was used as the cathode lead, which was kept in contact with copper.  $\text{UO}_2$  powder or  $\text{UO}_2+\text{C}$  pellet was placed at the bottom of the graphite crucible in the annular space between the boron nitride crucible and the graphite crucible. When  $\text{UO}_2+\text{C}$  pellets were used as the source of uranium, a high density graphite perforated disc was used to clamp the pellets down to prevent floating of the pellets in the higher density electrolyte. Premixed electrolyte was charged into the crucible. The steps of the experiments remained essentially the same as in phase 1 except the following variation. Here, the high density graphite cathode lead insulated with boron nitride was immersed into the cathode compartment at 1473K. Before the actual immersion, the graphite cathode lead was held just above the electrolyte to thermally equilibrate and avoid sudden thermal shock to boron nitride. After equilibration of  $\text{UO}_2$  in the electrolyte solvent, the desired voltage was applied across the electrodes. The electrolysis was conducted for a duration of 200-300 mins. After electrolysis, in the hot condition the graphite cathode lead was lifted above the crucible from the cathode compartment and the furnace was allowed to cool in a continuous stream of high purity argon at a rate of 200K/hr.

In the phase 2 the experiments with S-700 size cells and  $\text{LiF-BaF}_2-25\text{Wt}\% \text{UF}_4$  electrolyte three variations were tried with setup C, D and E respectively. In the experiments with the setup C,  $\text{UO}_2$  powder was placed at the bottom of the crucible. In the setup D,  $\text{UO}_2+\text{C}$  pellets were used as a source of  $\text{UO}_2$  and arrangement was made such that they will not float in the electrolyte.

In another variant of experiment with the setup E, a BN tube with perforations was used as the cathode chamber with centrally place tungsten rod of 2.4mm diameter as the cathode. No  $\text{UO}_2$  was added to the electrolyte and only electrowinning of uranium was planned in the experiment. Electrolysis was conducted at constant voltage as well as constant current density configurations.  $\sim 3.5\text{V}$  was applied in the constant voltage experiments. In constant current mode the cathode current density was studied at  $1.3\text{ A/cm}^2$  and  $\sim 12\text{A/cm}^2$ . Duration of the electrolysis was between 80mins and 600 mins.

In both the experiments with both  $\text{UO}_2$  powder and  $\text{UO}_2+\text{C}$  pellets, electrolysis did not yield any coalesced uranium that could be collected. The experiment with only electrowinning of uranium from  $\text{LiF-BaF}_2\text{-25Wt\% UF}_4$  also did not yield uranium. However, the contents of the cathode chamber BN crucible or BN tube were found to have higher concentration of  $\sim 28\%$  uranium as against  $18.9\%$  in the electrolyte. This shows that uranium ions were migrating towards cathode and probably reducing but quickly redissolving into the electrolyte. That the color near the cathode, which was brown or red (figure 6.9) indicating presence of  $\text{UF}_3$ , strengthened the inference of re-dissolution.

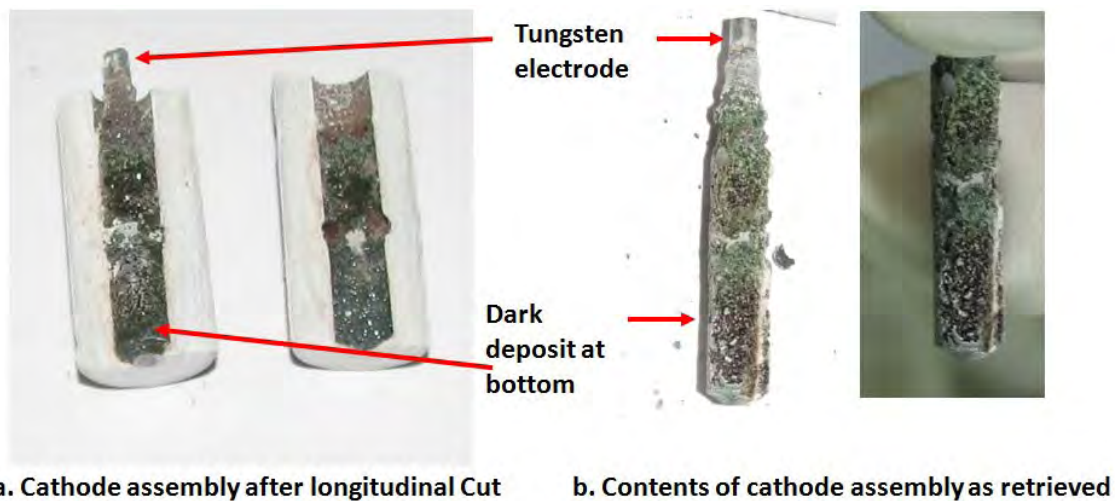


Figure 6.9 Photograph of the BN tube used in electrowinning of uranium

### 6.6.3 Phase 3 electrolysis experiments (ES10-ES19)

Although the results were encouraging for the cells S-80, S-350 and S-700 of small size, the electrolysis experiments did not yield any recoverable uranium. Hence the efforts were directed towards use of a liquid cathode of higher quantity which could alloy or trap and act as an immediate sink to the uranium produced, thereby reducing its activity. Special precautions were taken with the suspension of the liquid cathode chamber such that no undissolved oxide could settle or reach the BN cathode chamber. To accommodate the elaborate provisions of liquid cathode and anode designs, larger size cells were fabricated which would contain ~1400g of electrolyte. The setups F, G and H having capacities of 1400g were used for the experiments of phase 3. The objective of this phase of experiments was to use a sufficient amount of liquid cathode to trap the deposited uranium; and investigate the effect of different liquid metal cathodes and sources of uranium oxide.

### Liquid metal cathode selection criteria

In order to study the formation of uranium metal and prevent its re-dissolution from the cathode, a liquid metal cathode was planned. The choice of liquid metal cathode for electrolytic reduction process was based on the following considerations

1. The metal should be molten at 1473K and should not lead to boiling at the operational temperature, hence a metal should be chosen such that 1473K is well above its melting point and well below the boiling point.
2. Metal should have sufficient density difference with respect to electrolyte at 1473K to ensure separation between the layers.
3. Metal should remain inert to the electrolyte and the container at 1473K
4. Uranium shall have reasonable solubility in the liquid metal at 1473K and preferably much lower or nil solubility at room temperature, and
5. Metal should have low vapour pressure at 1473K to avoid evaporation and loss.

Copper and tin were chosen as they meet most of the criteria. They are inert to uranium oxide and have no thermodynamically feasible reaction between the metal and the electrolyte and also the boron nitride container at 1473K. The problem of uranium oxide settling in the lower density of copper or tin, was circumvented by the design of the electrolytic cell. Bismuth was used in only two experiments, and all the rest of the experiments were conducted with either copper or tin as the liquid cathode.

In the 1400g capacity cells, the high density graphite crucible was used only as a containment for the electrolyte and was kept electrically floating. A separate high density

graphite anode compartment was used to hold sintered  $\text{UO}_2$  or  $\text{UO}_2+\text{C}$  pellets. A boron nitride cup of 50mm OD, 40mm ID, and 20mm height was used as the cathode compartment with ~60g liquid metal cathode. The premixed electrolyte was charged into the crucible which was lowered into the alumina ceramic tube. As described in the previous phase experiments, the pretreatment of the electrolyte was conducted for 24hrs at 673K and another 24hrs at 1473K. Both the high density graphite anode and the boron nitride compartment were introduced into the uniform temperature hot zone for thermal equilibration, and were held slightly above the molten electrolyte. The anode compartment was then immersed into the electrolyte at 1473K and held for 24hrs for uranium oxide dissolution and equilibration. The desired voltage was applied across the electrodes and electrolysis was conducted for a duration of 200-300 mins. After the electrolysis, both the anode and the cathode compartments were lifted above the electrolyte level and cooling of the experimental setup was commenced at a rate of 200K/hr in high purity argon gas stream.

#### Experiments with bismuth liquid cathode (ES10-ES11)

Initially ~12g of bismuth was used as a cathode placed in a boron nitride cup of 50mm diameter and 40mm ID with depth of 8mm depth. Graphite rod of 10mm diameter with threaded tip was fixed into the BN cup, the rod was insulated with a BN sleeve. The length of the graphite rod was such that it dipped in the liquid cathode after heating it to 1473K. For using of  $\text{UO}_2+\text{C}$  pellets the anode was designed as shown in figure 6.6a. The anode essentially consisted of a graphite cylindrical chamber with perforations on the upper portion on the cylindrical surface, for the electrolyte to enter into the chamber. The bottom

portion of the anode was not having perforations to avoid undissolved  $\text{UO}_2$  reaching the cathode chamber if the pellet disintegrated. 1400g of electrolyte was used with ~68g of  $\text{UO}_2+\text{C}$  pellets for the electrolysis runs. The electrolysis was conducted at 3.5V with a cathode current density of  $\sim 2\text{A}/\text{cm}^2$  for 200-300 mins.

In the experiments where bismuth was used as the cathode and the  $\text{UO}_2+\text{C}$  pellets as the anode, the assembly was opened in the fume hood after cooling the contents, the uncoalesced uranium oxidized immediately on exposure to air. This confirmed that the uranium was indeed deposited but oxidized quickly as uranium was in the form of small globules. The reason for this behavior was that when during operation at 1473K for 24hrs, liquid bismuth evaporated and deposited on the radiation shields and other cold areas. Only a small amount of bismuth was left, which was not sufficient to form an alloy. The residual uranium, after evaporation of bismuth oxidized on exposure to air. Because of the failure to obtain any uranium product, the subsequent experiments were conducted with either copper or tin as a liquid cathode.

#### Experiments with tin liquid cathode (ES12-ES15)

Experiments with ~60g tin as the liquid metal cathode and  $\text{UO}_2+\text{C}$  pellets as the anode led to formation of  $\text{USn}_3$  compound with tin metal which was confirmed by XRD. The formation of  $\text{USn}_3$  compound indicates that the production of coalesced uranium metal requires a combination of favorable factors namely, availability of dissolved  $\text{UO}_2$ , formation and coalescence of uranium and reducing redissolution. The absence of any one factor might lead to either poor deposition or no deposition of uranium. It was expected that

the availability of dissolved  $\text{UO}_2$  at the anode and the presence of carbon together with  $\text{UO}_2$  would lead to depolarization. However, no change in the cell voltage was seen for a given cathode current density.

For a given cell configuration and electrolyte composition, increase in the cathode current consistently increases the cathode current efficiency. The anode current densities are limited by the onset of anode effect. Hence a high ratio of anode to cathode area is desirable. In the current experiment, cathode area was  $11.4\text{cm}^2$  and the anode area was  $\sim 110\text{cm}^2$ , hence no anode effects were observed even when the cell was operated at  $2\text{A}/\text{cm}^2$  cathode current density.

Coalescence of the deposited uranium metal was a major cause for the poor production of metal in all the small cell experiments. In the present experiment, the metal cathode was very useful to trap and collect the metal. As stated earlier, there was no continuous addition of  $\text{UO}_2$  and provision was made to ensure that the undissolved  $\text{UO}_2$  did not reach the cathode chamber during electrolysis.

With the tin cathode, the effect of the source of  $\text{UO}_2$  was also investigated.  $\text{UO}_2$  powder or sintered  $\text{UO}_2$  pellets were used in separate experiments in  $\text{LiF-BaF}_2\text{-}25\text{Wt}\% \text{UF}_4$  electrolyte with the identical configuration of cell and anode designs as shown in figure 6.6a and 6.6b respectively. The electrolysis conditions were maintained identical to those of the experiments with  $\text{UO}_2\text{+C}$  pellets. In these experiments  $\text{USn}_3$  formation was confirmed by XRD of the sample from the frozen tin cathode. There was no change in the potential to

maintain the cathode current density of  $2\text{A}/\text{cm}^2$ , either with  $\text{UO}_2$  powder or with sintered  $\text{UO}_2$  pellets compared to the required potential with  $\text{UO}_2+\text{C}$  pellets. The rate of dissolution of  $\text{UO}_2$  pellets might have been sufficient to maintain the requisite cathode current density, and hence no anode effect was also observed. One could conclude that the limiting dissolution rate of uranium oxide from  $\text{UO}_2$  powder, sintered  $\text{UO}_2$  pellets or  $\text{UO}_2+\text{C}$  pellets did not have any effect on these electrolysis runs. A major observation in these experiments was that the extent of uranium oxide in the cathode chamber was higher in the case of  $\text{UO}_2$  powder in comparison to the experiments with sintered  $\text{UO}_2$  pellets. Although a provision had been made to prevent settling of any undissolved oxide, due to the buoyancy driven natural convective currents due to the unavoidable minor thermal gradients occurring at high temperature, fine uranium oxide powders were carried from the anode to cathode. In all the subsequent experiments sintered  $\text{UO}_2$  pellets were used to avoid this phenomenon. Quantification of the convected  $\text{UO}_2$  in the cathode compartment was not carried out in this work.

#### Experiments with copper liquid cathode

Then the study was extended to determine the effect of the type of liquid cathode metal on the feasibility of uranium production. Tin was replaced with copper as the liquid cathode and the experiment with the identical configuration (setup H) and electrolysis parameters was conducted with sintered  $\text{UO}_2$  pellets. After the analysis of the cathode deposit, it was found that  $\text{Cu}_5\text{U}$  was present along with copper. This confirms that the deposition of uranium with both the types of liquid cathodes used. Figure 6.10 shows the photographs of the components, namely, cathode assembly, anode assembly and the pellets after the

electrolysis. Figures 6.11 and 6.12 show the typical XRD data on the formation of uranium compounds,  $USn_3$  and  $Cu_5U$  respectively. The typical uranium concentration in frozen tin and copper cathodes was 11.3 wt% and 10.9 wt% respectively. The total amount of uranium in cathode was analyzed by ICPMS and was used to estimate cathode current efficiencies for the electrolysis experiments. General cathode current efficiencies vary between 7 to 8%.

The investigations with copper cathode were extended to study the effect of the source of  $UO_2$ .  $UO_2$  powder or  $UO_2+C$  pellets were used in separate experiments in  $LiF-BaF_2-25Wt\% UF_4$  electrolyte again with the identical configuration and anode designs as shown in figure 6.6a and 6.6b respectively. The electrolysis conditions were maintained identical to those experiments with  $UO_2$  pellets described above. In these experiments also  $Cu_5U$  formation was confirmed by XRD.

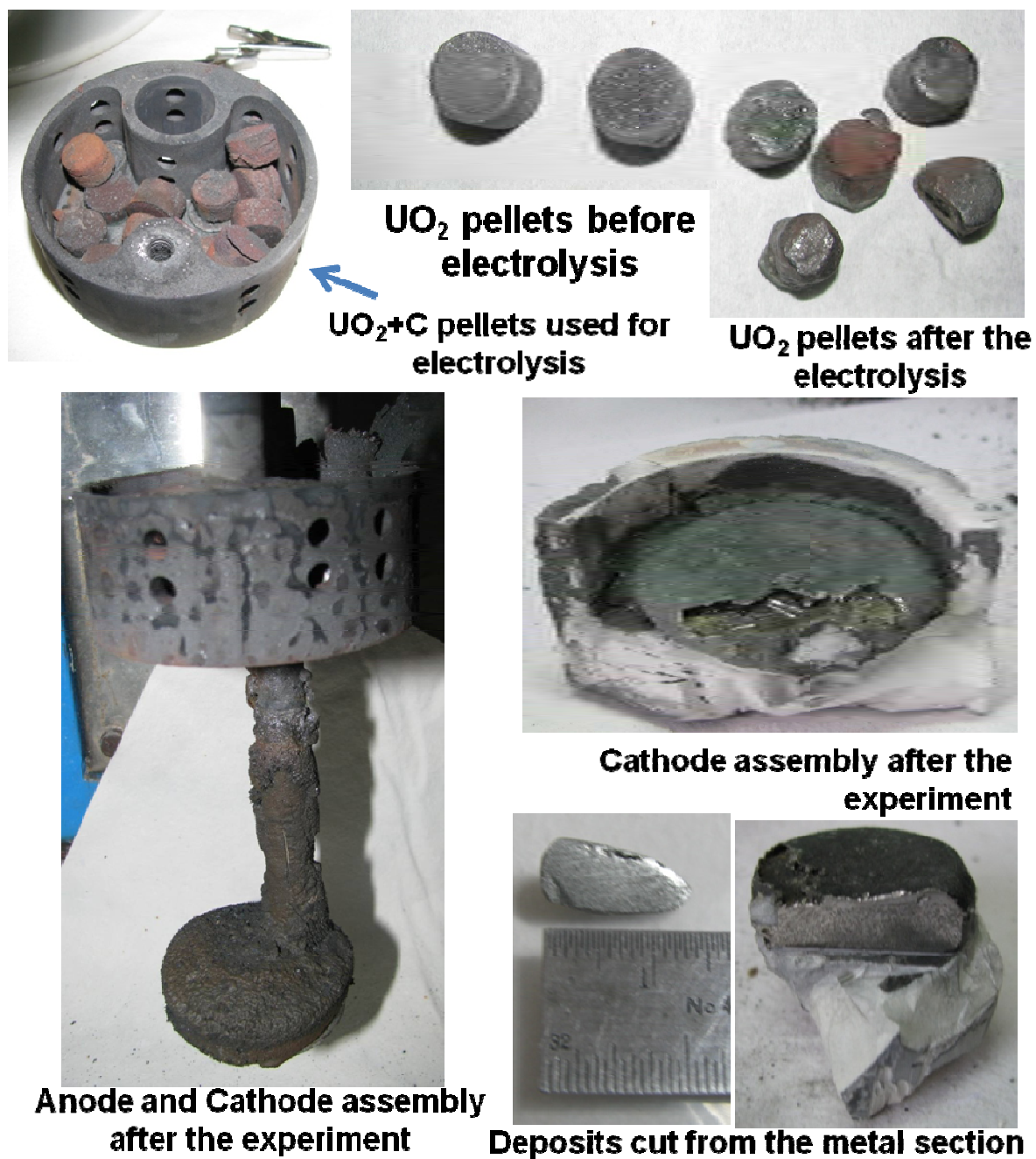


Figure 6.10 Photographs of components depicting their typical state after the electrolysis experiments in phase 3 with tin cathode

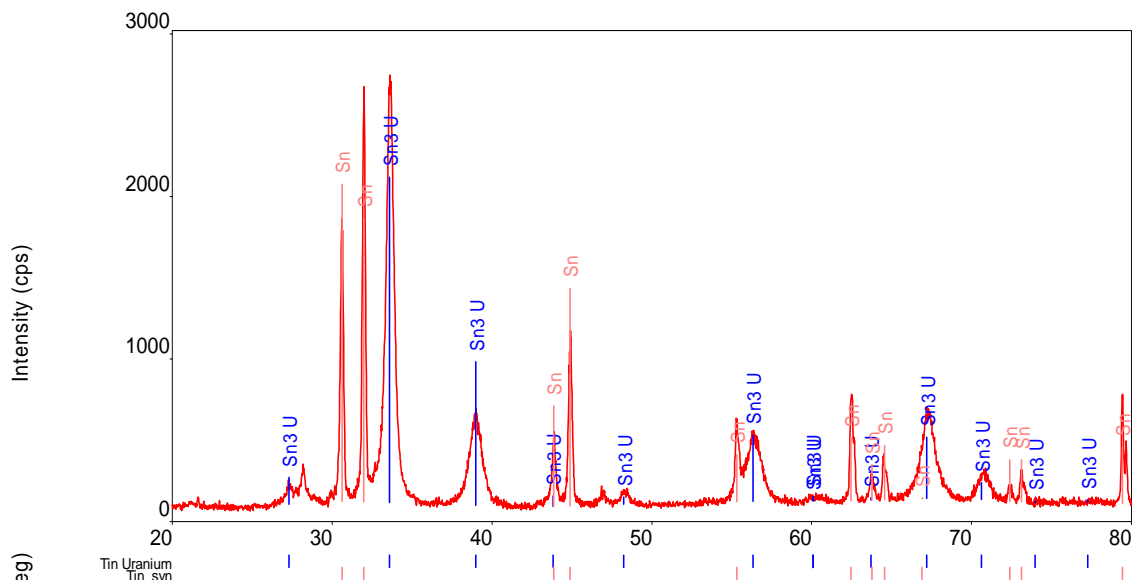


Figure 6.11 Typical XRD analysis of cathode deposit sample confirming the formation of  $USn_3$

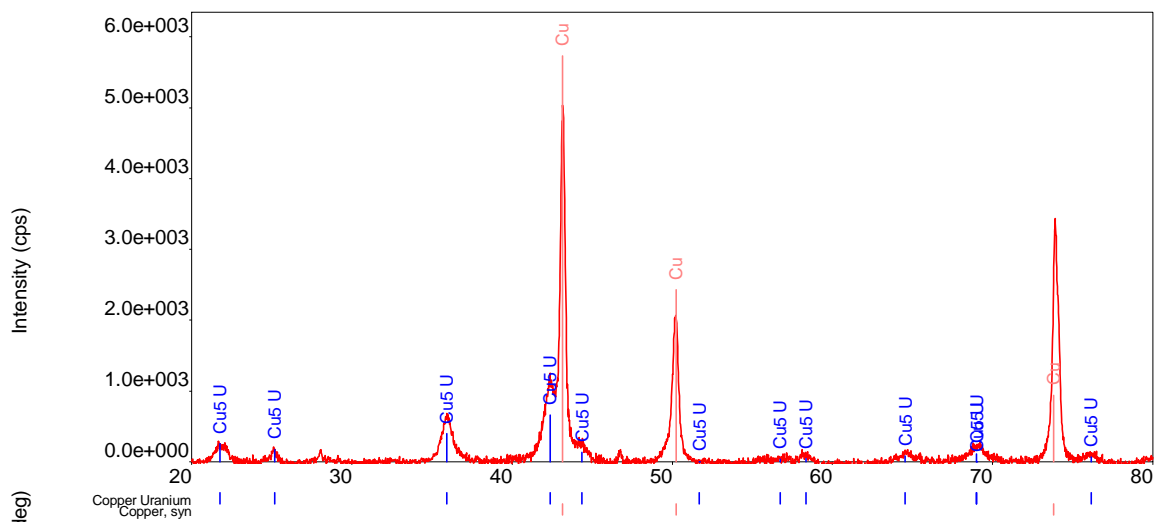


Figure 6.12 Typical XRD analysis of cathode deposit sample confirming the formation of  $Cu_5U$

#### 6.6.4 Electrolysis experiments in Phase 4 (ES17-ES21)

After establishing the uranium production in the widely reported electrolyte of LiF-BaF<sub>2</sub>-25Wt% UF<sub>4</sub> and that different sources of uranium oxide types and liquid cathodes do not have any significant effect on the uranium deposition, the effect of alternative additives in the electrolyte on the deposition of uranium was studied.

The effect of LaF<sub>3</sub> additive was studied by gradually replacing some portion of UF<sub>4</sub> with LaF<sub>3</sub> (termed here 'mixed electrolyte') and finally with only LaF<sub>3</sub> additive. Separate experiments with mixed electrolytes were conducted with LiF-BaF<sub>2</sub>-9.5Wt%UF<sub>4</sub>-15.5Wt%LaF<sub>3</sub> and LiF-BaF<sub>2</sub>-9.5Wt% LaF<sub>3</sub>-15.5Wt% UF<sub>4</sub> electrolyte, with sintered UO<sub>2</sub> pellets as the source of uranium oxide and copper as the liquid cathode. The cathode current density was maintained at 2A/cm<sup>2</sup>. The experiments were repeated for reliability in the results. Analysis of the metal in the cathode chambers confirmed the formation of Cu<sub>5</sub>U in all the cases. As mixed electrolytes resulted in uranium deposition, it was logical to replace all the UF<sub>4</sub> with LaF<sub>3</sub> and proceed further with experiments in LiF-BaF<sub>2</sub>-25Wt%LaF<sub>3</sub> electrolyte. All the other cell parameters were maintained constant during these experiments. The same experiment was repeated with UO<sub>2</sub>+C pellets to study the effect of source of UO<sub>2</sub> in LiF-BaF<sub>2</sub>-25Wt%LaF<sub>3</sub> electrolytes. It was observed that uranium deposition was obtained in all the experiments with LiF-BaF<sub>2</sub>-25Wt%LaF<sub>3</sub> electrolyte and Cu<sub>5</sub>U was present along with copper.

Some efforts were directed in all the experimental runs to determine the change in bath composition occurring during electrolysis by collecting samples of the frozen electrolyte. It

was observed that segregation occurs when the cooling was deliberately slow to protect the ceramic tube.

The detailed list of representative electrolysis experiments are presented in Table 6.4. It can be seen that electrolysis experiments in phase 1 and phase 2 with widely reported electrolyte  $\text{LiF-BaF}_2\text{-25Wt\% UF}_4$  did not yield any recoverable uranium. Electrolysis runs in phase 3 with  $\text{LiF-BaF}_2\text{-25Wt\% UF}_4$  electrolyte have led to deposition of uranium with tin or copper as liquid cathode. Mixed electrolyte with  $\text{LaF}_3$  as the additive also led to repeatable deposition of uranium. As seen from the phase 3 results, form of uranium oxide had no effect on deposition of uranium. Phase 4 experiments with  $\text{LaF}_3$  as the only additive to the electrolyte also confirmed the deposition of uranium, with different forms of uranium oxide.

Table 6.4 List of UO<sub>2</sub> electrolytic reduction experiments conducted with different cell designs in phases

Phase I experiments

Exp No	Cell design, electrolyte quantity	Cathode current density A/cm <sup>2</sup>	Anode current density A/cm <sup>2</sup>	UO <sub>2</sub> powder qty	Anode design	Electrolysis time, minutes	Inter-electrode distance	Results
ES1	A, 80g	1.2	0.1	5.8g	Graphite bucket	400 mins	10mm	No metal deposit
ES2	A, 80g	1.2	0.1	4.5g	Graphite bucket	205 mins	10mm	No metal deposit
ES3	A, 80g	1.2	0.1	4.3g	Graphite bucket	217 mins	20mm	No metal deposit
ES4	A, 80g	2.2	0.1	5.4g	Graphite bucket	205 mins	10mm	No metal deposit
ES5	B, 350g	~5.66	0.09	9.2g	Graphite bucket	205 mins	15mm	No metal deposit
ES6	B, 350g	~5.66	0.86	10.5g	BN floating bucket	200 mins	15mm	No metal deposit
ES7	B, 350g	~5.66	0.18	25.6g	Graphite perforated anode	307 mins	30mm	No metal deposit
ES7a	B, 350g	~5.66	0.18	25.5g	Graphite perforated anode	300 mins	15mm	No metal deposit

Phase II experiments

Exp No	Cell design, electrolyte quantity	Cathode current density $A/cm^2$	Anode current density $A/cm^2$	UO <sub>2</sub> powder qty	Anode design	Electrolysis time, minutes	Inter-electrode distance	Results
ES8	D, 700g	Constant voltage CCD~12	0.3	16g	Graphite crucible with UO <sub>2</sub> +carbon pellet	80 mins	~30mm	No metal deposit
ES9	E, 600g	1.38	0.04	NIL	Graphite crucible anode	600 mins	~25mm	No metal deposit

Phase III experiments

Exp No	Cell design, electrolyte quantity	Cathode current density $A/cm^2$	Anode current density $A/cm^2$	UO <sub>2</sub> powder qty	Anode design	Electrolysis time, minutes	Inter-electrode distance	Results
ES10	F, 1400g Bi, Cathode	~2	0.15	UO <sub>2</sub> +C pellets	Graphite bucket with lid	240mins	20mm	Metal, quickly oxidised
ES11	F, 1400g Bi, Cathode	~2	0.15	UO <sub>2</sub> +C pellets	Graphite bucket with lid	240mins	20mm	Metal, quickly oxidised
ES12	G, 1400g Sn, Cathode	~2.2	0.17	UO <sub>2</sub> +C pellets	Graphite bucket	217 mins	20mm	U-Sn compound

Exp No	Cell design, electrolyte quantity	Cathode current density A/cm <sup>2</sup>	Anode current density A/cm <sup>2</sup>	UO <sub>2</sub> powder qty	Anode design	Electrolysis time, minutes	Inter-electrode distance	Results
ES13	H, 1400g Sn, Cathode	~2.3	0.18	UO <sub>2</sub> +C pellets	Graphite bucket	240 mins	20mm	U-Sn compound
ES14	H, 1200g Sn, Cathode	~2	0.15	UO <sub>2</sub> powder	Graphite bucket	240 mins	20mm	U-Sn compound
ES15	H, 1200g Sn, Cathode	~2.3	0.18	UO <sub>2</sub> pellets	Graphite bucket	360 mins	20mm	U-Sn compound
ES16	H, 1200g Cu Cathode	~2.28	0.18	UO <sub>2</sub> pellets	Graphite bucket	360 mins	20mm	Cu <sub>5</sub> U compound
ES17	H, 1200g mixed Cu Cathode	~1.7	0.14	UO <sub>2</sub> pellets	Graphite bucket	70 mins	20mm	Cu <sub>5</sub> U compound
ES18	H, 1200g mixed Cu Cathode	~2.3	0.18	UO <sub>2</sub> pellets	Graphite bucket	360 mins	20mm	Cu <sub>5</sub> U compound
ES19	H, 1200g mixed Cu Cathode	~2.2	0.17	UO <sub>2</sub> +C pellets	Graphite bucket	360 mins	20mm	Cu <sub>5</sub> U compound

Phase IV experiments

<b>Exp No</b>	<b>Cell design, electrolyte quantity</b>	<b>Cathode current density A/cm<sup>2</sup></b>	<b>Anode current density A/cm<sup>2</sup></b>	<b>UO<sub>2</sub> powder qty</b>	<b>Anode design</b>	<b>Electrolysis time, minutes</b>	<b>Inter-electrode distance</b>	<b>Results</b>
ES20	H, 1200g UF <sub>4</sub> free Cu, Cathode	~2.2	0.17	UO <sub>2</sub> pellets	Graphite bucket	240 mins	20mm	Cu <sub>5</sub> U compound
ES21	H, 1200g UF <sub>4</sub> free Cu, Cathode	~2.2	0.17	UO <sub>2</sub> pellets	Graphite bucket	240 mins	20mm	Cu <sub>5</sub> U compound

## 6.7 Conclusions

The technical feasibility of a process for electrolytic reduction of uranium oxide to uranium metal in LiF-BaF<sub>2</sub>-25Wt%LaF<sub>3</sub> electrolytes at 1473K has been demonstrated in the laboratory scale for the first time. Under suitable operating conditions a continuous process for production of uranium by electrolytic reduction in LaF<sub>3</sub> solvent base electrolyte should be possible.

In all the electrolysis experiments with LiF-BaF<sub>2</sub>-25Wt%LaF<sub>3</sub> the form of uranium oxide was not found to have an influence on the formation of uranium. Also in all the electrolysis runs anode effect never occurred mainly because sufficient dissolved uranium oxide was available and the cyclic  $U^{4+} \leftrightarrow U^{3+}$  reaction contributed to depolarization of the anode, in addition to the fact that anode current density was one order less than the cathode current density. The current efficiencies were found to be in the range of 7-8% in all the experiments.

Although very high cathode current efficiencies have not been obtained, sufficient metal has been produced to indicate that kilogram level production is possible. Higher efficiencies should be possible in large size electrolytic cells than that were obtained in laboratory cells.

The general problem that always remains with the continuous process is the rate of uranium oxide addition to the electrolyte such that it will not lead to settling of undissolved oxide. Although problems of uranium oxide settling and improvement of efficiencies remain to be

solved, this process is very attractive, as a replacement for the present electrolytic reduction of uranium oxide. It can be implemented in the nuclear fuel cycle without elaborate steps for conversion of uranium oxide to  $UF_4$  of specific isotopic composition.

### References

- 6.1 Konstantin I. Popov, Stojan S. Djokic, Branimir N. Grgur, FUNDAMENTAL ASPECTS OF ELECTROMETALLURGY, 2002 Kluwer Academic/Plenum Publishers.
- 6.2 Niedarch L. W. and Dearing B. E., "The preparation of uranium metal by the electrolytic reduction of its oxides", Journal of the Electrochemical society, Vol 105, No. 6, pp 353-358, 1958.
- 6.3 Niedarch L. W., "New approach to electrolytic uranium", Nucleonics, Vol. 16, No 1, pp 64-65, 1958.
- 6.4 Niedarch L. W. and Glamm A.C., "Uranium purification by electrorefining", Journal of the Electrochemical society, Vol 103, No. 9, pp 521-528, 1958.
- 6.5 Niedarch L. W. and Dearing B. E., "Electrowinning of uranium from its oxides", Knolls Atomic Power Laboratory, Rep No KAPL-1761, 1957.
- 6.6 Niedarch L. W. and Schafer A. C., "Electrowinning of uranium from its oxides II A preliminary Engineering evaluation", Knolls Atomic Power Laboratory, Rep No KAPL-1668, 1957.
- 6.7 Henrie T. A., "Electrowinning rare-earth and uranium metals from their oxides", Journal of Metals, pp 978-981, 1964.
- 6.8 Piper R. D., and R.F. Leifield, "Electroreduction of uranium oxides to massive uranium metal", Mallinckrodt Chemical Works, Rep No. MCW-1447, 1960.

- 6.9 Piper R. D., and R.F. Leifield, "Electrolytic reduction of uranium metal from uranium oxides", I & EC Process Design and development, Vol 1, No. 3, pp 208-212, 1962.
- 6.10 Piper R. D., and Gay. E. C, "Process development quarterly progress report", Mallinckrodt Chemical Works, Rep No. MCW-1479, 1962.
- 6.11 Piper R. D., "Process development quarterly progress report", Mallinckrodt Chemical Works, Rep No. MCW-1480, 1963.
- 6.12 Piper R. D., Vie J.D., Reyland J.N., Kornfeld R.J., and D.E. Treadway, "Methods for tapping molten uranium from an electrolytic cell", Mallinckrodt Chemical Works, Rep No. MCW-1481, 1963.
- 6.13 Piper R. D., "Laboratory report of the uranium Electroreduction process", Mallinckrodt Chemical Works, Rep No. MCW-1500, 1966.
- 6.14 Stevenson J.W., "Electrolytic uranium project: Cell operation, terminal progress report", Mallinckrodt Chemical Works, Rep No. MCW-1514, 1966.
- 6.15 Varwig J.W., "Solubility of  $UO_2$  in molten salt", Mallinckrodt Chemical Works, Rep No. MCW-1490, 1964.
- 6.16 Haas P.A, Adcock P.W, Coroneos A.C. and Hendrix D.E, "Small cell experiments for electrolytic reduction of uranium oxides to uranium metal using fluoride salts", Metallurgical and Material transactions B., Vol 25B, pp 505-518, 1994.
- 6.17 Haas P.A and Stanley P. Cooper, "Solubility of uranium oxides in fluoride salts at  $1200^{\circ}C$ ", American chemical society, Vol 38, No. 1, pp 26-30, 1993.
- 6.18 Takeshi Shimda, Nobuo Tedzuka, Yuzo Shimizu and Masanobu Miyake, "Electrochemical reduction of uranium oxide in molten fluoride mixture", Journal of Alloys and compounds, 204, pp 1-4, 1994.

- 6.19 Takeshi Shimda, Nobuo Tedzuka, Yuzo Shimizu and Masanobu Miyake, “Electrode reactions of Uranium during electrolysis of its oxide in a molten fluoride bath”, Journal of Alloys and compounds, 206, pp 249-253, 1994.
- 6.20 W F Gale and T C Totemeier, Smithells metals reference book, 8th ed, ISBN: 978-0-7506-7509-3
- 6.21 Porter B., and Brown E.A., “Determination of oxide solubility in the Molten fluorides”, Bureau of Mines Report of investigation 5878, U.S. Department of interior, Bureau of Mines,(1961).
- 6.22 Belov G V, Trusov B G, ASTD Version 2.0, 1995
- 6.23 G.J. Janz, W. Dampier, G.R. Lakshminarayanan, P.K. Lorenz and R. P. T. Tomkins , “Molten Salts”, Vol 1. Electrical conductivity, Density and viscosity data, NSRDS-NBS 15, 1968.

## CHAPTER VII

# PREPARATION AND TESTING OF YTTRIA COATINGS

---

The success of the electrolytic reduction process largely depends on the availability of corrosion resistant materials for the engineering components. The cell material for containing the electrolyte was already addressed earlier in chapter III. This chapter deals with the development of components required for handling liquid uranium, its testing for thermal stability and compatibility with liquid uranium.

### 7.1 Introduction

For all the engineering components required for handling liquid uranium in large scale electrolytic cells, a protective barrier on metallic components is required as molten uranium is highly corrosive. These structural members should possess excellent resistance to liquid uranium and at the same time should not introduce any undesirable impurity into the uranium. The phase diagrams of various refractory metals with uranium indicate that there is a definite solubility of refractory of metal in uranium at 1473K, which makes them unfit to use in direct contact with liquid uranium directly as they would introduce impurities. [10.1]. In the literature, it is reported that certain ceramic oxides such as  $\text{Al}_2\text{O}_3$ , Calcia Stabilized Zirconia,  $\text{Y}_2\text{O}_3$ ,  $\text{LaPO}_4$  are capable of withstanding liquid uranium well [10.2-10.3]. The data on the compatibility of various refractory metals and ceramic materials with liquid uranium as available from the literature are summarized in Table 7.1. Although the ceramic

materials are superior in high temperature corrosion resistance, engineering components of an electrolytic cell are complex in construction and monolith shapes of ceramic materials are very difficult to fabricate. Instead a protective ceramic coating on metallic components of desired shapes, is a more feasible option.

Among the various coating technologies, plasma spray coating has been accepted as an established technique to produce ceramic coatings for protection against heat, corrosion and wear. It is one of the most versatile thermal spraying techniques to prepare refractory material coatings for improved surface characteristics. In this process almost all the materials that can be melted without decomposition can be deposited on substrates; in these cases the substrate invariably have heat resistance to temperatures lower than the melting point of the ceramic coating material. The main limitation of the plasma spray coating is its inferior mechanical strength in comparison with the corresponding ceramic monolithic materials [10.4]. Plasma sprayed coatings of various ceramics such as alumina, calcia/yttria stabilized zirconia, and other refractory materials have been well developed for various high temperature engineering applications [10.5].

Table 7.1 Materials of construction and their compatibility with liquid uranium

S.no	Material	M.point (K)	K W/m K	Compatibility with uranium	Ref
1	Tantalum	3290	57.5 (273K)	Exhibits brittleness and tears (~20hrs @ 1210°C)	[10.6]
2	Tungsten	3695	174 (273K)	Full penetration of 0.3 mm foil in 20hrs @ 1300°C	[10.7]
3	Molybdenum	2896	142 (273K)	Full dissolution of 0.3 mm foil in 0.25 hrs at 1160°C	[10.8]
4	Al <sub>2</sub> O <sub>3</sub>	2323	5.8 (1400K)	Used for short term handling	-

S.no	Material	M.point (K)	K W/m K	Compatibility with uranium	Ref
5	CSZ	2900	10.7 (1273K)	Attack observed in 0.5 hrs at 1400°C	[10.2]
6	Y <sub>2</sub> O <sub>3</sub>	2683	8 (1000K)	No reaction till 12.5hrs @ 1400°C	[10.3]
7	CaF <sub>2</sub>	1691	9.71 (273K)	Most compatible material, lacks hot strength.	-
8	LaPO <sub>4</sub>	2343	1.8 (973K)	No reaction upto 2hrs @ 1250°C	[10.9]

### 7.1.1 Yttria coating

Thermal spray grade yttrium oxide has been synthesized and used to produce adherent coatings of yttrium oxide with NiCrAlY bond coat on various substrates [10.13]. Yttrium oxide has excellent thermal stability up to its melting temperature and also possesses superior resistance to aggressive chemical attack by molten metals and some salt mixtures at high temperatures. Because of its thermodynamic stability, yttrium oxide exhibits better corrosion resistance to liquid metal corrosion and is used in the form of sintered shapes and protective coatings in several applications associated with high temperature corrosion [10.10, 10.11]. Toshiaki *et al.* have proposed yttrium oxide as a candidate material compatible with liquid uranium due to its greater thermodynamic stability in comparison with UO<sub>2</sub> [10.11]. Reduction of Y<sub>2</sub>O<sub>3</sub> by uranium metal is not thermodynamically feasible, as the Gibbs free energy of formation of Y<sub>2</sub>O<sub>3</sub> at 1573K is -1455 kJ/mole compared to -814 kJ/mole for UO<sub>2</sub>. Free energy minimization study of Y<sub>2</sub>O<sub>3</sub>-U system by Padmanabhan *et al.* indicates that yttrium oxide is chemically stable up to 3000K [10.12]. Thermodynamic analysis based on free energy suggests that yttrium oxide is chemically more stable in comparison to ZrO<sub>2</sub> and Al<sub>2</sub>O<sub>3</sub> against attack by uranium up to 3000 K [10.2-10.3,10.11]. The binary phase diagram of uranium and yttrium metal also indicates a

very low mutual solubility, with the maximum solubility of yttrium in uranium being 0.5 atom % at 1573K. Based on the reported superiority of yttrium oxide, in this work it was planned to study the thermal stability and the robustness of yttria coating, and also investigate the compatibility of the yttria coating with liquid uranium.

Yttrium oxide coating (sponge rub of yttria slip) on graphite crucibles had been proposed by Koger *et al.* as a solution for reducing the carbon pickup from the graphite crucibles [10.2]. Short term melting experiments by Koger *et al.* upto 30 mins between 1573K-1773K showed that yttria is stable against liquid uranium. However, in the reactivity study conducted [10.3] for the duration of 200hrs between liquid uranium and polycrystalline sintered yttrium oxide substrates at 1673K Tournier *et al.* concluded that oxidation of uranium occurs from the oxygen provided by yttrium oxide. They found that the  $UO_2$  layer formed at the uranium/yttria interface was gradually transformed into a solid solution of  $UO_2$ - $Y_2O_3$  [10.12]. Studies on corrosion resistance of  $Y_2O_3$  barrier coating are scanty.

Tantalum has been chosen as the substrate among the other refractory metals, keeping in view the following considerations: ease in fabrication and handling, availability, limited saturation solubility in liquid uranium (~2.5 wt%) at its melting point.

The yttria coating on the metallic materials used at high temperatures is required to have good thermal shock resistance to prevent peeling of the coated layer during operation, as peeling will lead to enhanced corrosion as well as other operational problems. Typically, plasma coated coatings have a two-layered structure consisting of a bond coat and a chemically resistant and thermally insulating ceramic topcoat.

The bond coat reduces the thermo-mechanical mismatch between the top coat and the substrate. When the coating serves as a chemical barrier and simultaneously as a thermal barrier, the bond coat is also required to be as chemically inert to the corrosive media as the substrate metal. In the intended applications, accidental failure of protective coating will expose the commonly used bond layer (Ni-Cr-Al-Y alloy) which is more severely attacked than tantalum by the molten uranium. Hence the  $Y_2O_3$  protective coating on tantalum without a bond layer is the preferred option. However, there is not enough reported literature available on the production methods and performance evaluation of the plasma spray coatings on substrates without a bond coat.

The work of development of corrosion resistant coatings involved two major objectives

- (i) The development of thermally stable coatings which had to begin at preparation of plasma spray grade yttrium oxide powder, and
- (ii) Experimental studies to study the reactivity of liquid uranium with plasma spray grade yttrium oxide on the tantalum substrate at 1573K for durations upto 400hrs, sufficient to demonstrate the suitability of the engineering components.

The two studies are presented respectively in Part A and Part B of this chapter.

## **PART A**

### **7.2 Yttria coating preparation and thermal stability testing**

The operating parameters that influence the plasma spray coating in general, and the yttria coating on tantalum without a bond coat are (a) the quality of the powder, (b) the electric power, (c) the powder feed rate, (d) primary gas flow and (e) the torch to base distance. Resistance to thermal shock was evaluated by subjecting the coated specimens, to controlled heating and cooling cycles between 300K to 1500K in an induction furnace. The experiment was designed to examine the sample tokens by both destructive and non-destructive techniques, after a pre-determined number of thermal cycles.

#### **7.2.1 Preparation of plasma spray grade Y<sub>2</sub>O<sub>3</sub> Powder**

Powders utilized in preparation of Y<sub>2</sub>O<sub>3</sub> coatings were in-house sintered and prepared from the raw material supplied by IRE Ltd (99.5% minimum assay) that had a size range of 5-10 micron. The powder was subjected to Cold Isostatic Pressing (CIP) at ~206 MPa to obtain a green density of ~ 50%. Sintering of the compact was done at 1873K for 4 hours. Microhardness test was conducted on the sintered blocks to ensure the sintering process. The sintered block was crushed to chunks followed by reduction to smaller size fractions in a planetary ball mill with alumina balls each weighing 20g. The ground powder was then sieved to obtain powders of size range 38-75µm and 76 -106µm.

#### **7.2.2 Preparation of coated samples**

The coating was done in an existing facility in the laboratory: The torch parameters in the experiments were thus around the optimized values regularly used in the facility.

The specimens used for test of coating were cut from a pure tantalum sheet into coupons of rectangular shapes having dimensions 25 mm x 10 mm x 1mm thk, and 40 mm x 8 mm x 1mm thk respectively. In order to reduce the stress raising points, the edges and corners of the rectangular tokens were rounded. A series of coating experiments were conducted by producing coatings of yttria with variations of the main parameters, namely, powder size, plasma power, the primary gas flow and the powder feed rate. Other coating factors that were maintained constant are the torch to base distance (TBD), the auxiliary gas flow, the feed gas flow and the surface roughness. Adhesion test was used as the response parameter for obtaining the optimum parameters for the coating process. The results, in terms of the adhesion strength, of the parametric experiments conducted and an analysis of the significant factors are presented in Table 7.2. It is observed from the table that in all the coating experiments conducted with 38-75 $\mu$ m powder always resulted in coatings with higher adhesion strength in comparison to 76 -106 $\mu$ m powder. It is seen that with 38-75 $\mu$ m powder maximum adhesion strength of 8MPa was obtained with 24.6kW of plasma power, with the other parameters maintained constant. The probable reason for reduced strength at higher power of plasma of 29.9 kW is that, for a given powder feed rate higher power resulted in excessive temperature of the particles, which could have led to a lower viscosity of the liquid, causing it to splash on impact on the substrate. Splashing would lead to the generation of a splat with additional small droplets of the coating, which degrade the interfacial strength of the coating. The optimized parameters which were selected and used for plasma spray coating for subsequent coatings are given in Table 7.3.

Table 7.2 List of parametric studies conducted for plasma coating of yttria

Coupon no	Carrier gas Ar, lpm	TBD mm	Powder Feed g/min	Substrate Material	Substrate Quantity	Powder Size $\mu\text{m}$	Power kW	Primary Gas lpm	Secondary Gas lpm	Coating Thickness ( $\mu\text{m}$ )	Adh. strength MPa	Avg strength
I A I B I	12	100	13	ASTM size SS specimen &Ta coupon	2 SS and 1 Tantalum	38-75	29.4	Ar. 30	N <sub>2</sub> 3	250	7.276 5.238	6.257
II A II B II	12	100	13	ASTM size SS specimen &Ta coupon	2 SS and 1 Tantalum	38-75	29.9	Ar. 25	N <sub>2</sub> 3	250	4.178 4.892	4.535
III A III B III	12	100	13	ASTM size SS specimen &Ta coupon	2 SS and 1 Tantalum	38-75	24.6	Ar. 30	N <sub>2</sub> 3	250	8.051 7.032	7.5415
IV A IV B IV	12	100	13	ASTM size SS specimen &Ta coupon	2 SS and 1 Tantalum	38-75	24.4	Ar. 25	N <sub>2</sub> 3	250	6.013 6.053	6.033
V A V B V C	12	100	14	ASTM size SS specimen &Ta coupon	3 SS and 1 Tantalum	76-106	29.9	Ar. 30	N <sub>2</sub> 3	280	5.605 6.053	5.829
VI A VI B VI C	12	100	14	ASTM size SS specimen &Ta coupon	3 SS and 1 Tantalum	76-106	29.9	Ar. 25	N <sub>2</sub> 3	280	4.280 3.322	3.801
VII A VII B VII C	12	100	14	ASTM size SS specimen &Ta coupon	3 SS and 1 Tantalum	76-106	24.6	Ar. 30	N <sub>2</sub> 3	280	4.994 5.911	5.5425
VIII A VIII B VIII C	12	100	14	ASTM size SS specimen &Ta coupon	3 SS and 1 Tantalum	76-106	24.6	Ar. 25	N <sub>2</sub> 3	280	4.076 3.689	3.8825
			$\Sigma_+ = 19.055$				$\Sigma_+ = 19.055$	$\Sigma_+ = 20.42$	$\Sigma_+ = 25.17$			
			$\Sigma_- = 24.366$				$\Sigma_- = 24.366$	$\Sigma_- = 22.99$	$\Sigma_- = 18.25$			
			$eff = -1.328$				$eff = -1.328$	$eff = -0.65$	$eff = 1.73$			
										$\Sigma_+ = 19.055$		
										$\Sigma_- = 24.366$		
										$eff = -1.328$		

Table 7.3 Optimized yttria coating parameters by plasma spray

S.no	Parameter	Value	Study
1.	Power	24.6 KW	Optimized
2.	Primary Argon gas flow	30 lpm	Optimized
3.	Secondary gas flow	3 lpm	Fixed
4.	Powder size	38-75 $\mu\text{m}$	Optimized
5.	Powder feed rate	13 g/min	Optimized
6.	Carrier gas flow	12 lpm	Fixed
7.	TBD	100 mm	Fixed
8.	Average coating thickness	240-270 $\mu\text{m}$	Optimized

### 7.2.3 Thermal cycling test of coatings

Around 50 coupons of 25 mm x 10 mm x 1mm thk and 40 coupons of 40 mm x 8 mm x 1mm thk were coated with the optimized parameters in different batches. Each batch for coating had around 15 coupons. Prior to the thermal cycling test of the coated coupons, visual inspection and optical micrography were conducted for around 100 coupons to evaluate the coating. Leica DMI 5000 optical microscope was used for optical microscope investigations. To qualify the coating for long term thermal cycling tests the plasma sprayed  $\text{Y}_2\text{O}_3$  coupons were heated with a 24 kW plasma flame to red hot condition and cooled to room temperature by putting off the flame. This quick method of thermal cycling was able to exclude poorly coated coupons. Microhardness evaluation of coatings was also done to study the nature of the deposited material. Generally, a sintered block with greater than 99% theoretical density exhibits a higher hardness in comparison to the coating, which

inherently has ~10-12% porosity. The hardness measurement serves as a quick method of determining approximately the porosity in the coating. For each batch of powder preparation, hardness values were measured for the sintered block. The batches of coated coupons were prepared and their hardness values as measured are shown in Table 7.4. It was found that the coating hardness of the batches was in the similar range, which indicates that the coatings produced with different batches of powders are likely to have similar properties.

Table 7.4 Microhardness values of sintered blocks of yttria and yttria coated coupons

<b>Component</b>	<b>unit</b>	<b>Powder Batch-1</b>	<b>Powder Batch -2</b>	<b>Powder Batch -3</b>
Sintered block	HV	543	508	538
Plasma coated coupon	HV	462	466	473

#### **7.2.4 Equipment for thermal cycling**

The experimental setup for the thermal cycling experiments, mainly consisted of a ceramic muffle either to provide an inert gas cover or a high vacuum atmosphere, along with a heating system to achieve the required temperature. The heating and cooling rates were controlled by a dedicated microprocessor based programmable PID controller with a R type thermocouple for temperature measurement. The design considerations of inert gas purity, structural materials, hot zone uniformity, leak tightness, sealing methods, cross section of the rods used inside the muffle, movement of internal through guides for the solubility experiments (discussed in the section on solubility study sec 4.3 of chapter 4) are also valid for this experimental setup. Additional considerations for the experimental setup for thermal cycling studies were as follows

- a) All the components used in the setup should be vacuum compatible with lower vapour pressure and out gassing rate.
- b) Wherever possible graphite should be avoided in vacuum to prevent reaction between the refractory metal samples and carbon from graphite.
- c) Vacuum better than or equal to  $5E-6$  mbar should be maintained during the experiments
- d) Detailed conductance calculations should be conducted to arrive at the vacuum pump specifications

All the weld joints and the O ring seals were leak tested with an Alcatel 142D Helium Mass Spectrometer Leak Detector (He-MSLD) to a sensitivity of  $1E-9$  mbar.l/s. The setup was characterized for the maximum attainable temperature, heating rate and uniform zone temperature. Ultimate vacuum achievable at room temperature was  $2E-6$  mbar, which proved the adequacy of the vacuum system. Before the actual experiments, the attainable vacuum level was measured at 1573K, and it was found to be around  $3E-6$ mbar, which was better than specified.

For the thermal cycling tests in argon atmosphere, experiments were conducted using a 10 kW induction furnace with a coil of 120mm diameter, 150mm height, which would accommodate a axially aligned ceramic tube upto 100mm OD. Based on the heat conduction calculations from the first principles and the experience from the previous assemblies, a recrystallized alumina tube with 80mm ID, 90mm OD and 800mm length, which was closed at one was found to be sufficient to maintain the temperature of the O

ring seal below 333K with forced convection cooling. A graphite susceptor was used for heating the coupons which rested on the floor at the closed end of the alumina tube.

For the thermal cycling tests in vacuum the open end of the alumina tube was connected to the vacuum system with the help of a tee. The flange at the far end of the tee had leak tight feed-throughs for coupon holders and thermocouple. The closed end of the tube was placed inside a resistively heated 6kW furnace. Vacuum of 1E-6 mbar was maintained by an oil diffusion pump of 260 lps pumping capacity backed by a rotary pump of 6 m<sup>3</sup>/hr displacement capacity. In both the argon gas and the vacuum thermal cycling setup, the open end of the tube had a set of flanges with O ring seals, which had provision for gas inlet, outlet and thermocouples. An alumina thermowell of 4mm ID 6mm OD 1000mm long and closed at one end was used to insert a R type thermocouple with 3mm diameter ceramic beads for temperature measurement. The coupons were hung using Kanthal wire of 0.5 mm diameter, and were shielded from the induction coil to prevent direct heating using an electrically grounded graphite cylinder. The general assembly of the experimental setup is shown in figure 7.1.

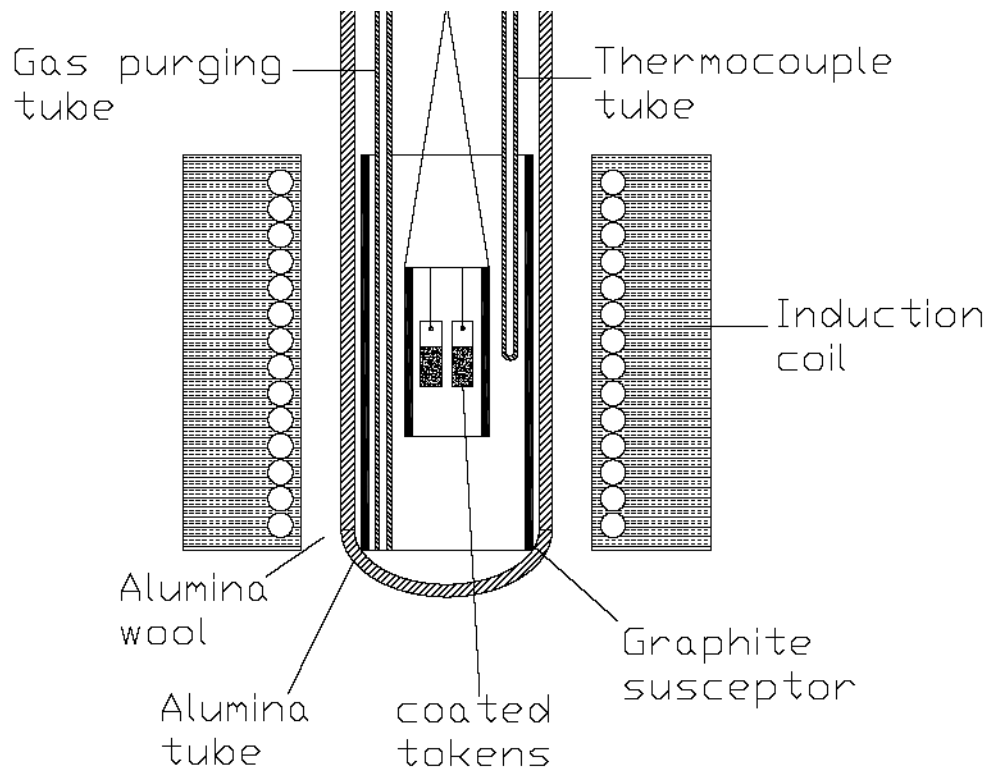


Figure 7.1: General assembly of the thermal cycling setup for thermal cycling test of plasma coated coupons

### 7.2.5 Thermal cycling test procedure

The thermal cycling tests were performed at 1523K with continuous purging of purified argon having  $\leq 0.1$ ppm oxygen. For vacuum thermal cycling tests the vacuum was of the order of  $1E-6$  mbar. Each cycle consisted of heating the coupons to 1523K in a controlled way at 200K/hr, and soaking at that temperature for 2 hours, followed by controlled cooling. The heating and cooling rates adopted for the cycling experiment are shown in figure 7.2. The weight changes of the coated samples were measured to a precision of 0.01 mg. For each reading, at least two samples were tested in identical conditions so that the average weight gain/loss of the samples could be obtained. The samples were observed at

100X magnification in an optical microscope for any defects caused due to thermal cycling. A test coupon was considered failed when cracks were observed at 100X at any location on the surface.

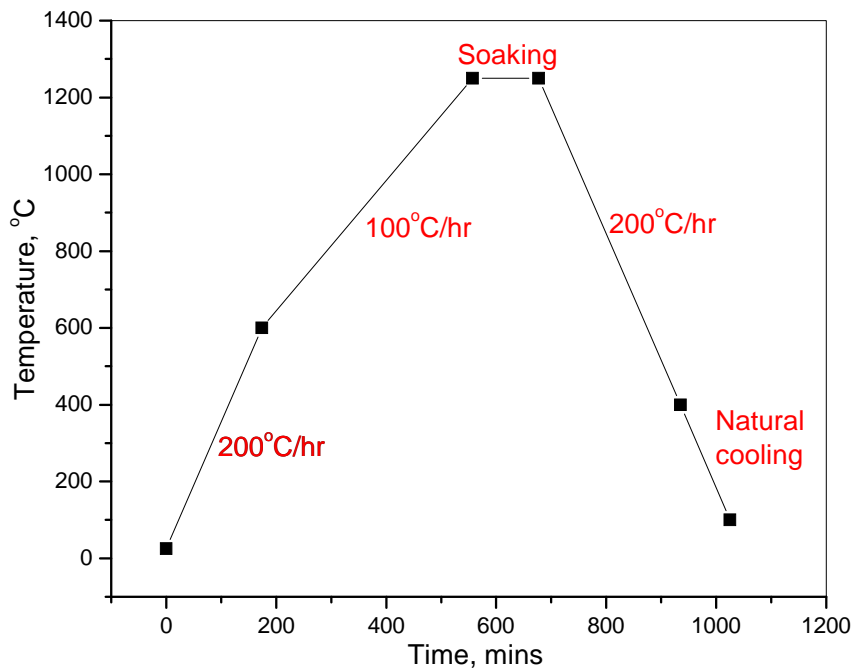


Figure 7.2: Heating and cooling cycle for thermal cycling experiments for test of yttria coating.

### 7.3. Results and Discussion for thermal cycling tests

Figures 7.3 and 7.4 show the microstructure of the yttria coating on the tantalum substrates. Two different kinds of morphologies were observed in the coatings. In figure 7.3, the surface is relatively rough when compared to the microstructure in figure 7.4. This feature was observed in the entire set of 15 coupons coated in the batch. Smooth surface was obtained on the first surface which was coated. Then the coupons were turned by 180° for coating on the second side. A rough structure was always obtained on the second side of the

rectangular coupon coated. This could be attributed to the slight oxidation that would occur on the uncoated surface during the coating of the first metal surface. This oxide layer might have increased the surface roughness, because of which the resulting coating surface obtained was also rough.



Figure 7.3. Ytria coating on tantalum rectangular token, as coated surface micrograph at 100X



Figure 7.4. Ytria coating on tantalum rectangular token, as coated surface micrograph at 100X

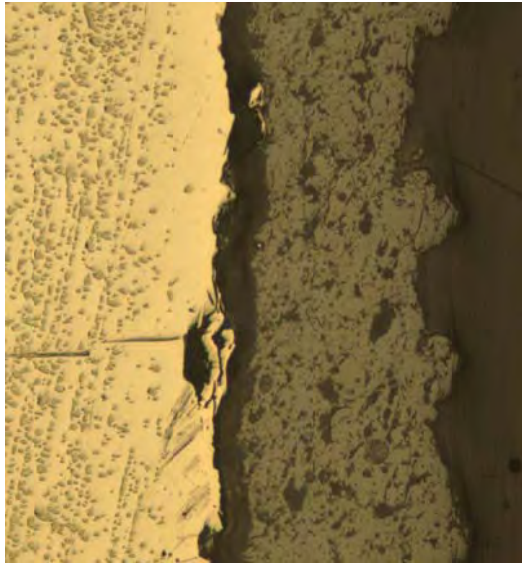


Figure 7.5. Optical micrograph of Yttria coating on Ta coupon

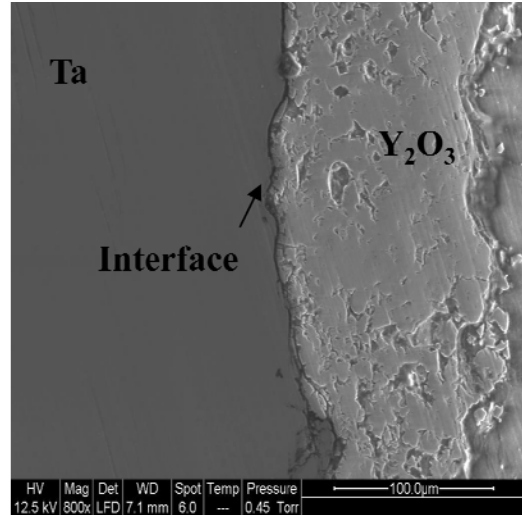


Figure 7.6. SEM Picture of Ta-Yttria interface of yttria coating

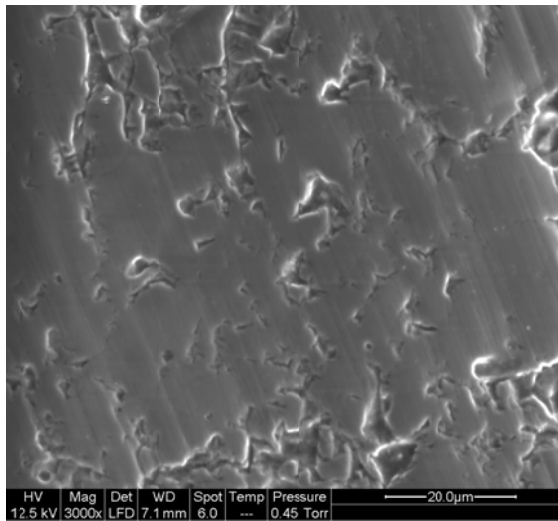


Figure 7.7. SEM picture of yttria coating

Figures 7.5 and 7.6 show the micrographs of the interface between tantalum and of yttria coating, and figure 7.7 shows only the yttria coating. It can be observed that the coating is uniform, and the absence of large open or closed pores show that the coating quality is good.

One of the findings was that the coatings produced by the in-house sintered and ground powder did not develop any cracks in the argon atmosphere upto 26 cycles. Further testing was not done as the process requirement criterion was sufficiently satisfied. In the case of the procured powder, thermal cycling of coupons was conducted upto 6 cycles, and no failures were obtained. When the coupons were tested in vacuum, it was observed that the coatings produced by both by the in-house sintered and prepared powder and the powder procured from reputed commercial sources did not develop any cracks upto 9 cycles.

The other findings were from unplanned variations in the experiment. In one of the experiment, a water bubbler used in the outlet had led to an accidental introduction of water into the experimental setup. Entry of moisture had led to the formation of oxide along with TaC by the reaction of hydrocarbon gases or CO produced by high temperature reaction of the moisture with the graphite susceptor and the graphite shield. In another experiment, atmospheric oxygen leak into the system due to a faulty outlet valve resulted in the oxidation of the tantalum coupons. Both the episodes resulted in peeling of the coating. Thus, both the oxygen and the moisture introduction led to undesirable reaction with the substrate and consequent peeling of the coating. In a practical application with yttria coated tantalum components, oxygen and moisture should be scrupulously avoided.

This study shows that thermally stable and robust yttria barrier coatings can be produced using the selected process parameters without the use of a bond coat. The coupons coated with optimal parameters were taken for further studies on liquid uranium compatibility.

## PART -B

### 7.4 Liquid uranium corrosion studies of yttria coatings

Different mechanisms by which liquid uranium can attack the substrate are direct dissolution from the surface limited by saturation concentration, inter-granular attack, reactions with impurity elements, alloying and compound reduction. Except for compound reduction, all the other mechanisms are predominant when refractory metals like tantalum, molybdenum, tungsten and tungsten-rhenium alloys are used for containing liquid uranium [10.6-10.8, 10.14,10.15]. However, when ceramic materials specifically the oxides are used, compound reduction is the primary mode of attack, along with inter-granular attack and impurity reactions. The microstructure of the plasma spray coating is another important parameter which decides the extent of grain boundary penetration. The inter-splat voids and the microcracks in the splat offer path for penetration of the liquid metal. The degree and the nature of the liquid uranium attack is strongly influenced by the conditions prevailing at the interface between the liquid and the substrate, the wettability of the contact surface with the liquid metal, and the thermodynamic stability of the material in contact with the liquid uranium. Temperature, liquid pool velocity, heating and cooling conditions are the other factors that affect the degree of attack.

Many oxides of importance in high temperature technologies ( $ZrO_2$ ,  $Y_2O_3$ ,  $TiO_2$ ,  $UO_2$  etc.) exhibit significant ranges in non-stoichiometry. Tournier et al. have observed that these non-stoichiometric oxides have a strong influence on the wettability of liquid metals [10.16]. At 1673K, stoichiometric  $Y_2O_3$  has a contact angle of  $106^\circ$  with pure liquid

uranium, whereas the solid solution of  $\text{UO}_2$ -  $\text{Y}_2\text{O}_3$  offers a contact angle of  $52^\circ$ . The  $\text{UO}_2$ - $\text{Y}_2\text{O}_3$  solid solution is reportedly formed by reaction of molten uranium with  $\text{Y}_2\text{O}_3$  [10.3].

However, there is no data available on the liquid uranium corrosion resistance of the plasma spray coated yttria. Hence progressive, experimental studies were conducted progressively to study the reactivity of liquid uranium with the plasma sprayed yttrium oxide on a tantalum substrate at 1573K for long duration. The objective was to investigate the stability and compatibility of the plasma spray coated yttria on tantalum substrates without the use of bond coat in a pool of liquid uranium.

#### **7.4.1 Experimental setup for liquid uranium compatibility studies**

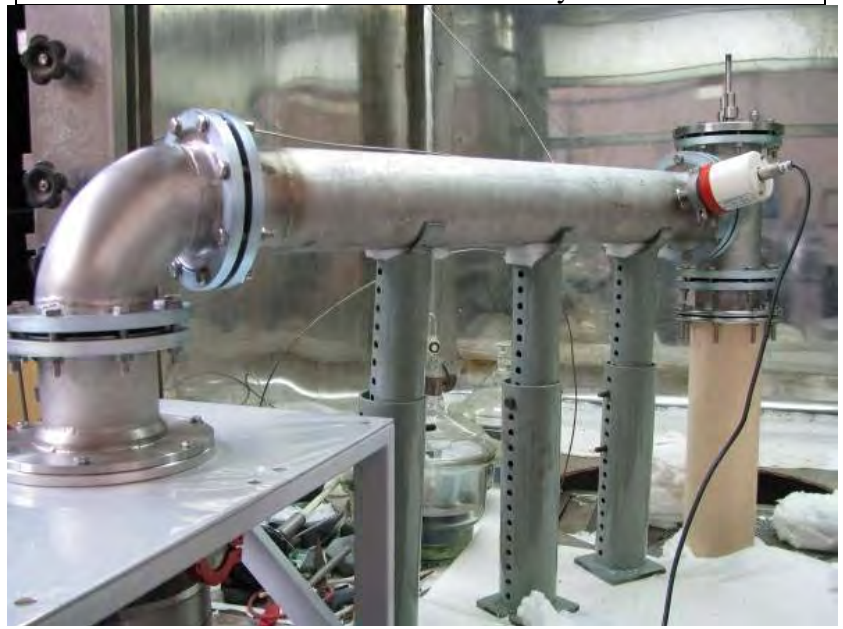
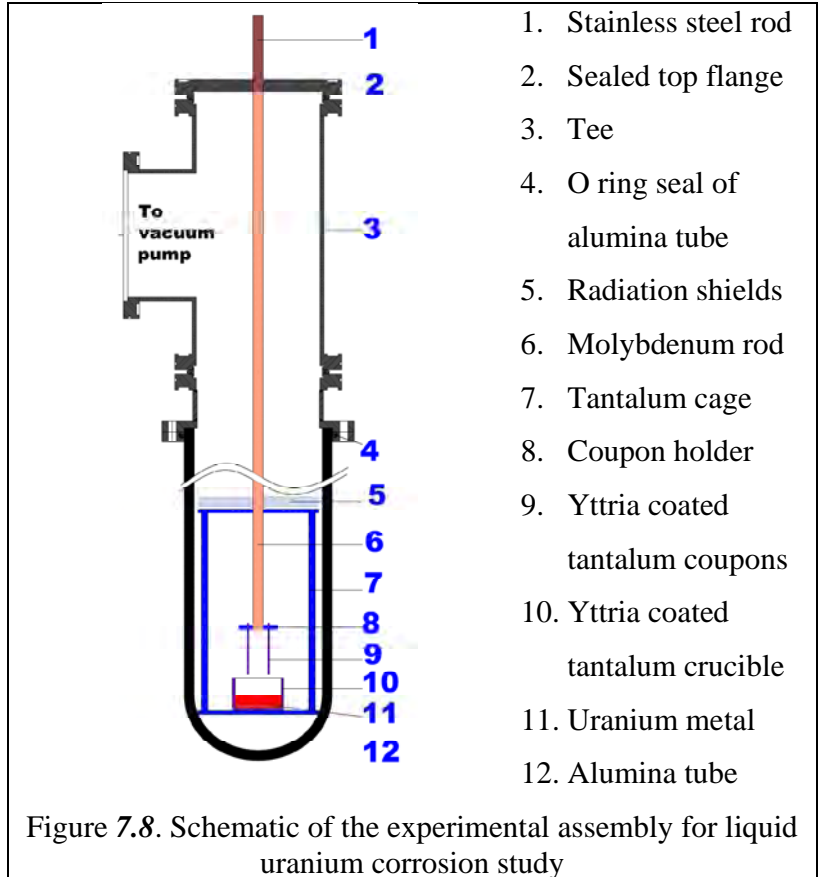
The design considerations of vacuum pumping system adequacy, structural materials, hot zone uniformity, leak tightness, sealing methods, arrangement of internals and movement of the internals through guides discussed for thermal cycling tests in section 7.2.4 remained valid for the present experiments. In addition to that, defense in depth approach was followed for safety of equipment and personnel by providing multiple barriers for containing the liquid uranium. The first barrier was the crucible containing the liquid uranium, the second containment was the alumina tube and as the third containment a copper block of 100mm diameter 150mm height with a cavity to accommodate 300g of uranium was provided below the alumina tube. The complete experimental setup was housed inside a fumehood to prevent any release of powder or vapours of uranium into the laboratory.

The setup was built with a one end closed alumina tube of 100mm ID, 115mm OD and 800mm long with the open end connected to the vacuum system with the help of a tee. Similar to the earlier arrangement, the flange at the other face of the tee had leak tight feed-throughs for coupon holder and thermocouple. The closed end of the tube was placed inside a resistively heated furnace. The length of the alumina tube was so chosen that forced air cooling sufficed to keep the temperature of O ring seals below 373K. Vacuum of 1E-6 mbar was maintained by an oil diffusion pump (pumping speed 480 lps) backed by a rotary pump (6000 lph). A pack of radiation shields above the crucible ensured a uniform temperature over 150mm length in the hot zone. A tantalum cage was used to support the crucible containing uranium. The crucible having dimensions of 50mm outside diameter and 30mm height was formed from a 2mm thick tantalum sheet. This tantalum crucible was plasma spray coated with 80-110 $\mu$ m thick yttrium oxide. It contained about 230g of nuclear grade uranium, which on melting gave a pool depth of about 8mm. The experimental setup was tested for its thermal profile. The experimental setup went through a formal safety audit and approval process.

It was planned to change the uranium charge after the experiment if any scum was formed on the surface. In the experiments reported, there was no scum observed. Hence the same melt was used for all the experiments. The tantalum coupons used were 40mm x 8mm x 1mm thick with rounded edges and corners to reduce the stresses in the yttria coating. The coating was done up to 15mm length from one 8mm end of the coupon. The other end 8mm had a provision to fix the coupon in a rigid tantalum coupon holder. The coating thickness varied from 60 $\mu$ m-110 $\mu$ m. The coupon holder was a tantalum plate of 30mm x 30mm x

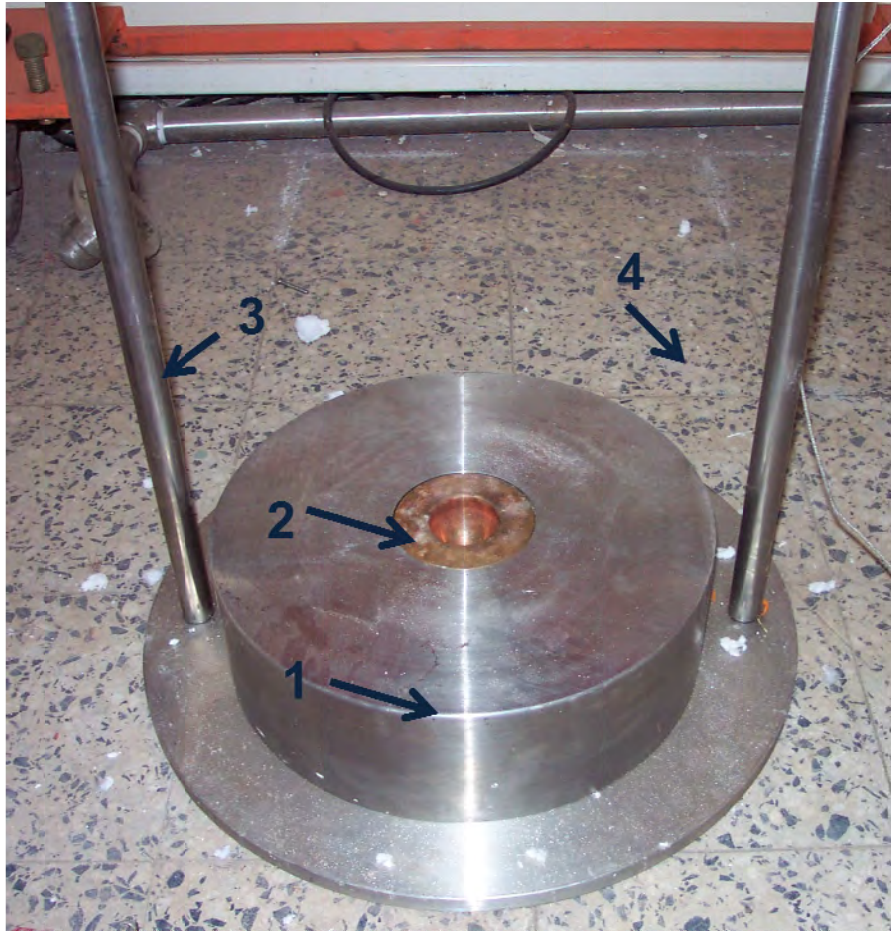
3mm thick with rectangular slots to insert the coupons, this did not allow the coupon to disorient during dipping in the melt. The coupon holder was connected to a molybdenum rod, which was in turn connected to a stainless steel rod, projecting out through a vacuum feed-through mounted on the flange. The rod was moved to immerse or remove the coupons from the metal pool. At least two coupons were used in each experiment. The pre-experimental qualification for defect free coupons was done by optical microscopy at 200X as was done for the thermal cycling experiments, and also by conducting thermal cycling tests of a few coupons of the batch. The schematic of the experiment assembly is shown in figure 7.8. Figure 7.9 shows the photograph of the experimental setup inside the fumehood.

Initially, a tantalum free crucible namely, high density graphite crucible was tried, to study the tantalum pickup in the uranium metal coming from tantalum coupons. Several trials were carried out to contain pure, liquid uranium at 1573K in the high density graphite crucibles with and with out pyrolytic carbon coating. Reaction of uranium with graphite was observed in both the high density graphite crucibles and the pyrolytic carbon coated crucibles, which made them unfit for liquid uranium containment.



1. Alumina tube
2. Sealed top flange with feed through for coupon holder
3. Connection to the vacuum line
4. Complete setup assembled inside a fumehood

Figure 7.9. Photograph of the experimental assembly for liquid uranium corrosion study



- |   |   |   |                                     |
|---|---|---|-------------------------------------|
| 1 | Stainless steel holder for copper block               | 3 | Ceramic tube support rods           |
| 2 | Copper block with cavity for quenching liquid uranium | 4 | Laboratory flooring inside fumehood |

Figure 7.10 Engineering safety arrangement of copper block to quench accidentally spilled liquid uranium inside the fumehood

### 7.5 Plasma spray coating on coupons and crucible

As discussed in the previous section attempts to use a tantalum free crucible did not yield meaningful results. It was thus decided to conduct all the melting and immersion experiments in a yttrium oxide coated tantalum crucible, where the liquid metal corrosion effects would be studied only on the coupons. The optimized process described in section 7.2.1 was used to prepare spray grade powder starting with pure yttrium oxide from M/s

Indian Rare Earths Ltd. Sintering was carried out in air at 1873K for 2 hrs for ensuring conversion of all non-stoichiometric oxides, if any, to stoichiometric  $Y_2O_3$ . No, further investigation of stoichiometry was done. The plasma spray parameters used for coating the coupons and crucible are as shown in Table 7.3.

#### **7.6. Experimental procedure for liquid uranium corrosion studies**

The heating, cooling and holding cycles adopted in the experiments consisted of heating the setup to 723K at 200K/hr and holding it for 2 hours, followed by heating to 873K at 200K/hr and holding for 2 hours for complete outgassing of the system. Heating was continued at 100K/hr to 1573K to melt the uranium charge, and thermally equilibrate the metal pool and coupons for 2hrs before immersion. The coated coupons were then dipped into metal pool upto a depth of 7mm. The experiments were conducted by continuous immersion of the coated coupons for 10, 20, 40, 80, 120, 200 and 400hrs durations. Around 20 experiments were conducted in this study, and the time of immersion was the only variable, all other parameters like temperature, level of vacuum, depth of immersion, heating and cooling rates were maintained constant. In each experiment, at least two control coupons were immersed which provided information about the measure of the reaction with liquid uranium at 1573K. The coupons were removed from the metal pool and held above the pool for 1hr for the adhering liquid uranium, if any, to trickle down. Post experiment analysis includes observation of the full area under an optical microscope at 200X for any defects. Defect free coupons were cold mounted and cut with a diamond wheel of 300 $\mu$ m thickness to observe the cross-section. Polishing was intentionally not done to retain the

micro structural features. A Zeiss EVO 40 SEM was used along with a Bruker EDX analyzer for micro-structural and chemical analysis.

### **7.7 Results and Discussions for liquid uranium compatibility studies**

The list of the experiments conducted, corresponding temperature, duration of immersion, and the observations of optical microscopy and SEM analysis are presented in Table 7.5. There were no cracks or pores observed on the surface of the coating of the unimmersed coupons, when viewed at 200X. Figures 7.11-7.14 show the micrographs of the as coated coupons. Surface porosity was studied using the SEM, and pore sizes ranging from 2-10 $\mu$ m were observed. It can also be seen from the cross-sectional micrograph that the coating is relatively free of interconnected pores which has a direct effect on the extent of penetration of uranium through the pores. Further, the optimized coating conditions had led to better adherence between the splats which is indicated by the absence of voids (5000X). The thickness of the coating on the coupons varied between 60-110 $\mu$ m. The density of the coating was found to be 90% of the theoretical density.

Table 7.5 List of the liquid uranium corrosion study experiments conducted and observations

<i>S.no</i>	<i>Sample Name</i>	<i>Duration of immersion, hrs</i>	<i>Temperature, K</i>	<i>Optical microscopy observations of immersed surface</i>	<i>SEM analysis observations of cross section immersed coupon</i>
1.	UCOR-4	10	1573	No cracks, spalling, chipping or delamination of coating observed at 200X	No corrosion reaction products are observed at the uranium/yttrium oxide interface. Uranium inside the coating was below detectable limits.
2.	UCOR-6	20	1573	No cracks, spalling, chipping or delamination of coating observed at 200X	No corrosion reaction products are observed at the uranium/yttrium oxide interface. Uranium inside the coating was below detectable limits.
3.	UCOR-8	40	1573	No cracks, spalling, chipping or delamination of coating observed at 200X	No corrosion reaction products are observed at the uranium/yttrium oxide interface. Uranium inside the coating was below detectable limits.
4.	UCOR-12	80	1573	No cracks, spalling, chipping or delamination of coating observed at 200X	No corrosion reaction products are observed at the uranium/yttrium oxide interface. Uranium inside the coating was below detectable limits.

<i>S.no</i>	<i>Sample Name</i>	<i>Duration of immersion, hrs</i>	<i>Temperature, K</i>	<i>Optical microscopy observations of immersed surface</i>	<i>SEM analysis observations of cross section immersed coupon</i>
5.	UCOR-14	120	1573	No cracks, spalling, chipping or delamination of coating observed at 200X	No corrosion reaction products are observed at the uranium/yttrium oxide interface. Uranium inside the coating was below detectable limits.
6.	UCOR-16	200	1573	No cracks, spalling, chipping or delamination of coating observed at 200X	No corrosion reaction products are observed at the uranium/yttrium oxide interface. Uranium inside the coating was below detectable limits.
7.	UCOR-18	400	1573	No cracks, spalling, chipping or delamination of coating observed at 200X	No corrosion reaction products are observed at the uranium/yttrium oxide interface. Uranium inside the coating was below detectable limits.
8.	Yttria coated tantalum crucible	840 (cumulative)	1573	No cracks, spalling, chipping or delamination of coating observed at 200X	SEM analysis was not conducted as the crucible was planned to be used for further experiments.



Figure 7.11 Typical optical micrograph of surface of yttria coating on tantalum substrate (as coated)

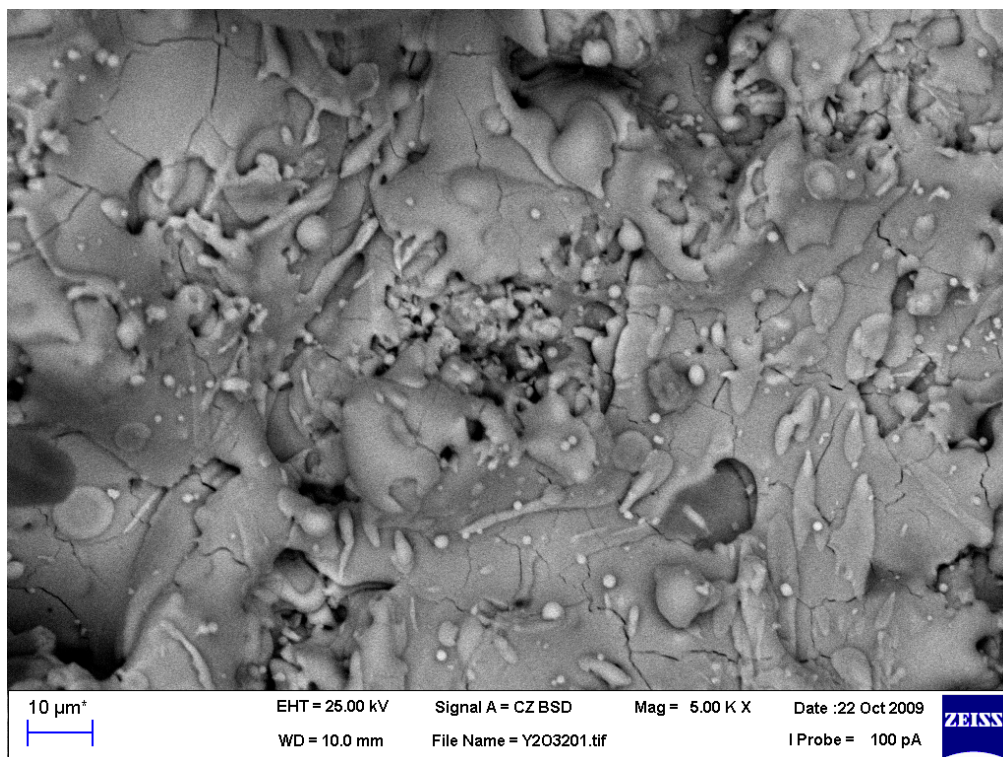


Figure 7.12. Typical SEM micrograph of surface of yttria coating on tantalum substrate (as coated)



Figure 7.13 Typical optical micrograph of cross-sectional view of tantalum /yttria coating interface (as coated)

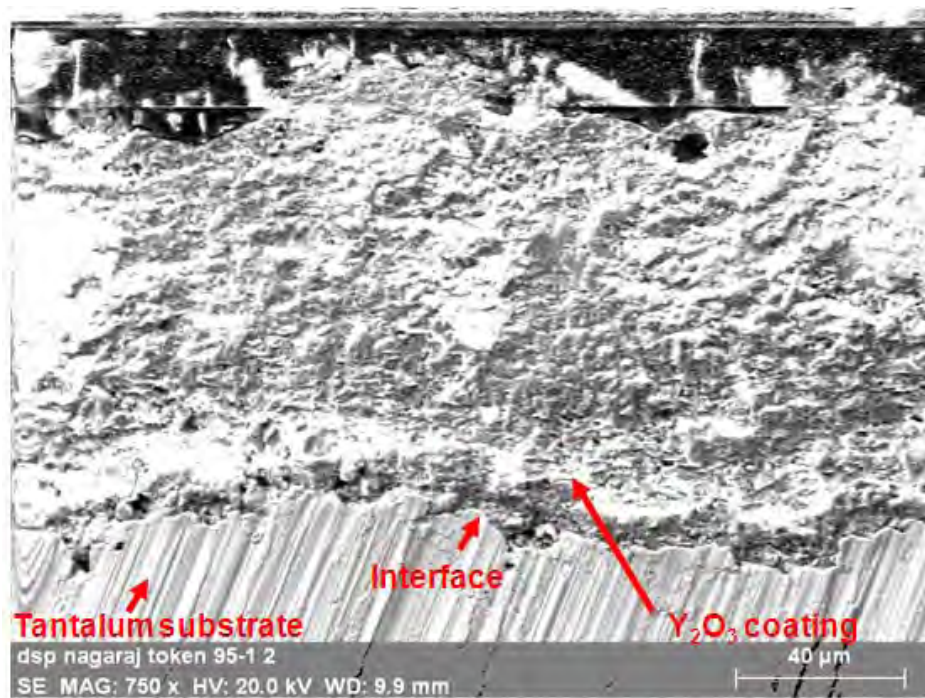


Figure 7.14. Typical SEM micrograph of cross-sectional view of tantalum /yttria coating interface (as coated)

After the corrosion experiments, the coating was examined for interface integrity. None of the coupons showed delamination or interfacial cracks. No significant change was observed in the average thickness of the coating after immersion. The coupons always reported a weight gain (in the range of 0.5 to 1.3 g) due to adherence of uranium, and no scum was observed on top of the melt that would have resulted from either reduction of yttrium oxide by uranium metal or due to spalling of the coating. Figures 7.16-7.22 show the cross-sectional view of the coupons of the seven different runs where the coupons were immersed for 10, 20, 40, 80, 120, 200 and 400 hrs respectively in liquid uranium at 1573K. No specific reaction products were observed at the interface of liquid uranium and  $Y_2O_3$  in the coupons immersed for 10, 20, 40, 80, 120, 200 and 400 hrs durations. The gradual conversion of white stoichiometric  $Y_2O_3$  to black non-stoichiometric  $Y_2O_3$  with increasing contact time with liquid uranium was observed by Tournier *et al* at 1673K [10.3]. This non-stoichiometric oxide was not observed across the thickness of coating even after 400 hrs of contact time with liquid uranium as reported by Tournier *et al* [10.12]. This possibly suggests that kinetics of the formation of non-stoichiometric oxides was very slow as the temperature of the experiment was lower by 100K than that of Tournier's. However, black or brown color was observed on the surface of the immersed area of the coupon, which might be due to oxidation of uranium that was adhering to the coupon after removal from the metal pool.

The photographs of the as coated coupon, of a coated coupon after immersion in liquid uranium and that of coated crucible which has been in contact with liquid uranium for 840 hrs(cumulative) are shown in figure 7.15..

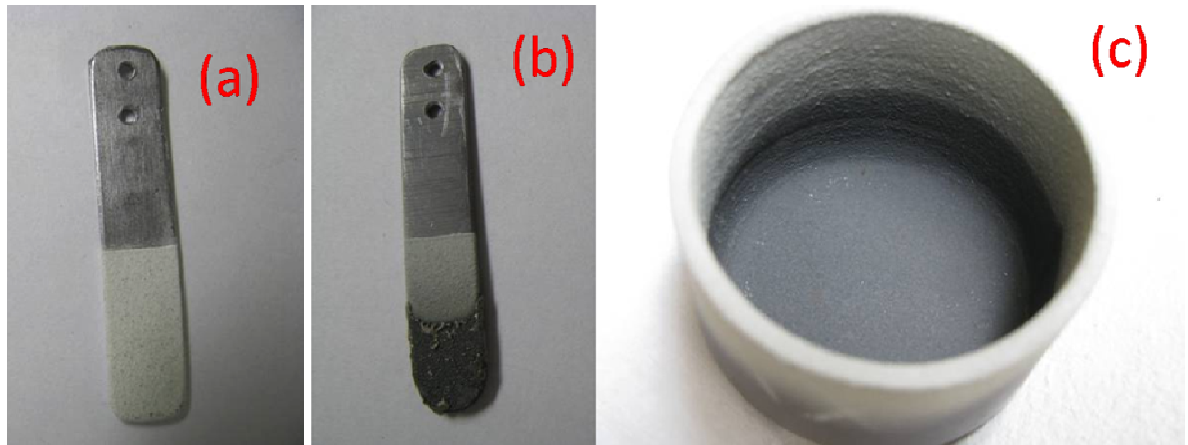


Figure 7.15. Photographs of the Y<sub>2</sub>O<sub>3</sub> coated tantalum coupons a) As coated b) After immersion in liquid uranium and c) crucible (Grey area represents contact area with liquid uranium for 840hrs)

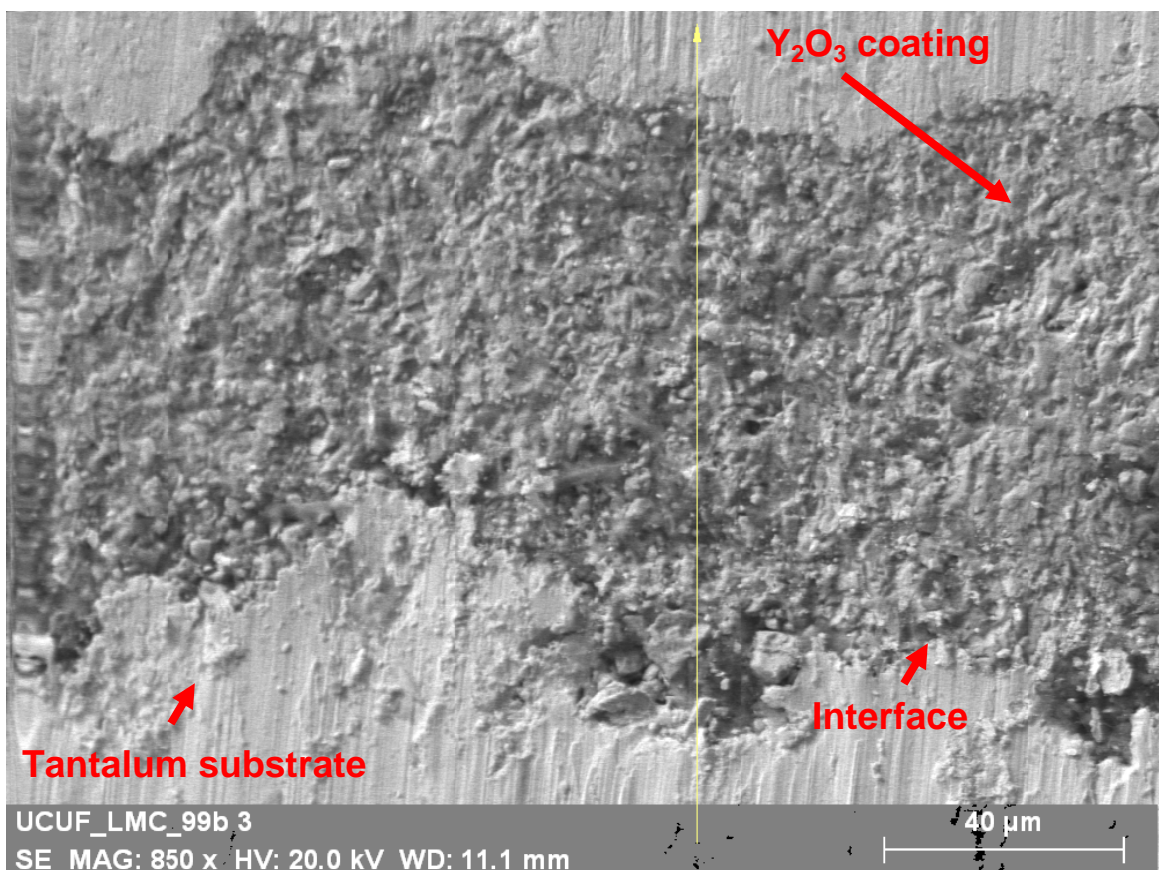


Figure 7.16 Cross-sectional view of tantalum /yttria coating interface after 10hrs of immersion (Sample UCOR-4)

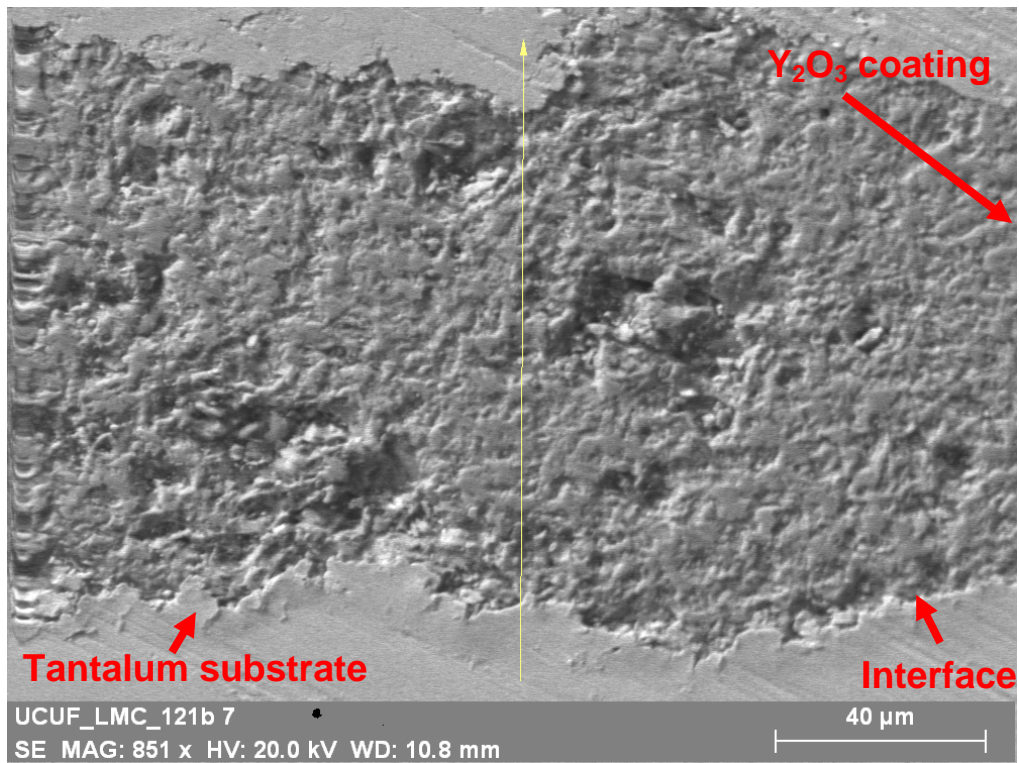


Figure 7.17 Cross-sectional view of tantalum /yttria coating interface after 20hrs of immersion (Sample UCOR-6)

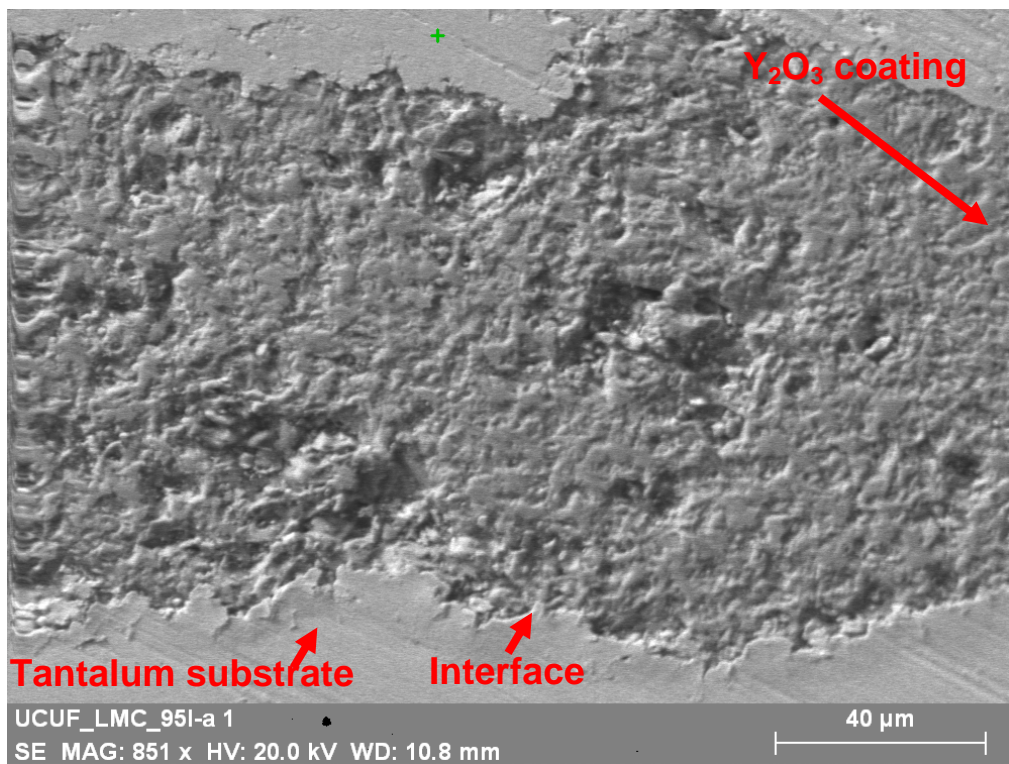


Figure 7.18 Cross-sectional view of tantalum /yttria coating interface after 40hrs of immersion (Sample UCOR-8)

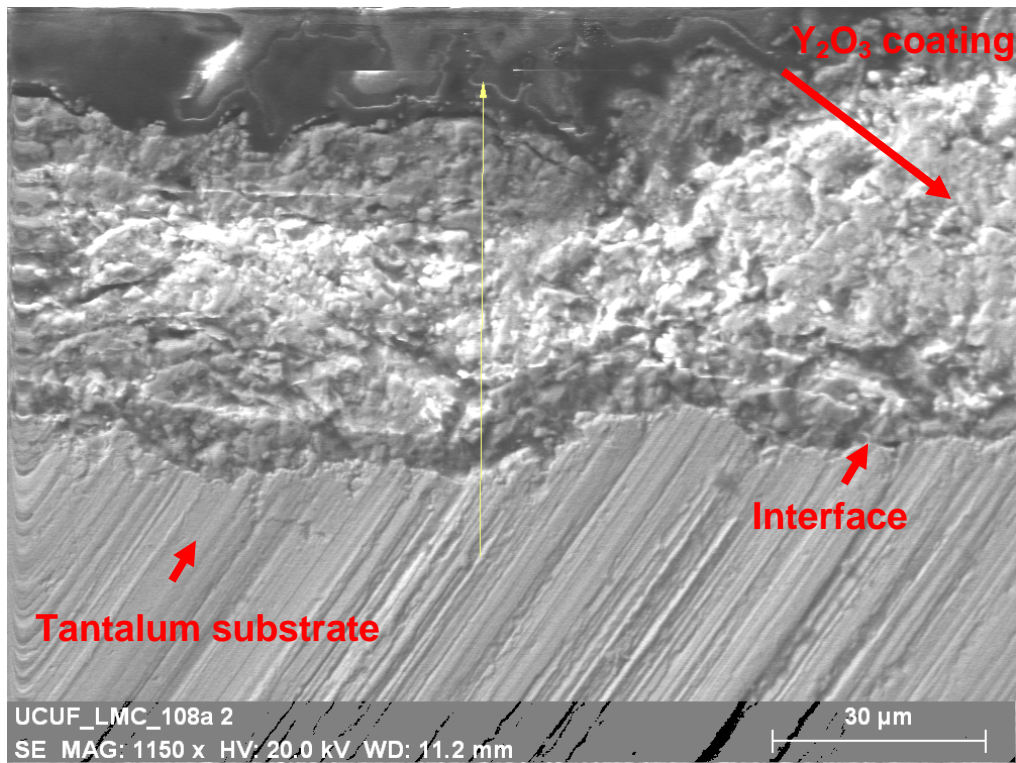


Figure 7.19 Cross-sectional view of tantalum /yttria coating interface after 80hrs of immersion (Sample UCOR-12)

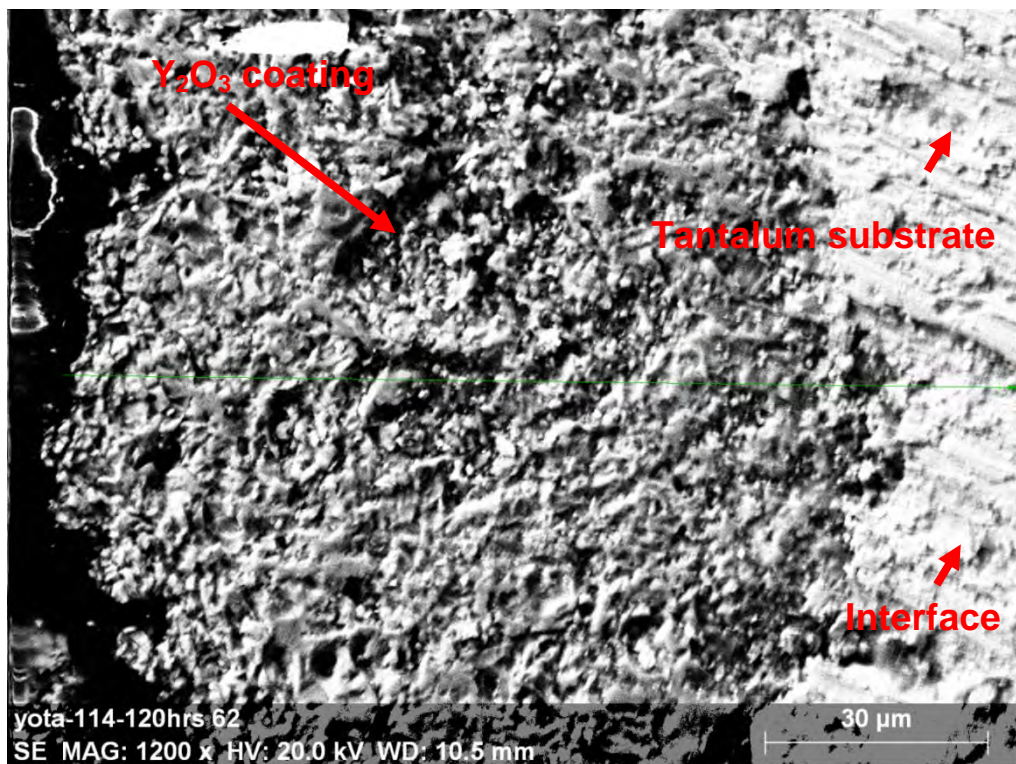


Figure 7.20 Cross-sectional view of tantalum /yttria coating interface after 120hrs of immersion (Sample UCOR-14)

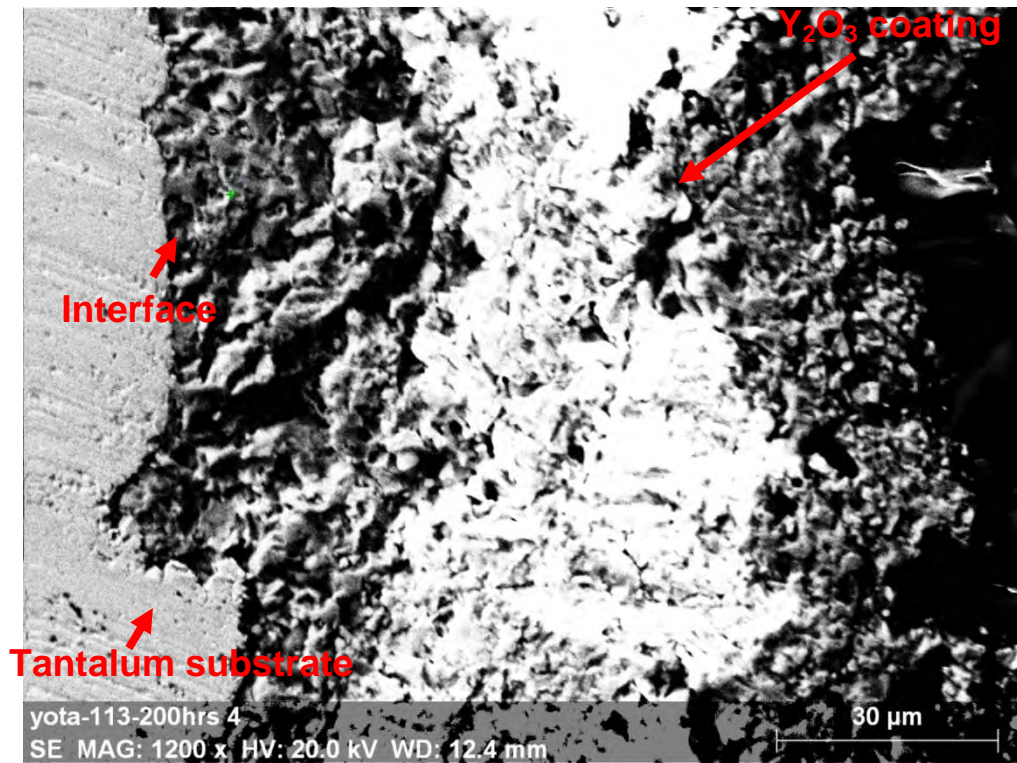


Figure 7.21 Cross-sectional view of tantalum /yttria coating interface after 200hrs of immersion (Sample UCOR-16)

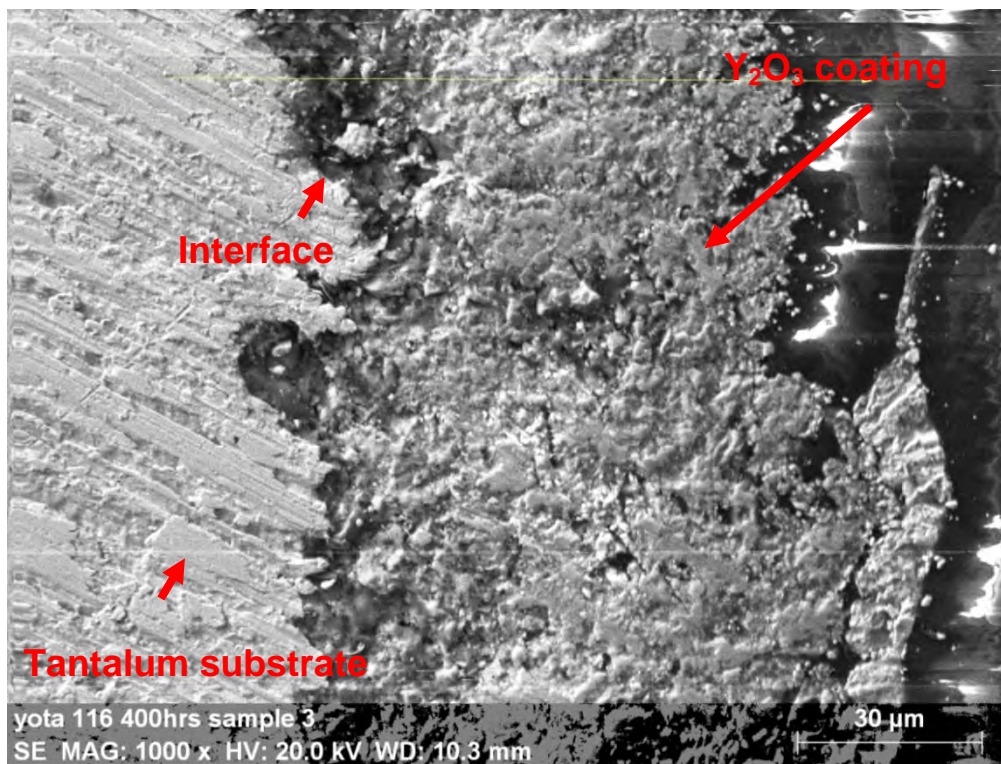


Figure.7.22 Cross-sectional view of tantalum /yttria coating interface after 400hrs of immersion (Sample UCOR-18)

### 7.7.1 Analysis of penetration of uranium into pores of coating

It is observed from the above micrographs that uranium has not penetrated through the pores on the surface. Penetration of liquid uranium into these pores is dependent on the surface tension and the contact angle. The rate of capillary penetration of the liquid metal is given by the Washburn equation (Eq 7.1). The Washburn equation is written as

$$\frac{dh}{dt} = \frac{1}{8\mu h} \left[ \Delta P' - \rho gh \right] r_o^2 \quad \dots\dots\dots(7.1)$$

where  $\mu$  is the viscosity of the liquid,  $\rho$  is the liquid density,  $r_o$  is the capillary radius,  $h$  represents the distance of penetration from a given datum line,  $g$  acceleration due to gravity and  $\Delta P'$  is the capillary pressure which is given by

$$\Delta P' = \left( \frac{1}{D} \right) 4\sigma \cos \theta \quad \dots\dots\dots (7.2)$$

where  $D$  is the pore diameter,  $\sigma$  the surface tension of liquid uranium and  $\theta$  the contact angle between the liquid uranium and yttrium oxide, all in consistent units. Here ' $\rho gh$ ' is the static pressure exerted by the liquid uranium.

The surface tension of liquid uranium between 1406K to 1850K is given by J.A. Cahilla and A.D. Kirshenbaum by the following equation 7.3 [10.17].

$$\sigma(\text{dyn/cm}) = 1747 - 0.14T(K) \quad \dots\dots\dots(7.3)$$

Considering a maximum pore size of 10 $\mu$ m on the surface, with the value of the surface tension at 1573K of liquid uranium being 1.5267 N/m and contact angle of 106 $^\circ$ , the pressure required to penetrate is 0.164 Mpa. The total hydraulic head, ' $\rho gh$ ' available considering an 8mm metal pool is only 1486.5 Pa which is a few orders below the required pressure. This explains the observation of liquid uranium not penetrating the

yttrium oxide coating. This also explains the fact that the solidified uranium from the yttrium oxide coated tantalum crucible was always easily removable at the end of each experiment.

Penetration of uranium vapour through the pores or inter-splat voids by Knudsen diffusion would have resulted in the accumulation of uranium by condensation, through all the interconnected channels. To confirm the penetration of uranium vapors, EDS analysis was performed.

### **7.7.2 EDS analysis of the cross section of immersed coupons**

The evidence of the absence of reaction between liquid uranium and yttrium oxide was further confirmed by line scans across the cross-section of the coating immersed in liquid uranium for different durations. Figures 7.23-7.29 show the line scans for different elements across the interface, in which the uranium concentration in all the cases was below the detection limits and was a part of the background noise. The variation in the signal counts was due to the surface roughness. The uranium peak seen in the figure 7.24 corresponds to the uranium adhering to the coating surface. Point analysis and quantification conducted at different locations across the cross-section also revealed that the uranium presence was below the detection limit. During the EDS line scan analysis the uranium concentration present in the coating on the tantalum substrate was below the detection limits of the instrument and hence was not observed. This further confirms the absence of interconnected porosity, hence, penetration of uranium vapour was not observed. From the results presented it is seen that the plasma sprayed yttrium oxide is compatible with liquid uranium at 1573K. It is also of interest to note

that the yttrium oxide coated tantalum crucible had been exposed to liquid uranium for 840hrs (cumulative) and was still in a good condition for use in more experiments.

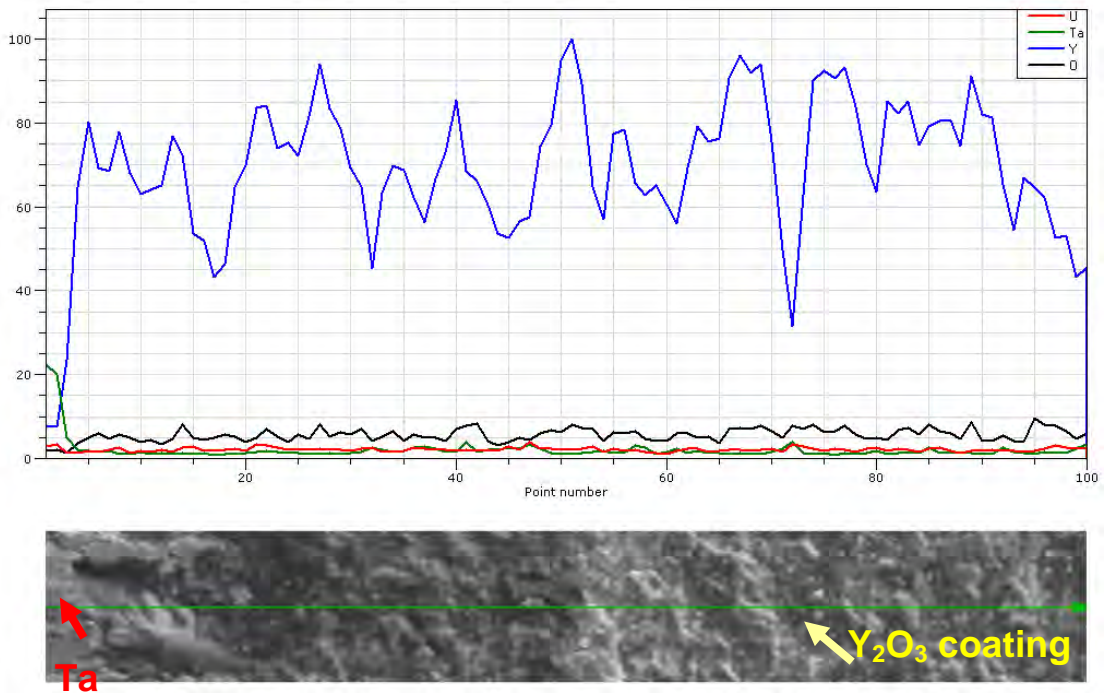


Figure 7.23 EDS line scan of the cross-section of tantalum /yttria coating interface after 10hrs of immersion (Sample UCOR-4)

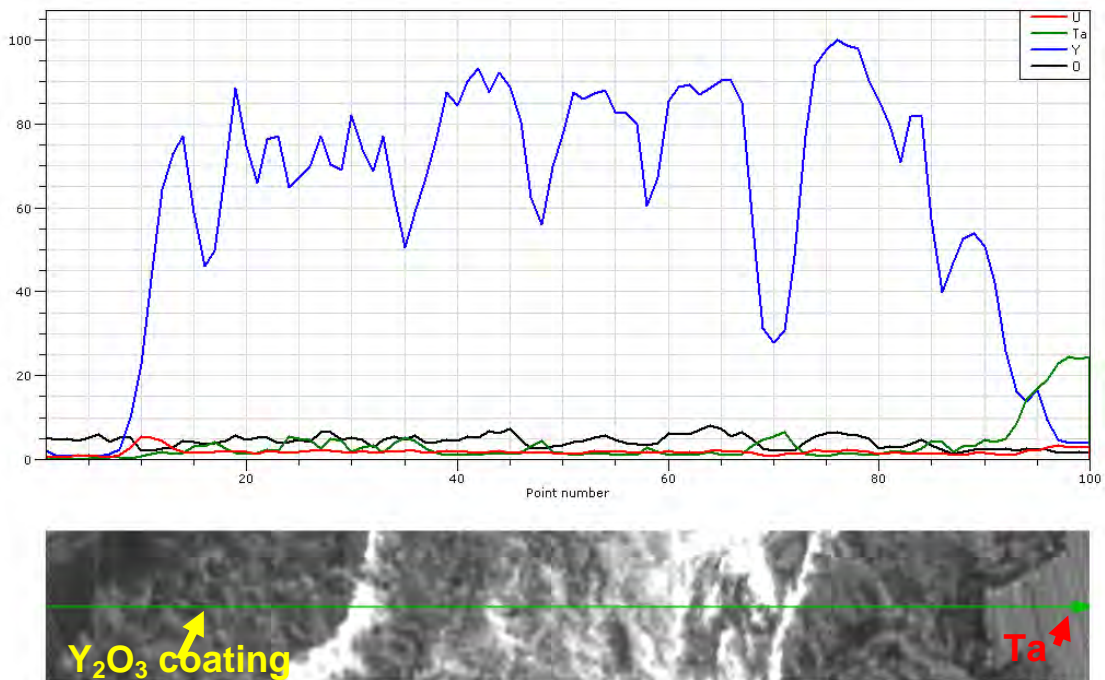


Figure 7.24 EDS line scan of the cross-section of tantalum /yttria coating interface after 20hrs of immersion (Sample UCOR-6)

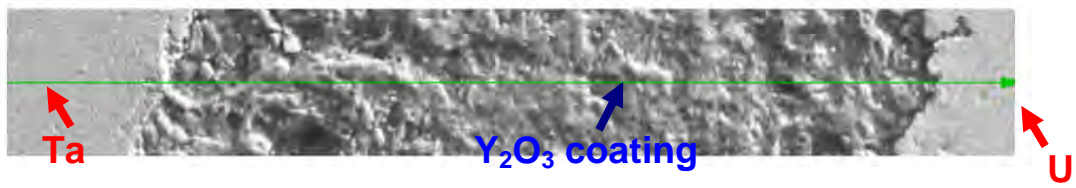
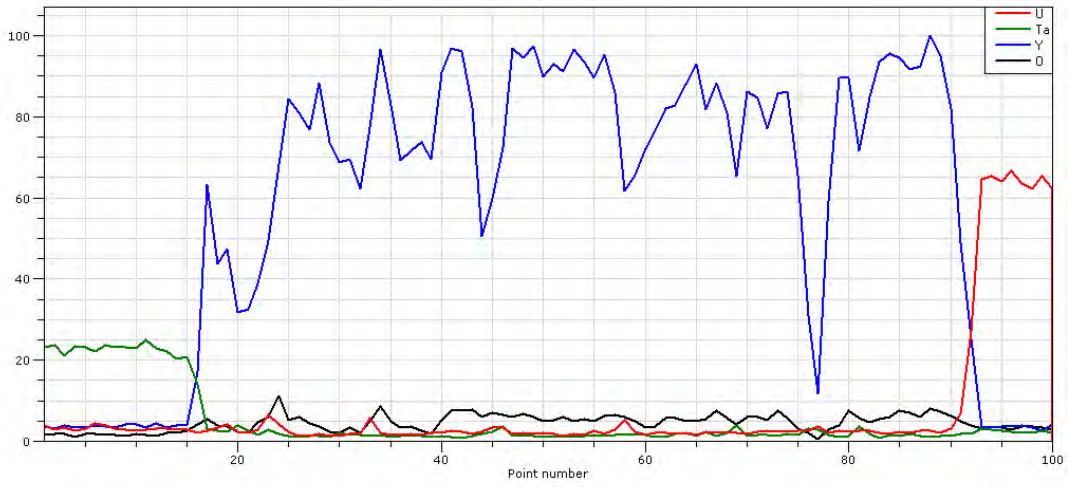


Figure 7.25 EDS line scan of the cross-section of tantalum /yttria coating interface after 40hrs of immersion (Sample UCOR-8)

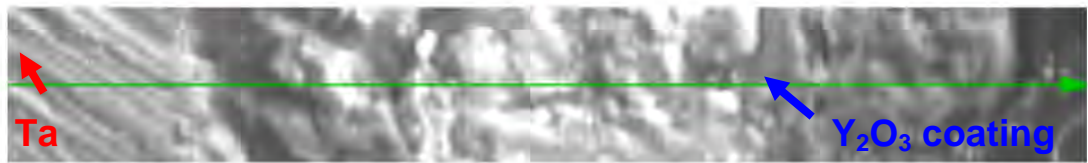
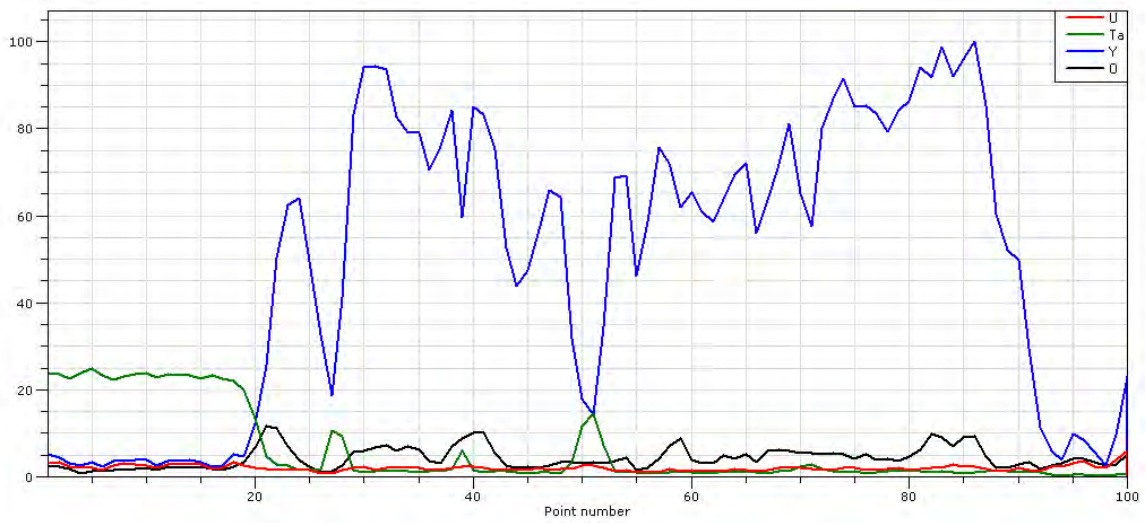


Figure 7.26 EDS line scan of the cross-section of tantalum /yttria coating interface after 80hrs of immersion (Sample UCOR-12)

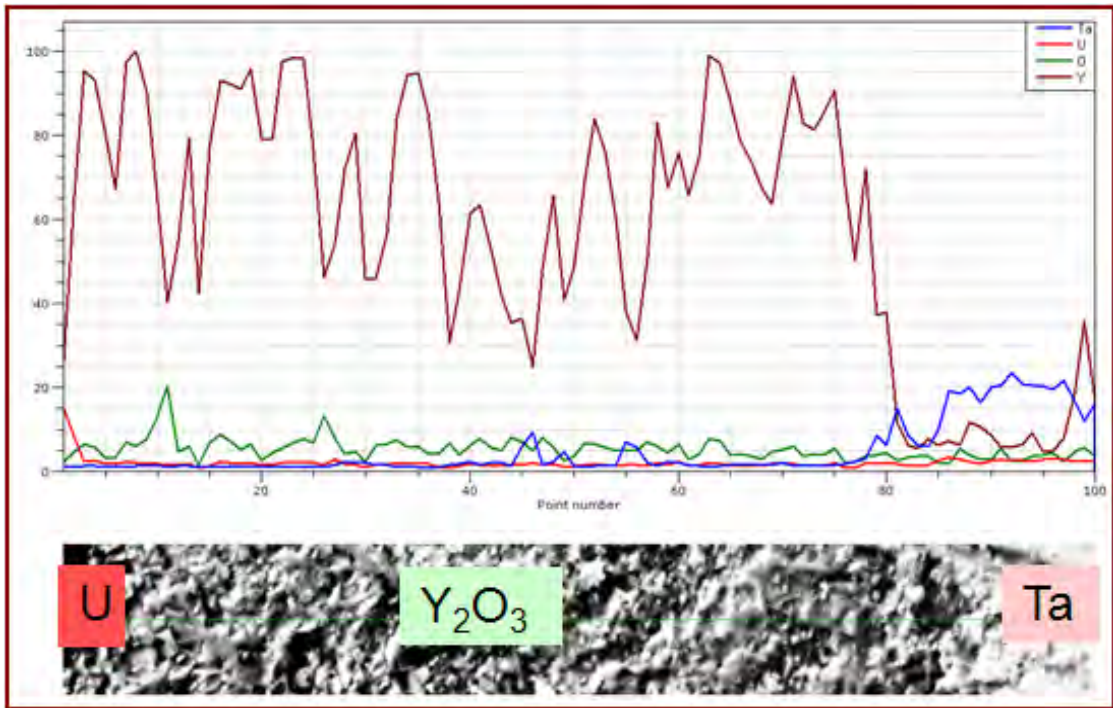


Figure 7.27 EDS line scan of the cross-section of tantalum /yttria coating interface after 120hrs of immersion (Sample UCOR-14)

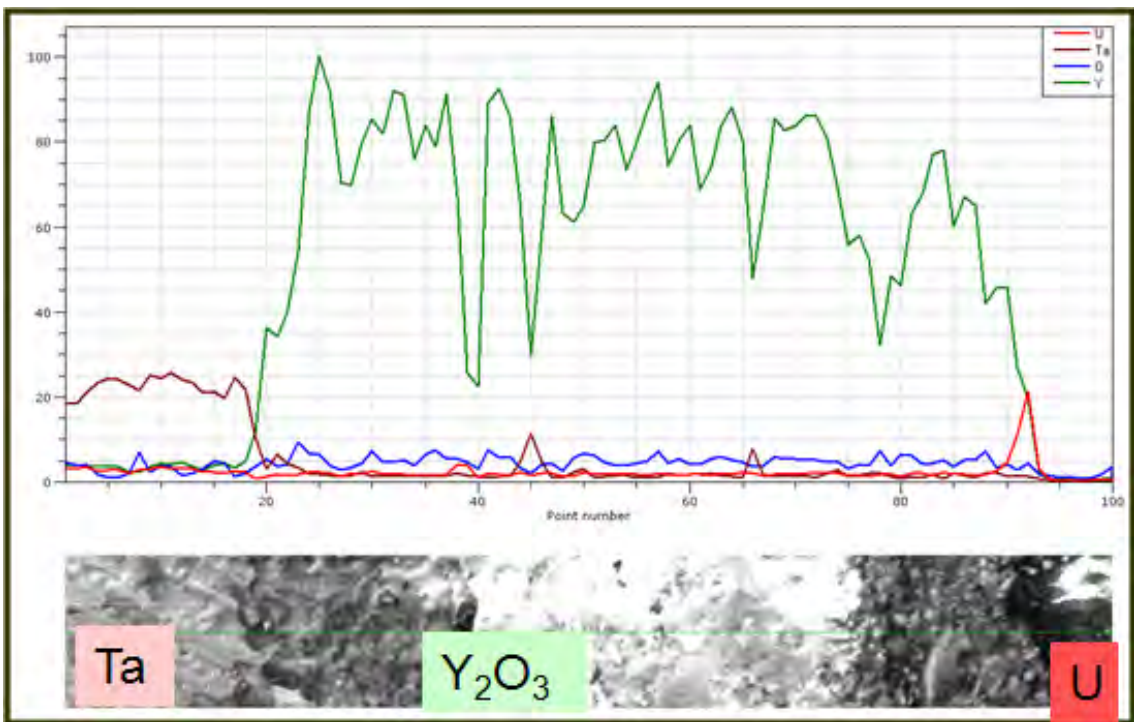


Figure 7.28 EDS line scan of the cross-section of tantalum /yttria coating interface after 200hrs of immersion (Sample UCOR-16)

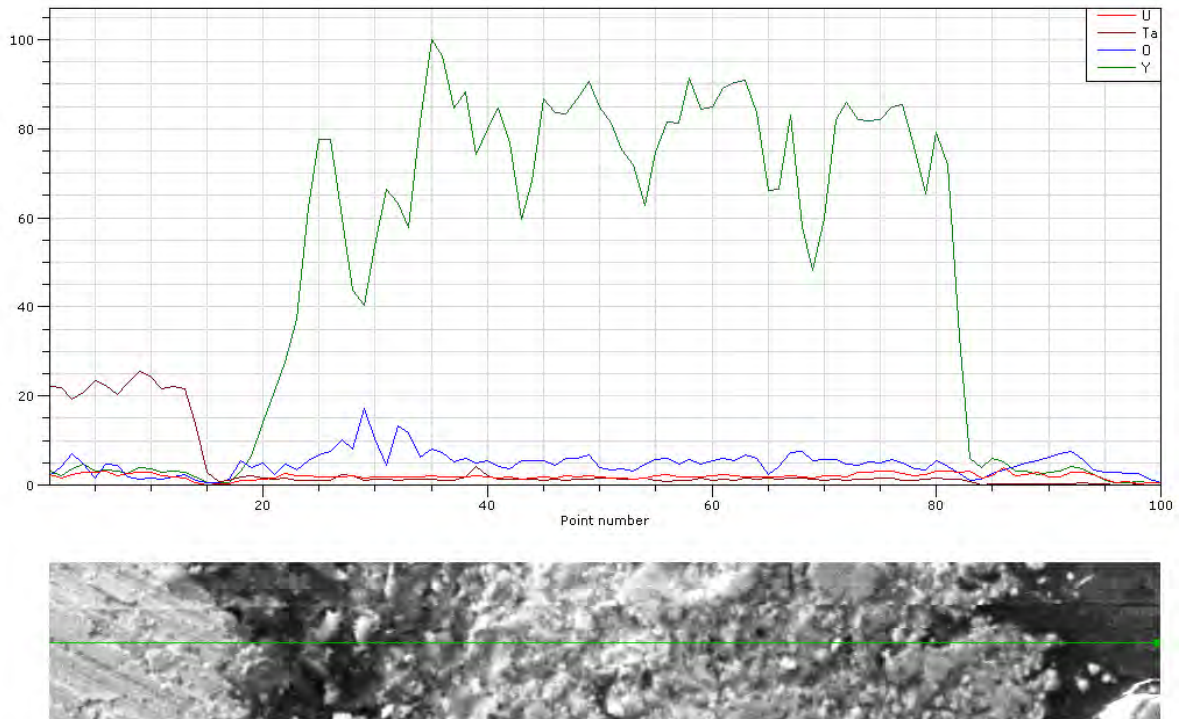


Figure 7.29 EDS line scan of the cross-section of tantalum /yttria coating interface after 400hrs of immersion (Sample UCOR-18)

## 7.8 Conclusions

- i. (a) One of the primary objectives of the experimental program was to produce durable coatings of yttria on tantalum substrate without the use of any bond coat for liquid uranium containment applications. This was accomplished by establishing the optimized plasma spray coating parameters, which were qualified by the adhesion test. The coatings prepared with the selected parameters using both the in-house powder and the commercially procured powder respectively could withstand stress from thermal cycling.
- (b) In addition, it was found that moisture and oxygen have a deleterious effect on the performance of the coating on tantalum substrate.
- (c) Yttrium oxide by thermal plasma spray was found to be a stable protective barrier against liquid uranium at 1573K upto 400hrs at least. The reaction products

are not observed at the uranium/yttrium oxide interface. The EDX line scan confirmed that uranium was unable to diffuse into yttrium oxide coating. Immersion of the coupons in uranium had not resulted in any coating instabilities leading to cracks or spalling of the coating.

- ii. The analysis showed that the surface pore sizes and surface tension of liquid uranium was such that the liquid uranium was not able to penetrate into the pores on the surface.
- iii. The protective coating was also free of interconnected porosity; hence migration of uranium vapour through the coating had not taken place. The results were utilized for preparing the engineering components of yttria coated tantalum.

#### **References:**

- 10.1. ASM Binary phase diagrams, 2002.
- 10.2. J. W. Koger, C. E. Holcombe, J. G. Banker, Coatings on graphite crucibles used in melting uranium, *Thin solid films* 39 (1976) 297 303.
- 10.3. C. Tournier, B. Lorrain, F. Le Guyadec, L. Coudurier, N. Eustathopoulos, Kinetics of interfacial reactions in molten U/solid Y<sub>2</sub>O<sub>3</sub> system, *J Nucl Mater* 254 (1998) 215 220.
- 10.4. *Metallurgical and Ceramic Protective coatings*” Ed. By Kurt H. Stern, Pg 264-266.
- 10.5. P. V. Ananthapadmanabhan, K. P. Sreekumar, K. V. Muraleedharan, N. Venkataramani, Plasma-sprayed composite coatings for high temperature engineering applications, *Surf Coat Tech* 49 (1991) 62 66.
- 10.6. Moshe Kuznietz, ZviLivne, Carlos Cotler, GidonErez, Diffusion of liquid uranium into foils of tantalum metal and tantalum 10 wt% tungsten alloy upto 1350°C, *J Nucl Mater* 152 (1988) .

- 10.7. Moshe Kuznietz, Zvi Livne, Carlos Cotler, Gidon Erez, Effect of liquid uranium on tungsten foils upto 1350°C, *J Nucl Mater* 160 (1988) 69-74.
- 10.8. Moshe Kuznietz, Carlos Cotler, Progressive dissolution of molybdenum foils in liquid uranium at 1160°C, *J Nucl Mater* 160 (1988) 196-200.
- 10.9. P.V. Ananthapadmanabhan, K.P. Sreekumar, T.K. Thiyagarajan, R.U. Satpute, K. Krishnan, N.K. Kulkarni, T.R.G. Kutty, Plasma spheroidization and high temperature stability of lanthanum phosphate and its compatibility with molten uranium, *Materials Chemistry and Physics*, 01/2009; 113(1):417-421.
- 10.10. X. Q. Cao, R. Vassen, D. Stoeber, Ceramic materials for thermal barrier coatings, *J Eur Ceram Soc* 24 (2004) 1-10.
- 10.11. Toshiaki Yoneoka, Takayuki Terai, Yoichi Takahashi, High temperature liquid metal corrosion and high temperature electrical conductivity of Y<sub>2</sub>O<sub>3</sub>, *J Nucl Mater* 248 (1997) 343-347.
- 10.12. P. V. A. Padmanabhan, S. Ramanathan, K. P. Sreekumar, R. U. Satpute, T. R. G. Kutty, M. R. Gonal, L. M. Gantayet, Synthesis of thermal spray grade yttrium oxide powder and its application for plasma spray deposition, *Mater Chem Phys* 106 (2007) 416-421.
- 10.13. Nagaraj A, Anupama P, Jaya Mukherjee, Sreekumar K P, R U Satpute, P V A Padmanabhan and L M Gantayet, "Thermal stability studies of plasma sprayed yttrium oxide coatings deposited on pure tantalum substrate", *J. Phys. Conf. Ser.*, 208, 2010.
- 10.14. C E Holcombe, G. L. Powell, The reaction of aluminum titanate crucibles with molten uranium, *J Nucl Mater* 49 (1973) 238-240.
- 10.15. D. Das, S. R. Dharwadkar, M. S. Chandrasekharaiah, Containment of molten uranium alloys in powder metallurgical tungsten containers, *J Nucl Mater* 97 (1981) 88-92.
- 10.16. C Tournier, B. Lorrian, F. Le Guyadec, N. Eustathopoulos, The influence of non-stoichiometry of oxides on their wettability by liquid metals, *J Mater Sci Lett* 15 (1996) 485-489.
- 10.17. J A Cahill, A.D. Kirshenbaum, The surface tension of liquid uranium from its melting point, 1406°K to 1850°K, *J Inorg Nucl Chem* 27 (1965) 73-76.

## CHAPTER VIII

### SUMMARY AND CONCLUSIONS

---

#### Summary of the work

In the present thesis, the research work was directed towards the development of a molten salt electrochemical process for production of uranium metal from uranium oxide. Due to several advantages in the nuclear fuel cycle, the process operating above the melting point of uranium and in the molten fluoride electrolyte bath was chosen. Due to the difficulties of producing  $UF_4$  additive of specific isotopic composition in the nuclear fuel cycle, a new bath without uranium additive as solvent, namely,  $LaF_3$  has been developed. In this work studies were conducted to determine the thermophysical and electrochemical properties of molten fluoride  $LiF-BaF_2$  baths with  $LaF_3$  additive, understand the mechanism of uranium reduction in fluoride baths, to establish the feasibility of uranium metal production in  $LaF_3$  electrolytes, and with due emphasis on the development of materials and components for handling liquid uranium and electrolyte at high temperature.

Due to the safety hazards associated with the handling of radioactive materials, all the operations involved in the experiments were done in fumehoods designed to handle radioactive materials. The experiments were conducted with utmost safety precautions, and personal protection equipment where required. Several customized experimental assemblies were built with leak tightness of  $1E-9$  mbar l/s to prevent ingress of impurity gases, characterized, tested and used for specific studies. Safety features were provided in all the experimental setups, to contain the spread of

radioactivity in the event of an accident. Safety clearances were obtained from the regulatory authorities before conducting the experiments.

### **8.1 Thermo-physical characterization and preparation of electrolytes**

Thermo physical characterization studies were carried out on several salt mixtures related to the production of Uranium metal by molten salt electrolysis technique. Thermo Gravimetry/ Differential Thermal Analysis and X-Ray Diffraction studies were done to determine the melting points, high temperature losses due to evaporation and phases present after the sample is cooled to room temperature. A detailed conditioning procedure was developed. Linear sweep voltammetry had been used as a diagnostic tool for measurement of the impurities present in the electrolyte, as impurities give rise to a higher background current.

### **8.2 Selection of materials to for the electrolysis setup**

Selection of materials to handle fluoride baths had been done based on thermodynamic analysis and experiments simulating the electrolysis process. For conducting the electrolysis experiments two types of materials are required a) electrically insulating and resistant to both liquid uranium and molten fluoride electrolyte and b) electrically conducting and resistant to molten fluoride electrolyte at 1473K. Towards these material requirements  $\text{Al}_2\text{O}_3$ ,  $\text{Y}_2\text{O}_3$ ,  $\text{SiO}_2$ , low density graphite, high density graphite, hexagonal boron nitride,  $\text{LaPO}_4$  were tested with different electrolytes. It was observed that high density graphite ( $\sim 1.95 \text{ g/cc}$ ) is the best suited for the anode compartment. High density graphite is conducting and resistant to electrolytes of  $\text{LiF-BaF}_2$  with  $\text{UF}_4/\text{LaF}_3$  additive upto 1573K. For the cathode compartment applications, electrically insulating hexagonal boron nitride is

found to be a suitable material which has corrosion resistance to liquid uranium, U alloys with copper and tin, and electrolytes of LiF-BaF<sub>2</sub> with UF<sub>4</sub>/LaF<sub>3</sub>. Based on this study the materials of construction for the electrolytic cells have been chosen.

### **8.3 Solubility studies of UO<sub>2</sub> in the electrolyte baths**

The molten fluoride salt mixture LiF-BaF<sub>2</sub> with varying amounts of UF<sub>4</sub> and LaF<sub>3</sub> was equilibrated with a sintered uranium oxide pellet at 1473K, 1523K and 1573K, and the salt samples were collected after 48hrs of equilibration. Studies were conducted with 10%, 30% and 50% LaF<sub>3</sub> additions in LiF-BaF<sub>2</sub> base electrolyte. The solubility of UO<sub>2</sub> generally increased with rise in LaF<sub>3</sub> concentration in the electrolyte at any temperature in the range of 1423K-1523K. The solubility variation between 30% LaF<sub>3</sub> and 50% LaF<sub>3</sub> was within the standard deviation of the analytical results. At a given concentration of LaF<sub>3</sub>, the UO<sub>2</sub> solubility increased monotonously with temperature. To study the effect of mixed electrolyte, UF<sub>4</sub> had been added as a replacement of LaF<sub>3</sub> in LiF-BaF<sub>2</sub>-10%LaF<sub>3</sub> and LiF-BaF<sub>2</sub>-30%LaF<sub>3</sub> in a manner that the sum of UF<sub>4</sub> and LaF<sub>3</sub> remained at 10% and 30% respectively. The addition of 1.9% UF<sub>4</sub> to the LaF<sub>3</sub> resulted in increase of UO<sub>2</sub> solubility in the mixed electrolyte in comparison to the UF<sub>4</sub> free electrolyte. The effect of the UF<sub>4</sub> addition seems to indicate, the formation of a complex of UO<sub>2</sub> and UF<sub>4</sub> resulting in higher dissolution. The new data of solubility of uranium oxide generated in this work has been used for molten salt electrolysis.

### **8.4 Electrochemical studies of uranium in the molten fluoride bath at 1473K**

Electrochemical studies on UF<sub>4</sub> in LiF-BaF<sub>2</sub> eutectic have been carried out with and without addition of UO<sub>2</sub> at 1473K by cyclic voltammetry and chronopotentiometry.

Tungsten and Molybdenum wires of 0.5mm diameter were used as the working electrode, and the crucible served as the counter electrode. The potentials were referred to a platinum wire (1mm diameter) acting as a quasi-reference electrode (QRE). The sweep rate was varied from 50mV/s to 1000mV/s in the voltammogram recordings. For the chronopotentiometric experiments, the current was varied from 50mA to 300 mA to study the chronopotentiometric wave. In the electrolyte LiF-BaF<sub>2</sub>(1:1)25 wt% UF<sub>4</sub>, two redox peaks were observed in the cyclic voltammograms which could be attributed to two redox reactions of U<sup>4+</sup>→U<sup>3+</sup> and U<sup>3+</sup>→U. The measured reduction potentials versus platinum (QRE) of U<sup>4+</sup>→U<sup>3+</sup> and U<sup>3+</sup>→U are -0.804V and -0.999V respectively at 1473K. It was observed that the cathodic peak potentials shifted more cathodically with an increase in the scan rate, indicating a quasi-reversible reduction process. The linearity of the peak current versus square root of scan rate indicates the electrochemical reduction process is a diffusion controlled process. Chronopotentiograms exhibited two waves corresponding to the two peaks observed in the same potential range as observed in the cyclic voltammogram, which could be associated to the reduction of uranium ions. The product of current applied and the transition time  $\tau^{1/2}$  in the chronopotentiogram has been found to follow the Sand's law. With the addition of UO<sub>2</sub> to the LiF-BaF<sub>2</sub>(1:1)-25 wt% UF<sub>4</sub> electrolyte, in place of two redox peaks, which had been observed without UO<sub>2</sub>, only a broad peak appears indicating that uranium may be present as an oxy-fluoride complex. The deposition potentials thus determined were utilized in choosing the cell voltages for electrolyte conditioning and the electrolysis experiments.

## 8.5 Electrolysis of $\text{UO}_2$ to U metal

Several electrolysis experiments were conducted and the effects of the following were studied: a) Variation of the size of the cell, b) anode and cathode configurations, c) cathode or liquid cathode materials, d) anode materials and e) type of electrolytes. The targeted cathode current density was attained by providing an insulating BN liner to the graphite crucible, exposing only the desired area of the graphite surface. The experimental procedure involved first pretreating the electrolyte at 673K and 1473K with a dwell time of 24hrs at each temperature; and then equilibrating the electrolyte and uranium oxide source (Sintered  $\text{UO}_2$  pellets,  $\text{UO}_2+\text{C}$  pellets,  $\text{UO}_2+\text{C}+\text{biomass tar}$  pellets and  $\text{UO}_2$  powder). Four cell sizes S-80, S-350, S700 and S-1400 were used in the experimental plan for capacities of 80g, 350g, 700g and 1400g of electrolyte respectively. Different anode and cathode design configurations were used in the four types of cells. Several electrolysis experiments were conducted in  $\text{LiF}:\text{BaF}_2$  (1:1)-25 Wt %  $\text{UF}_4$  salt mixtures in different electrolytic cell designs to arrive at the cell configuration which could replicate the results of uranium deposition with standard electrolyte reported by the previous authors. Thereafter, the experiments were continued for production of uranium in the electrolytes proposed in the study. The electrolysis experiments with ~60g tin or copper as the liquid cathode in BN container and  $\text{UO}_2$  as anode with ~1400g of electrolyte with a current density of ~2  $\text{A}/\text{cm}^2$  yielded mixture of Tin- $\text{USn}_3$  and Cu- $\text{Cu}_5\text{U}$ , respectively; this confirmed the formation of uranium metal. Process repeatability in  $\text{LiF}:\text{BaF}_2:25\%\text{LaF}_3$  electrolyte was established. ~8% cathode current efficiency was observed in  $\text{LiF}:\text{BaF}_2:25\%\text{LaF}_3$  electrolyte. XRD analysis of salt mixture was conducted to identify the uranium phase in the salt. Chemical analysis was done by ICPMS and EDXRF to estimate the quantity.

Higher efficiencies than those reported in this study can be achieved by careful design of electrolytic cell and also supplementing with additional data on the solubility of uranium metal in LiF-BaF<sub>2</sub>-LaF<sub>3</sub> metals. Choice of the electrolyte mixture with low solubility of uranium metal and which offers a medium in which UF<sub>3</sub> is unstable may lead to higher current efficiencies by reduction of parasitic cyclic reaction current.

### **8.6 Preparation of Y<sub>2</sub>O<sub>3</sub> coatings as chemical barrier**

A systematic and comprehensive study has been reported for the preparation of robust yttria coatings on components. Tantalum was chosen as the substrate for coatings among other refractory metals, keeping in view the following considerations; ease in fabrication and handling, limited saturation solubility in uranium (~2.5% w/w), and availability. In house spray grade powder was made from the raw material supplied by M/s IRE Ltd that had a size range of 5-10 micron. The IREL powder was subjected to Cold Isostatic Pressing (CIP) at 30,000 PSI to obtain a green density of ~ 50% theoretical density. Sintering of the compact was done at 1873K for 4 hours, and the compact was ground. The powder was then sieved to separate into size ranges of 38-75µm and 76 -106µm. The specimens used for testing of coatings were cut from pure tantalum sheet into coupons of rectangular shapes having dimensions 25 mm x 10 mm x 1mm thk, and 40 mm x 8 mm x 1mm thk, respectively and their edges were rounded off. A series of coating experiments were conducted by producing the coatings of yttria with variation of powder size, plasma power, primary gas flow and powder feed rate. Other coating factors such as torch to base distance (TBD), auxiliary gas flow, feed gas flow and surface roughness were maintained constant as

practiced in the existing lab facility. Adhesion test was used as the response parameter for obtaining the optimum coating parameters.

### **8.7 Qualification of coatings by thermal cycling**

Prior to the thermal cycling test of coated coupons, visual inspection and optical micrography were conducted to evaluate the coating. Thermal cycling experiments were conducted both in high purity argon gas and vacuum environment. In the experiments conducted in argon, each cycle consisted of heating the coupons to 1523K in a controlled way, and soaking at that temperature for 2 hours, followed by controlled cooling. The changes in weight of the coated samples were measured to a precision of 0.01 mg. The samples were considered as failed when cracks were observed at 100X magnification in an optical microscope. The coatings produced by the powder prepared in-house did not develop any cracks upto 26 cycles. To study the thermal stability of coating in vacuum operations, thermal cycling tests were done at a vacuum of 1E-6 mbar. The coatings produced by both the in-house powder and the powder procured from reputed commercial sources withstood 9 cycles. The environmental influence on the performance of the coating was investigated; both oxygen and moisture introduction resulted in reaction with the substrate and peeling of the coating. In the case of contamination with moisture at high temperature hydrocarbon gases and CO are produced by reaction with graphite susceptor. Reaction with these gases resulted in the formation of tantalum oxide as well as TaC. The oxygen leak into the system resulted in direct oxidation of tantalum coupons and peeling of the coating.

## **8.8 Compatibility of yttria coating with liquid uranium**

For studying the compatibility of the coated coupons with liquid uranium, several experiments were conducted by immersing the coated coupons into liquid uranium at 1573K for different durations. The crucible for containing liquid uranium was formed from a 2mm thick tantalum sheet having dimensions of 50mm outside diameter and 30mm height. This tantalum crucible was coated with 80-110 $\mu$ m thick yttrium oxide and contained about 230gm of nuclear grade uranium to provide a molten pool depth of about 8mm. This experimental setup went through a formal safety audit and approval process. The tantalum coupons used were 40mm x 8mm x 1mm thick with rounded edges and corners to reduce the stresses in the coating. Two coupons were used in each experiment. Pre-experimental qualification for defect free coupons was done by optical microscopy at 200X, and thermal cycling tests of a few coupons of the batch.

The heating, cooling and holding cycles adopted in the experiments consisted of heating the setup to 723K at 200K/hr and holding it for 2 hours, followed by heating to 873K at 200K/hr and holding for 2 hours for complete outgassing of the system. Separate experiments were conducted by continuous immersion for 10, 20, 40, 80, 120, 200 and 400hrs durations. Coupons were removed from the metal pool and held above the pool for 1hr for liquid uranium to trickle down. Post experiment analysis had included observation of full area under an optical microscope at 200X. Defect free coupons were cold mounted and cut with a diamond wheel of 300 $\mu$ m thickness to observe the cross-section. Polishing was intentionally not done to retain the micro structural features. The cross-sectional micrograph had shown that the coating is relatively free of interconnected pores which have a direct effect on the extent of

penetration of uranium through the pores. The density of the coating was found to be 90% of the theoretical density. The surface porosity was studied using a SEM, and pore sizes ranging from 2-10 $\mu$ m were observed. After the corrosion experiments, the coating was examined for interface integrity. None of the coupons showed delamination or interfacial cracks. No specific reaction products were observed at the liquid/Y<sub>2</sub>O<sub>3</sub> interface in all the coupons. Non-stoichiometric yttrium oxide was not observed across the thickness of coating even after 400 hrs of contact time with liquid uranium. Considering a maximum pore size of 10 $\mu$ m on the surface, with the value of surface tension of liquid uranium being 1.5267 N/m and contact angle of 106°, the pressure required to penetrate is 0.164 Mpa. The total hydraulic head available in 8mm metal pool being only 1486.5 Pa, which was a few orders below the penetrating pressure, and hence the liquid uranium had not penetrated into the yttrium oxide coating.

## 8.9 Important Conclusions

The important conclusions from the work are enumerated below

1. LaF<sub>3</sub> has been identified as an additive in the fluoride salt mixture. Salt mixtures of LiF-BaF<sub>2</sub> (1:1) equimolar mixture with different concentrations of LaF<sub>3</sub> have been prepared and characterized.
2. Melting point and high temperature losses have been determined by TG-DTA for LiF-CaF<sub>2</sub> (6:4 mol%) with 5, 10 and 20 wt% LaF<sub>3</sub> as well as for LiF-BaF<sub>2</sub> (1:1) with different UF<sub>4</sub> and LaF<sub>3</sub> compositions.
3. Compatibility of several materials for different fluoride electrolytes has been determined and suitable materials have been successfully used in the experimental work.

4. The fluoride salt pretreatment procedure has been developed with linear sweep Voltammetry (LSV) as a diagnostic tool and has been implemented in all the experiments.
5. Design, development, fabrication and testing of tailor made experimental setups for working at 1573K have been made for conducting solubility studies, electrolysis studies and material compatibility studies in liquid uranium.
6. Solubility studies of  $\text{UO}_2$  in  $\text{LiF-BaF}_2\text{-LaF}_3$  mixtures with  $\text{LaF}_3$  varying from 10wt% to 50 Wt% have been conducted in the range of 1423K-1523K. Solubility studies in a few  $\text{UF}_4$  containing mixtures have also been conducted at 1473K. It is concluded that increase in the  $\text{LaF}_3$  concentration leads to increase in uranium oxide solubility. Similar increasing trend has been observed with rise in the temperature. Addition of a small quantity of  $\text{UF}_4$  to  $\text{LaF}_3$  increases the solubility further.
7. Electrochemical investigations (CV and chronopotentiometry at 1473K) in  $\text{LiF-BaF}_2$  base salt mixtures with  $\text{UF}_4$  or  $\text{LaF}_3$  and with out addition of  $\text{UO}_2$  have been conducted and deposition potentials of uranium have been determined.
8. Durable coating of yttria on tantalum substrate without the use of any bond coat has been developed and tested for thermal stability upto 26 cycles by establishing the optimized plasma spray coating parameters; they were qualified by adhesion test.
9. Environmental influence on the performance of the coating has been studied by introducing air and moisture leaks into the system during the thermal cycle.

It has been established that both moisture and oxygen have a deleterious effect on the coatings.

10. Liquid uranium corrosion with yttrium oxide has been evaluated at 1573K upto 400hrs. Yttrium oxide by thermal plasma spray has been found to be a stable protective barrier against liquid uranium at 1573K upto 400hrs.
11. Feasibility of uranium deposition in LiF-BaF<sub>2</sub> base salt mixtures with UF<sub>4</sub>/LaF<sub>3</sub> mixed electrolytes and LaF<sub>3</sub> containing electrolyte has been established by conducting electrolysis with different anode/cathode configurations.

### **8.10 Major contributions**

Some of the major contributions made in the research work are listed below

1. Thermo-physical characterization of LaF<sub>3</sub> containing with LiF-BaF<sub>2</sub> electrolytes has been carried out for the first time.
2. Experimental setups have been designed, developed, fabricated, tested and installed for electrolytic process related experiments at 1573K, the setups qualified for regulatory safety clearance for uranium experiments.
3. New data on UO<sub>2</sub> solubility in LiF-BaF<sub>2</sub>-LaF<sub>3</sub> mixtures in the range of 1423K-1523K have been generated.
4. Deposition potentials of uranium ions in fluoride melts at 1473K have been determined.
5. Stable protective barrier against liquid uranium at 1573K have been developed and tested upto 400hrs of continuous contact.
6. The feasibility of uranium production in LiF-BaF<sub>2</sub>-LaF<sub>3</sub> electrolytes has been demonstrated.

### 8.11 Future work

For further development of the proposed new electrolysis process and systems, the following areas are identified.

- i. Conducting electrolysis of  $\text{UO}_2$  in  $\text{LiF-BaF}_2\text{-LaF}_3$  electrolytes with liquid uranium as the cathode.
- ii. Development of a high temperature reference electrode for electrochemical studies in the range of 1423K to 1523K (in place of pseudo reference electrode), and comparison of deposition potential of uranium in different molten fluoride electrolytes.
- iii. Determination of the saturation concentration and the rate of dissolution of liquid uranium metal in  $\text{LiF-BaF}_2\text{-LaF}_3$  electrolytes.
- iv. Optimizing the yield and purity of the metal produced with parametric studies of cathode current density, cell voltage and inter electrode distance.
- v. Improving the high temperature electrochemical cell design, which includes improvement in electrode design, product collection mechanism, arrangement for avoiding  $\text{UO}_2$  settling at the metal electrolyte interface, and prevent dissolution of liquid uranium.
- vi. Mathematical modeling of electrochemical process for optimization.

### **List of International Journal Publications included in the present thesis**

1. Nagaraj Alangi, Jaya Mukherjee, L M Gantayet, “Solubility of uranium oxide in LiF-BaF<sub>2</sub> electrolyte with LaF<sub>3</sub> additive”, J. Nucl. Mat, Vol 470, 2016, 90-96.
2. Nagaraj A, Jaya Mukherjee, Anupama P, Mukesh K V, Y.Chakravarthy, P V A Padmanabhan, A K Das and L M Gantayet, “Liquid uranium corrosion studies of protective yttria coatings on tantalum substrate”, J. Nucl. Mat, Volume 410, Issues 1–3, 2011, Pages 39–45.
3. Nagaraj A, Anupama P, Jaya Mukherjee, Sreekumar K P, R U Satpute, P V A Padmanabhan and L M Gantayet, “Thermal stability studies of plasma sprayed yttrium oxide coatings deposited on pure tantalum substrate”, J. Phys. Conf. Ser. , 208, 2010.

### **Manuscripts under review:**

1. Nagaraj Alangi, Jaya Mukherjee, L M Gantayet, “Development of LaF<sub>3</sub> based fluoride bath for high temperature electrolytic reduction of uranium oxide”, communicated to Mineral Processing and Extractive Metallurgy (Trans. Insti. Min. Metall. C)
2. Nagaraj Alangi, Jaya Mukherjee, L M Gantayet, “Electrochemical study of uranium in molten fluoride media at 1473K”, to be communicated to Journal of applied electrochemistry.

### **Presentations in International and national conference included in the present thesis**

1. Nagaraj A., Anupama P., Jaya Mukherjee, K. P. Sreekumar, R. U. Satpute, P. V. A. Padmanabhan, L. M. Gantayet, “Studies on thermal stability of plasma sprayed yttrium oxide coatings deposited on pure tantalum substrate”, NMD-ATM 2007.

2. Nagaraj A, Trupty Chavan, D.N.Wagh, Anupama P., R.Verma, L.M.Gantayet, "Determination of Uranium in molten fluoride salts using Energy Dispersive X-ray fluorescence (EDXRF)", NUCAR 2009.
3. Nagaraj Alangi, Jaya Mukherjee, Anupama P, M K Verma, Y Chakravarthy, "Thermal and chemical stability studies of protective plasma sprayed yttrium oxide coatings on tantalum substrate against liquid uranium", International Conference on Electron Nanoscopy, EMSI50, 2011.
4. Nagaraj Alangi, Anupama P., Jaya Mukherjee, L. M. Gantayet, "Evaluation of a molten salt electrolyte for direct reduction of actinides", Advances in Nuclear Materials, ANM-2011.
5. Nagaraj Alangi, A K Suri and L M Gantayet, " Electrochemical study of uranium in molten fluoride media at 1473K", NuMat 2012: The Nuclear Materials Conference, Osaka, Japan, 22-25 October, 2012.
6. Nagaraj Alangi, Jaya Mukherjee, Anupama P, K Dasgupta, "Electrolytic reduction of uranium oxide in molten fluoride baths", Thorium energy conference, ThEC2015, Dec 2015.